Imaging Spectroscopy of salt-affected soils: Model-based integrated method

Jamshid Farifteh

Jamshid Farifteh (2007)
Imaging Spectroscopy of salt-affected soils: Model-based integrated method, International Institute for Geo-information Science and Earth Observation (ITC) and Utrecht University

Universiteit Utrecht

P.O. Box80.115
Utrecht, The Netherlands

International Institute for Geo-information Science and Earth Observation (ITC), P.O. Box 6, 7500 AA, Enschede, The Netherlands

May 2007
ITC dissertation number: 143
ISBN: 978-90-6164-259-6

Printed by International Institute for Geo-information Science and Earth Observation, Enschede, The Netherlands

E-mail: Farifteh@itc.nl

Imaging Spectroscopy of salt-affected soils: Model-based integrated method

Beeldvormende spectroscopie van door verzouting aangetaste bodems: Model-gedreven geïntegreerde methodiek

(Met een samenvatting in het Nederlands)

PROEFSCHRIFT

ter verkrijging van
de graad van doctor aan de Universiteit Utrecht
op gezag van de Rector Magnificus,
Prof. dr. W.H. Gispen,
ingevolge het besluit van het College voor Promoties
in het openbaar te verdedigen
op woensdag 9 mei 2007 des ochtends te 12.45 uur

door

Jamshid Farifteh

Promotoren:

Prof. dr. F. D. van der Meer
Prof. dr. S. M. De Jong

Co-promotoren:

Dr. M. van der Meijde
Dr. E. J. M. Carranza

Leden Promotiecommissie:

Prof. Dr. C. Ritsema
Dr. E.L.H. Cammeraat
Prof. Dr. J. Hill
Prof. Dr. J. Poesen
Prof. Dr. V. G. Jetten

In memory of my brother
Abdolhossein

Contents

Chapter 3
Spectral characteristics of salt-affected soils: A laboratory experiment

Chapter 4
Similarity measures for spectral discrimination of salt-affected soils

Chapter 5
Interference of salt and moisture on soil reflectance

Chapter 6

Quantitative analysis of salt-affected soil reflectance spectra: A comparison of two adaptive methods

Chapter 7

Synthesis: Information on soil salinity modelling; integration of surface and near-surface remotely sensed measurements

References

Summary

ITC Dissertation List

List of Figures

List of Tables

List of Acronyms

A	Area within the Gaussian curve
ANN	Artificial neural network
ASD	Analytical Spectral Devices, Inc.
AVIRS	Air-borne Visible/Infrared Imaging Spectrometer
BRDF	Bidirectional reflectance distribution function
CR	Continuum removal
CV	Cross-validation
CV%	Coefficient of variation (standard deviation/Mean)
DAIS	Digital Air-borne Imaging Spectrometer
DEM	Digital Elevation Model
e	Mean error of prediction
e %	Relative e
EC	Electrical Conductivity
ECa	Apparent Electrical Conductivity
ECav	Apparent Electrical Conductivity (vertical dipole)
ECah	Apparent Electrical Conductivity (horizontal dipole)
$\mathbf{EC_e}$	Electrical Conductivity of saturated soil extract
EM	Electromagnetic
EM-38	Geophysical instrument
FCC	False Colour Composite
FOV	Field Of View
GER	Geophysical and Environmental Research Corporation
GIS	Geographic Information System
GPR	Ground-Penetrating Radar
H_0	Null hypothesis
H_a	Alternative hypothesis

IG	Inverted Gaussian
LWs	Loading Weights
MAE	Mean absolute errors
MAE%	Relative MAE
ME	Model Efficiency
MSC	Multiplicative Signal Correction
MSE	Mean Squared Error
NIR	Near Infrared
PCA	Principal Component Analysis
pH	Hydrogen Potency
PLSR	Partial Least Squares Regression
R^2	Coefficient of determination
R^2_{CV}	Cross-validated coefficient of determination
Rd	Amplitude
RMSE	Root Mean Square Error
RMSE%	Relative RMSE
$RMSE_{CV}$	Cross-validated root-mean-square error
RPD	Ratio of prediction to deviation
σ	Distance to the inflection point
SAM	Spectral Angle Mapper
SEM	Standard error of the mean
SID	The spectral information divergence
SMC	Soil Moisture Contents
SNR	Signal to Noise Ratio
SSC	Soil salt content
SSV	Spectral Similarity Value
SWIR	Short Wave Infrared
TDS	Total Dissolved Solids
TIR	Thermal Infrared
TM	Thematic Mapper

TSC	Total Concentration of Soluble Cations
UV	Ultra Violet
VIS	Visible

Chapter 1

Salt-affected soil: Research overview

Abstract

Soil salinity is one of the main environmental problems affecting extensive areas of land in both developed and developing countries. It is the product of a complex interaction of many variables, which lessen the current and /or potential capability of soil to produce goods and services. In general, the consequent changes in land use mainly due to the common policy of agricultural intensification, together with unfavourable natural conditions, have accelerated soil salinity in many parts of the world. In this chapter, the research plan and strategies used to estimate degree of salinity are discussed. In general, the research focuses on characterizations of salt-affected soils by integrating earth observation data of the earth's surface and near surface at various scales (experiment, field and image). The overview presented in this chapter discusses (i) the major issues concerning soil salinity; (ii) research objective and questions; (iii) some key concepts and definitions; and (iv) the rational of the research reported in this dissertation.

1.1 The issue of soil salinity

Concentration of soluble salts in the surface or near-surface soil horizon is a major problem with severe worldwide economical and social consequences. In terms of agricultural consequences, excessive salts in soil accelerate land degradation processes and increases impact on crop yields and agricultural production. The increase of salts in soil also affects other major soil degradation phenomena such as soil dispersion, sealing and crust formation and structural changes, which results in unstable and compacted soil (Agassi et al., 1981; Frenkel and Meiri, 1985; FAO, 1988; Mainguet, 1991; De Jong, 1994; Metternicht and Zinck, 2003). In urban areas, increased levels of salt cause significant problems by damaging roads, buildings, underground services and contaminating drinking water (Spenneman, 1997). The consistent identification and monitoring of soil salinization is essential to control degradation trends and secure sustainable land management, especially, in semi-arid areas where harsh climatic conditions together with rapidly increasing population demand agricultural intensification and land use changes.

Salt-affected areas can be found worldwide under almost all climatic conditions, however, they are most widespread in the arid and semiarid regions (Figure 1.1). Geological formations, climate factors, geomorphology and human activities are considered responsible for accumulation of salt in soil. Geological formation consisting of salt accumulated sediments can provide large volume of salts to be carried by surface or ground water (Maingute, 1991). Climate factors such as low precipitation and high evaporation can increase the concentration of salts in soils, surface and ground water and contribute to salinity problems. Geomorphology has substantial affects on accelerating salinization/ alkalinization within closed basin or lowland areas, where groundwater rises due to a poor drainage system. Improper use of land and irrigation with water containing high levels of soluble salts are human-induced factors causing secondary salinity.

Detection of salinization, assessment of the degree of severity and the extent, particularly in its early stage is vital in terms of sustainable agricultural management. In general, most of the salinity studies in past decades have focused on mapping severely saline areas and have given less attention to quantification of salinity levels (see chapter 2), due to limitations in available technology and methodological techniques. However, the advances in the field of data acquisition and modelling techniques that has been discussed in chapter 2, stimulates the necessity for new development of modelling techniques with predictive capabilities. The new developed method is founded on establishing empirical relationships between soil properties and is based on the assumption of being applicable to non-surveyed areas with similar conditions. In addition, since the entire soil profile is involved in the process, it should be based on integrating surface and near surface measurements.

Figure 1.1: Global distribution of salt-affected soils (Sparks, 1995).

A review of techniques and methods that are used to detect salt-affected areas (see chapter 2) allows establishing a discussion leading to development of a new conceptual framework for the research. The new conceptual framework focuses on defining the underlying problems that prevent accurate estimation of soil salinity levels from remote sensing and is based on the philosophy of solving one problem at a time and providing answers that contribute to solve another problem in hand. Following such an ideology, the research needed to be started with an experimental study under controlled laboratory conditions to provide the basic but very essential information with regard to spectral characteristics of salt-affected soils and the underlying factors. It is followed by field application of laboratory experiment achievements and up-scaling using air-borne hyperspectral imageries in combination with field geophysics measurements. Finally, data from various scales (experiment, field and image) are employed to predict soil salinity using statistical and mathematical modelling tools. The findings of the research support integration of surface remote sensing and near-surface geophysics measurements for more accurate estimation of salinity levels.

The aim of this chapter is to present an overview of the research plan and strategy which includes the world wide problem of soil salinity, the research objective and questions, the research foundation and the thesis structure.

1.1.1 Processes of salinization and alkalinization

The accumulation of soluble salts at the surface or near-surface of soil horizon is called salinization (Szabolcs, 1974). As a consequence, dominant salts in soil

change to chlorides and sulphates of sodium, calcium and magnesium and soil properties such as electrical conductivity (EC) will be affected depending on the amount of accumulated salts. Besides the occurrence of salt crystals, salt crusts and salic horizons, saline soils often have some typical characteristics such as the presence of loose and quite porous granular structure, in the topsoil. With large amount of sodium sulphate (Na_2SO_4) in soil, the topsoil is puffy and the presence of $CaCl_2$, $MgCl_2$ or nitrates gives the soil a moist appearance.

Alkalinization is a process leading to the formation of soils with high percentage of exchangeable sodium. The presence of carbonates and bicarbonates leads to formation of soils with high pH values, between 8.5 and 10 (FAO, 1988; Sparks 1995). The main cause of alkaline reaction of soils, as described by FAO (1988), is the hydrolysis of either exchangeable cations or of salts such as $CaCO_3$, $MgCO_3$, and Na_2CO_3.

1.1.2 Classification and characteristics of salt-affect soils

In general, the two major salt-affected soil groups are *saline* and *alkali* (*sodic*) (Figure 1.2). These two groups can be distinguished on the basis of physico-chemical and biological properties, and their geographical and geochemical distribution (Szabolcs, 1974). Although the aforementioned two categories account for a very large fraction of salt affected soils the world over, there are transitional or borderline formations which are likely to have intermediate properties (FAO, 1988).

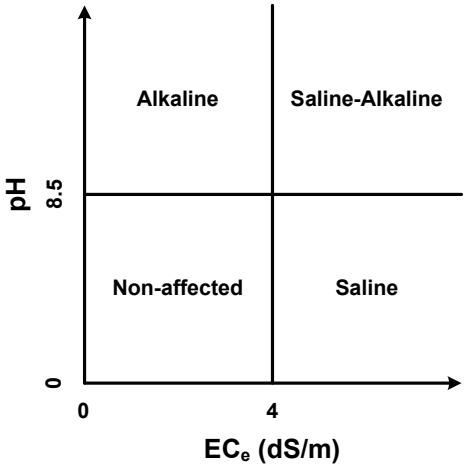

Figure 1.2: Traditional classification of soils into saline, alkaline, and saline-alkaline soils (Richards, 1954).

Salinity in soil and water is expressed by different terms and units namely total dissolved solids (TDS) in milligrams per litre, total concentration of soluble cations (TSC) and total concentration of soluble anions (TSA) in equivalents per litre/kilogram (Tanji, 1990). The most frequently used indicator of salinity is electrical conductivity of saturated soil extract (EC_e). Electrical conductance (the reciprocal of resistance) is a quick and sufficiently accurate measure for soil salinity which is independent of the size of the sample (Richards, 1954). EC_e increases with the concentration of soluble salts. Table 1.1 shows standard salinity classes proposed by the US salinity laboratory (Richards, 1954). The standard unit of electrical conductivity (EC) is expressed in deci Siemens per metre (dS/m) at 25° C. EC measurements of soils can be converted to standard reference temperature by a 2 percent increase of the measured value at 25° C per degree Celsius in temperature (Richards, 1954).

No exact relationship between these various measures of salinity parameters has been reported in published literatures. According to Tanji (1990), however, the EC (dS/m) values can be used to derive the TDS, TSC and TSA measurements. The TDS may be approximated by multiplying EC (dS/m) by factor of 640 and 800 for lesser and hyper saline samples, respectively. In order to obtain TSC or TSA, the EC (dS/m) values can be multiplied by a factor of 0.1 and 10.0 for $mol_{(c)}/l$ and $mmol_{(c)}/l$, respectively.

Table 1.1: Soil Salinity classes in terms of EC_e (Richards, 1954).

Salinity class	EC_e (dS/m)	Salinity effects on crops
Non-saline	< 2	Salinity effects are negligible
Slightly saline	2 - 4	Yields of very sensitive crops may be restricted
Moderately saline	4 - 8	Yields of many crops restricted
Very saline	8 - 16	Only tolerant crops yield satisfactory
Extremely saline	> 16	Only a few very tolerant crops yield satisfactorily

1.1.3 Salt minerals

The salt minerals found in salt-affected soils are various proportions of the cations sodium, calcium, magnesium, and potassium and anions chloride, sulphate, carbonate, bicarbonate, and nitrate (Richards, 1954). The salts in soil appear in the form of crust (as a result of evaporation), deposit as a result of precipitation, and solution as a result of dissolving in water in soil profile (FAO, 1988). Basically, salt minerals in nature are rarely pure, since trace elements are often trapped in crystal lattices during crystallization and thus affect the colour

and other reflectance properties of minerals (Hunt and Salisbury, 1970). The salt minerals mainly responsible for salinity of soil are found within four chemical groups namely carbonates, halides, sulphates, and borates.

The carbonates are common constituents of the earth's near-surface crust. They are a complex group of minerals built around the CO_3^{-2} ion where a carbon atom resides at the centre and an oxygen atom at every corner of the triangle sits. Calcite ($CaCO_3$), dolomite CaMg $(CO_3)_2$, magnesium carbonate ($MgCO_3$), and sodium bicarbonate ($NaHCO_3$) are some of the carbonates minerals, which can be found in salt-affected soils.

The halides are a group of minerals whose principle anions are halogens such as fluorine (F^-), chlorine (Cl^-), and bromine (Br^-) and iodine (I^-) combined with an alkali metal. The halogens are present as large negatively charged cations, linked with a pure ionic bond to a small metal positive cation such as sodium (Na^+) or calcium (Ca^{++}). Some of the most common halide minerals found in salt-affected soils are halite (NaCl), bischofite ($MgCaCl_2 {}^*6H_2O$), and antarcticite ($CaCl_2 {}^*6H_2O$).

Sulphate minerals are compounds of oxygen and sulphur creating the sulphate ion, SO_4^{2-}, combined with one or more metals. Many of the minerals are strongly hydrated species, meaning that they are bound with water molecules in the crystal. Mirabilite ($Na_2SO_4 {}^*10H_2O$), gypsum ($CaSO_4 {}^*H_2O$), and kieserite ($MgSO_4 {}^*H_2O$) are some of the sulphates minerals, which can be found in salt-affected soils.

Borates are a complex minerals group containing boron and oxygen in combination with other elements, forming boric acid, or inorganic salts. There is little variation in the chemistry of these minerals and the most found in salt-affected soils are sodium, calcium and magnesium borates.

These mineral groups and their characteristics are extensively discussed in literatures, namely by Klein and Hurlbut (1999).

1.1.4 Salt-affected soil-water system

Mineral solubility, in principle, controls water chemistry and salinity in soils. With water as solvent, the evaporites are the most soluble types of minerals; first to dissolve and last to precipitate. The resistates and hydrolyzates are the least soluble minerals followed by oxidates and carbonates (Tanji, 1990). A simplified interpretation of the Hardie-Eugster model for evaporative salinization of water indicates that the first mineral to precipitate in large quantities is calcite and further evapoconcentration depends on relation between molarity of Ca and carbonate alkalinity (Drever, 1982). In a soil

solution where ratio of water to soil is considerably small, other mechanisms may also play a significant role (Tanji, 1990). Chemical interactions between the solution, solid, exchanger and gas phase in soil are illustrated in Figure 1.3. The composition of the soil solution results from numerous, interdependent, multi-phase chemical interactions (Tanji, 1990). Irrigation, rainfall or evapotranspiration are the main factors that cause changes in soil-water contents and therefore alter the soil equilibrium. Such changes occur due to mineral precipitation or dissolution, association or dissociation of ion pairs, adsorption of cations, and emission or adsorption of gases (Paul et al., 1966). A detailed explanation of salt-affected soil chemistry can be found in Tanji (1990).

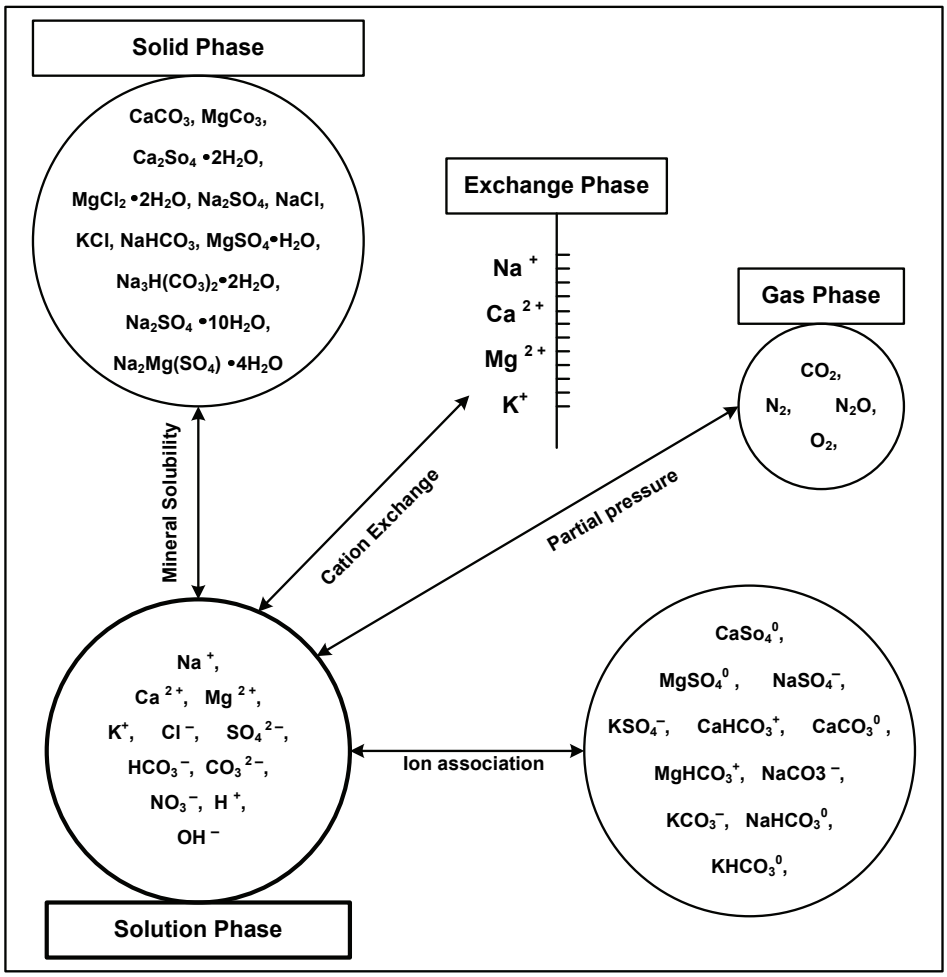

Figure 1.3: Chemical reaction in soil solution (Tanji, 1990).

1.1.5 Effect of salts on soil

The detrimental effect of adsorbed sodium on the physical properties of soils results in low water infiltration rate, low permeability to water and gases, increase of osmotic pressure of the soil, and poor soil structure. The increase of salts in soil also results in chemical dispersion, which increases susceptibility of soil to sealing and crust formation (FAO, 1988). Increasing exchangeable sodium promotes structural changes resulting in unstable and compacted soil (Mainguet, 1991). This is due to dispersion of soil particles and swelling of soil clay contents. Mainly in sodic soils, the content of organic matter tends to drop or does not decompose satisfactorily. Changes in soil properties (higher EC or ESP) as a result of salts accumulations in soil reduce soil productivity. The damaging effects of salt on plants are also caused by osmotic forces, as well as by toxic levels of sodium and chloride. This effect is mainly indirect by pulling moisture out of roots and reducing the uptake of water and nutrients (FAO, 2006).

1.1.6 Definition; Spectroscopy, Imaging spectrometry

Spectroscopy is derived from spectro-photometry, the measure of photons as a function of wavelength that has been emitted, reflected, or scattered from a solid, liquid, or gas (Clark, 1999). It is often used for the identification of substances through the spectrum emitted from them or absorbed in them. Historically, it referred to application of visible light for studies on the structure of matter. Recently, however, the definition has broadened, including many other forms of electromagnetic and non-electromagnetic radiation.

Imaging spectroscopy, also named imaging spectrometry or hyperspectral, is the simultaneous acquisition of spatially co-registered images in many, narrow, contiguous bands to provide information on the major features of the spectral reflectance of a given object (Vane and Goetz, 1993). A hyperspectral image, also referred to as an image cube, is a 3-dimensional data set with two spatial and one spectral dimension. In general, the spectral range includes the visible (0.4 - 0.7 μm), near-infrared (0.7 - 1 μm) and short wave infrared (1 - 2.5 μm). However, there are other wavelength ranges that are in use such as ultraviolet (UV, 0.001 to 0.4 μm), the mid-infrared (3.0 to 30 μm) and the far infrared (30 μm to 1 mm) (Lide, 1993).

Hyperspectral remote sensing is mostly performed using hand-held or air-borne sensors. A hand-held spectrometer is used for recording a spectrum in laboratory and field. Common hand-held spectrometers are the field-spectrometers from Geophysical and Environmental Research Corporation (GER), Analytical Spectral device (ASD) and Integrated Spectronics (PIMA). ASD FieldSpec, used in this study, is a field portable instrument with a spectral

range of 350 - 2500 nm and a spectral resolution of 3 and 10 nm for the regions 350 - 1000 nm and 1000 - 2500 nm respectively. Hyperspectral imageries are mostly obtained by aircrafts. Air-borne platforms are operated by a number of companies including HyVista (The HyMap system), SpecTIR (The ProSpecTIR and HyperSpecTIR systems) and the Galileo Group (The AISA Eagle and Hawk systems). The HyMap provides contiguous spectral coverage (except in the atmospheric water vapour bands) across the wavelength region of 450-2500 nm. The sensor has bandwidths between 15 – 20 nm and a signal to noise ratio of >500:1 (HyVista, 2004). A few hyperspectral satellite systems are operational, of which Hyperion is the most well-known. Hyperion sensor is one of the three primary instruments on the EO-1 spacecraft. The instrument can image a 7.5 by 100 km area per image, and provide detailed spectral information with high radiometric accuracy (USGS, 2007). It is capable of resolving 220 spectral bands (from 400 to 2500nm) with a 30 metre spatial resolution.

1.1.7 Spectral features of salt minerals

The reflectance properties of salt minerals are affected by a number of factors including the impurities, elemental composition, and crystalline structure (Hunt and Salisbury, 1970). The spectral features associated with salt minerals (Tables 1.2 and 1.3) are distinguishable on the basis of their appearance, and general location in the spectrum. The V-NIR-SWIR absorption bands in the spectra of saline minerals are mainly associated with internal vibration modes due to the excitation of overtones and combination tones of the fundamental modes of anion groups such as HOH, -OH, CO_3^{-2}, and SO_4^{2-} or of molecules such as water or carbon dioxide, which are trapped, adsorbed or associated with the crystal structure (Hunt and Salisbury, 1971). The fundamental vibration of anions occurs generally in the mid infrared region 4000 - 600 cm^{-1} (2700 - 17000 nm) and far infrared region 600 – 40 cm^{-1} (17000 – 25000 nm).

The bands associated with OH stretching vibrations of water and hydroxyl groups occur between 3200 and 3700 cm^{-1}. Considering the hydroxyl (-OH) group, there is only one fundamental stretching mode, which produces a strong sharp band in the region 3700 - 3650 cm^{-1} (somewhere near 2750 nm) depending on what the OH is directly attached to, and where it is located in the mineral. While water of hydration usually exhibits strong sharp bands near 3600 cm^{-1} and one or more near 3400 cm^{-1} and a medium band (often multi-component) due to H-O-H bending motion in the region 1650 - 1600 cm^{-1} which is used to differentiate it from the hydroxyl group (Nyquist and Kagel, 1971; Herzberg, 1945). Free water has a strong broad absorption centred in the region 3400 - 3200 cm^{-1}.

Table 1.2: Characteristic frequencies and fundamental vibrations of inorganic anions (Nyquist and Kagel, 1971). The vibration frequencies noted for carbonate and sulphate ions are from Nakamoto (1963) and Bhagavantan and Venkatarayuda (1939).

Element	Formula	Ion	Characteristic absorption (cm^{-1}) *	Point group	Vibration (cm^{-1})
Carbon	CO_3^{2-}	Carbonate	1320 - 1530 stg (OD), 1040 - 1100 wk (OD), 800 - 890 wk-m, 670 - 745 (owk)	D_{3h}	v_1 (a_1') 1087, v_2 (a_2'') 874, v_3 (e) 1432, v_4 (e') 706
Sulfur	SO_4^{2-}	Sulfate	1040-1210 stg (OM or SMAX), (960-1030, often 1 or 2 wk sp bands), 570-680 m (OD or M)	T_d	v_1 (a_1) 983, v_2 (e) 450, v_3 (f_2) 1105, v_4 (f_2) 983
Halogen	Cl^- Br^-	Chloride Bromide			

* (O) = often; (owk) = often weak, but not always detected; wk = weak; m = medium; stg = strong; bd = broad; sp = sharp; (SD) = sometimes doublet; (OD) = often doublet; (M) = multiple; (SMAX) = with sub maximum.

Table 1.3: Wavelength positions of absorption bands in spectra of salt minerals used in this study.

Mineral	Formula	Absorption Band Position		
		V-NIR-SWIR (350 - 2.500 nm)[+]	Mid-infrared (3800 - 600 cm^{-1})[++]	Far-infrared (600 - 40 cm^{-1})[◊]
Bischofite	$MgCl_2*6H_2O$	758,985, 1190, 1451, 1556, 1824, 1952	3420, 3235, 1630, 612	470
Halite	NaCl	14, 401, 933		264, 164
Sylvite	KCl			
Epsomite	$MgSO_4*7H_2O$	793, 999, 1240, 1490, 1631, 1760,1946	3400, 3270, 1660, 1125, 1100, 986, 750, 630	430
Thenardite	Na_2SO_4			

[+] This study, [++] Moenke, 1962, [◊] Ferraro, 1971.

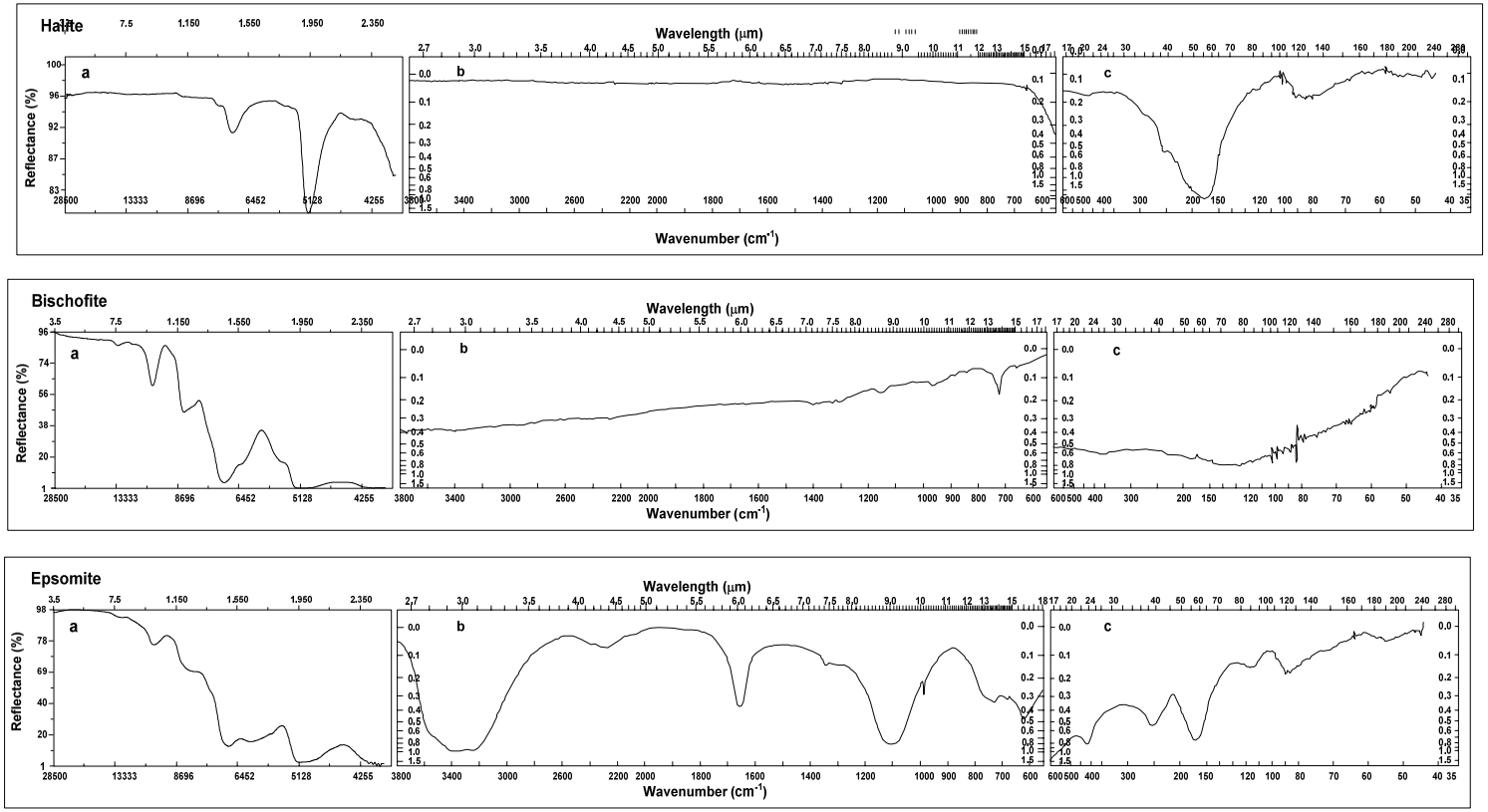

Figure 1.4: Spectra of a few examples of salt minerals in region between 400 to 24000 nm. a = V-NIR-SWIR (350 – 2500 nm) measured in this study, b = mid-infrared (3800 – 600 cm^{-1}) and c = far-infrared (600 – 35 cm^{-1}) taken from Nyquist and Kagel (1971).

Characteristic infrared frequencies, band intensities and the fundamental vibrations of inorganic anion groups are summarized in Table 1.2. The halide ion possesses no internal modes, and the metal-halide stretching fundamentals all occur in the far-infrared (Hunt et al., 1972; Ferraro, 1971). The halides are commonly used as window and matrix materials in the mid infrared region since the frequencies are low, and the overtones are weak. Lattice vibrations, which are unique for a specific crystalline compound and are useful fingerprints for identification of metal and alkali halides, can occur as high as 600 cm^{-1} but usually below 300 cm^{-1} (Nyquist and Kagel, 1971). The infrared spectral features seen in the sulphate spectra arise from the S-O bond oscillations of the sulphate anion. The sulphate ion (SO_4^{-2}) has four modes of vibration (Table 1.2) when it retains its full (T_d) symmetry (Ross, 1974). The frequencies of the CO_3^{-2} ion are difficult to define since it does not exist except in compounds or solution (White, 1974). The carbonate ion CO_3^{-2} has four modes of vibration (Table 1.2). The vibration frequencies v_1 (a_1') 1064, v_2 (a_2'') 897, v_3 (e′) 1415 and v_4 (e′) 680 reported by White (1974) do not correspond with the frequencies as cited by Nyquist and Kagel (1971).

The infrared spectra of evaporated salt minerals are dominated by internal and external vibrations of the above discussed anion groups and water molecules. A few examples of the spectra of salts minerals used in this study (NaCl, $MgCl_2$ *$6H_2O$, $MgSO_4$*$7H_2O$) are illustrated in Figure 1.4 and the location of the absorption bands are presented in Table 1.3. The Raman and infrared spectral characteristic of these minerals are extensively discussed by Farmer (1974), Ferraro (1971), Nyquist and Kagel (1971) and Moenke (1962). The bands observed in the NIR/SWIR spectra of these salt minerals are due to the first overtone of the OH stretch (e.g., near 1.4 mm), or combination bands of fundamental stretch with e.g., Mg –OH bending fundamental, or due to the OH stretch in combination with some lattice or vibration mode. The absorption bands in the halite spectrum (short of 2500 nm) resulted from the 8 or 9^{th} overtone of fundamental stretch, and the handing fundamentals occur at still lower frequencies (Hunt et al., 1972). Pure halite mineral displays some very weak water bands from water in fluid inclusions near 1950 and 2250 nm. Nearly all vibration features in the V-NIR-SWIR spectra of sulphate minerals are due to OH vibrations (Hunt et al., 1971).

1.2 Problem statements

The excessive concentration of soluble salts at the surface or near-surface of the soil horizon is due to existence of primary minerals in the exposed layer of the earth's crust. During the process of chemical weathering, they are gradually released and transported by surface or groundwater streams. Their accumulation at the surface or near the surface increases through either natural

process or human activities. Apart from the occurrence of salt crystals, several other features are formed at the soil surface. If the accumulation of salts continues the site further develops to the formation of salt-affected soils, to the extent of toxic levels and to the creation of wasteland (Figure 1.5). Apart from affecting the physical, chemical and biological properties of the soil, excessive concentration of salt leads to partial or complete loss of soil productivity. It is also a major concern at local and global scales, since it is a progressive phenomenon, particularly when the land is subjected to mismanagement, and thus rapidly non-saline soils become saline as a result.

Field investigation of salinity usually involves measurements and monitoring activities that are very costly and also limited with respect to the temporal and spatial variability meaning that frequent field studies on a fine grid would be required. Even though, salinization can be measured directly in the field, the measurements only provide information for the observed locations at a given time.

In past decades, the use of remote sensing is widely investigated for collecting information on soil properties such as salinity (see chapter 2). Considering the complexity of the salinization process and its influence on different soil properties (both physical and chemical), detecting salt-affected soils with remote sensing is not an easy task. The main limitations of remote sensing in salinity studies can be summarized as the following (Irons et al., 1989; Csillag et al., 1993):

- Variations in the reflectance spectra of soils cannot be attributed to a single soil property.
- Remote sensing data do not contain information on the third dimension of the soil body (the profile and other subsurface properties).
- Salinization is hidden at its inception and thus, can often go undetected by remote sensing sensors.
- Many of the salts' diagnostic spectral signatures occur in water regions at around 1400 and 1900 nm and hence, are obscured by the presence of water.
- In general, most absorption features indicative of salt minerals are in the far infrared, whereas spectral features in the visible, near and short wave infrared (400 - 2500 nm) are very weak and limited.
- Salt concentrations in soils need to be high to influence the soil reflectance.
- Moisture contents of soils and salts (depending on the types) have similar affects on soil reflectance spectra and causes large anomalies in predicting salinity levels from remotely sensed data.

These constraints have limited the operational use of remote sensing for mapping only severely saline soils and neglecting the marginal areas, which must actually be the future targets. The salt-affected soils, however, can be mapped more distinctively by use of remote sensing, when salinity-related features are more pronounced at the surface, if high percentage of bare-soil is available or when other indicators such as vegetation types and density are used. With regard to modelling and estimating soil salinity levels accuracy can be increased if the following questions are answered:

1. What are the spectral characteristics of salt-affected soils? How far does spectral information derived from the salt minerals contribute to identification of the minerals and discrimination of saline areas?

2. Do different salinity levels of soils result in different spectral signatures? Can spectral classes or clusters be generated on the basis of the quantified similarity or dissimilarity values?

3. What would be the influence of soil moisture on reflectance spectra of salt-affected soils and how does it influence modelling of salinity?

4. Is it possible to model and predict salt concentrations in soils at regional scale on the basis of their spectral reflectance?

Figure1.5: Severe salinity in Dasht-e-Kavir, Iran (Wasteland)

Considering the problems and related research questions, the main focus of this study is the development of modelling tools that use both spectral reflectance and electromagnetic measurements (geophysics). The developed models provide the possibility to progress from two non-unique salt identification techniques towards a unique and new integrated multi-disciplinary approach. The new methods aim at predicting the degree of soil salinity from remotely sensed imageries that have not been possible by the use of common image processing techniques. The principal concept of the developed methods is applicable, however, to any salt-affected area since they have been tested on various data sets (experiment-, field- and image-scale) from four different field areas.

1.3 Research objective

This study aims at developing predictive models for quantitative salt contents in soils on the basis of the integrated use of soil reflectance and geophysical surveys. The main question in this research is: Can a salinity warning system that employs modelling techniques be developed to detect areas in the early stage of salinity where the soils are potentially at risk? The specific research objectives were:

1. To develop a conceptual model for quantification and modelling of salt versions in soil using soil reflectance.

2. To study the information content of soil spectra with respect to salt concentration and salt types under laboratory conditions.

3. To investigate whether quantitative spectral indicators of saline and non-saline soils can be related to internationally used salinity classes as defined by US salinity laboratory (Richards, 1954).

4. To study the impact of soil moisture contents on soil spectra and the consequences for estimating soil salinity.

5. To examine the suitability of statistical and mathematical techniques as empirical modelling tools to predict salt concentrations in soils based on reflectance spectra.

1.4 Outline of the thesis

The research presented in this dissertation is described in seven chapters. It is essentially a collection of five papers, chapters 2-6, which either have been published or will be published in international peer-reviewed journals.

Chapter 1 presents an overview which includes the research objective and problem and a short introduction to the test sites and the key concepts regarding the research topic.
A review of the current state of the most used methods and techniques for identification of salt-affected soils is presented in chapter two. It discusses, in details, the constraints and advantages of each method in order to outline a conceptual framework for the research. The results suggest the feasibility of detecting early stage of soil salinity via integrating surface and near-surface information into a modelling process in a GIS environment.

In order to understand the main problem in remote sensing of salt-affected soils, a carefully designed laboratory experiment was carried out and presented in chapter three. The focus of this experimental study was on the use of laboratory spectroscopy to examine the contribution of the spectral information derived from the salt minerals in identification of the minerals in soil samples. To ensure the quality of data, published literature concerning guidelines for laboratory methods were carefully followed. The results provide detailed information on salt-induced spectral features and their potential involvement in predicting soil salinity. The analysis of the relationship between salt concentrations in soil samples and their spectral responses revealed the complexity of salts identification and quantification of salinity levels. The context of this chapter provides a perspective for developing spectrometric techniques to recognize the presence and abundance of salts in soils.

Several spectral similarity measures techniques were introduced in chapter four in order to quantify dissimilarity between the spectra measured from soil sample of same type but of different salinity. Besides providing an insight and a better understanding of soil spectral response due to salt variations, it is illustrated that spectral similarity measures can be used as diagnostic indicators to differentiate among salt-affected soils spectra. It was shown that differences observed in absorption strength, absolute reflectance and spectral angle in the near and shortwave infrared regions of salt-affected soils are proportionally varied with the amount of salts in soils. The results of numerical classification method applied to spectral similarity values showed that the spectral variations are sufficient to provide bases for aggregation in classes that are in agreement with standard international salinity classes. The statistical test show that the differences between the reflectance spectra associated with the observed salinity classes are statistically significant. The results confirm that wavelengths regions in the near and shortwave infrared contain the most crucial information and can be used to as a guideline to select diagnostic wavebands. The results showed that the established spectral parameters in experiment data can not be fully employed considering up-scaling to image spectra and thus calls the attention for further investigations.

Findings of experimental study, discussed earlier, suggested that the soil salt and moisture content has substantially similar affect on soil reflectance spectra. This means prediction of both salt and moisture content from reflectance values, largely depend on the presence or absence of one of the two. In order to evaluate the affects, inverted Gaussian modelling techniques that have been successfully used to estimate soil moisture contents were applied to experiment data and field in situ measurement to estimate both salinity and moisture. Findings presented in chapter five shows that the accuracy of soil salinity largely depends on availability of free water (moisture content) in soil and vice versa. The results suggest further experimental study to define the magnitude of effects and provide a better understanding of the process.

In the last paper (chapter six), prediction of salt concentrations in soils on bases of variations in their spectral reflectance was tested by use of partial least squares regression (PLSR) and artificial neural network (ANN) analysis. The results suggest that the both algorithms have a vast potential on predicting soil salinity at different scales (experiment, field and image). It also showed that the combination of surface and subsurface measurements leads to an early detection of salinization. The developed method can be considered as a major advance in terms of management of agricultural practices and would be a great benefit to both farmers and states.

Finally, the main findings and conclusions of the research and some recommendations for application of the current results and for the further research are synthesised in chapter seven.

1.5 Test areas

The data sets used in this study were collected from four different areas (Table 1.4). The soil samples used in a laboratory experiment were collected from the island of Texel in the northwest of The Netherlands located between 52° 99' to 53°17' N and 4° 48' to 4° 72' E, and an area (Tedej) in northeast Hungary located between 47° 39' to 47° 89' N and 21° 0' to 21° 43' E (Figure 1.6).

The Texel island has a gently sloping and undulating landscape (mostly flat) with height varies between 15.30 m and –70 cm above sea level. The climate of the island is moderate and humid with no dry season. It has a mean annual of approximately 733 mm and average annual temperature varied between 2.6 and 17.8° C (Abdulghani, 1963). The landscape has mainly been formed in the Pleistocene period which mostly covered by sand (Vink 1949). In Texel island the sea water intrusion is the major factor responsible for increase of salts in groundwater and soils. The detailed soil information of the area is given in Kloosterhuis et al. (1986).

The study area (Tedej) in northeast Hungary is approximately 1500 hectares of intensively cultivated agricultural land situated in Hajdu-Bihar County (Figure 1.6b). It has characteristic of plain landscape with dominant Solonchaks and Solonetz soil types (Keränen et al., 2003). The climate of the area is moderately warm and dry. In this area groundwater rise due to poor drainage system are considered the major factors responsible for salt accumulation in soils.

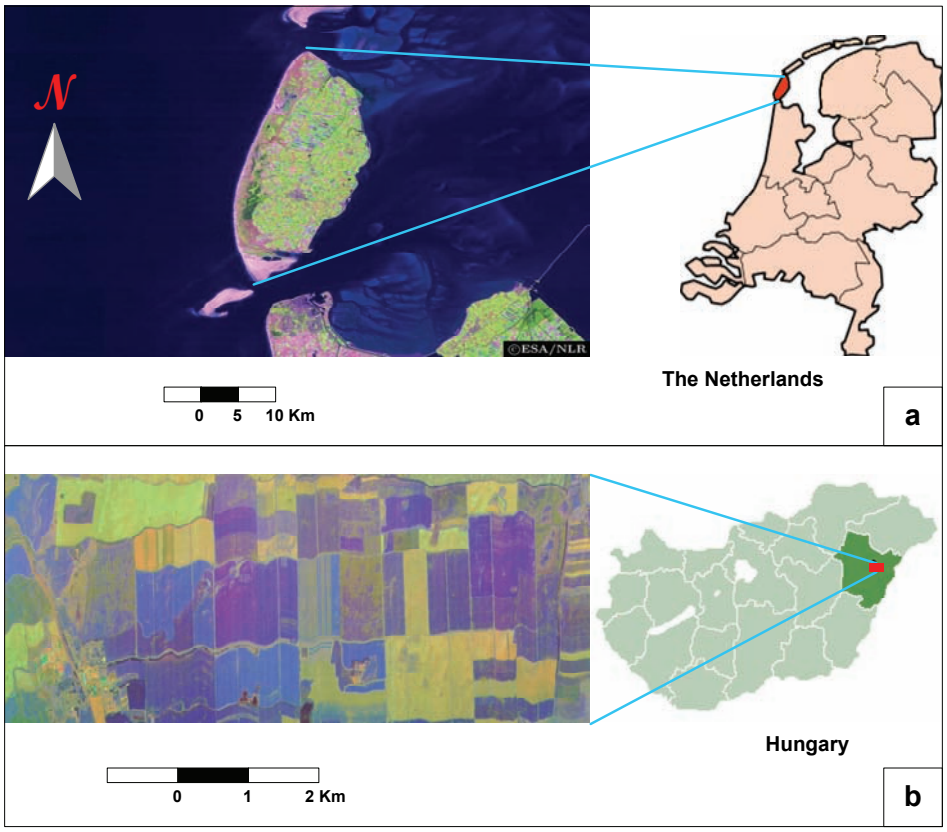

Figure 1.6: The study areas: a) Texel island in northwest of the Netherland and b) Tedej area in northeast Hungary. Soil samples used for laboratory experiment were collected from these two sites.

The test site in Northeast Thailand (Muangpia) covers an area of approximately 55 square km situated near Khon Kaen city between 16° 00′ to 16° 05′ N and 102° 38′ to 102° 43′ E. Figure 1.7a shows the research area and the location of grids along which a number of detailed observations and measurements were carried out during a fieldwork operation. The climate of the test area in Northeast Thailand belongs to tropical savanna type, characterized by hot wet

season between May to October and mild dry season from November to April (Yamamoto and Sukchan, 2003). The average annual rainfall of about 1200 mm and average annual temperature of 27.5° C recorded for Khon Kaen city is representative for the area. A minimum monthly average of 23.5° C and a maximum monthly average of 30.1° C occur in December and March respectively, indicating slight seasonal variation in temperature. Geomorphology of this area indicates an undulating topography with top hills at 180 m height and lowland area forming wide flat valley bottoms at height of approximately less than 160 metres. Although the difference in height is minor, with only 30 metres differences between highest and lowest points, the effects on salinity spatial distribution is large. In general, the lowlands in this area are highly affected by salinization. In general, the lowlands in this area are highly affected by salinization. According to the salinity map of LDD (1991) more than 50 % of the lowland area is considered to be salt-affected. The parts of lowland that have not been affected by salinity are mainly used as paddy fields. The upland areas, mainly, are not saline and used for sugarcane and cassava plantations. According to Mitsuchi et al. (1989), soils such as skeletal, sandy, saline and vertisol can be found mainly in this area. Skeletal soils contain gravel or rock fragments more than 35% by volume while the texture of saline and vertisol is varied between clayey to sandy.

Table 1.4: Description of the data used in this study.

Location	Country	Geographic Coordinates	Type of data sets	Soil texture
Texel Island	The Netherlands	52° 99' to 53° 17' N 4° 72' to 4° 48' E	Laboratory experiment	Sandy loam Sand
Tedej	Hungary	47° 39' to 47° 89' N 1° 0' to 21° 43' E		Silty clay loam
Muangpia	Thailand	16° 00′ to 16° 05′ N 102° 38′ to 102° 43′ E	Field measurements	Sand Sandy loam Loam Sandy clay loam
Toolibin Lake	Western Australia	32°54′ to 32° 55′ S 117° 36′ to 117° 37′ E	Hyperspectral imagery and field measurements	See Table 1.5

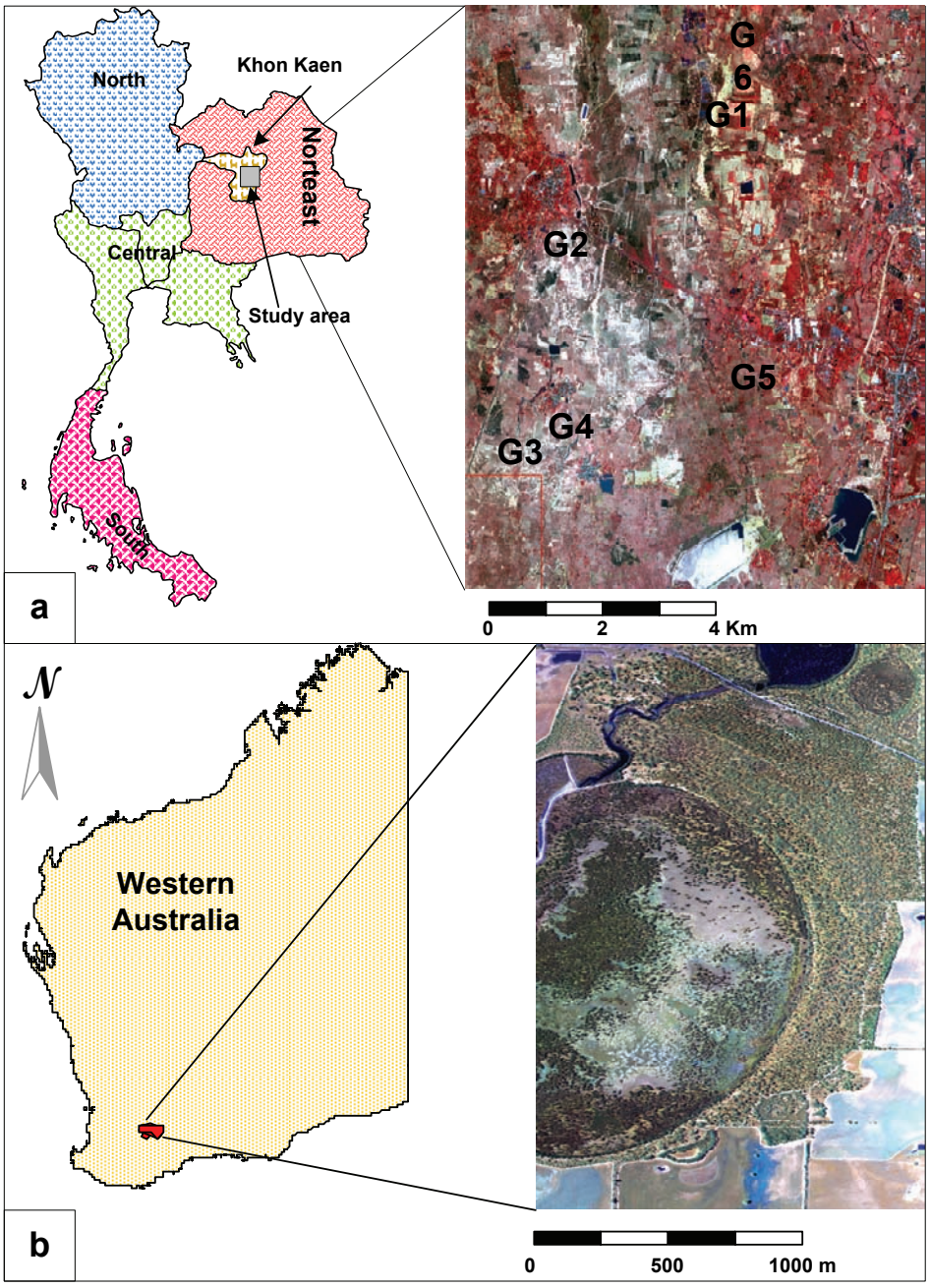

Figure 1.7: The study areas: a) Northeast Thailand and location of the grid areas (see Figure 6.1) along which field measurements took place, b) Toolibin Lake in Western Australia.

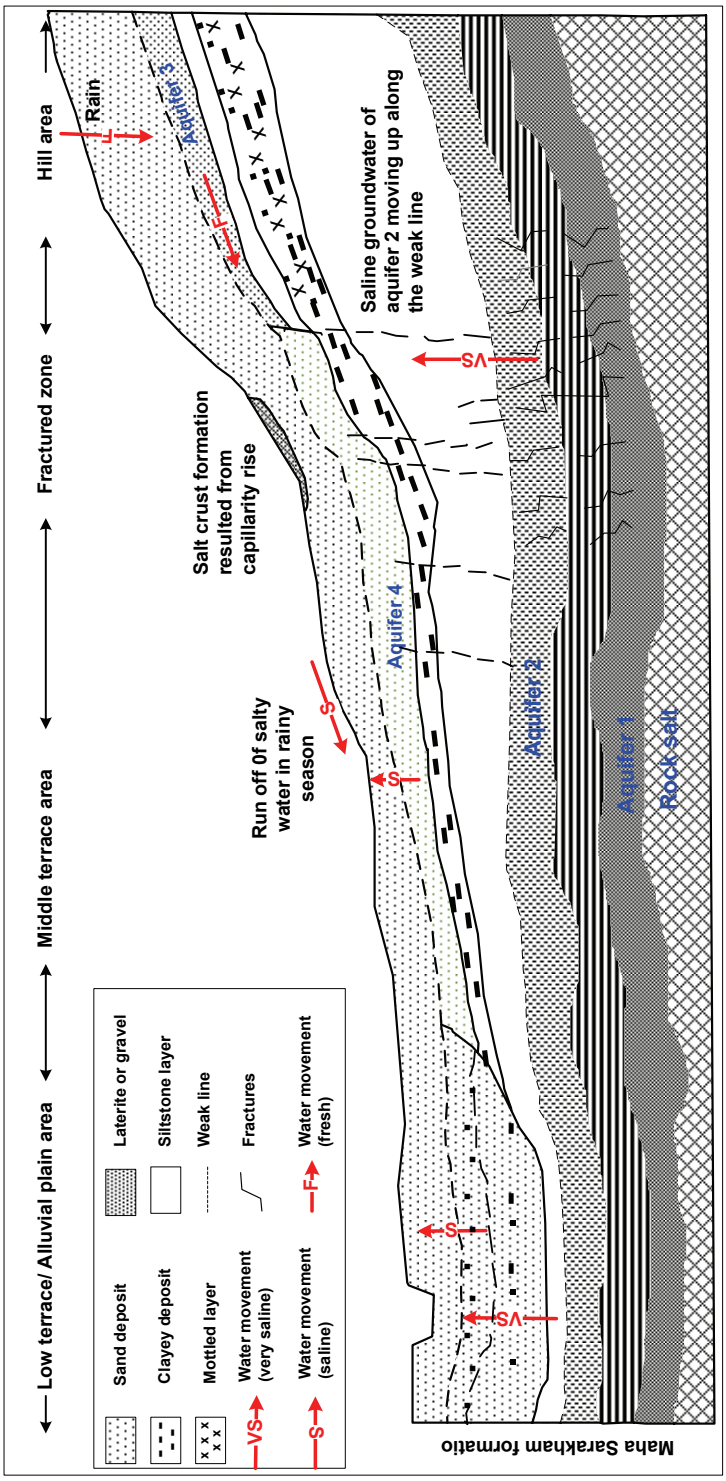

Figure 1.8: Schematic model of soil salinization in Thailand study area (adapted from Kohyama et al., 1993).

The test area in the Western Australia (Toolibin Lake) situated at approximately 200 km south-east of Perth close to the town of Narrogin between 32° 54′ to 32° 55′ S and 117° 36′ to 117° 37′ E (Figure 1.7b). The area lies at about 300 m above sea level and has been referred to as the most important wetland in terms of its ecological significance. Clearing of native vegetation, the lower water use of agricultural plant species and saline inflows have increased salts concentration in this area (Pracilio et al., 1998). A mean salinity of close to 50.000 mgL^{-1} and groundwater rises of around 0.05 ma^{-1} around Lake Toolibin has reported by George and Bennett (2000). The region has a Mediterranean climate with very dry summers and most of its rain falling in the winter growing season. The average annual rainfall ranges from about 379 mm at Toolibin up to 421 mm in the west and 417 mm in the east. Average pan evaporation for the area is about 1900mm. The soil type in the area is illustrated in Figure 1.9 and descriptions of soil units are given in Table 1.5. Detailed description of the area can be found in (Pracilio et al. 1998, Hearn, 1988).

The field data in this area were collected by department of agriculture and department of conservation and land management in Western Australia. The hyperspectral imagery of the area was provided by The Commonwealth Scientific and Industrial Research Organization (CSIRO) located in city of Perth.

Number of pictures from salt-affected areas, salt-induced surface futures and field work activities are given in Figures 1.10, 1.11, 1.12 and 1.13.

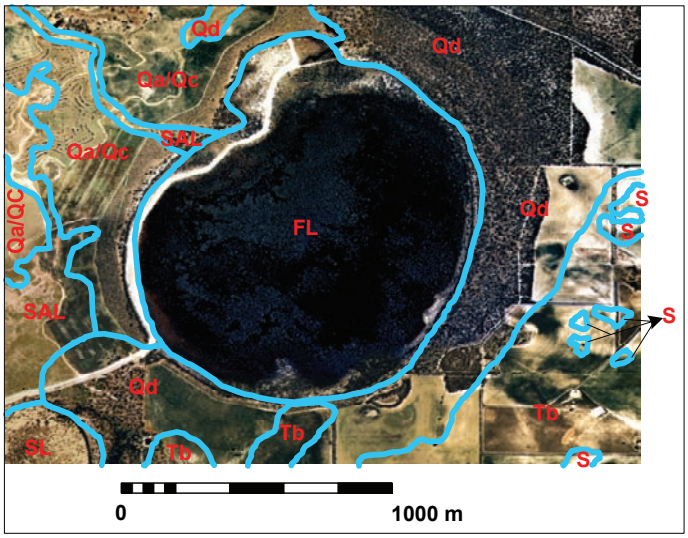

Figure 1.9: Soil Units in the field work area of Toolibin Lake (data from department of Agriculture and department of conservation and land management in Western Australia). The legend of the soil units is provided in table 1.5.

Table 1.5: Description of soil units in area of Toolibin Lake, legend of soil map Figure 1.9

Soil Unit	Description
FL	Lake deposit
Tb	Lateritised landscape: Pale sandy surfaced gravely duplex soils 50% Pale sands over sandy gravel over reticulite and clay 30% Shallow sandy gravel over duricrust and gravel over clay 10%
Qa	Dominated by old alluvium: Acid to neutral grey deep sandy duplexes 35% Alkaline grey shallow loamy and sandy duplexes 40% Grey clays 10%, Low recharge Recent alluvium 10%
Qc	Lateritic colluviums and residual soil: Pale sandy surfaced gravely duplex soils 30% Pale sands over sandy gravel over reticulite and clay 30% Yellow gravely sand plain over reticulite over clay 10% Gradational soil derived from Granite 10% Duplex soils derived from Granite 10%
Qd	Alluvial soils: Alkaline grey shallow loamy and sandy duplexes 40% Acid to neutral grey deep sandy duplexes 10% Grey sodic clays 20%, Low recharge Aeolian soils: Brown and grey deep sands 20% Calcareous loamy earths 10%
SL	Salt Lake
SAL	Saline soil
S	Pale deep acid sands

Figure 1.10: Pictures of salt-affected areas in study site located in d north of the Netherlands.

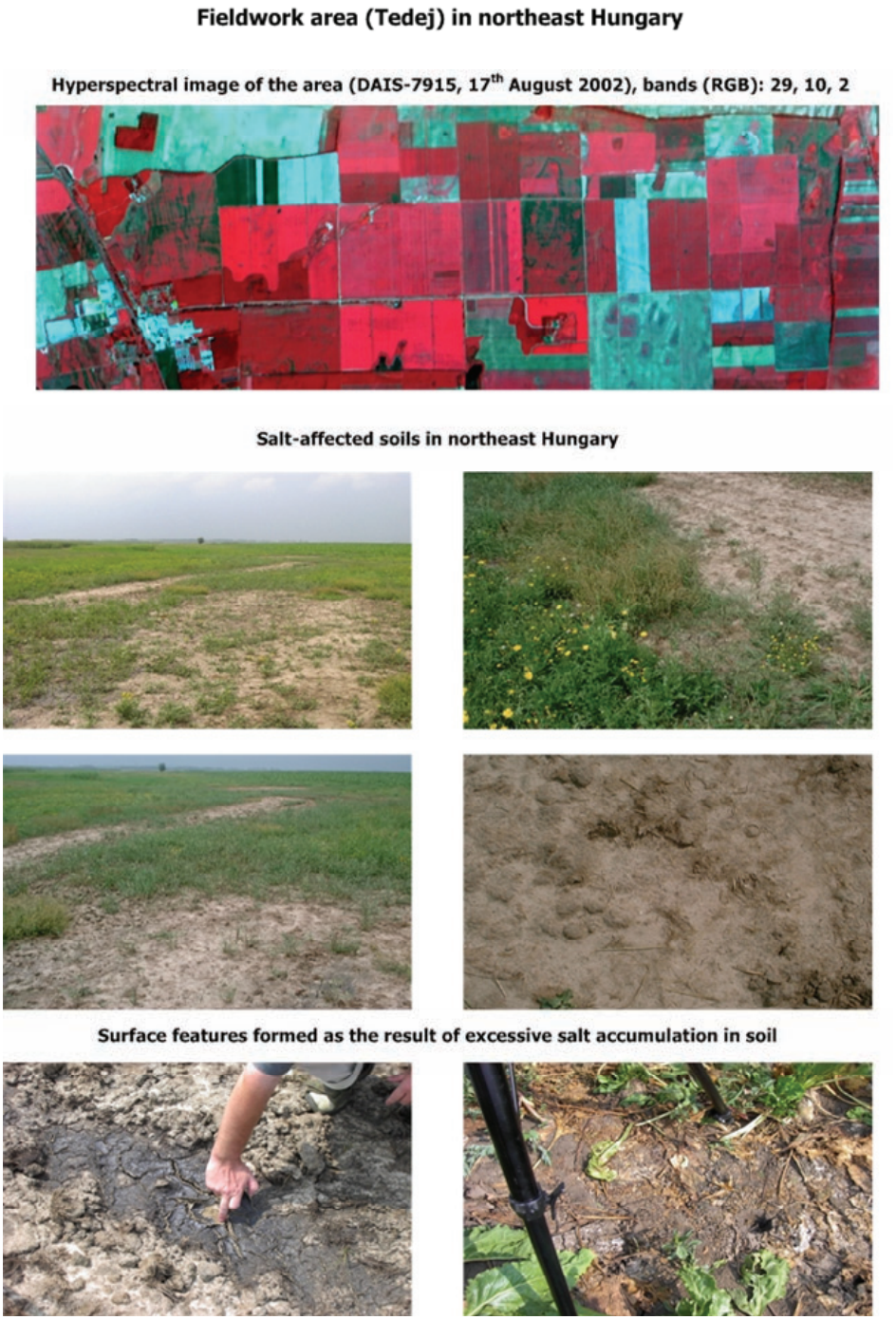

Figure 1.11: Pictures of salt-affected areas in study site located in northeast Hungary.

Figure 1.12: Pictures of salt-affected areas and fieldwork activities in northeast Thailand.

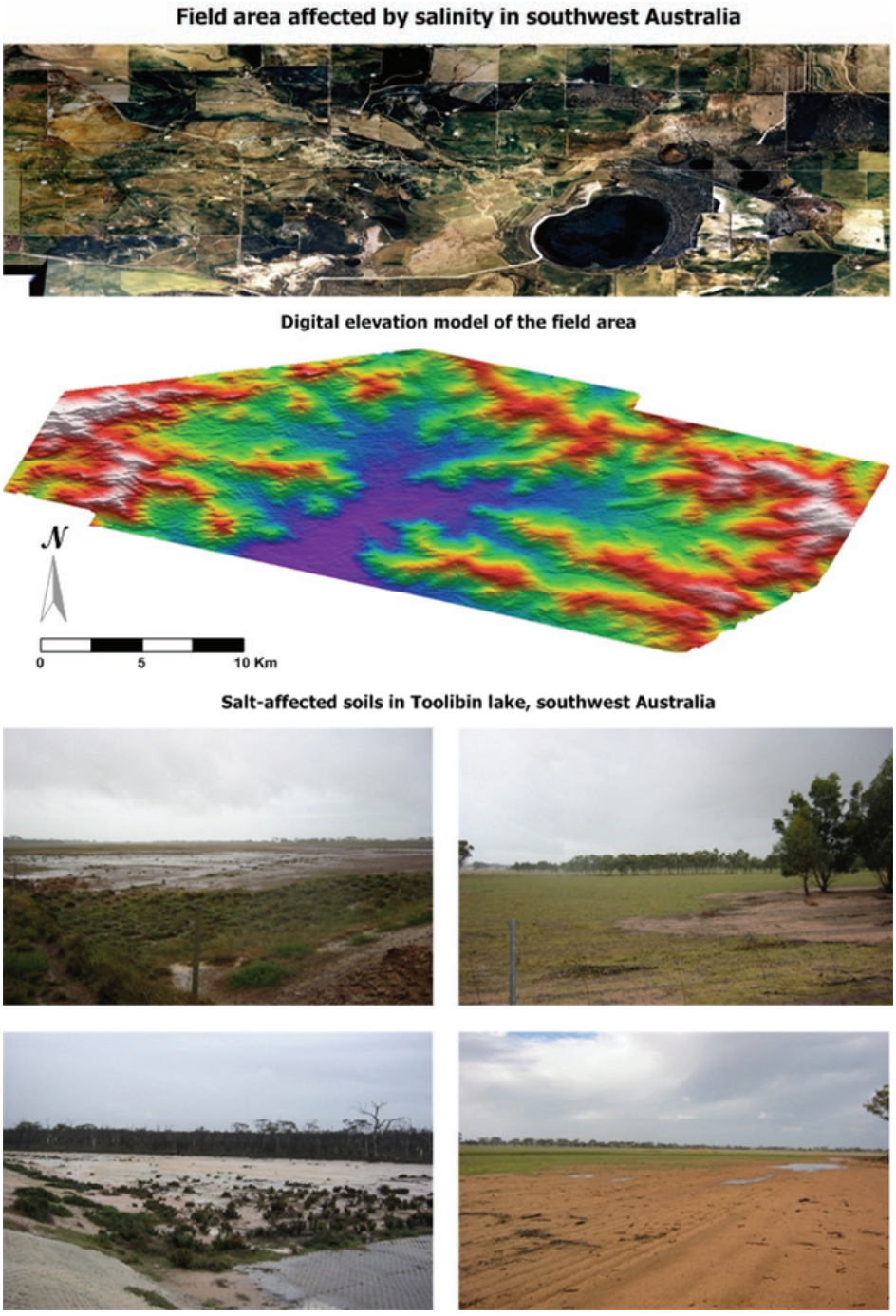

Figure 1.13: Pictures of salt-affected areas in southwest Australia.

Chapter 2

Assessing salt-affected soils using remote sensing, solute modelling, and geophysics*

Abstract

Salinization and alkalinization are the most common land degradation processes, particularly occurring in arid and semi-arid regions, where precipitation is too low to maintain a regular percolation of rainwater through the soil. Under such a climatic condition, soluble salts are accumulated in the soil, influencing soil properties and environment to cause lessening of the soil productivity. The consistent identification of the processes is essential for sustainable soil management.

Identification, large scale mapping and monitoring of salt-affected areas have been done, generally, using three different techniques. Optical remote sensing is a widely used technique to detect and map salt-affected areas, since thousands of medium to high-resolution imageries from the earth surface are available. In practice, remote sensing applications have focused mostly on severely saline areas and have given less attention to the detection and monitoring of slightly or moderately affected areas. The major constrain is related to the nature of the

---

* This Chapter is based on:
Farifteh, J., Farshad, A., & George R.J. (2006). Assessing salt-affected soils using remote sensing, solute modelling, and geophysics. *Geoderma*, Volume 130, 3-4, 191-206.

satellite images, which do not allow extracting information from the third dimension of the 3-D soil body, e.g., where salts concentrate in subsoil. Solute transport modelling is another technique used widely to predict the salt distribution in the subsoil. It has the advantage of providing subsoil information on dynamics of the salt movement regimes. This technique provides complementary data on salt movement in the soil profile which can be used in combination with remote sensing data. Since a few years, near-surface geophysics sensors, particularly airborne, have been widely used to map and monitor salt-affected areas. This technology has the advantage of effectiveness for cropped land and can efficiently be used to highlight conductive areas where no surface expression of salt is evident.

The paper outlines the conceptual framework of a method where the data obtained from optical remote sensing sensors are integrated with results of simulation models and geophysical survey in order to predict different levels (low, moderate, severe) of salinization/alkalinization in a cost-attractive and efficient way. In the proposed integrated method, data are combined not only to demarcate existing salt-affected soils, but also to monitor salinization as a pedogenic process. Such an approach focuses on the integration of the data with different natures and scales, meaning that data fusion and up-scaling are strongly involved.

2.1. Introduction

In the literature, a compound process (a series of processes, together) termed as salinization/alkalinization, is referred to as the most frequently occurring land degradation type in (semi-) arid regions. These processes are the product of a complex interaction of various factors, which cause changes within a time period of about a decade, generally irreversible, leading to a lower production potential of the soil (Szabolcs, 1974; Fauck, 1977).
Salinity problems have a large impact especially in semi-arid regions since these areas with harsh climatic conditions are under high pressure to supply the required food and fibre for their rapidly increasing population. This pressure results from changes in land use, which is mainly due to the common policy of agricultural intensification. Usage in this manner accelerates land degradation processes, among others salinization/alkalinization, and eventually reduction in yield. Therefore, timely detection of salinization/alkalinization, assessment of its degree of severity and the extent, particularly in its inception is vital. In this respect, three different non-unique techniques (remote sensing, solute modelling and geophysics) can be used to identify, detect and predict the areas affected by salts.

Remote sensing data and techniques have been widely used to map salt-affected areas (Hunt and Salisbury, 1976; Hick *et al.*, 1984; Goetz et al., 1985; Goetz and Herring, 1989; Hick and Russell, 1990; Crowley, 1991a; Mougenot *et al.*, 1993; Verma *et al.*, 1994; Ben-Dor et al., 2002, Dehaan and Taylor, 2003). The potentiality of remote sensing in the study of salt-affected soils and in particular slightly to moderately affected areas is usually restricted (Metternicht and Zinck, 2003; McGowen and Mallyon, 1996; Jain et al., 1988; Manchanda and lyer, 1983). The sensors scan only the soil surface, while the entire soil profile is involved and should be considered. This limitation highlights the necessity of using other data and techniques, in combination with remote sensing. Modelling of salt movement and advanced geophysical survey, which have recently been used successfully to detect and predict salt-affected areas, considered in many literature as promising tools (Doerge *et al.*, 2002; George and Bennett, 2000; Lund *et al.*, 2001; McNeill, 1980a; Street *et al.*, 2002). Modelling of solute transport (vertically and laterally) in soil provides vital information on understanding the dynamic of salt movement regime and assessing the impact of salt accumulation under various conditions (Jury, 1982; Schoups and Hopmans, 2002). This technique can be used as an integrated approach to provide data on salt movement in the soil profile in space and time. Geophysics sensors, particularly airborne, are now widely used to map and monitor salt-affected areas, since they are capable of gathering rather cheaply subsurface information. This technology has the advantage of effectiveness for cropped land (Johnson *et al.*, 2001) and can efficiently be used to highlight conductive areas where no surface expression of salt is evident (Howlett *et al.*, 2001).

In brief, the need to focus more on detecting and monitoring of slightly to moderately salt-affected areas, where the soils are potentially at risk, is obvious. The intention of this paper is to present an overview of approaches and supporting techniques implemented to detect salinity. The overview outlines a conceptual framework of a method where the data obtained from optical remote sensing sensors and geophysical survey can be integrated with the results of a simulation model in order to predict different levels (low, moderate, severe) of salinization/alkalinization in a cost-attractive and efficient way.

2.2 Remote sensing and salt-affected soils

All ground-based, air-borne and space-borne sensors have been used to identify and monitor salt-affected soils. In environmental studies, air-borne or space-borne remotely sensed data are generally complemented with field measurements in order to determine relations between the spectral signature and the surface or object properties. Ground-based spectroradiometers such as GER3700 and FieldSpec FR (ASD) measure reflectance spectra in narrower,

continuous spectral bands. The spectra measured by these instruments are basically stored as spectral library and used as end members to classify air-borne or space-borne data (Shepherd and Walsh, 2002). A large number of research works have been conducted in the last two decades to identify diagnostic absorption bands in spectrum of evaporate minerals and salt crust either in the field or in the laboratory (e.g., Hunt et al., 1971 and 1972; Hunt and Salisbury, 1971; Gaffey, 1987; Crowley 1991a and 1991b; Drake, 1995; Howari et al., 2002). This information is basically used to establish a relationship between spectral properties of salt-affected soils and presence or abundance of salt minerals in soil (Farifteh et al., 2004).

Airborne sensors (e.g., AVIRIS; DAIS-7915) are generally designed to serve as a prototype for future space-borne sensor systems. Basically, airborne sensors provide high spectral and spatial resolution imageries. Many of them collect data in continuous spectral channels (bands) with wavelengths from 400 to 2500 nanometres and have a spectral bandwidth of approximately 10 nm (Clark, 1999; Clark et. al., 2003). Calibration of air-borne data is vital and can be achieved by removing effects of the atmosphere (scattering and absorption) and converting from radiance values received at the sensor to reflectance values of the land surface (Clark et al., 2002).The potentialities of hyperspectral imagery in salinity studies have been recently addressed (Taylor and Dehaan, 2000; Ben-Dor, 2002; Dehaan and Taylor, 2003). These studies show that soil organic matter, soil moisture and salt-affected areas with different degrees of severity can be successfully mapped by combining air-borne hyperspectral data with field measurements.

Space-borne sensors have provided global coverage of the earth's surface conditions at different spatial and temporal resolutions. In general, they are sensitive to reflected solar energy (400 to 2500 nm), to emitted thermal energy (8000 to 14000 nm) or radiation at longer wavelengths known as microwaves. Basically, the radiation reflected from soil surface can vary depending on the soil constitutes, soil surface conditions and wavelengths (Csillag et al., 1993). Soil elements have characteristic features mostly occurring in narrow wavelength regions. In general, such detailed spectral signatures are masked when the bandwidths are wide and/or the spectral bands are limited (Cloutis, 1996; Kumar et. al., 2001). This is the case with broad-bands sensors such as Landsat TM, SPOT and ASTER that average the reflectance over a wide range. Most of the studies using conventional remote sensing data are focused on mapping severely saline areas or successfully differentiating between saline and non-saline soils (e.g., Hick et al., 1984; Mougenot et al., 1993; Dwivedi, et al., 1999). That is partially due to higher spectral reflectance of severely saline soil as compared to non-saline soils (De Jong, 1994; Rao et al., 1995). However, restriction due to spectral resolution of broadband sensors, which affects the quality and quantity of the information have been improved. Hyperion is the

first operational hyperspectral imager to orbit the earth and provides 242 spectral bands over the 400 to 2500 nm range with 30 m ground resolution (NASA, 2001). The spatial resolution of satellite data can also play a restrictive role in detection of salt-affected areas where size of the affected area is smaller than the pixel size. The advantage of space-borne data is their high temporal resolution since salt concentration in soil changes, at least seasonally.

2.2.1 Factors affecting salt-affected soils reflectance

The major soil components are inorganic solids consisting primarily of crystalline minerals and non-crystalline substances, organic matter, air, and water or a solution containing a variety of dissolved compounds (Irons et al., 1989; Jackson et al., 1986). There is a high correlation between soil reflectance and several soil properties such as mineralogy, organic matter content, moisture content, particle size distribution, iron oxide content, and surface conditions (Baumgardner et al., 1985; Bowers and Hanks, 1965; De Jong, 1992; Demattê, et al., 2004; Epema, 1993; Hunt, 1980; Irons et al., 1989; Stoner and Baumgardner, 1981). Ground observations and radiometric measurements indicate that the main factors affecting the reflectance are quantity and mineralogy of salts, moisture content, colour, and surface roughness (Mougenot et al., 1993). Examples of salt-affected soil spectra and the effect of salts on soil reflectance are illustrated in Figure 2.1. Most of the features seen in spectrum of saline minerals (400 – 2500 nm) can be attributed to internal vibration modes of certain molecular groups, particularly carbonate, borate, hydroxyl anion groups and neutral water molecules (Hunt, 1980; Crowley, 1991a). The reflectance of these salts can be quantitatively measured by laboratory or field spectroradiometers.

Surface features common in salt-affected areas also cause variation in soil reflectance and can be used for identification when using remotely sensed data. These features can be divided in two main categories such as soil-related and performance-oriented indicators. Presence of white salt crusts on the surface, puffy soil surface, dark greasy surface of pure alkali soils, dehydration cracks of 1 – 2 cm wide and coarser topsoil texture (Driessen and Schoorl, 1973; Mabbut, 1977 and 1984; Thomas, 1997) are soil related indicators. Performance-oriented indicators used to distinguish saline/alkaline soils are spotty growth of crops, presence of dead trees, a blue-green tinge, and moisture stress condition (Matternicht and Zinck, 2003).

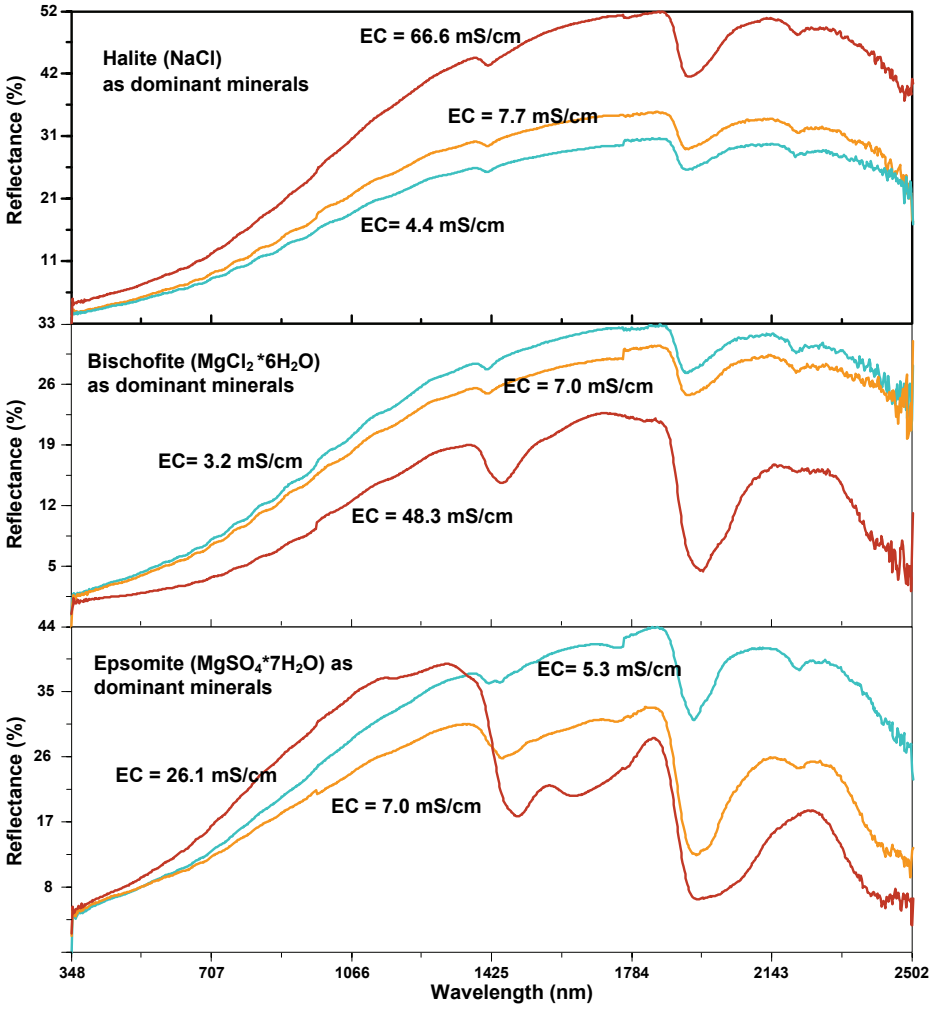

Figure 2.1: Examples of salt-affected soils' spectra, obtained in laboratory, from soil materials impregnated by different evaporate minerals.

2.2.2 Constraints and advantages of remote sensing in salinity

Remote sensing has repeatedly been used as a promising tool to obtain information regarding soil properties and land degradation processes (De Jong, 1994; Dehaan and Taylor, 2002; Van der Meer et al., 1999). Thousands of medium to high-resolution imageries from the earth surface are available, which can be used to detect and monitor salinization/alkalinization spatially

and temporally (Escadafal, 1994). To make use of satellite remote sensing an appropriate scene model is needed to convert multi-spectral reflectance into thematic information (Hill et al., 1996). Potential contribution from remote sensing to salinization/alkalinization study can be analyzed applying the approach suggested by Verstraete et al. (1994) and used by Pinty et al. (1996). Dealing with remote sensing data, three types of variable are distinguished, namely the measurable, the retrievable, and the hidden ones. The potential contribution of remote sensing techniques depends on whether or not the number of hidden variables is larger or smaller than the other two sets of variables. As an extreme case, if the behaviour of the system under study is entirely explained by the hidden variables, then there is little hope that remote sensing data can provide useful information for this particular application.

In studies where basically visual interpretation techniques are applied to map salt-affected areas on the hardcopy of the satellite images (Verma et al., 1994), an integrated approach of image interpretation (TM bands 2, 3, 4 and 6) coupled with field study are used (Dwivedi and Sreenivas, 1998; Rao et al., 1998; Sharma and Bhargava, 1988; Evans and Caccetta 2000).

In some attempts where digital analysis techniques are applied to detect salinity from broadband remote sensing data (Figure 2.2), use is made of the relationship between soil reflectance and the salinization-related soil characteristics (Szilagyi and Baumgardner 1991). Metternicht and Zinck (1996) applied a synergistic approach to map salt-affected soils and found that a combination of six Landsat TM bands (1, 2, 4, 5, 6, 7) provide the highest separatability among salt- and sodium-affected soil classes. The incorporation of the TM thermal band 6 improves the separatability of alkaline areas neighbouring saline-alkaline, saline and non-affected areas. Everitt et al. (1988) found that colour-infrared composite and red narrowband video images were superior to green and near-infrared narrowband images for distinguishing areas of soil salinity. They used some criteria (indicators), such as less plant cover and crusted surfaces of saline soils, to differentiate between saline and non-saline soil. In practice, use is also made of indirect indicators such as crops growth performance, leaf angle orientation (leaf roll), and increased chlorosis, which is best observed in the near- and middle-infrared bands (Bastiaanssenet al., 2000; Steven et al., 1992).

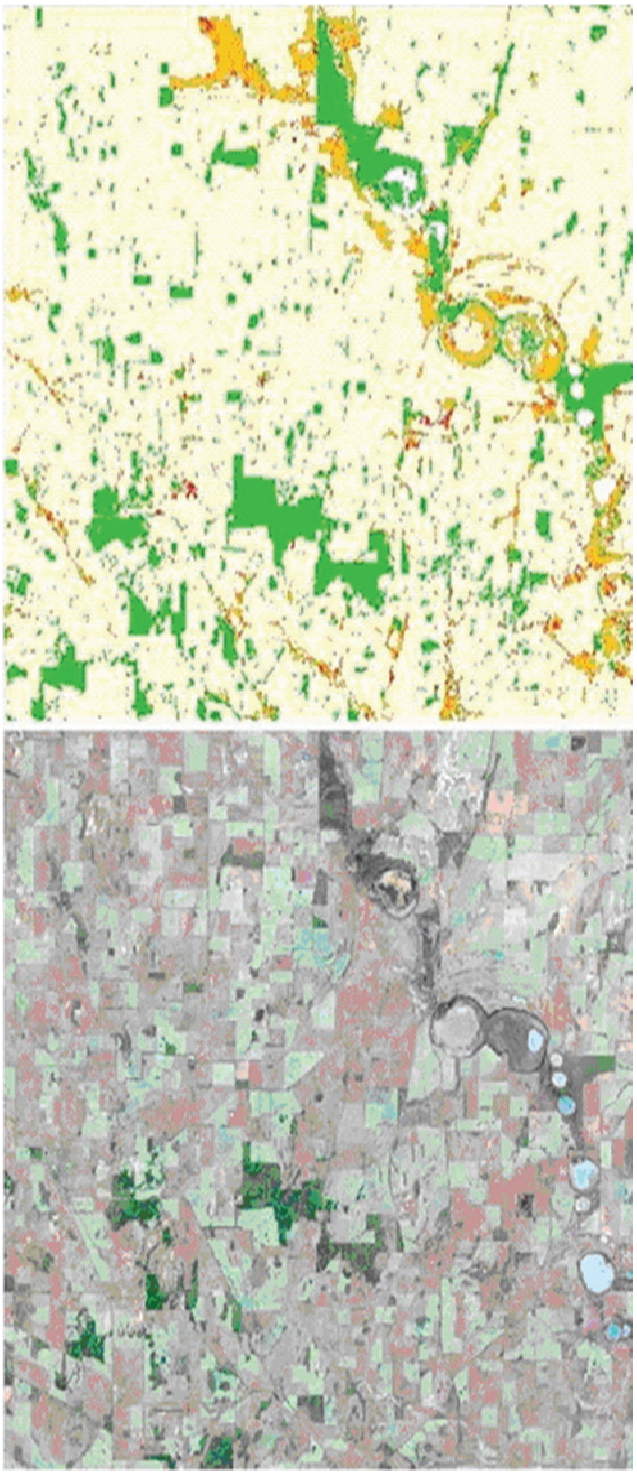

Figure 2.2: Image classification of salt-affected soil using Landsat TM images (CSIRO, Western Australia).

In works where absorption feature analysis using laboratory spectroscopy are used, Hunt and Salisbury (1976) found that gypsiferrous soils can be differentiated from non-gypsiferrous group because of the presence of a broad water absorption region from 1330 to 1650 nm. Calcareous soils are more complicated as they have several absorption bands at 2250, 2350, 2380 and 2465 nm due to the internal vibration of the carbonate ion in $CaCO_3$. Stoner (1979) found that soil generally high in soluble salts had the highest average reflectance over the spectral range from 520 to 900 nm. Soils with electrical conductivity of more than 4 dS/m gave lower reflectance values through the spectral range from 500 to 2380 nm. The reflectance increases when the electrical conductivity is reduced (Baumgardner *et al.*, 1985). Figure 2.3 shows some spectra of chloride, chloride hydrate and sulphate hydrate minerals measured in the visible to middle-infrared range (400 to 2500 nm) by means of laboratory spectrometer. The analysis of absorption bands was also applied to hyperspectral imagery (Clark et al., 2003) to detect and map salinity (Taylor and Dehaan, 2000; Ben-Dor et al., 2002, Dehaan and Taylor, 2003).

Most of the studies discussed above attempt to unravel the contribution of individual soil properties to reflectance. In the context of salinity/alkalinity, broadband remote sensing observations have often concentrated on severely saline soils neglecting the slightly affected areas, which must actually be the target when dealing with soil degradation. This concentration is basically related to the complex nature of the salinization/alkalinization process and its influence on different soil properties, both physical and chemical (Csillag et al., 1993). Another limiting factor stems from the nature of the conventional satellite images, which by definition does not allow extracting information from the third dimension of the 3-D soil body e.g., where salts concentrate in subsoil (Figure 2.4). Other constraints related to remote sensing are the combined reflectance or mixed pixel and limited number of salinity indicators (variables) directly measurable by remote sensors. However, dealing with slightly and moderately salt-affected soils using remotely sensed data, the observed reflected spectra may be successfully simulated if the mentioned sensors-related problems and the scene model are worked out in an appropriate research approach. For example, in the study conducted by Peng (1998), TM imageries were used in combination with non-remote-sensing data to map salinity classes ranging between non-saline to severely saline.

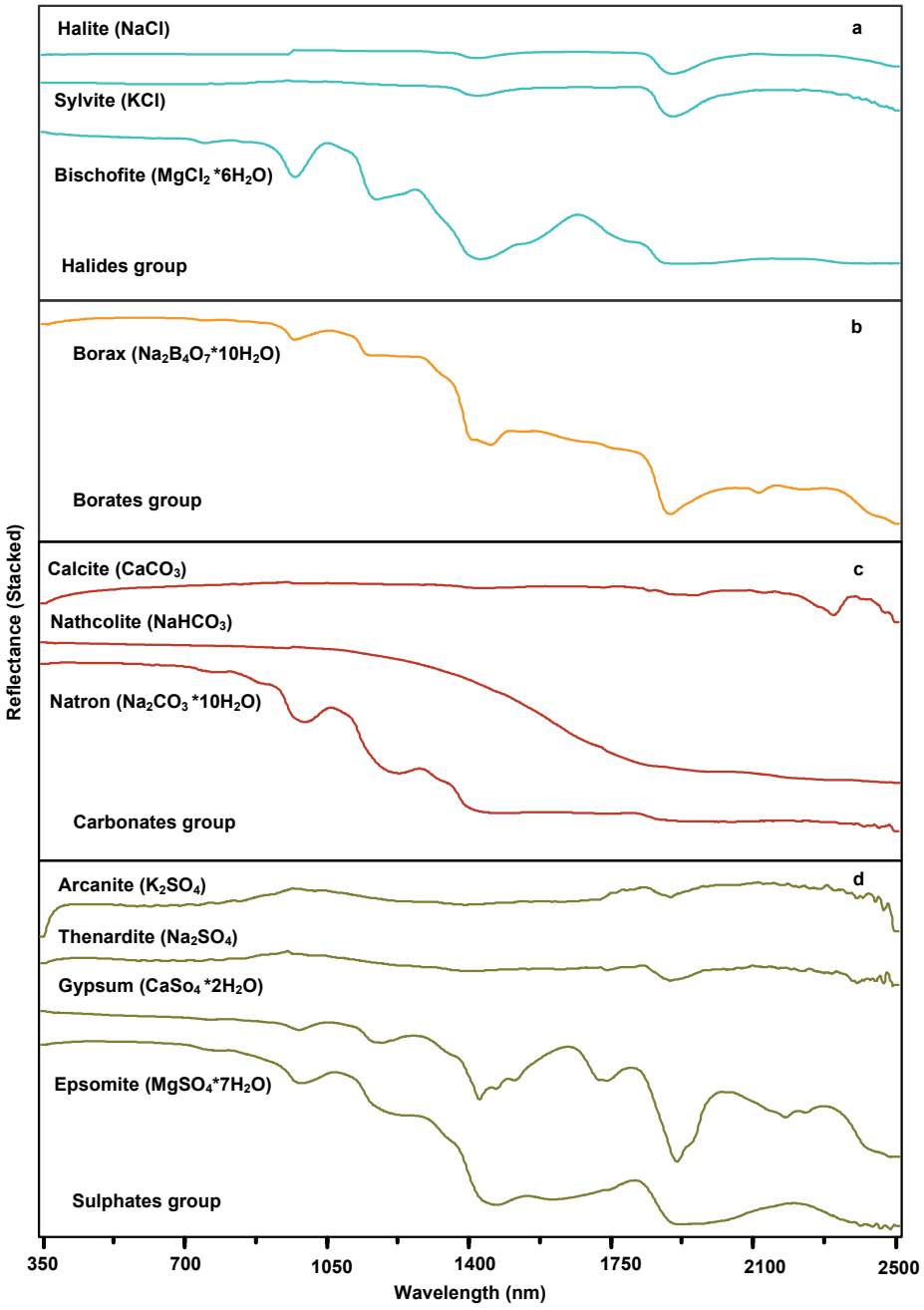

Figure 2.3: Laboratory-derived spectra of salts minerals, (a) halide group, (b) Borax, (c) carbonate group and (d) Sulphate group.

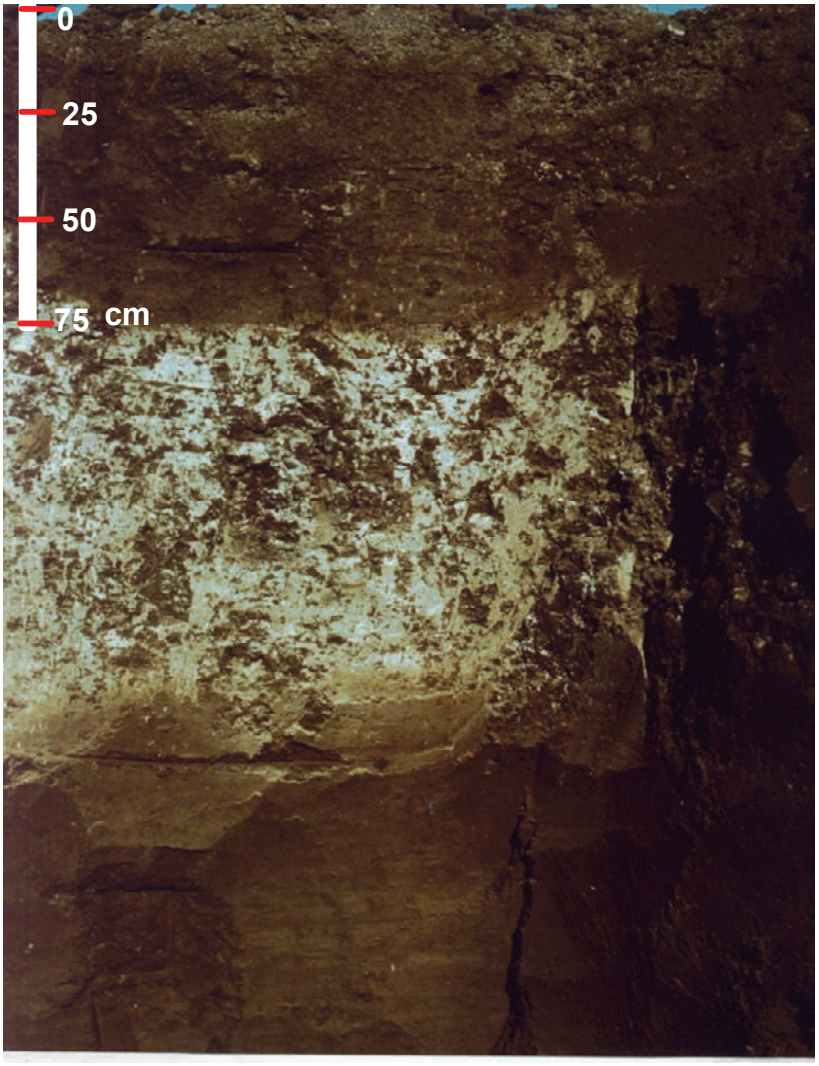

Figure 2.4: Subsurface concentration of salt (Salic horizon in Hamadan province, Iran), where salts do not appear at surface and hence go undetected by remote sensing sensors. The salic horizon is a surface or shallow subsurface horizon which contains a secondary enrichment of readily soluble salts.

2.3 Groundwater modelling and salinization

In arid and semi-arid areas, many soils and often groundwater are potentially saline. In other words, any disturbance of the delicate hydrological balance may lead to the mobilization of the inheritably available salt. The salt transport mechanism is often highly complex, the understanding of which necessitates the use of computer modelling, preferably in combination with field studies and geostatistics (Jolly, 1998; Pishkar 2003). Usually, salt-transport modelling aims at predicting the salt distribution in the subsurface as a result of water percolation, groundwater level changes and groundwater flow.

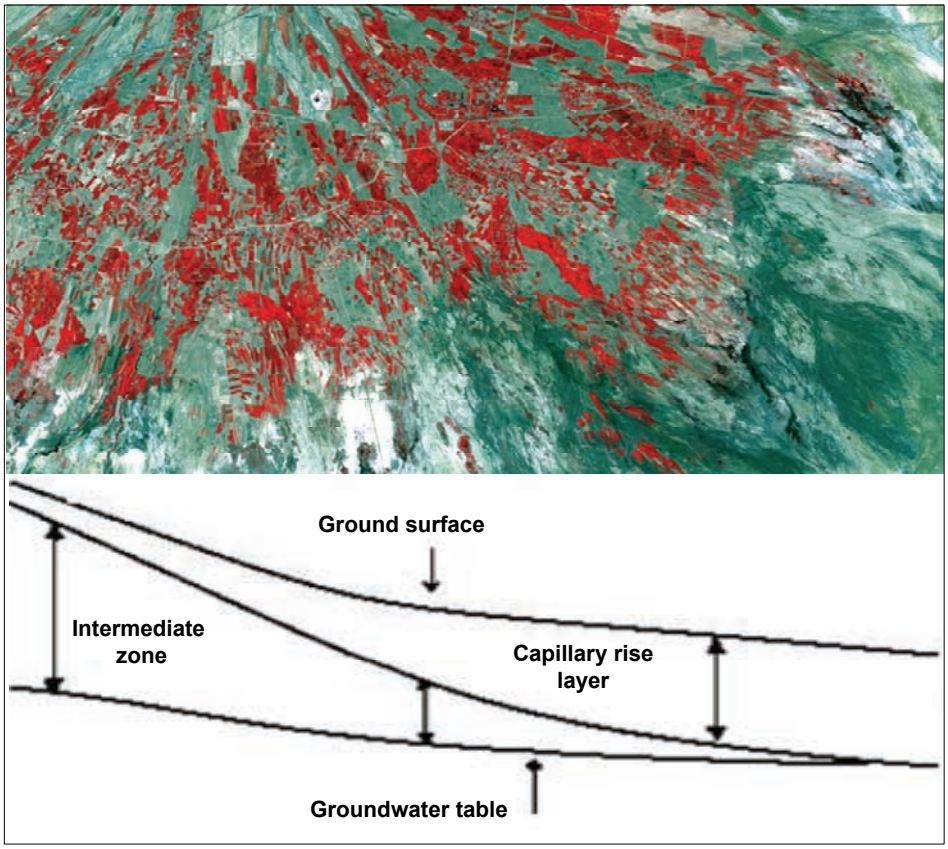

Figure 2.5: Landsat TM imagery (FCC) of a part of a piedmont (coalesced alluvial fans), with clear surface (distributary) drainage pattern.

Many options are available to model solute movement in the vadose zone (Spitz and Moreno, 1996; Trudgill, 1995). Mathematical models of one, two or three dimensional type, or of unsaturated-saturated flow, and/or of transport of a solute are used to simulate water flow and solute transport processes and to

determine or estimate the average concentration of the salt in soil profile (Van Dam *et al.*, 1997). For example, Jury (1982) used a transfer function model to predict average values of solute concentration as a function of depth and time, through highly variable field systems. In an integrated approach, a GIS system was coupled with a numerical model to study the solute transport (El-Kadi *et al.*, 1994). A stochastic-convective model was used successfully to predict solute and to estimate the leading edge of solute migration (Butters and Jury, 1989). A multiple linear regression model in conjunction with GIS was used to study the development of salinity considering four soil salinization factors: soil permeability, depth to the groundwater, groundwater quality, and leaching fraction (Corwin *et al.*, 1989). Geopedologic models were used in two piedmont areas in Iran to link salinization with rather easily mapable geopedologic patterns (Figure 2.5). Geostatistical analysis of the data collected in grids helped to justify the relations that could then be used to model the salinity trend, using a rule-based, fuzzy logic, or any other GIS-oriented method (Pishkar, 2003).

2.3.1 Prospective of modelling in salinity study

Assessing the impact of salt accumulation on physical and chemical soil properties is a key component to slowing down the salinization process and protecting the soil from further progression. Assessment also includes understanding the dynamics of the salt movement regimes. For better preparation and analysis of the numerous data, an interactive system, such as Geographic Information System (GIS), should be coupled with groundwater model (Burrough, 1996; Corwin, 1996; El-Kadi *et al.*, 1994; Gilliland and Baxter-Potter, 1987; Van Wesenbeeck and Kachanoski, 1994; Vaughan *et al.*, 1996; Wagenet and Hutson, 1996). Such integration should basically take care of data transformation and information sharing between the different components through integrated layers of constituent spatial information. The coupled GIS with the solute model would integrate the subsurface information, obtained from model, with the component of remote sensing providing surface data. Therefore, modelling is used complementary to provide data on salt movement (Figure 2.6) in the soil profile, while remote sensing provides information on the presence of salt at the soil surface. As Corwin (1996) described, limitations that result from the integration of a GIS with a deterministic model can be minimized by selecting an appropriate model, scale, and defining the required accuracy of the simulated output data. The cost of data collection can be minimized by implementing sensitivity analysis, which determines the most and the least sensitive parameters and variables, which can be measured and estimated, respectively. The reliability of the output data should be determined by performing an uncertainty analysis.

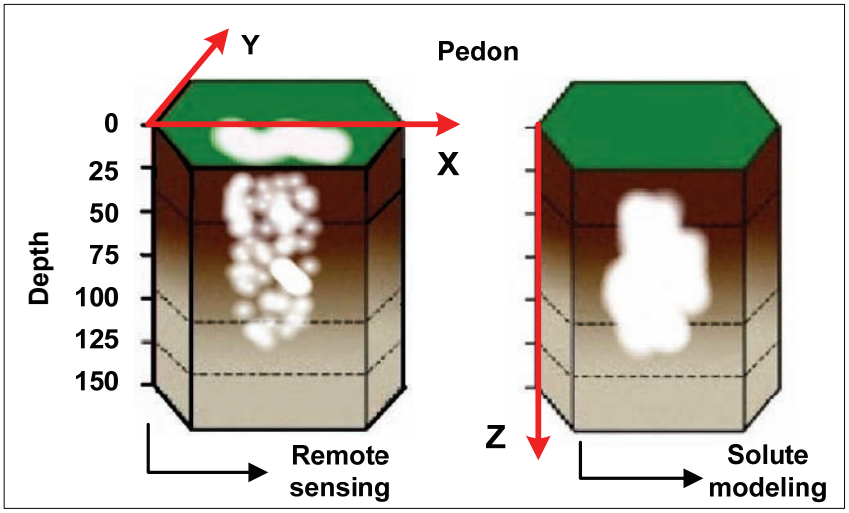

Figure 2.6: Surface is detected by remote sensing while solute modelling is used to obtain information on soil profile.

2.4 Geophysical exploration and salt-affected soils

Geophysical sensors have been used since the early 20th century in environmental studies and more recently, are being increasingly used to extract information from the near-surface and subsurface, also in regolith and soil profile. Concerning salt-affected soils, geophysical sensors, particularly airborne, can provide comprehensive data (George and Bennett, 2000; George and Woodgate, 2002; Street *et al*., 2002). The geophysical devices are designed to cover the range of depths and have several applications, namely, mapping saline intrusions, mapping terrain conductivity, soil and rock layers, and some general geological features such as fault and fracture zones.

2.4.1 Geophysical methods used in salinity studies

Electromagnetic (EM) induction and contact electrode are two techniques used to measure soil EC in the field (Figure 2.7). The EM surveys are conducted by inducing electromagnetic energy into soil profiles without physical contact. The sensor is composed of a transmitter and a receiver coil (Figure 2.7a) installed usually 1.0 m (3.3 ft) apart in a non-conductive bar in the opposite ends of the instrument (Upadhyaya and Teixeira, 2002). The transmitter coil (Tx) induces a current into the soil (assumed uniform), generating a time-varying magnetic field in the earth. The resulting secondary electromagnetic field (H_s) set up by any ground conductors is then measured at a receiver coil, together with the

primary field, H_p. In general this secondary magnetic field is a complicated function of the inter coil spacing (l), the operating frequency (f), and the ground conductivity (σ). Under certain constrains, the secondary magnetic field is a very simple function of these variables (McNeill, 1980b) Eq. [1]:

$$EC_a = \frac{4}{\omega \mu_o l^2}\left(\frac{H_s}{H_p}\right), \quad \omega = 2\pi f, \qquad [1]$$

where, f = frequency (Hz), μ_0 = permeability of free space, EC_a = ground conductivity (mho/m), and l = inter-coil spacing (m). The measured conductivity depends on salt concentration in soil, type and amount of clay and soil moisture and soil porosity. This technique has been used in EM conductivity meters such as EM-38 manufactured by Geonics. The application of EM series instruments and their efficiencies in soil salinity assessments have been addressed in Rhoades and Corwin (1981), Williams and Fiddler (1983), Rhoades et al. (1989), and Lesch et al. (1995).

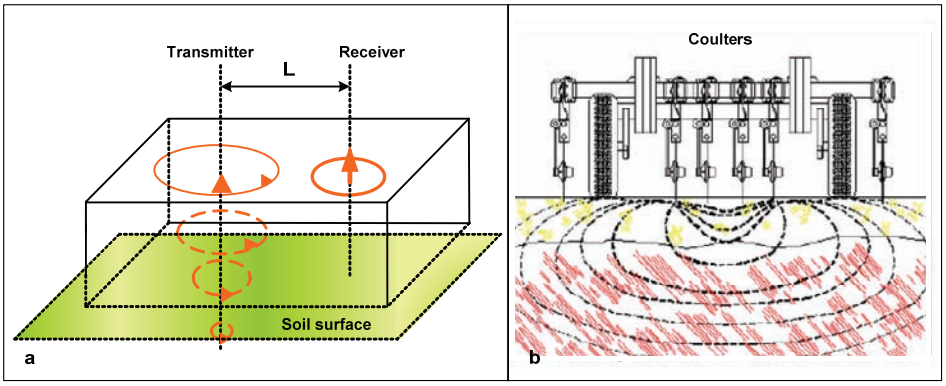

Figure 2.7: Direct measurement of soil electrical conductivity. a) electromagnetic induction method, b) contact electrode system.

The contact electrode system (Figure 2.7b) measures EC_a with a system of coulters that are in direct contact with soil through insulated metal electrodes that penetrate the soil surface (Doerge et al., 2002). These devices directly measure the voltage drop between a source and a sensor electrode. The depth to which EC can effectively be related to soil properties depends on the spacing width of coulter-mounted electrodes for contact methods and on the orientation (vertical vs. horizontal), height, and spacing of the source electrical coils for the EM methods. Most of soil EC devices are designed to be effective for depth of 3 to 5 feet. The Veris 3100, manufactured by Veris Technologies, Inc., is a soil

conductivity sensor in which contact electrode technique is used. Output from the instrument data Logger reflects conductivity of soil mass, which is the conversion of soil electrical resistance. The application of the instrument and their efficiencies in soil salinity assessments are discussed in Hartsock et al., (2000) and Farahani (2004).

Airborne geophysical techniques are widely used because of their speed and cost-effectiveness and availability of large number of different systems (Kearey and Brooks, 1994). The most commonly used systems are deployed from helicopters as they can be operated most easily at low flying heights and are much more manoeuvrable than fixed-wing aircraft (Reynolds, 1997).

2.4.2 Application of geophysics exploration in salinity

Traditional methods for field measurements and analysis to obtain soil parameters on a fine grid are expensive, laborious and time consuming. Geophysical sensors are capable of gathering rapidly and cheaply subsurface information with sufficient accuracy for an adequate interpretation to be made (Griffiths and King, 1981; Johson et al., 2001). Figure 2.8 shows an example of apparent conductance image of the Toolibin catchment in Western Australia provided by an airborne sensor. This technology has the advantage of effectiveness of salt mapping for cropped land while optical remotely sensed imagery is typically applied effectively to topsoil where soil has no vegetation cover (Johson et al., 2001). Furthermore, the EM data can be used efficiently to highlight areas of elevated conductivity where no surface expression of salt is evident (Howlett et al., 2001). The airborne EM system also measures information that is required to derive three-dimensional conductivity estimates of the subsurface (Lane et al., 2000).

Geophysical methods such as EM, magnetic and radiometric survey have all been employed in salinity studies. EM survey is the most used method to map the three-dimensional variation in the soil (bulk) resistivity (conductivity), caused by changes in mineralogy, intensity of alteration, water content or salinity (Diaz and Herrero, 1992; Hartsock et al., 2000; Howlett et al., 2001). In combination with EM method, the magnetic and radiometric methods are used to gather soil body-related information.

Magnetic survey defines the local variations in strength and direction in the earth's magnetic field, which can indirectly be related to salinity. It can accurately locate the position of shear zones and faults, which enables more accurate prediction of future outbreaks of salinity and also helps explain the current distribution of salinity (George et al., 1998).

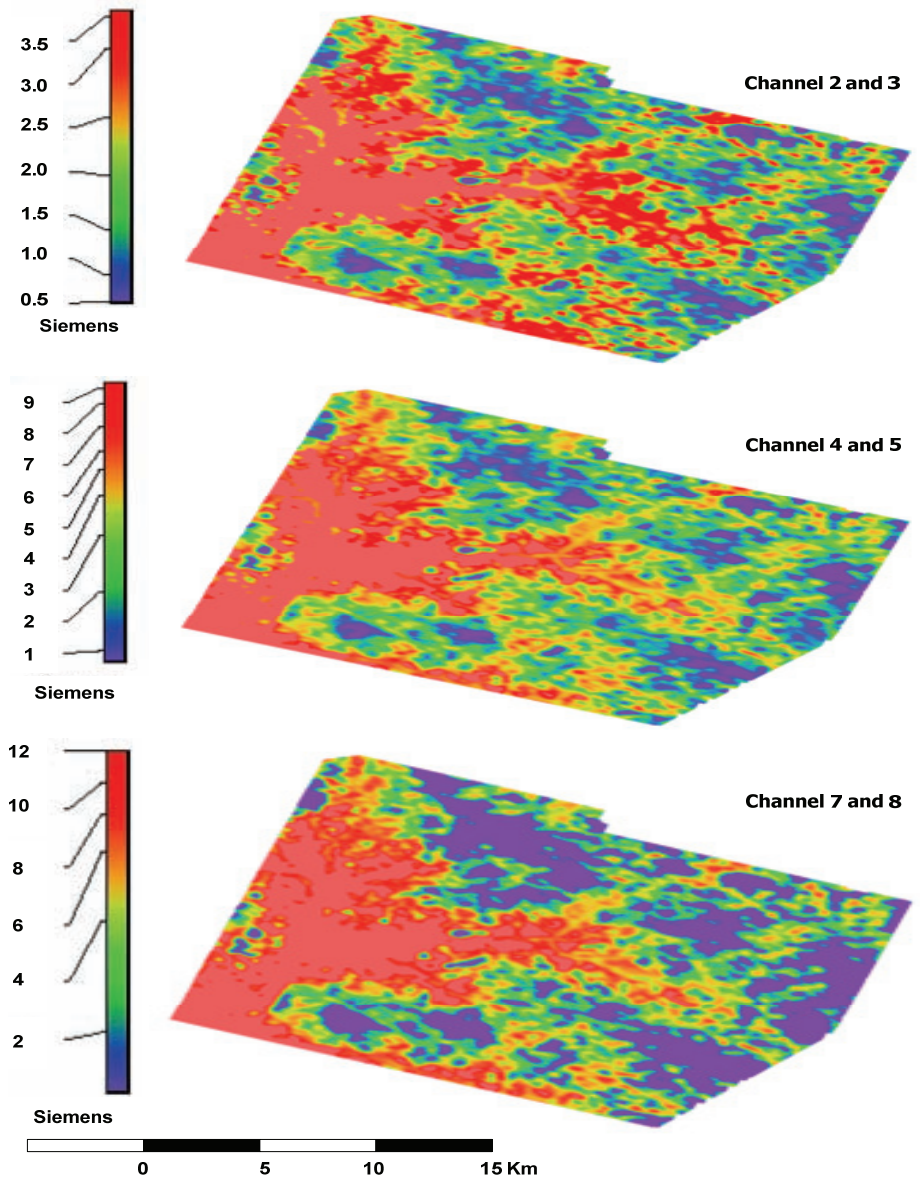

Figure 2.8: Airborne apparent conductance image of the Toolibin catchment in Western Australia (George et al., 1998). It shows apparent conductance for early (channel 2 and 3), mid (channel 3 and 4) and late time (channel 7 and 8). Conductance is reported in Siemens, while conductivity is reported in mS/m or dS/m. The data obtained by SALTMAP™ system which is a fixed wing, time-domain airborne electromagnetic system that combines magnetic, radiometric and digital elevation models to define soil conductivity, thickness, etc.

The salt-affected soils can be identified efficiently when an integrated interpolation of all available data, including geophysical data, is applied (Street *et al.*, 2002). Interpretation of EM data, which requires ample skill, becomes an important new technique in soil survey (Vlotman, 2000). However, the conversion from EM measurements to soil salinity (EC_e) requires knowledge of soil properties and an appropriate calibration, which can be easily obtained using the salinity probe (Rhoades and Corwin, 1981). Calibration involves geostatistical analysis of data to establish a relationship between soil electrical conductivity of saturated paste extract (EC_e) and soil apparent conductivity (EC_a) (Triantafilis, 2001).

2.5 The proposed integrated approach

Considering the complexity of salinization, depending on responsible factors and causes, its detection in the early stages remains difficult. Normally, high concentration of salts influences some of the physical and chemical soil properties, which might be detectable, even without salt efflorescence on the soil surface. The process in its inception, however, does not harm the soil, to a detectable degree. Timely detection of the process as one of the most harmful degradation types, in order to take proper conservation measures before it is too late, is a must (Farifteh and Farshad, 2002).

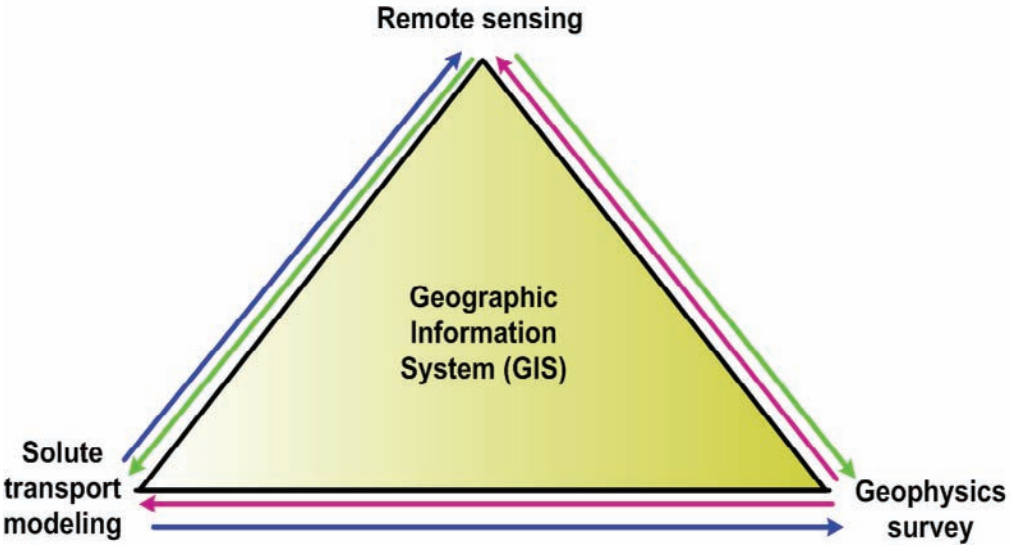

Figure 2.9: The proposed conceptual framework of the integrated methodology for the assessment of salt-affected soils.

Having already indicated both possibilities and limitations of the most common techniques in the detection of salinity, an integrated approach is conceptualized in this paper, which should to a great extent, overcome the limitations. Figure 2.9 illustrates the proposed conceptual approach.

Following the principles of geopedologic modelling, a discrete model of salinity spatial distribution in a given area can be obtained. The result of such a modelling does not only provide qualitative information on salt-affected areas but also indicates areas prone to salinization. Remotely sensed (RS) data used at this phase confines to the conventional Landsat and in particular aerial photographs that are preferably obtained at the time when salinity-related features are most pronounced, for example, at the end of hot and dry season and/or when high percentage of bare-soil is available, especially in areas under intensive agriculture. An example of general strategy to detect salt-affected soils using the proposed integrated method is presented in Figure 2.10.

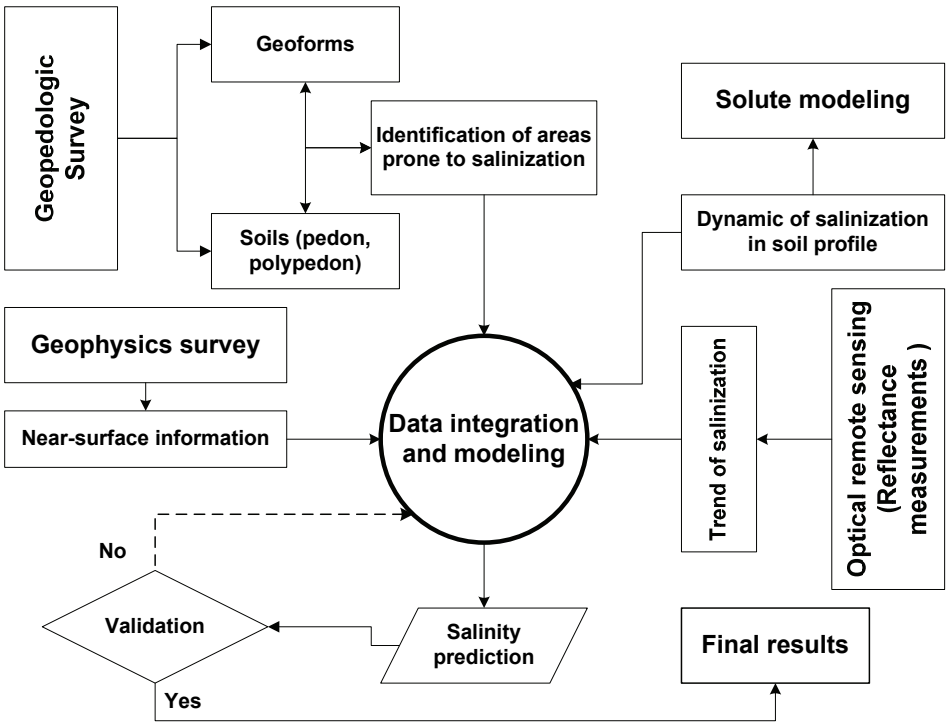

Figure 2.10: General Methodological approach; integration of remote sensing, solute modelling and geophysical survey.

The soil resistivity (conductivity), which can be related to the degree of salinity, can be measured using geophysical sensors. Geophysical technologies, preferably airborne, can provide comprehensive data, which have the advantage of effectiveness for cropped land and can efficiently be used to highlight areas of elevated conductivity where no surface expression of salt is evident while optical remotely sensed imagery is typically applied to topsoil where soil has no vegetation cover or being severely affected (Howlett et al., 2001). The data obtained through geophysical survey represent an average apparent conductivity of the materials (as bulk) at a certain depth depending on the frequency (the higher the frequency the shallower the depth). An example of general strategy to determine relationship between the spectral reflectance of salt-affected soils measured by a spectrometer and electrical conductivity measured through a geophysical survey is presented in Figure 2.11.

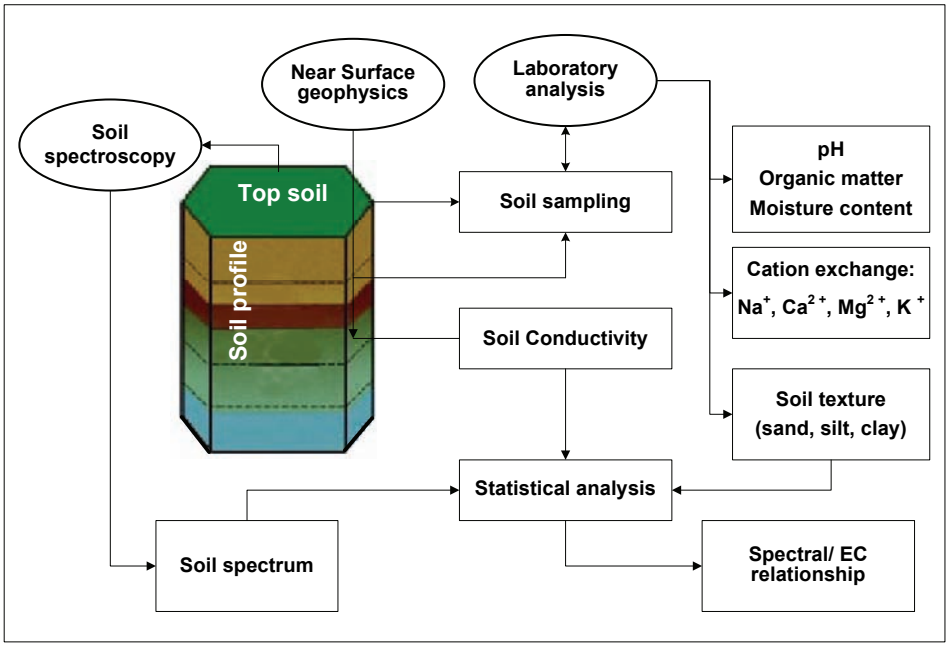

Figure 2.11: General strategy to integrate soil spectra with soil electrical conductivity measured by geophysical instruments such as EM-38 (at approximate depths of 075 and 1.5 m).

Modelling of solute (vertically and laterally) in soil should provide valuable information on understanding the dynamic of salt movement regime, assessing the impact of salt accumulation, and prediction of soluble salts under various conditions especially in areas where soils and often groundwater are potentially saline and any disturbance of the delicate hydrological balance results in mobilization of the stored salt. Since the information derived from a model

represents the points where the field data were collected, the results have to be interpolated. While geophysical survey, carried out in pre-selected locations, indicates slightly to moderately affected areas, the solute modelling would highlight salinization in its inception.

However, the issue of integration is vital and is assigned to a well designed GIS environment, where next to geostatistics use is also made of a rule-based technique. Such an integrated methodology should involve an up-scaling approach, because both the process and the obtained data are scale dependent (Figure 2.12).

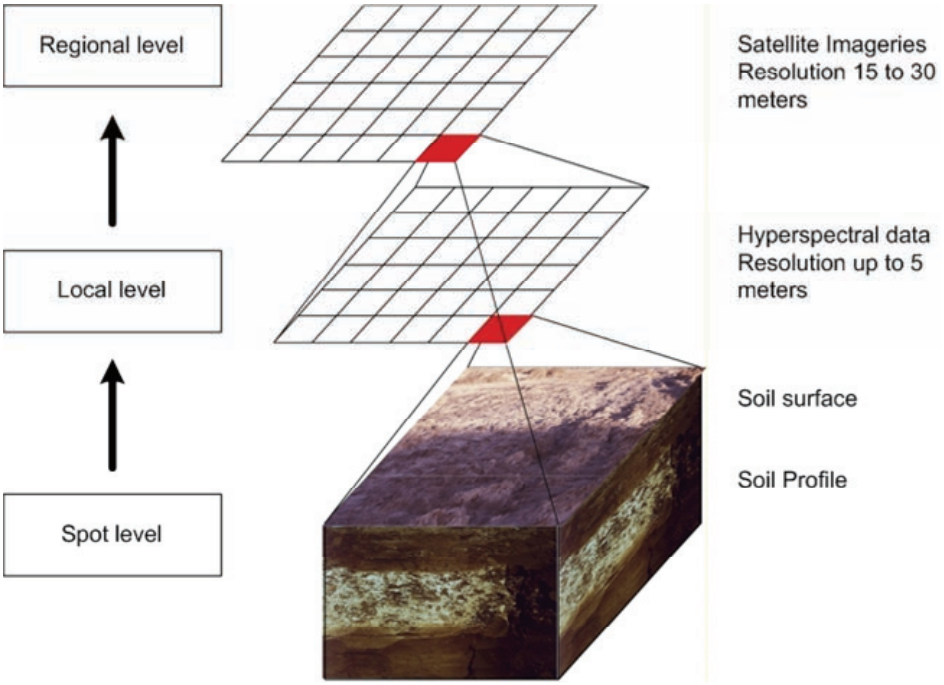

Figure 2.12: Up-scaling approach to assess salt-affected soils.

2.5.1 Applications of proposed integrated approach

A research framework is proposed to improve the currently used techniques of tracking down of salinization as a degradation process and to map salt-affected areas via integrating soil surface and near-surface information into modelling process in a GIS environment. The full application of the suggested research framework has not been evaluated yet (as it is a part of the research program in the coming years). However, there are several investigations in which integration approach have been applied to improve the products derived from remotely sensed data concerning salinity mapping and prediction (Sah et al., 1995; MacGowen and Mallyon, 1996; Eklund, et. al., 1998).

Overlaying approach is one of the most used techniques to integrate the derived information at a given grid cell. In this approach digital data obtained from space-borne or air-borne sensor can simply be combined with ancillary data such as DEM (digital elevation model), soil map, groundwater quality map, geological map and land use map. This approach was found effective in classifying salt-affected areas (Sah et. al., 1995; Eklund et. al, 1998). The method also allows categorizing the attribute maps according to the impact of the elements influencing the process by assigning different weight-values to each of the layers involved (Pishkar, 2003).

Conditional probability has also been used to integrate several GIS layers from databases including also remotely sensed data. In this context Bayes theory can be used to update the probability of rules that certain degree of salinity occurs at a given location based on predefined piece of evidence (Duda and Hart, 1973). Such approach was used by Skidmore (1989) and Schmidt et al. (2004) for mapping Eucalypt forest type and coastal vegetation respectively.

Techniques such as knowledge based systems offer more potential for extracting information from remotely sensed data. It is based on use of remote sensing data, explicit knowledge about the objects and processes, ancillary data, and an iterative procedure to adjust the measurements (Mulder 1994; Moon and Bonham-Carter, 1992). Peng (1998) used this technique to integrate remote sensing data with groundwater mineralization data, groundwater depth data, topography, and surface water data to map salinity classes. The artificial neural networks and evidential reasoning are also used to involve GIS data layers in the process of image classification Wilkinson (1996).

2.6. Conclusion

Remote sensing data, geophysical survey, and solute transport modelling are the most commonly used tools and techniques in the detection and mapping of soil salinity. The constraints and advantages of these techniques suggest that an

integrated approach using techniques and facilities that remote sensing, in particular image spectrometry, solute transport modelling and advanced geophysical survey offer to timely detect salinization (of different degrees) must be introduced. Application of such an integrated methodology, in a GIS environment, follows also a relevant up-scaling approach, from spot through local to regional, realizing that both the process and the data are scale dependent.

Chapter 3

Spectral characteristics of salt-affected soils: A laboratory experiment*

Abstract

This study focuses on the use of laboratory spectroscopy to recognize the presence and abundance of salts in soils. To create soil samples with large variations in soil salinity, six different saline solutions in various densities were prepared (containing either $MgCl_2$, NaCl, KCl, K_2SO_4, $MgSO_4$ or Na_2SO_4). The saline solutions were used to sub-irrigate three sets of soil samples with silty clay loam (nobs = 65), sandy loam (nobs = 41) and sand textures (nobs = 41). After sub-irrigation, soil spectra and soil salinity were measured for each of the 147 samples. Statistical techniques were used to detect and characterise diagnostic absorption bands and to develop predictive regression models between spectral signature and soil salinity levels.

Spectral analyses revealed that salt-affected soil samples do not exhibit all of the diagnostic absorption features that were found in the spectra of salt minerals used to treat them. It also showed that the number and clearness of diagnostic

---

* This chapter is based on:

Farifteh, J., van der Meer, F., van der Meijde, M., Atzberger, C. (2006). Spectral characteristics of salt-affected soils: A laboratory experiment. Under review, *Geoderma*.

bands reduces as the salt concentration in the samples decreases. Even if salts were present in high concentrations (EC ≥ 8 dS/m), two commercially available software packages (PimaView and TSG algorithm) were unable to correctly recognize presence of different salts.

To quantify salt-abundances across soil types, none of the investigated regression models proved optimal for all salts. In general, predictive models using continuum-removed absorption features gave higher accuracies compared to models using either spectral reflectances at selected wavelengths or models based on overall albedo. Amongst the investigated salts, $MgCl_2$ and $MgSO_4$ were estimated with the highest accuracies (cross-validated $R^2_{CV} \geq 0.80$ and $PRMSE_{CV} < 40\%$). For NaCl, estimation of soil salinity gave an accuracy ($R^2_{CV} = 0.65$ with $PRMSE_{CV} = 50.3\%$). Only weak relations could be established to quantify KCl and Na_2SO_4. Given the high $PRMSE_{CV}$ values for these two salts (67.2% and 60.6%, respectively), application of these models must be considered very limited. No useful relation could be established between K_2SO_4 and the investigated spectral features.

The results highlight the limitations of remote sensing for mapping soil salinity. With regard to up-scaling from experiment data to field and eventually to air-borne and space-borne sensors, a number of constraints have to be considered. The main limitation is that most diagnostic spectral features occur close to the water absorption bands around 1400 and 1900 nm and are very small and not diagnostic. Hence, their detection would require a very high spectral resolution, continuous spectral sampling and high signal-to-noise ratio. The recognition of presence and abundance of salts in soils is further complicated by the fact that in natural conditions, soil water and roughness effects, organic matter content, soil mineralogy and BRDF (Bidirectional reflectance distribution function) effects are superimposed on the measured signal. This illustrates the complexity of the implementation of laboratory findings in the analysis of air- and space-borne data where the crucial spectral information is not completely available and/or influenced by other soil constituents.

3.1 Introduction

Identification of salt-affected areas is essential for sustainable agricultural management, especially in (semi-) arid environments. Salt-affected soils contain various proportions of cations (Na^+, Mg^{++}, K^+, and Ca^{++}) and anions (Cl^-, SO_4^{--}, CO_3^{--} and HCO_3^-) that lead to different degrees of salinity. The main source of salt constituents are the primary minerals found in soils and exposed rocks, which appear in the form of a (1) salt crust as a result of evaporation, (2) deposit as a result of precipitation, or (3) solution as a result of dissolving in water in a soil profile (FAO, 1988; Richards, 1954). The minerals mainly responsible for soil

salinity are found within four chemical groups namely carbonates, halides, sulphates, and borates. The mineral groups and their characteristics are extensively discussed by Klein and Hurlbut (1999). Soil salinity is generally measured by soil electrical conductivity (EC) with values ranging between 2 to more than 32 dS/m (Richards, 1954).

Remote sensing has been widely used to identify and map saline areas at various scales (e.g., Farifteh, et al., 2006a; Dehaan and Taylor, 2003; Metternicht and Zinck, 2003; Ben-Dor et al., 2002, Evans and Caccetta, 2000; Dwivedi and Sreenivas, 1998; De Jong, 1992; Everitt et al., 1988; Sharma and Bhargava, 1988). Application of broadband remote sensing (e.g. Landsat, SPOT, Aster) in salinity studies is restricted due to the limitations in spatial and spectral resolution and sampling bandwidth that masks detailed spectral signatures (Cloutis, 1996). Three major problems interfere in the detection of salt-affected soils by means of remote sensing: (1) the process goes often undetected, especially when salt minerals have not (yet) severely affected the soils, (2) the physical boundaries separating saline areas of different degrees are fuzzy, and (3) the process of salinization occurs not only at the soil surface but also in the soil profile, which can not be detected by optical sensors. Moreover, in nature, salt minerals are rarely pure, since trace elements are often trapped in crystal lattices during crystallization. This affects the reflectance properties of minerals (Hunt and Salisbury, 1970, 1971) and thus hampers the use of already established experimental models.

To map saline soils, different direct and indirect methods have been developed. Besides detecting altered soil optical properties, salt-induced roughness changes and/or modified plant growth pattern can be detected (Ben-Dor 2002; Dehaan and Tayor, 2002; Szilagyi and Baumgardner, 1991; Baumgardner, et al., 1985; Stoner and Baumgardner, 1981). For the analysis of altered soil optical properties, various analytical techniques have been developed. Methods encompass monovariate regressions to multivariate approaches. Recently, partial least squares regression (PLSR) has been extensively used for quantitative analysis of reflectance spectra (Yang et al., 2003; Udelhoven et al., 2003; Wold et al., 2001; Anderson and Bro, 2000; Haaland and Thomas, 1988a, b). Despite all efforts, differentiation between saline areas of different degrees and automatic salt identification are still not sufficiently researched.

Technological advances such as (airborne) imaging spectrometry offer considerable potential as the instruments provide high spatial resolution data in a large number of narrow contiguous spectral bands in the VNIR-SWIR region (400 to 2500 nm). As salt minerals have characteristic features occurring in the VNIR-SWIR region, they can be distinguished from one another (Drake, 1995; Crowley, 1991a, b; Gaffey, 1987; Hunt et. al., 1971, 1972).

Success in discrimination of saline areas of different degrees can be increased if the spectral characteristics of salt-affected soils and the underlying factors are examined. In this regard, more attention should be given to the analysis of reflectance spectra obtained from soils containing various amount of salts. Through carefully designed laboratory experiments, the contribution of the spectral information derived from the salt minerals in identification of minerals and discrimination of saline areas can be examined. At the same time, the strength of the relationship between amount of salts in soils (electrical conductivity) and their influence on soil spectral characteristics can be analysed in more detail. Consequently, the main aim of this chapter is to provide insight spectral information that leads to a better understanding of spectral behaviour of salt-affected soils and to define a guideline for development of spectrometric techniques with capabilities of recognizing the presence and abundance of salts in soils. To study the relationship between salt concentration in soil samples and its spectral response, a laboratory experiment was designed involving soils with three textures and six salt minerals. The artificially induced soil salinity covered the whole range from non-saline (EC_e < 2 dS/m) to extremely saline soils (EC_e > 16 dS/m). For predicting salinity levels focus was on monovariate linear regression approaches between EC and spectral features. For salt identification in the soil reflectance spectra, two commercially available software packages (PimaView and TSG algorithm) were used and evaluated.

3.2 Materials and methods

3.2.1 Laboratory experiment design

Ideally, it is desired to obtain direct and simultaneous measurements of soil properties, including reflectance, as salinization process progress under natural conditions. To obtain such ideal set of data, essentially requires lysimeter[1] facilities, which allow study of soil profiles under various conditions as salinity levels progress due to changing depths of saline water table. However, for practical reasons, a simpler laboratory experiment was designed to control salt accumulation in soil samples. In such a controlled experimental set up, salt concentration in soil samples were varied by simulation of ground water rise and of evaporation processes while soil constituents were kept almost constant in the short period of the experiment. This means any change in soil reflectance

[1] The lysimeter is much like a pot that sits in the ground and can accommodate soil, plants, air and water resources. It was developed by Bill Pruitt, and has been used in hundreds of experiments to study e.g., the water and material movement in soil profile, the effects of different soil surface formations and plant covers on the water regime of the soil.

spectra is mainly due to variations in salt content of the soil samples because the other soil properties remain almost the same.

Quality assurance and control were formulated according to the published literature concerning guidelines of field and laboratory methods. The fieldwork activities and data collection and their relevance are described separately (see fieldwork actives and materials). The quality control of the experiment activities can be present in steps of samples preparation and measurements. The preparation of the solution was guided by the published methods namely Handbook of chemistry and physics (Lide, 1993). The preparation of the soil samples was guided by soil survey laboratory methods (Burt, 2004; Van Reeuwijk, 1993). The spectral measurements followed procedures found in Hunt and Salisbury (1970 and 1971), Csillag (1993), Crowley (1991a, b), Congalton and Green (1999), NASA (2001) and USGS websites. The ASD user manual (Hatchell, 1999) was consulted for calibration of the spectrometer and the spectral data collection.

3.2.2 Sample preparation

Soil material was air-dried, crushed and passed through a 2 mm sieve (Van Reeuwijk, 1993). The soil samples were, according to texture, divided in three sets. In total, 147 top-open Kubiena boxes were prepared in three sets (65, 41 and 41) each representing a soil texture. The Kubiena boxes in each set were filled with about 50 to 60 grams of soil after a sponge was placed at the bottom of each box (Figure 3.1). The samples were placed in bigger plastic boxes in such a way that added salt solution could move up to the soil through the sponge (simulating groundwater level change).

The aqueous salt solutions were prepared in 100 cc of distilled water using standard methods applied in laboratories (Max et al., 2001, Lide, 1993). The technical-grade salts used to prepare the solution are listed in Table 3.1. All salts were purchased as pure (99 or 98 %) from Merck Bv. (http://www.merck.nl). The soil samples were sub-irrigated with saline water and left to dry at room temperature (simulating evaporation process). One sample of each set was treated with distilled water. Different levels of soil salinity were artificially created in this way.

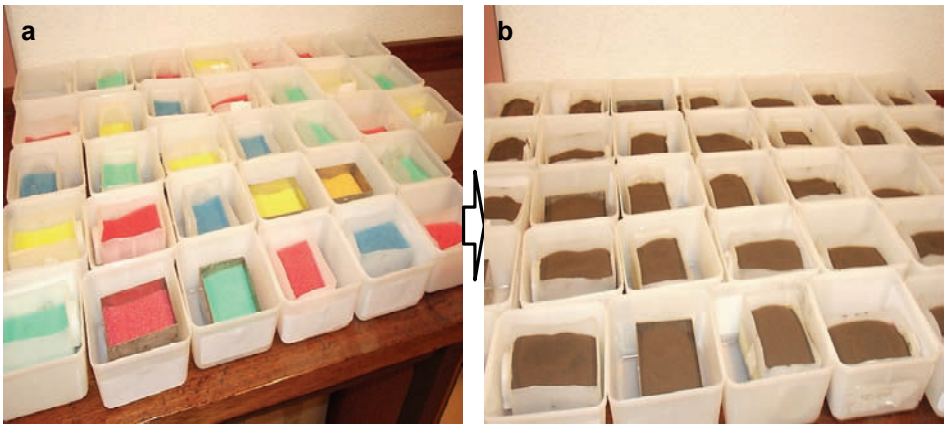

Figure 3.1: a) Kubiena boxes including sponges. b) Kubiena boxes including sponges and soil.

Table 3.1: Salt minerals and their maximum solubility at various temperatures (in ^{o}C). Data from Lide (1993) and Verkerk et al. (1992).

Mineral	**Formula**	**Maximum solubility in water [gr/100cc]**		
Bischofite	$MgCl_2*6H_2O$	117.0** at 25^{o}		
Halite	NaCl	35.7* at 0^{o}	35.9** at 25^{o}	
Sylvite	KCl	34.0* at 25^{o}	35.9** at 25^{o}	
Arcanite	K_2SO_4	12.0* at 25^{o}	12.0* at 25^{o}	24.1** at 100^{o}
Epsomite	$MgSO_4*7H_2O$	71.0* at 20^{o}	91.0* at 40^{o}	
Thenardite	Na_2SO_4	4.67* at 0^{o}		

* From Handbook of chemistry and physics (Lide, 1993). ** From Binas (Verkerk et al., 1992)

3.2.3 Laboratory procedures for soil analysis

Soil properties that are known to be influenced by accumulation of salts and/or affecting soil optical properties were determined for each soil prepared soil sample by known laboratory methods (Van Reeuwijk, 1993). The following soil properties were measured: soil particle size distribution, electrical conductivity (EC), pH, moisture content and soluble salt content. The proportions of clay, silt and sand were measured using a pipette method. The soil texture triangle and

distribution percentages measurements were used to define the soil texture of the samples (Table 3.2). The EC of the samples were determined from soil water extract (1:2 by weight) using air-dry soil and distilled water. The amount of salt cations present in each sample was measured using the ICP-AES (liberty series II Inductively Coupled Plasma Atomic Emission Spectrometer).

3.2.4 Laboratory procedures for spectral data acquisition

A portable ASD FieldSpec FR spectrometer (manufactured by Analytical Spectral Devices, Inc.) was employed for the reflectance measurements. The instrument covers the visible to short-wave infrared wavelength range (350 to 2500 nm) using three separate detectors: the VNIR (350 – 1050 nm), the SWIR1 (1000-1800 nm), and the SWIR2 spectrometer (1800 -2500 nm). The spectrometer has a sampling interval of 1.4 nm for the region 350 - 1000 nm and 2 nm for the region 1000 - 2500 nm with a spectral resolution of 3 and 10 nm, respectively (Hatchell, 1999).

Reflectance measurements were acquired in a laboratory setting using a 25° foreoptic. A light source (Lowel Light Pro, with JCV 14.5V-50WC halogen lamp) illuminated the sample surface with a 45º zenith angle from a distance of 20 cm. Spectral measurements were taken from nadir at 3 cm height above the sample. Integration time was set to 1 sec. Reflectance was calibrated against a white panel of known reflectance (Spectralon Diffuse Reflectance Panel). All spectral measurements were made in a completely dark room to avoid contamination by stray light.

3.2.5 Laboratory measurements

The soil samples used in this study were collected from field area in northeast Hungary (silty clay loam soil) and from Texel island in the northwest of The Netherlands (sandy loam and sand).The properties of these soil samples under field conditions are given in Table 3.2. Once the treated samples were dried, their properties were measured. The experimental set-up ensured that soil moisture contents remained low, thus minimizing the effect of soil moisture on the measured spectra. Soil moisture content never exceeded 0.05 %, with more than ¾ of samples having moisture contents of less than 0.02 percent (Figure 3.2). The number of samples per salinity class is shown in Table 3.3 for each of the six salt minerals. Sample numbers varied between 12 (arcanite) and 37 (halite).

Table 3.2: Soil properties of soil samples under field conditions.

	Soil type		
	L	**SL**	**S**
Soil Texture	**Silty clay loam**	**Sandy loam**	**Sand**
% Sand	18.5	54.1	91.4
% Silt	48.8	44.6	3.7
% Clay	32.7	1.3	4.9
pH	8.2	6.4	5.6
Moisture content (%)	0.0088	0.0095	0.0023
EC (dS/m)	2.1	0.4	0.2
Total cations (me/L)	10.7	11.3	10.4
Number of sub-samples (nobs)	65	41	41

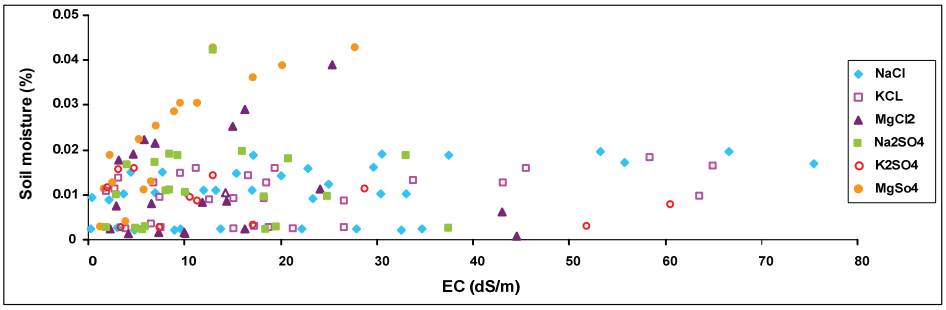

Figure 3.2: Scatter-plot of soil sample moisture content versus EC at the time of spectral measurements. The various symbols represent different salt minerals.

Table 3.3: Number of soil samples per salinity class and salt mineral used for sub-irrigation. Three samples were treated with distilled water and served as a control sets. For each sample, EC and spectral reflectance were measured.

	Salt minerals for soil sub-irrigation						**Total**
	Halite NaCl	**Sylvite KCl**	**Bishofite $MgCl_2$**	**Epsomite $MgSO_4$**	**Thenardite Na_2SO_4**	**Arcanite K_2SO_4**	
Un-treated	n.a.						3
Slight (< 4 dS/m)	2	4	3	5	3	3	20
Moderate/strong (4-16 dS/m)	11	7	12	9	11	5	55
Extreme (> 16 dS/m)	24	21	7	5	8	4	69
Total	37	32	22	19	22	12	147

In total, 147 laboratory derived spectra were collected from the saline and air dried soil samples. Reflectance spectra of the six salt minerals (will be discussed later) that were used for sub-irrigating soil samples were also measured. In addition, the spectra of the aqueous solutions of the technical-grade salts (Table 3.1) were measured almost at the limit of their solubility range. The salts in the solution are completely ionized and the ions by themselves do not exhibit absorptions features in the range of 400 - 2500 nm (Figure 3.3). However, the salts solvated water have distinctive spectra which are slightly different from that of pure water and can be analyzed using various techniques (Max and Chapados 2001; Max et al., 2001). Nevertheless, such detailed differences in spectra of salt aqueous solutions do not have a significant impact on remote sensing application of salt-affected soils.

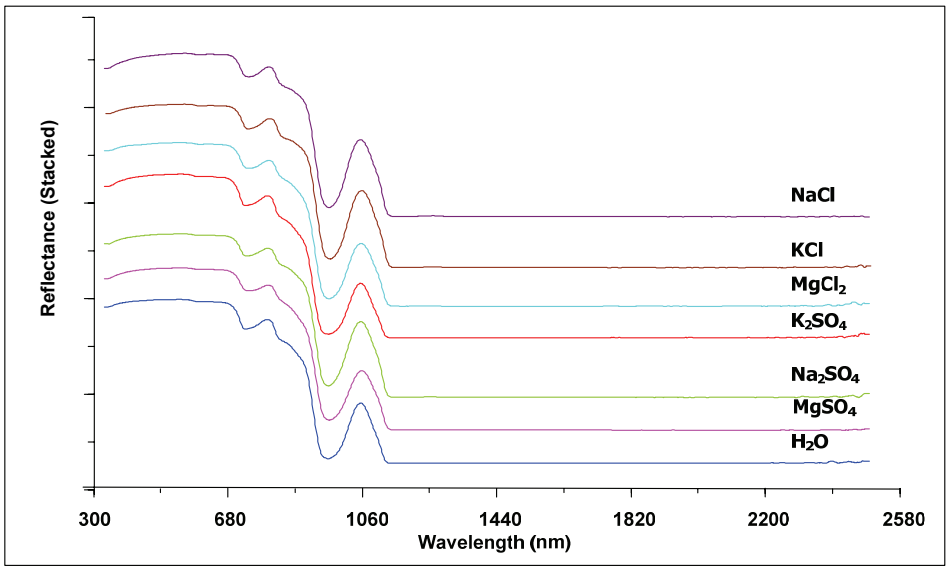

Figure 3.3: The spectra of pure water and salt solutions at maximum concentration. The white reference panel was placed under the solution to enhance the measured spectra. The spectra presented in this figure are offset vertically for viewing purpose.

To further reduce noise present in the soil spectra, a (polynomial) Savitzky-Golay filter (Savitzky and Golay, 1964) was applied to the measured spectra (order of 2 and frame size of 51 nm). The salt induced variability in soil reflectance is depicted in Figure 3.4 for each soil type separately. The graph shows the spectral signature of the soil treated with distilled water (solid line), as well as the 5% and 95% percentiles per wavelength (dashed lines). For later analysis, only the spectral range between 1000 and 2400 nm has been considered.

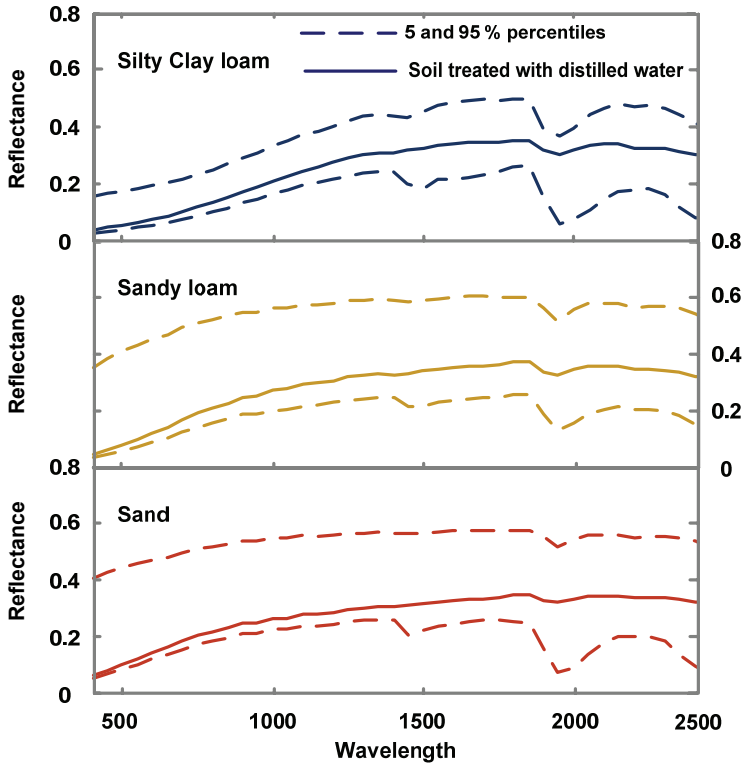

Figure 3.4: Soil reflectance variability (5% and 95%-percentiles) resulting from sub-irrigation of three soils with saline solutions of various densities (dashed lines). The solid lines correspond to the soils treated with distilled water. All soil spectra were measured in air-dried conditions.

3.2.6 Spectral analysis techniques

To analyse and exploit relationships between soil salinity and soil optical properties, linear relations between EC and spectral characteristics were assumed. Two categories of spectral characteristics were analyzed: (1) soil reflectances and (2) absorption features. The measured soil reflectances were either analyzed as a function of wavelength (yielding spectral correlograms in steps of 50 nm) or were spectrally integrated into overall albedo values before analysis. In both cases, analysis was restricted to the wavelength range between 1000 and 2400 nm. As regards the absorption features, characteristics such as depth, depth position (λ_d) and area of the absorption feature were considered (van der Meer, 2000b; Kruse, 1995). These characteristics were calculated from continuum-removed spectra to enhance absorption features in the recorded soil reflectance spectra. Clark and Roush (1984) were the first to suggest

continuum–removal (CR) analysis to isolate individual absorption features of interest. The continuum is a convex "hull" of straight-line segments fitted over the top of a spectrum that connect local spectral maxima and represents the "background" absorption onto which other absorption features are superimposed (Huang et al., 2004). The continuum is removed by dividing the reflectance value for each point in the absorption feature by the reflectance level of the convex hull at the corresponding wavelength. The local shoulder positions were determined through visual analysis and fixed independent of soil type. They are indicated by circles in the right hand side of Figure 3.5.

To assess the validity and accuracy of the various regression models, the cross-validation procedure was used (Duckworth, 1998). In this approach (also called leave-one-out method), n different regression equations are calculated from n-1 samples (n being the sample number). Each time a regression variant is calculated, the calibration model is used to predict the observation that was left out. As the predicted samples are not the same as the samples used to establish the model, the cross-validated root-mean-square error ($RMSE_{CV}$) and coefficient of determination (R^2_{CV}) are good indicators of the accuracy of the model in predicting unknown samples. To make the effects of different salts more comparable, differences in average salinity levels were corrected by calculating the cross-validated percentage root-mean-square error ($PRMSE_{CV}$). Using standard statistical software (SPSS), statistics were tested for significance at the 0.01 level.

Two commercially available mineral identification algorithms were used to identify salt minerals from the recorded soil spectra (PimaView user manual, 1999; TSG user manual, 2005). The algorithms are based on statistical methods identifying an unknown mineral from a reference library. The PimaView algorithm finds the mixture percentage of that mineral in relation to other minerals identified (PimaView user manual, 1999). The TSG algorithm calculates similarities between mineral spectral and soil samples spectra in 3 spectral regions (1304-1400, 1600-1850 and 2100-2496 nm), thus excluding the water absorption bands. The matching value is scaled between 0 and 1 and is a measure of the "goodness of fit" with 1 being a perfect match and 0 indicating no similarity between reference (i.e. mineral) and sample spectra.

3.3. Results and discussion

3.3.1 Spectral features of salt minerals

The reflectance spectra collected from pure salt minerals are shown in Figure 3.5. The absorption features identified in the spectra of these minerals corroborate well with other published results (Drake, 1995; Crowley, 1991a;

Gaffey, 1987). Only occasionally, the positions of the absorption features are slightly different probably related to variations in mineral purity, grain size, shape and structural order (Drake, 1995).

The VNIR-SWIR absorption features seen in most of these mineral spectra are mainly associated with internal vibration modes of anion groups such as HOH, -OH, and SO_4^{-2} or of water, molecules which are trapped, adsorbed or associated in some way with the crystal structure (Crowley, 1991a; Hunt and Salisbury, 1970). For example, the absorption features seen near 1000, 1200, 1400 and 1900 nm in the spectra of hydrated minerals such as epsomite and bischofite are related to vibrations of these anion groups. They show relatively broad absorption features, due to the overlapping bands of water molecules while less hydrated species show narrower absorption bands (Crowley, 1991a). The broad absorption bands near 1400 and 1900 nm in spectra of halite and thenardite are related to the presence of fluid inclusions and/or absorbed water (Crowley, 1991a).

3.2.2 Salt-induced absorption features in CR-spectra

Continuum-removed (CR) reflectance spectra of soils treated with six different salt minerals are displayed in Figure 3.6 with different colours representing three levels of salinity. The soil samples in Figure 3.6 (a) and (b) contain halite (NaCl) and sylvite (KCl) as the dominant evaporite minerals. In arid and semi-arid regions, these minerals are amongst the most widespread. The salts mainly occur in form of crystals or efflorescence as a result of evaporation of trapped bodies of salt water. The continuum-removed soil spectra show consistent absorption features at approximately 1440 and 1933 nm, which are also present in the pure mineral spectra of halite and sylvite (Figure 3.5). The features noted at 1440 nm in the spectra of the minerals appear at around 1420 nm in the soil spectra. For both minerals, there is a slight trend of increasing absorption depths with increasing salt concentration.

The band at approximately 2204 nm becomes less developed as samples become more saline. The degradation of this band may occur as a result of loss of crystallinity in the clay minerals. This result coincides with findings of Dehaan and Taylor (2002).

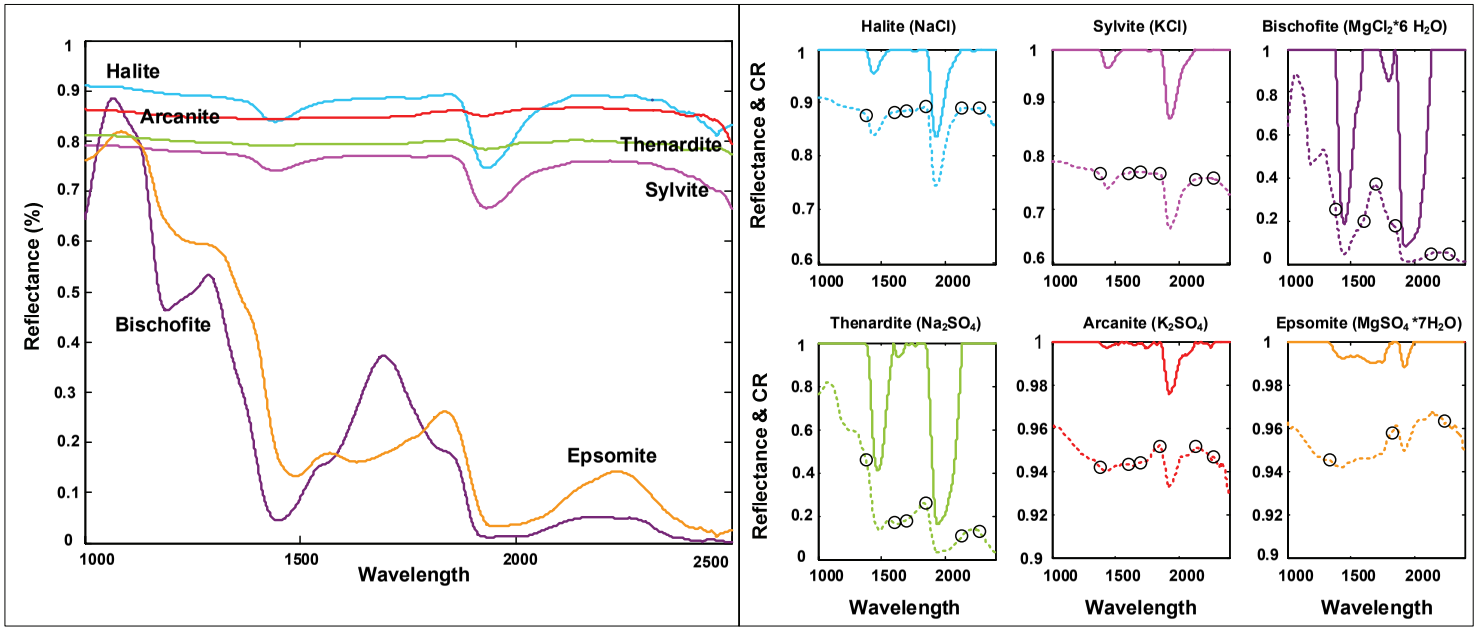

Figure 3.5: Laboratory spectra (1000-2500 nm) of six salt minerals used in this study: (left) reflectance spectra; (right) absorption features enhanced through continuum removal (solid lines) and reflectance spectra (dashed lines). All measurements have been filtered with a Savitzky-Golay (polynomial) smoothing filter (polynomial order of 2 and frame size of 51 nm) before display. On the right hand side, the original reflectance spectra (dashed lines) are displayed together with the approximate positions of the absorption shoulders (circles). Occasionally, the reflectance spectra had to be offset for better display.

The spectra in Figure 3.6c (bischofite) were obtained from soil samples treated with $MgCl_2$ solution. Compared to the bischofite spectra (Figure 3.5), they lack the absorption features at wavelength 1190 and 1824 nm. The shoulder observed at 1556 nm is comparable with the one noted in the spectrum of bischofite. The features at around 1451 and 1952 nm are weaker in the soil spectra and their positions shift as the amount of the salt abundance in the soil decreases. This is due to the fact that soil absorption features around 1400 and 1900 nm broaden as the salt concentration in soil increases.

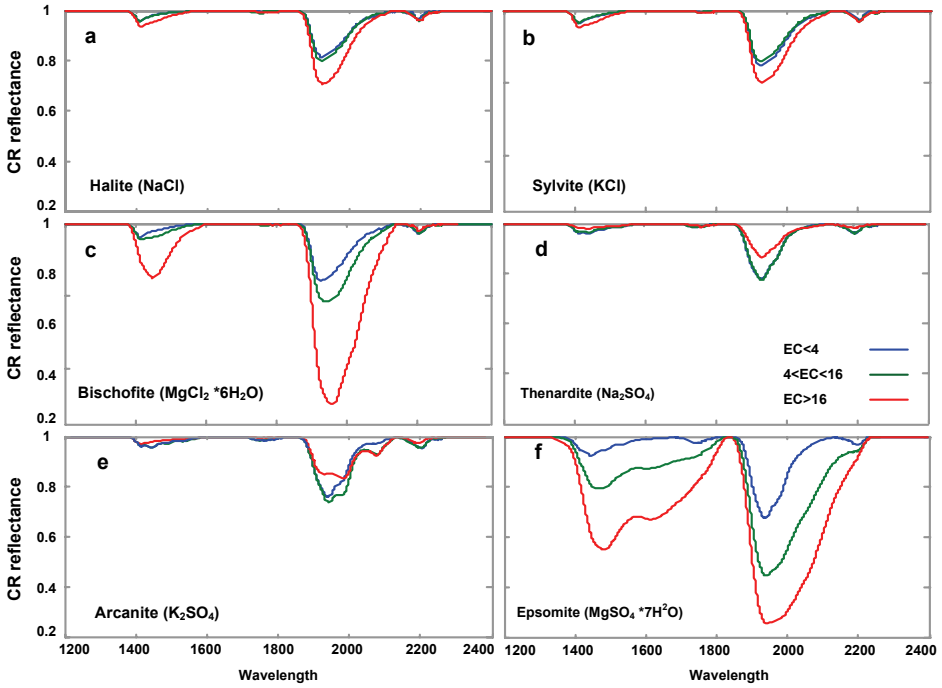

Figure 3.6: Continuum-removed reflectance spectra of soils treated with different salt minerals. Colours correspond to different levels of salinity: EC< 4 (blue line), 4 < EC < 16 (green line), and EC > 16 (red line). The results are calculated across soil types. The numbers of observations per class are given in Table 3.3.

The absorption bands (1410 and 1929 nm) noted in the thenardite spectrum (Na_2SO_4; Figure 3.5) are also found in saline soils spectra (Figure 3.6d), albeit we observe a slight shift in their positions. The CR-spectra indicate a strong negative correlation between increase of soil EC and changes in absorption bands parameters (depth, width and area).

Absorption features at 1430, 1932 and 2080 nm noted in the spectra of arcanite (K_2SO_4; Figure 3.5) also appear in the spectra of saline soil samples (Figure 3.6e). However, the soil spectra lack the absorption features at 2279 nm and the band at 2080 nm appears only in the spectrum of moderately to severely saline soils. In general, the positions of the absorption bands in the soil samples are slightly different from arcanite. For this mineral, the absorption features around 1420 and 1930 nm are flattened and slightly reduced in size when the salt concentration increases (Figure 3.6e). However, there is no strong correlation between salt concentration and the clearness of CR absorption features for this salt mineral.

The spectra of epsomite ($MgSO_4$) and saline soils samples treated with this mineral are almost identical in the range between approximately 1300 to 2400 nm (Figure 3.5 and Figure 3.6f). All spectra, however, lack the band at 1234 nm. The band at 1631 nm is only exhibited by severely saline soils. All the spectra of severely affected samples rich in epsomite lack the absorption band at around 2204, while slightly to moderately affected samples exhibit the band at this region. The results also indicate that the position of the maximum reflectance shifts toward shorter wavelengths as the salt concentration increases.

3.3.3 Salt-induced reflectance and albedo changes

The normalized albedo of saline soil samples is plotted as a function of soil salinity (EC) in Figure 3.7. The normalized albedo is the albedo of a saline sample ($\Sigma\rho_\lambda$) divided by the albedo of the same soil treated with distilled water. The graph illustrates that the overall albedo may increase or decrease with salt amount, depending on the salt mineral and soil texture (see also Table 3.5). Results indicate that the abundance of thenardite (Na_2SO_4) causes much higher soil albedo. The same holds for arcanite (K_2SO_4). In the latter case, however, the increase in albedo is restricted to the sandy loam and sand samples (Figure 3.7 and Table 3.4). A strong decrease in soil albedo is observed for samples treated with epsomite ($MgSO_4$) and bischofite ($MgCl_2$). In both cases, the decrease in soil albedo with increasing soil salinity can be observed across soil types. The effects of halite (NaCl) and sylvite (KCl) on overall albedo do not reveal a strong and consistent trend in relation to soil EC.

The influence of soil texture is clearly visible from samples treated with thenardite (Na_2SO_4) and epsomite ($MgSO_4$). The effect of both salt minerals on overall albedo increases as soil textures changes from silty clay loam to sandy loam and to sand (Table 3.4). This behaviour can be related to the specific soil surface which decreases from silty clay loam to sand. Variation in soil albedo can also be related to the surface conditions. In general, salts crystals or efflorescence were formed at the surface of the most severely affected soil

samples. Samples treated with epsomite, generally, showed a harder surface than e.g., samples treated with halite. However, a detail description of surface conditions can be very long since this experiment used more than 140 samples with salinity level varies between non to severely, which imply a large variety of surface conditions.

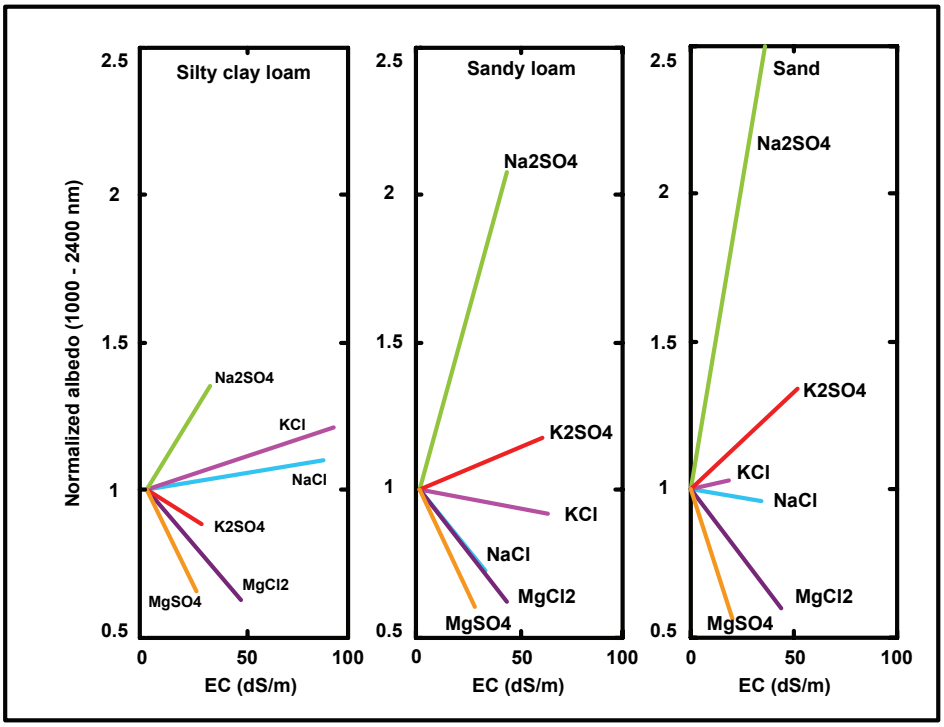

Figure 3.7: Normalized albedo (1000 – 2400 nm) as a function of soil salinity (EC) for six salts and three different soil types. The normalized albedo is the albedo of a saline sample (Σρλ) divided by the albedo of the same soil treated with distilled water. The different colours represent different salts. The strength of the relations is indicated in Table 3.4.

To illustrate the spectral dependence of the relation between soil reflectance and soil salinity, so called correlograms have been calculated across soil types for all salts (Figure 3.8). The correlograms report the coefficient of correlation (r) between soil reflectance and soil salinity as a function of wavelength. They have been calculated from reflectance spectra convoluted with a median filter (size 50 nm) using non-overlapping block processing.

A consistently positive correlation is observed for the samples treated with thenardite (Na_2SO_4) and arcanite (K_2SO_4). The results for the samples treated with bischofite ($MgCl_2$) and epsomite ($MgSO_4$) indicate a strong negative correlation, in particular in the spectral region above 1400 nm. Below 1400 nm, the influence of epsomite on soil reflectance is inconsistent, with correlations varying between positive and negative values. The correlograms of the samples treated with halite (NaCl) and sylvite (KCl) indicate no wavelength with a significant relationship between EC and soil reflectance. For these two salts, the coefficient of correlation (r) always remains between ± 0.5 for all wavelengths (Figure 3.8).

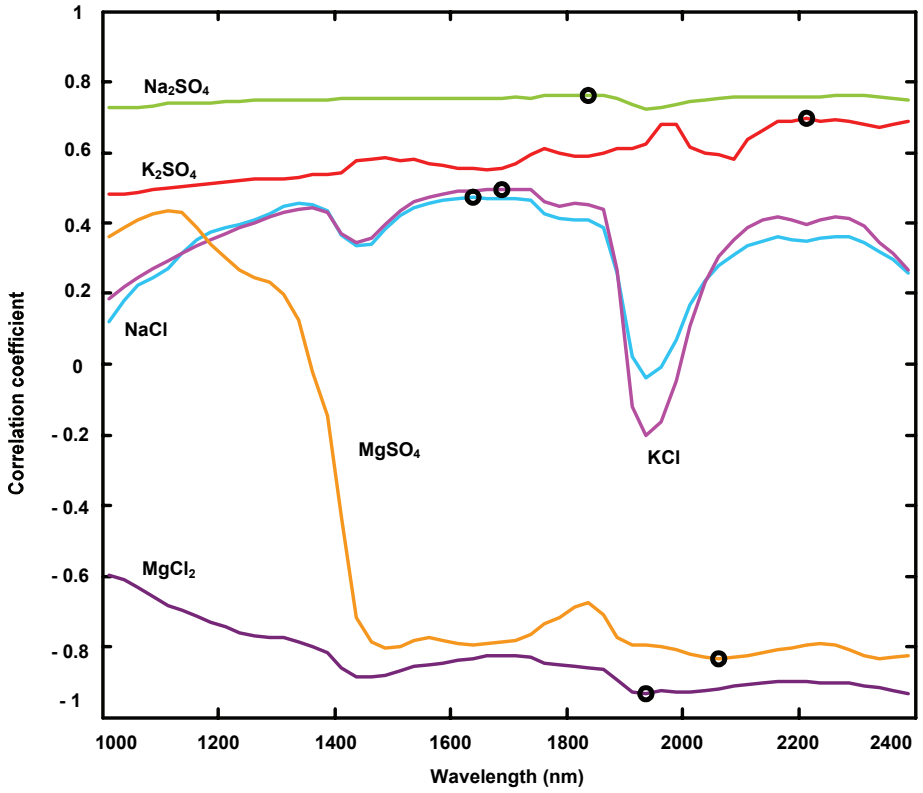

Figure 3.8: Coefficient of correlation (r) as a function of wavelength between soil reflectance and soil salinity (EC) across soil types. The different colours indicate six different salts. The circles indicate the positions of maximum (positive or negative) correlation. To reduce calculation time, the correlogram is calculated from reflectance spectra convoluted with a median filter (size 50 nm) using non-overlapping block processing.

Even though it is possible to identify the positions of maximum correlation from these curves (marked by circles in Figure 3.8), outstanding "optimum" bands can not be identified. On the contrary, the generally smooth and more or less horizontal curves indicate that the different wavelengths behave very similar (except $MgSO_4$). Apparently, for the six investigated salts strong diagnostic features do not exist in this wavelength range.

Table 3.4: Coefficient of correlation (r) between normalized albedo (1000 - 2400 nm) and soil salinity (EC) per soil texture class. The normalized albedo is the albedo of a saline sample ($\sum\rho_\lambda$) divided by the albedo of the same soil treated with distilled water.

	Soil texture		
	Silty clay loam	**Sandy loam**	**Sand**
NaCl	0.28	- 0.11	- 0.35
KCl	0.64	- 0.21	0.06
$MgCl_2$	- 0.88	- 0.82	- 0.98
Na_2SO_4	0.81	0.86	0.96
K_2SO_4	- 0.15	0.89	0.86
$MgSO_4$	- 0.69	- 0.99	- 0.98

3.3.4 Predictive regression models

In sections 3.2 and 3.3, the effects of salinity (EC) on the spectral characteristics of soil samples (overall albedo, spectral reflectances and salt-induced absorption features) were presented. In the present section, these relationships have been quantified to predict soil salinity on the basis of monovariate linear regression models. Again, the analysis has been restricted to the wavelength range between 1000 - 2400 nm and models have been established across soil types.

The best predictive results are depicted in Figure 3.9, for each of the six salts with different symbols representing different soil textures. The accuracies of the cross-validated relationships are summarized in Table 3.5. The cross-validated coefficient of determination (R^2_{CV}) is used to quantify the strength of the models. The root mean square error ($RMSE_{CV}$) and percentage $PRMSE_{CV}$ (Table 3.5) indicate the accuracy of the predictions for unknown samples based on overall albedo, spectral reflectance and absorption band parameters, respectively.

The results suggest that only for five of the six salts, predictive regression models could be established with $R^2_{CV} \geq 0.52$: NaCl, KCl, $MgCl_2$, Na_2SO_4 and $MgSO_4$ (Table3.5). No valuable predictive model was found for K_2SO_4. Amongst the five remaining salts, only for two salts ($MgCl_2$ and $MgSO_4$) the salinity levels could be predicted with $RMSE_{CV}$ lower than 6 dS/m (roughly equivalent to $PRMSE_{CV}$ lower than 40%). For the remaining three salts (NaCl, KCl and Na_2SO_4), $RMSE_{CV}$ were in the range $7.9 \leq RMSE_{CV} \leq 16.9$ dS/m ($PRMSE_{CV}$ between 50.3 and 67.2%).

In most cases, predictive models using absorption band features gave better results than models using spectral reflectances or overall albedo (Table 3.5). Visual inspection of Figure 3.9 reveals that the salinity level of sandy soil samples is often slightly overestimated, while the loamy samples have a tendency to be underestimated (e.g. Na_2SO_4). However, statistical test revealed that the differences related to soil texture are not statistically significant (at the 0.01 level).

3.3.5 Salt identification

The mineral identification algorithm (PimaView user manual, 1999) was applied to the 144 (exclude 3 samples representing field conditions) spectra obtained from salt-affected soil samples. The results of the mineral identification are summarised in a confusion matrix (Table 3.6). The results indicate that the accuracy and reliability of mineral identification is very low for all minerals. The calculated overall accuracy of 20.8 % and average reliability and accuracy of 27.1 % and 17.0 %, respectively, indicate low potential for identifying salt types in soils using spectral measurements in the VNIR-SWIR region.

The similarity between mineral spectra and the spectra obtained from the saline soil samples was also examined using 'The Spectral Geologist' software (TSG user manual, 2005). The spectral matching technique was used to calculate the spectral similarity between the salt minerals and severely to extremely saline soil samples (EC ≥ 8) treated with the minerals ($n_{obs} = 100$). A soil sample was said to be correctly identified if the goodness-of-fit value for the correct salt was higher than those of all other minerals. The results (not shown) confirm again the low potential of the VNIR-SWIR to correctly identify the different salt minerals, even for severely to extremely saline samples.

Table 3.5: Cross-validated coefficient of determination (R^2_{CV}), root mean square error ($RMSE_{CV}$) and percentage RMSE ($PRMSE_{CV}$) between measured and estimated soil salinity (EC) for six different salt minerals. Analysis was restricted to the wavelength range between 1000 and 2400 nm. Monovariate regression models were established across soil types. All statistics are cross-validated (leave-one-out method).

	Based on overall albedo			Based on spectral reflectances				Based on absorption features			
	R^2_{CV}	$RMSE_{CV}$	$PRMSE_{CV}$	R^2_{CV}	$RMSE_{CV}$	$PRMSE_{CV}$	λ (nm)	Features* (nm)	R^2_{CV}	$RMSE_{CV}$	$PRMSE_{CV}$
NaCl	0.01	23.1	85.2	0.11	21.6	79.9	1675	Area (1930)	0.65	13.6	50.3
KCl	0	25.4	101.1	0.1	23	91.8	1725	Depth (1430)	0.52	16.9	67.2
$MgCL_2$	0.75	6.7	49	0.87	4.9	35.7	1925	Area (1950)	0.84	5.5	40.1
Na_2SO_4	0.51	8	61.9	0.53	7.9	60.6	1825	Area (1650)	0.15	10.7	82.4
K_2SO_4	0.11	17.5	121	0.2	16.4	113.6	2275	λ_d (2210)	0.05	18.4	127.2
$MgSO_4$	0.49	5.8	62.2	0.69	4.5	48.3	2375	Area (1580)	0.8	3.7	39.1

*The positions of the absorption features are approximate.

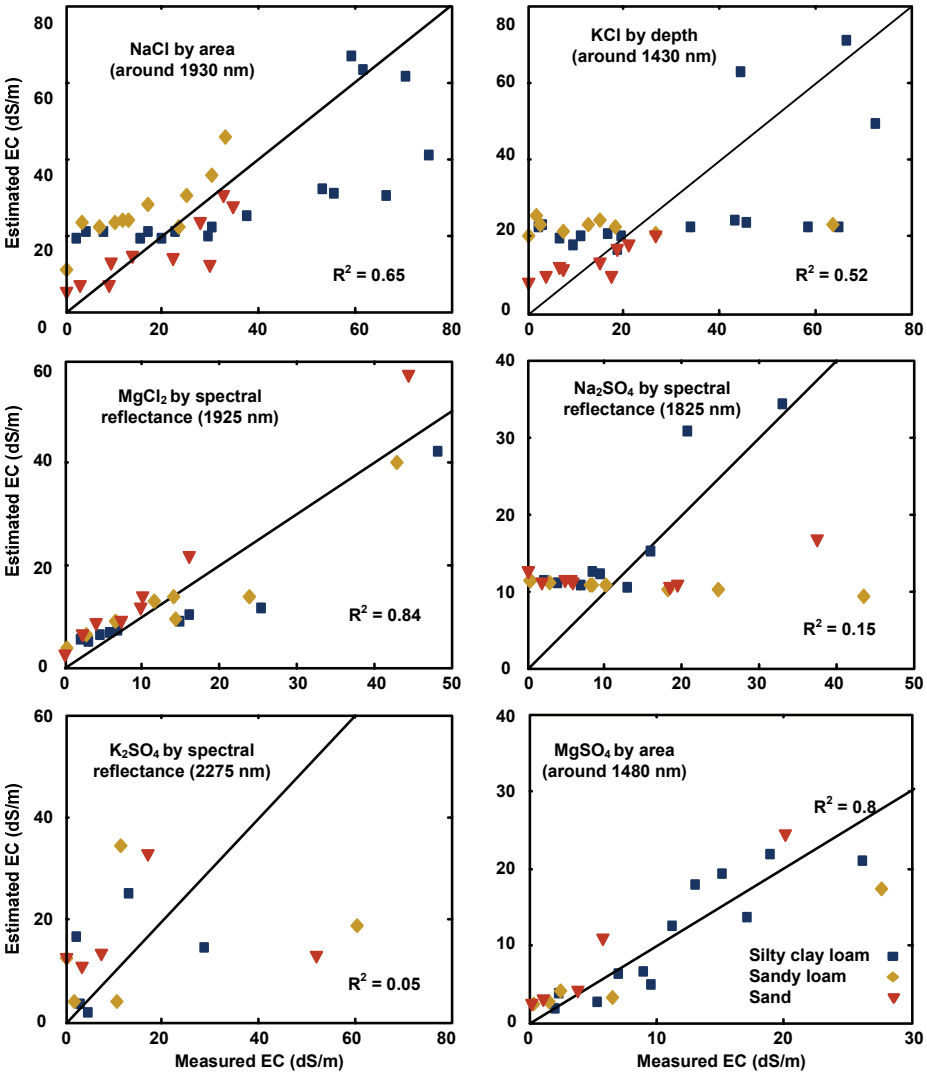

Figure 3.9: Measured against estimated EC. All estimations are cross-validated (leave-one-out). For each salt mineral, only the result of the best predictive model is shown. The different symbols represent different soil types: Silty clay loam (■), Sandy loam (◆) and Sand (▼). The corresponding cross-validated statistics are listed in Table 3.6.

Table 3.6: Summarized results of the PimaView mineral identification algorithm applied to spectra obtained from salt-affected soil samples treated with six salt minerals.

Minerals	Ha	Sy	Bi	Ep	Th	Ar	Un.	Total	ACC
Halite (Ha)	2	26	0	1	1	0	7	37	0.05
Sylvite (Sy)	1	24	0	0	0	0	7	32	0.75
Bischofite (Bi)	6	7	0	0	0	0	9	22	0.00
Epsomite (Ep)	2	11	0	3	0	0	3	19	0.16
Thenardite (Th)	5	12	0	0	1	0	4	22	0.05
Arcanite (Ar)	2	10	0	0	0	0	0	12	0.00
Total	18	90	0	4	2	0	30	144	0.21
REL	0.11	0.27	0.00	0.75	0.50	0.00			

ACC = Accuracy, REL = Reliability, Un. = Unclassified

3.4 Conclusion

The results presented in this chapter provided insight spectral information concerning salt-affected soils. It revealed positive aspects and limitations of remote sensing applications in monitoring and mapping saline areas. The results obtained from this experimental study allow drawing the following conclusions:

- The results showed that an increase in soil salinity induces changes in soil reflectance for wavebands higher than 1300 nm, particularly in the water absorption bands (around 1400 and 1900 nm). It also revealed that the relation between salinity level and albedo and/or spectral reflectance may be positive or negative, depending on salt mineral and soil type.

- It was found that the observed absorption features at further than 1400 nm were broaden, the position of maximum reflectance were shifted toward shorter wavelengths and overall reflectance were changed proportionally as salts concentration were increased in soil. The continuum-removed (CR) spectra indicate a strong negative correlation between increase of soil EC and changes in absorption bands parameters (depth, width and area).

- For all except one salt (K_2SO_4), statistically significant predictive regression models could be established. Linear spectral models to predict salinity level (EC) across soil types gave cross-validated root

mean square errors ($RMSE_{CV}$) between 3.7 and 16.9 dS/m ($0.51 \leq R^2_{CV} \leq 0.87$). Amongst the investigated spectral variables, those based on continuum-removed absorption features were generally the most accurate. However, the most accurate predictive models were based on spectral reflectances of selected wavelengths previously identified from spectral correlograms. The least accurate were models based on overall albedo.

- The results showed that soil samples with large variations in salts did not exhibit all of the diagnostic absorption features that can be found in the spectra of the dominant salt minerals. It showed that the number and clearness of diagnostic bands reduces as the salt concentration in the samples decreases.

- The present study also revealed number of limitations for salt identification and salinity mapping. The results showed that the absorption bands in the reflectance spectra of pure minerals were less distinctive in saline soil samples, even when salt concentrations were high (EC≥8 dS/m). In some cases, the number and/or position of absorption features varied between pure minerals and salt affected soils. Moreover, in spectra of salt-affected soil, most salt diagnostic absorption features occur close to known water (vapour) absorption bands.

- The results suggests that further studies are required to unravel the influence of soil status (e.g. soil composition, soil roughness, soil water content) on the relation between salinity level and spectral signature. The results also suggest that the quantification of salt-affected soil spectra should largely focus on spectral variations in NIR and SWIR region of soil spectra rather than individual diagnostic absorption signature. At up-scaling phase, quantification of salt-abundances in soil, should mainly focus on using general shape of spectrum rather than absorption bands parameters (depth, area, etc.), since most of the spectral features that are diagnostic of salt minerals or salt-affected soils are masked in an image due to atmospheric effect.

Chapter 4

Similarity measures for spectral discrimination of salt-affected soils*

Abstract

This paper illustrates a pilot study designed to examine spectral response of soils due to salts variations. The aim of the study includes determining whether salt-affected soils can be discriminated based on their spectral characteristics, by establishing relationship between soil properties and soil spectra and by testing if variations in the spectra of salt-affected soil samples are statistically significant.

To answer the research questions, a laboratory experiment was designed to simulate salt transport to a column of soil in order to provide direct measurements of soil spectra and soil properties when salt concentration in soil sample changes. The measured spectra were examined by application of spectral matching techniques to quantify the variations and ascertain a relationship that support spectral identification of saline soils. The Ward's grouping method was conducted as an exploratory tool to statistically create

---

* This chapter is based on:

Farifteh, J., van der Meer, F., Carranza, E.J.M. (2006b). Similarity measures for spectral discrimination of saline soils. In Press: *International Journal of Remote Sensing*.

homogeneous classes among data, which were obtained from application of the spectral matching techniques on salt affected soil spectra. A nonparametric statistical test (Mann-Whitney U-test) was used to determine whether the differences between the classes are statistically significant.

The results of spectral matching techniques showed differences in absorption strength, absolute reflectance and spectral angle in the near and shortwave infrared regions. The results also showed significant correlations between soil EC and spectral similarity measures, indicating that similarity between the samples' spectrum decreases as the salt concentration in soil increases. The generated clusters indicate two classes at the highest level, which were subdivided at the next level and further subdivided into multiple subclasses as the dissimilarity decreases. The spectral data were grouped in classes and were used to test the null hypothesis applying the Mann-Whitney U-test. The results indicate a significance level of $\alpha < 0.02$ between salinity classes and $\alpha < 0.05$ per waveband, meaning variations between the classes are higher than with in each class.

4.1. Introduction

Relationships between salt concentration in soil and the spectral characteristics of salt- affected soils have been the subject of research for decades, since thousand hectares of agricultural land are destroyed as the results of salinity every year (Rozanov, 1990). It has been established that quantity and chemistry/mineralogy of salts are among the main factors affecting the spectra of saline soils (Mougenot, et al., 1993). High salt concentrations in soil result in increase of surface albedo and affect the spectral properties of clay minerals (Ben-Dor 2002; De Jong, 1992). Concentration of soluble salts in soils directly affects soil spectra and absorption band parameters. Recently, it has also been shown that soil electrical conductivity (EC) is significantly correlated with diagnostic absorption band parameters such as depth, width, area and asymmetry (Farifteh et al., 2004). Schwarzott et al (2001) showed that dominant ions in saline soils (e.g., Na^+, Mg^{2+}) form highly hygroscopic salts ($MgCl_2$, and NaCl), which absorb water vapour and lead to an increase of soil moisture. Dehaan and Tayor (2002) have established a number of criteria, based on field-derived spectra of four different soil types, to characterize and discriminate saline areas using hyperspectral data. Their results show that saline soils have distinctive spectral features in the visible (VIS) and near-infrared (NIR) parts of the electromagnetic spectrum.

Studies of relationships between salt concentrations and spectral characteristics of salt-affected soils are important in development of methods for spectral discrimination of saline areas using air or space-borne data. Spectral discrimination between salt-affected soils using optical remote sensing remains

complicated, however, because variations in soil reflectance cannot be attributed to a single soil property and due to the complex nature of the salinization process that effects both physical and chemical properties of soil (Csillag et. al, 1993). This is especially the case where salinization is not severe such that neither salt crystal nor effloresce formation takes place at the soil surface, which means no subtle corresponding change in albedo or in parameters of diagnostic absorption bands. With the technological advance in the field of imaging spectroscopy, however, the prospect of improving the discrimination between salt-affected areas of different degree of salinity has been increased. Nonetheless, the possibility to evaluate the degree of salinization from spectral reflectivity values requires further examination of the relationship between certain properties and reflectivity of soil, such as in the case mentioned earlier.

The aim of this exploratory study was to determine the spectral response of soils in relation to variations in salt concentration. This chapter presents results of a laboratory experiment and statistical data analysis of relationships between salt concentration and reflectance of soils. The main strategy was to quantify variations in reflectance spectra of salt-affected soil samples and to determine, by way of correlation analysis, whether the variations in soil reflectance correspond proportionally to the variations in salt contents of soils. The techniques used to quantify variations in soil reflectance spectra are referred to as similarity measures (spectral matching), which are commonly applied to define (dis)similarity between spectra of an unknown substance (in this case salt-affected soil) and spectra of a reference substance (in this case non-saline soil) (Du et al., 2004; Van der Meer, 2000a, b). The potential to generate spectral classes or clusters from obtained values of similarity measures was explored by performing hierarchical cluster analysis. This numerical classification method allows creating clusters within which the degree of association is strong between the cluster members and substantially different from the members of other clusters (Webster and Oliver, 1990). The study also included statistical testing to analyze spectral differences between salt-affected soil samples that were grouped according to the standard international salinity classes defined by Richards (1954). The Mann-Whitney U-test was used to examine whether the variance of reflectance between the soil salinity classes is greater than within each class. The findings of this study are relevant to quantitative estimation of salt content in soils based on their spectral differences at the laboratory and field levels. The results would also constitute essential information to improve discrimination and classification of salt-affected areas using hyperspectral data.

4.2. Methods and materials

4.2.1 Laboratory measurements of soil properties

The soil samples used for laboratory analysis were collected from northeast Hungary and from the Texel island in the northwest of The Netherlands. Table 4.1 shows the properties of these different soil types under field conditions.

Table 4.1: Soil properties of soil samples under field condition.

Soil Texture	Particle size (%)			pH	SMC (%)	EC (dS/m)	Cations (me/L)				
	Sand > 2 mm	Silt < 50 μm	Clay < 2 μm				Mg^{++}	Ca^{++}	Na^{+}	K^{+}	Total
Silty clay loam	18.5	48.8	32.7	8.2	0.009	2.1	5.9	0.4	1.4	3.0	10.7
Sandy loam	54.1	44.6	1.3	6.4	0.009	0.4	0.1	0.1	9.9	1.2	11.3
Sand	91.1	3.7	4.9	5.6	0.002	0.2	1.2	4.5	3.6	1.1	10.4

SMC = soil moisture content

4.2.2 Spectral similarity measure

Two types of spectral matching techniques were used to determine differences between reflectance spectra of saline and non-saline soil samples: stochastic, deterministic. Stochastic techniques, such as spectral information divergence, are used to define spectral variation by modelling spectral information as a probability distribution (Chang, 2003). In general, stochastic techniques use sample properties and develop spectral criteria such as divergence, probability, etc. to measure dissimilarity between two spectra. Deterministic techniques are based on angle, distance, and correlation between two spectra. Recently, a new algorithm has been introduced to combine deterministic and stochastic techniques (Du et al., 2004). In the following discussion of different spectral similarity techniques, unknown spectra (for salt-affected soils) is denoted as X_i and reference spectra (for non-saline soil) is denoted Y_i, both measured for i (=1, 2, …,n) spectral bands.

4.2.2.1 Deterministic methods

Deterministic spectral similarity measures were calculated here based mainly on distance, angle and correlation between a set of spectra. Euclidean distance (d_e) measures the difference in magnitude of two spectra and can be defined as:

$$d_e = \sqrt{\sum_{i=1}^{n} (x_i - y_i)^2} \quad [1]$$

In order to remove the dependence on the number of spectral bands, the de is modified by inserting the factor 1/n (Keränen et al., 2003). Low values of de mean high similarity and vice versa. The de can be converted to a similarity index, SI, if it is scaled (normalized) so that it lies in the range of zero (for maximum dissimilarity) to one (for maximum similarity). The SI is calculated as (Webster and Oliver, 1990):

$$SI = 1 - de \quad [2]$$

The distance, De, can also be scaled between 0 and 1 (Homayouni and Roux, 2004) by:

$$D_e = (d_e - m) / (M-m) \quad [3]$$

where m and M are the minimum and maximum of d_e values, respectively.

Values of d_e are used in the Spectral Similarity Value (SSV) algorithm (Keränen et al., 2003). The SSV is calculated as:

$$SSV = \sqrt{d_e^2 + (1-\rho^2)^2} \quad [4]$$

$$\rho^2 = \left(\frac{\frac{1}{n-1}\sum_{i=1}^{n} (x_i - \mu_x)(y_i - \mu_y)}{\sigma_x \sigma_y} \right)^2 \quad [5]$$

where μ_x and μ_y are the means, σ_x and σ_y are standard deviations of unknown and reference spectra, respectively. Low values of SSV mean high similarity and vice versa.

The Spectral Angle Mapper (SAM) calculates the angle (α) between an unknown spectrum and a reference spectrum by applying the following equation (Kruse et al., 1993):

$$\alpha = \arccos\left(\frac{\sum_{i=1}^{n} x_i y_i}{\sqrt{\sum_{i=1}^{n} x_i^2} \sqrt{\sum_{i=1}^{n} y_i^2}} \right) \quad [6]$$

The α values range between 0 and $\pi/2$. Low values of α indicate high similarity between the unknown and the reference spectra. For comparison reasons, the results can be rescaled in range of 0 to 1 by dividing 2α to π (Schwarz and Staenz, 2001).

4.2.2.2 Stochastic techniques

Two stochastic similarity measures were used to compare the salt-affected soil and non-saline soil reflectance spectra. The spectral information divergence (SID) is defined as (Chang, 2003):

$$\text{SID}(x_i, y_i) = \text{D}(x_i \,||\, y_i) + \text{D}(y_i \,||\, x_i), \quad [7]$$

It measures discrepancy between spectral signatures of two vectors x_i and y_i in terms of their corresponding probability mass functions p and q, respectively (Chang, 2003). A combination of the SID and the SAM, a new measure referred to as the SID-SAM (Du et al., 2004). The SID-SAM between two spectral signatures x_i and y_i is given by:

$$\text{SID (TAN)} = \text{SID}(x_i, y_i) \tan(\text{SAM}(x_i, y_i))$$
$$\text{Or}$$
$$\text{SID (SIN)} = \text{SID}(x_i, y_i) \sin(\text{SAM}(x_i, y_i)) \quad [8]$$

The product of the SAM and the SID considerably increases spectral discriminability, because it makes two similar spectral even more similar and two dissimilar spectral more distinct. Low values of SID, SID (TAN) or SID (SIN) indicate high similarity and vice versa.

The detailed description of the algorithms of the methods is available in Chang (2003) and Du et al (2004).

4.2.3 Numerical spectral classification

4.2.3.1 Cluster analysis

Cluster analysis is an exploratory data analysis tool, which is used to statistically create homogeneous classes of data by minimizing within-class and maximizing among-class variability. It generates classes or clusters within which the degree of association is strong between the members and substantially different from the members of other classes (Webster and Oliver, 1990). An agglomerative hierarchical cluster analysis based on Ward's grouping method and correlation matrix (Webster and Oliver, 1990) was conducted to evaluate whether classes of salt-affected soils based on their spectral similarity values would correspond to international soil salinity classes defined by US soil salinity laboratory based on soil EC.

Hierarchical algorithms combine or divide existing classes to produce a hierarchical structure displaying the order in which classes are merged or divided. Agglomerative methods start with each observation in a separate class and proceed until all observations are in a single class. As described by Webster and Oliver (1990), Ward's method aims to minimize the sum of squares of the distance between individuals and their class centroids (Σd^2). For fusion of two classes A and B with n_A and n_B members, respectively, this is equivalent to:

$$\frac{n_A n_B}{n_A + n_B} d_{AB}^2, \qquad [9]$$

where d_{AB} is the distance between the class centroids (Wishart, 1969).

4.2.3.2 Mann-Whitney U-test

In general, statistical testing is performed to determine whether the differences between two classes are meaningful. There are several statistical tests for this and the suitability of each test depends on the data types and data distribution. The Mann-Whitney U-test is recommended, because it can be used with various types of data, is ideally dependent on random selection, it can be used for small sample sets (between 5 and 20), and is a nonparametric test whereby normal distribution of data is not necessary (Lehmann, 1998). Assumptions of the Mann-Whitney test are: (1) random sampling from populations, (2) independency within and between samples, and (3) at least ordinal scale of measurement. In this study, this test was used to analyze differences in reflectance spectra of salt-affected soil samples grouped into five salinity classes and to determine whether the variance of reflectance between the salinity classes is greater than within the class. The Mann-Whitney U-test, like all statistical tests, involves testing a null hypothesis (H_0) against an alternative

hypothesis (H_a). In this case, the null hypothesis means there is no significant difference between the median of individual waveband reflectance measurements for soil samples within each salinity class while difference between two classes is statistically significant. Thus, the null hypothesis for n salinity classes and i spectral wavebands reflectance measurements is:

$$H_0: \eta_n (i) = \eta_{n+1} (i) \quad [10]$$

where η_n is the median of reflectance measurements at i (= *1, 2, 3, …n*) wavebands for soil samples in N (= *1, 2, 3, …(N - 1)*) salinity classes (Moore and McCabe, 2003; Schmidt and Skidmore, 2003). The number of possible pairs from N salinity classes that has to be tested is the set of combinations of N' out of N and is given by the binominal distribution. If the null hypothesis is rejected for a pair of salinity classes, the alternative hypothesis, H_a, is that there is significant difference between medians of waveband reflectance measurements for soil samples in two salinity classes. This means that reflectance measurements in each salinity class represent different populations:

$$H_a: \eta_n (i) \neq \eta_{n+1} (i) \quad [11]$$

The significance level at which the null hypothesis is tested illustrates the probability of wrongly rejecting H_0, if it is in fact true. Usually, the significance level is denoted by α and initial level is here chosen to be 0.05 (or 5%). The probability value (p-value) of the hypothesis test represents the significance level indicating the strength of evidence for rejecting or accepting the null hypothesis. The smaller the p-value, the more convincing is the rejection of the H_0. However, a p-value suggesting acceptance of the 'H_0' does not necessarily mean that the null hypothesis is true; it only suggests that there is no sufficient evidence against H_0 in favour of H_a.

4.3. Results

4.3.1 Data collection

4.3.1.1 Sample characteristics

A summary of descriptive statistics of measured properties of the salt-affected soil samples is given in Table 4.2. The soil moisture content of each soil sample is very low, indicating that the effect of moisture on reflectance of each soil sample is minimal. The values of EC of the soil samples are highly variable, ranging from around 0.2 to 75 mS/cm.

4.3.1.2 Soil spectra

There were 97 laboratory-derived reflectance spectra measured from soil samples in five sets (Table 4.2), with each sample set sub-irrigated with saline water containing only one type of salt ($MgCl_2$, NaCl, KCl, $MgSO_4$, Na_2SO_4). The Savitzky-Golay smoothing algorithm (window size = 11) was used to smooth the measured reflectance spectra in order to enhance absorption features (Savitzky and Golay, 1964). Figure 4.1 presents smoothed reflectance spectra obtained from NaCl-irrigated soil samples having sandy loam (Figure 4.1a) and sandy (Figure 4.1b) texture. The reflectance spectra of the soil samples show that the absorption features at approximately 1420 and 1930 nm become wider as values of EC of the soil samples increase.

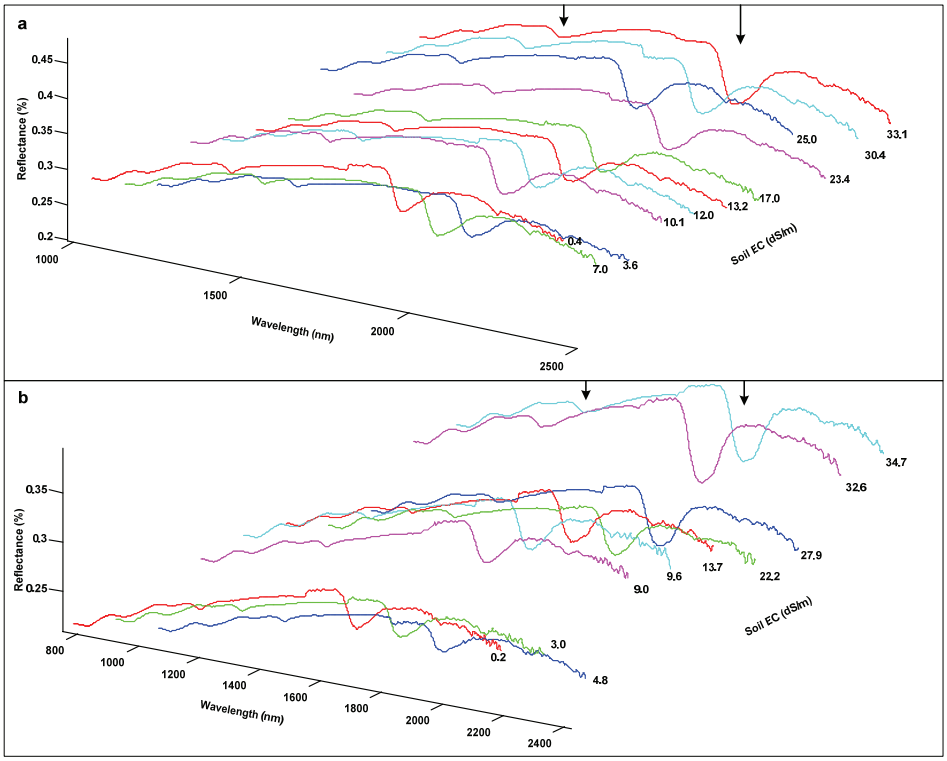

Figure 4.1: A 3D view of Laboratory reflectance spectra of NaCl-irrigated soil samples with (a) sandy loam and (b) sandy texture. Arrows represent wavelengths of 1420 and 1930 nm, where large variations in exhibited absorption bands occur due to variations in soil EC. Each number attached to a spectrum corresponds to EC value of soil sample.

Table 4.2: Descriptive statistics of measured properties of soil samples after being sub-irrigated with saline water and dried at room temperature. The number of samples in each sample set is 22, 37, 32, 19 and 22 for samples rich in $MgCl_2$, NaCl, KCl, $MgSO_4$ and Na_2SO_4, respectively.

Soil texture+	pH			SMC* (%)			EC (mS/cm)		
	L	LS	S	L	LS	S	L	LS	S
Rich in NaCl									
Minimum	6.9	6.0	5.1	0.014	0.009	0.002	4.4	0.4	0.2
Mean	7.0	6.3	5.3	0.017	0.011	0.002	33.6	15.9	15.8
Median	7.0	6.4	5.3	0.017	0.010	0.002	29.6	13.2	11.7
Maximum	7.4	6.6	5.7	0.020	0.012	0.003	75.4	33.1	34.7
Standard Dev.	0.2	0.2	0.2	0.002	0.001	0.000	22.7	10.8	12.7
SE mean	0.0	0.1	0.1	0.001	0.000	0.000	6.3	3.3	4.0
Skewness	1.5	0.2	1.0	0.077	0.545	0.071	0.6	0.3	0.4
Kurtosis	1.9	-0.2	-0.3	-1.65	1.332	-0.28	-0.8	-1.1	-1.5
CV%	0.02	0.03	0.04	0.12	0.08	0.09	0.68	0.68	0.80
Rich in KCl									
Minimum	6.93	5.81	4.77	0.01	0.0085	0.0023	3.20	1.90	3.90
Mean	7.09	6.01	5.07	0.03	0.0096	0.0027	38.2	18.6	14.7
Median	7.09	5.88	5.01	0.02	0.0092	0.0026	38.5	13.9	16.2
Maximum	7.30	6.54	5.72	0.11	0.0113	0.0036	96.1	63.6	26.6
Standard Dev.	0.10	0.26	0.30	0.03	0.0009	0.0004	27.8	20.0	7.9
SE mean	0.03	0.09	0.11	0.01	0.0003	0.0001	6.94	7.06	2.81
Skewness	0.31	1.44	1.56	1.93	0.9963	1.4899	0.52	1.96	-0.01
Kurtosis	-0.4	1.39	2.85	2.70	-0.108	2.4691	-0.7	4.34	-1.2
CV%	0.01	0.04	0.06	1.00	0.0987	0.1541	0.73	1.08	0.54
Rich in $MgCl_2$									
Minimum	6.8	5.5	4.6	0.02	0.006	0.001	3.2	2.9	2.3
Mean	7.0	5.8	5.1	0.03	0.009	0.002	15.7	16.7	13.5
Median	7.0	5.8	5.1	0.02	0.008	0.002	11.0	14.2	10.0
Maximum	7.2	6.0	5.5	0.09	0.011	0.002	48.3	43.0	44.5
Standard Dev.	0.2	0.2	0.3	0.03	0.002	0.001	15.2	13.4	14.4
SE mean	0.1	0.1	0.1	0.01	0.001	0.000	5.4	5.1	5.4
Skewness	0.2	0.6	0.3	2.5	0.310	0.240	1.7	1.4	2.1
Kurtosis	-2.0	-0.8	-0.4	6.3	-0.30	-0.59	2.8	2.3	4.9
CV%	0.02	0.03	0.06	0.76	0.20	0.36	0.96	0.80	1.06
Rich in $MgSO_4$									
Minimum	7.2	5.6	4.8	0.019	0.011	0.003	2.3	1.6	1.2
Mean	7.2	5.9	4.9	0.039	0.025	0.024	12.2	9.6	7.8
Median	7.2	6.0	4.8	0.030	0.013	0.008	11.3	4.5	4.9
Maximum	7.4	6.0	5.2	0.084	0.063	0.079	26.1	27.7	20.2
Standard Dev.	0.1	0.2	0.2	0.019	0.025	0.037	6.8	12.3	8.5
SE mean	0.0	0.1	0.1	0.006	0.013	0.018	2.1	6.1	4.2
Skewness	0.4	1.4	1.7	1.488	1.994	1.943	0.6	1.8	1.7
Kurtosis	-0.5	1.6	2.7	2.302	3.982	3.794	0.3	3.4	3.1
CV%	0.01	0.03	0.04	0.49	1.01	1.51	0.56	1.28	1.09
Rich in Na_2SO_4									
Minimum	7.4	6.2	5.1	0.017	0.009	0.002	4.0	2.9	1.9
Mean	7.5	6.3	5.5	0.021	0.010	0.003	14.0	16.6	13.4
Median	7.5	6.3	5.5	0.019	0.010	0.003	11.2	10.1	5.9
Maximum	7.7	6.3	5.9	0.042	0.011	0.003	33.0	43.6	37.5
Standard Dev.	0.1	0.1	0.3	0.009	0.001	0.000	9.4	14.0	12.7
SE mean	0.0	0.0	0.1	0.003	0.000	0.000	3.3	5.3	4.8
Skewness	0.5	0.8	0.5	2.756	0.244	0.251	1.3	1.4	1.3
Kurtosis	0.4	-0.4	0.0	7.699	-2.05	-1.69	1.7	1.8	1.3
CV%	0.01	0.01	0.05	0.40	0.06	0.11	0.67	0.84	0.95

*SMC = soil moisture contents, + L = silty clay loam; LS = sandy loam; S = sand

Table 4.2: Continued

Soil texture+	Mg (me/l)			Ca (me/l)			Na (me/l)			K (me/l)		
	L	LS	S	L	LS	S	L	LS	S	L	LS	S
Rich in NaCl												
Minimum	3.0	0.1	1.2	11.1	0.1	4.5	269	10	4	1.2	1.2	1.1
Mean	12.0	1.3	6.9	52.2	4.9	27.2	3375	1412	1036	2.5	3.1	1.7
Median	12.8	1.2	7.2	57.2	4.7	26.7	2001	874	974	1.9	3.3	1.6
Maximum	21.2	2.6	14.0	93.6	11.0	55.3	9095	3127	2572	6.5	5.7	2.7
Standard Dev.	5.2	0.8	4.5	23.7	3.4	17.6	2988	1286	959	1.5	1.4	0.5
SE mean	1.4	0.2	1.4	6.6	1.0	5.6	829	388	303	0.4	0.4	0.2
Skewness	0.3	0.2	0.2	0.2	0.2	0.3	1.0	0.4	0.4	1.9	0.3	0.8
Kurtosis	-0.2	-0.6	-1.1	-0.3	-0.7	-1.2	-0.1	-1.9	-1.3	3.6	-0.6	-0.2
CV%	0.43	0.61	0.64	0.45	0.70	0.65	0.89	0.91	0.93	0.59	0.45	0.31
Rich in KCl												
Minimum	5.4	3.45	0.34	21.6	14.97	1.42	2.83	1.25	0.37	3	11.2	10.2
Mean	11.2	6.31	0.48	54.2	26.6	1.91	4.80	1.60	0.49	154	61.2	29.9
Median	10.8	6.26	0.50	54.1	26.6	1.97	4.89	1.45	0.41	168	56.3	28.7
Maximum	16.9	8.84	0.57	84.7	36.8	2.45	6.70	2.27	0.85	322	122	63.9
Standard Dev.	3.6	1.72	0.07	18.8	7.16	0.35	1.08	0.38	0.17	106	36.1	17.8
SE mean	0.9	0.61	0.03	4.7	2.53	0.12	0.27	0.13	0.06	26	12.8	6.32
Skewness	0.07	-0.09	-1.0	-0.02	-0.3	0.003	-0.1	1.26	1.88	0.07	0.40	0.94
Kurtosis	-1.0	-0.01	0.47	-0.9	-0.4	-1.1	-0.6	0.01	3.67	-1.5	-0.3	0.63
CV%	0.33	0.27	0.16	0.35	0.27	0.18	0.23	0.24	0.34	0.69	0.59	0.60
Rich in $MgCl_2$												
Minimum	9.6	8.6	6.5	17.9	16.4	1.8	1.7	0.8	0.2	1.1	0.9	0.8
Mean	147	134	61.4	55.5	36.1	2.8	3.4	1.2	0.3	1.5	1.6	1.0
Median	75.8	130	58.4	42.8	39.1	3.1	3.0	1.1	0.3	1.4	1.5	1.0
Maximum	614	303	150	106	47.6	3.3	6.1	1.8	0.4	2.2	2.2	1.3
Standard Dev.	199	103	49.3	35.4	11.2	0.5	1.5	0.3	0.1	0.3	0.5	0.2
SE mean	70.6	39	18.6	12.5	4.2	0.2	0.5	0.1	0.0	0.1	0.2	0.1
Skewness	2.3	0.6	1.0	0.6	1.0	1.7	1.0	0.9	0.2	1.9	0.2	0.1
Kurtosis	5.6	-0.4	0.7	-1.4	0.1	2.6	0.3	0.1	-2.3	4.4	-0.7	-0.5
CV%	1.36	0.77	0.80	0.64	0.31	0.18	0.43	0.28	0.32	0.23	0.30	0.19
Rich in $MgSO_4$												
Minimum	35.8	7.8	5.5	27.7	15.9	1.4	2.6	0.9	0.2	1.1	0.9	0.6
Mean	286	101	48.6	30.5	28.7	2.3	4.0	1.1	0.2	1.4	1.3	0.8
Median	241	51.6	29.4	30.9	31.8	2.3	4.0	1.0	0.2	1.4	1.2	0.8
Maximum	616	294	130	34.9	35.2	3.2	6.4	1.4	0.3	1.9	1.9	1.0
Standard Dev.	188	131	56.9	2.4	8.7	0.9	1.1	0.2	0.0	0.2	0.5	0.2
SE mean	56.7	65.5	28.4	0.7	4.4	0.5	0.3	0.1	0.0	0.1	0.2	0.1
Skewness	0.5	1.8	1.5	0.5	1.7	0.0	1.1	1.7	1.7	0.7	0.4	0.4
Kurtosis	-0.8	3.3	2.1	-0.6	3.1	-5.7	1.6	3.3	3.3	0.6	2.5	1.6
CV%	0.66	1.29	1.17	0.08	0.30	0.41	0.28	0.20	0.16	0.16	0.36	0.20
Rich in Na_2SO_4												
Minimum	3.6	2.0	0.0	15.7	9.4	0.5	19.8	6.1	1.6	0.9	1.2	0.6
Mean	6.1	3.9	0.2	25.9	21.1	1.1	37.4	71.5	18.4	1.3	1.6	0.9
Median	6.7	3.0	0.3	26.0	20.7	1.1	40.8	32.8	9.4	1.3	1.6	0.9
Maximum	9.2	8.3	0.4	30.6	27.0	2.0	43.3	272	60.8	1.6	2.5	1.2
Standard Dev.	2.1	2.2	0.1	4.8	6.3	0.6	8.2	92.8	20.4	0.3	0.4	0.2
SE mean	0.7	0.8	0.0	1.7	2.4	0.2	2.9	35.1	7.7	0.1	0.2	0.1
Skewness	0.1	1.6	0.8	1.5	1.1	0.6	1.8	2.2	1.9	0.0	1.6	0.3
Kurtosis	-1.5	2.4	-0.2	2.9	1.1	-1.1	2.6	5.0	3.6	-2.3	3.5	-1.2
CV%	0.35	0.58	0.51	0.18	0.30	0.52	0.22	1.30	1.11	0.22	0.26	0.26

*SMC = soil moisture contents, + L = silty clay loam; LS = sandy loam; S = sand

4.3.2 Spectral variations

The reflectance spectra associated with the soil samples with different values of EC were statistically analyzed to quantify the spectral differences and establish a relationship between soil salinity and spectral similarity values. The spectral similarity measures (described in section 4.2.2) were applied only to the infrared portion of the spectra (1350 - 2350 nm), because reflectance of soils in this range of the electromagnetic spectrum is highly affected by variations in salt concentration in soils.

The correlation coefficients between values of EC and spectral similarity values vary differently with textures of the soil samples. This is due to the fact that the size and arrangement of the soil particles in relation to the soil air and water has an impact on soil reflectance (Bowers and Hanks 1965; Baumgardner et al., 1985). The results presented in Table 4.3 suggest that (a) variations in reflectance spectra of the soil samples treated with NaCl, KCl and Na2SO4 are influenced not only by variations in salt concentration but also by variations in texture and (b) variations in reflectance spectra of the soil samples treated with MgCl2 and MgSO4 are influenced mainly by variations in salt concentration and only very slightly by variations in texture.

Table 4.3: Correlation coefficients between values of EC and spectral similarity values of the soil samples treated with NaCl, KCl and Na_2SO_4.

Dominant salt in soil sample	Nr.	Soil texture	Deterministic methods				Stochastic methods		
			de	SAM	SSV	S_{ind}	SID	SID(TAN)	SID(SIN)
NaCl	17	L	0.85	0.73	0.85	-0.85	0.64	0.57	0.57
	10	SL	0.86	0.74	0.86	-0.86	0.79	0.79	0.79
	10	S	0.29	0.75	0.29	-0.67	0.73	0.72	0.72
KCl	16	L	0.68	0.72	0.68	-0.68	0.71	0.68	0.68
	8	SL	-0.26	-0.35	-0.26	0.26	-0.41	-0.32	-0.32
	8	S	0.39	0.87	0.40	-0.39	0.85	0.85	0.85
Na_2SO_4	8	L	0.73	0.004	0.73	-0.73	-0.02	-0.005	0.004
	7	SL	-0.47	-0.30	-0.47	0.47	-0.30	-0.30	0.04
	7	S	0.50	0.69	0.50	-0.50	0.69	0.54	0.54

L, LS and S represent silty clay loam, sandy loam and sandy texture, respectively. S_{ind} = Similarity index, Nr. = number of sample

The slight influence of texture on variations of correlation coefficients between values of EC and spectral similarity values of the soil samples treated with $MgCl_2$ and $MgSO_4$ was further verified by combining the subsets of spectral similarity values according to texture into one set of spectral similarity values for the soil samples treated with $MgCl_2$ and one set of spectral similarity values for the soil samples treated with $MgSO_4$. Combining the subsets of spectral similarity values into one set of spectral similarity values was achieved by standardizing the data using the formula (Webster and Oliver, 1990; Yemefack et al., 2005):

$$S'_s = \left(\frac{S_{sj}}{\overline{S}_s} \right) \overline{S} \qquad [12]$$

where S'_s is the standardized spectral similarity value for sample s, S_{sj} is the original spectral similarity value for sample s in data subset j; $\overline{S}_j$ is the mean of original spectral similarity values of samples in data subset j; and $\overline{S}$ is the mean of original spectral similarity values in the whole data set. The correlation coefficient between values of EC and standardized spectral similarity values was then calculated. Table 4.4 shows that the correlation coefficients between values of EC and standardized spectral similarity values for soil samples treated with $MgCl_2$ and $MgSO_4$ are still high rather than becoming low as would be expected due to combination of data from the different subsets. This verifies the interpretation above that variation in reflectance spectra of the soil samples treated with $MgCl_2$ and $MgSO_4$ are influenced mainly by salt concentration and only slightly by soil texture. This interpretation is further supported by scatter plots shown in Figure 4.2, in which all soil samples treated with either $MgCl_2$ or $MgSO_4$ show better linear relationships between values of EC and spectral similarity values, whereas subsets of soil samples with silty clay loam texture and treated with either NaCl, KCl or Na_2SO_4 show poor linear relationships between values of EC and spectral similarity values.

Table 4.4: Correlation coefficients between values of EC and spectral similarity values for soil samples treated with $MgCl_2$ and $MgSO_4$.

Dominant salt in soil samples	**Nr.**	**Deterministic methods**				**Stochastic methods**		
		de	**SAM**	**SSV**	**S_{ind}**	**SID**	**SID(TAN)**	**SID(SIN)**
$MgCl_2$	22	0.92	0.92	0.91	-0.89	0.90	0.90	0.90
$MgSO_4$	19	0.74	0.90	0.74	-0.72	0.93	0.92	0.92

S_{ind} = Similarity index, Nr. = number of sample

The results shown in Table 4.4 indicate that spectral similarity values for the soil samples treated either $MgCl_2$ or $MgSO_4$ decrease as the concentrations of either of these salts increase. The strong correlations between values of EC with values of d_e, SAM and SSV indicate that the absolute reflectance, the shape of spectra and the combination of absolute reflectance and shape of spectra are strongly influenced by concentrations of either $MgCl_2$ or $MgSO_4$ in the soil samples. The results further suggest that, in the case of soils affected by either $MgCl_2$ or $MgSO_4$, the different spectral similarity values are useful for spectral classification of varying degrees of soil salinity due to either of these salts.

In the case of soils affected by NaCl, KCl or Na_2SO_4, the usefulness of the different spectral similarity measures for remote sensing of varying degrees of soil salinity due to either of these salts is limited by variations in soil texture. However, further analysis of the results for soil samples treated with NaCl, KCl or Na_2SO_4 suggests which properties of reflectance spectra could be useful in spectral discrimination of varying degrees of soil salinity due to either of these salts. For example, there is moderate to strong correlation between values of EC and spectral similarity values for soil samples with silty clay loam and sandy loam textures and treated with NaCl and KCl (Table 4.3). This suggests that, for NaCl- and KCl-affected soils with silty clay loam and sandy loam textures, shape and magnitude of reflectance spectra can be useful in spectral differentiation of varying degrees of soil salinity. As another example, there is significant correlation between values of EC and values of SAM and stochastic similarity measures for soil samples with sandy texture and treated with NaCl and KCl (Table 4.3). This suggests that, for NaCl- and KCl-affected soils with sandy texture, shape of reflectance spectra can be useful in spectral differentiation of varying degrees of soil salinity. For soil samples treated with Na_2SO_4, however, the results are inconclusive. In general, the results for soil samples treated with NaCl, KCl or Na_2SO_4 indicate that there are no clear relationships between spectral similarity values and values of EC. This suggests, in general, that for soils affected by NaCl, KCl or Na_2SO_4, reflectance spectra have limited usefulness in spectral discrimination of varying degrees of soil salinity.

4.3.2.1 Correlation of spectral similarity values

Figure 4.3 shows scatter plots of similarity values obtained by the deterministic and the stochastic techniques for each reflectance spectra of individual salt-affected soil samples as compared to the reflectance spectra of a non-saline soil sample. There is high correlation among spectral similarity values obtained using the three stochastic techniques (SID(SIN), SID(TAN), SID). The correlation between d_e values and SSV values is very high, whereas the correlation between SAM values and SSV values is relatively lower. Considering that d_e is based on

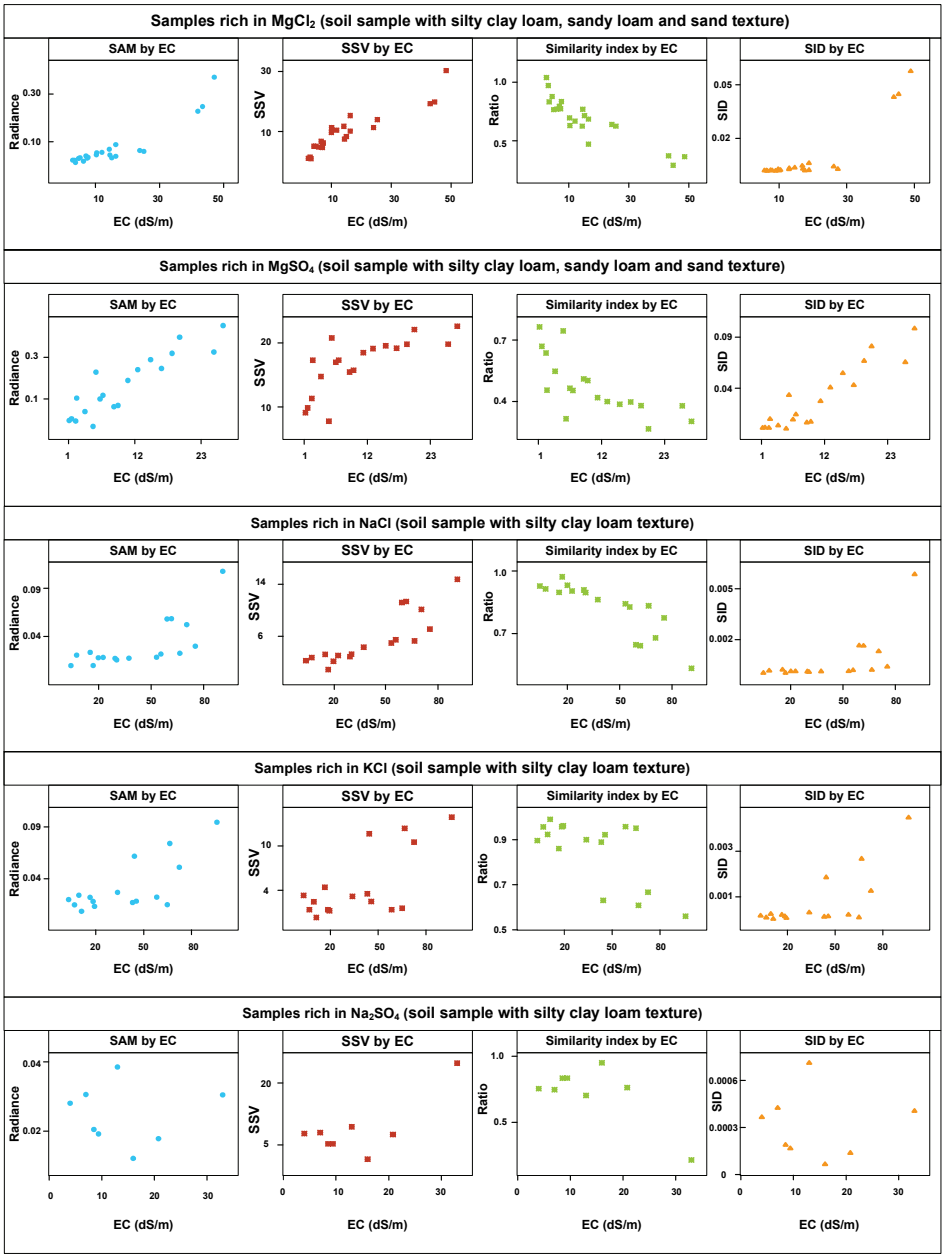

Figure 4.2: Scatter plots between values of spectral similarity and values of EC of the different sets of salt-affected soil samples. The Correlation coefficients for each plot is given in Table 4.3 and 44.

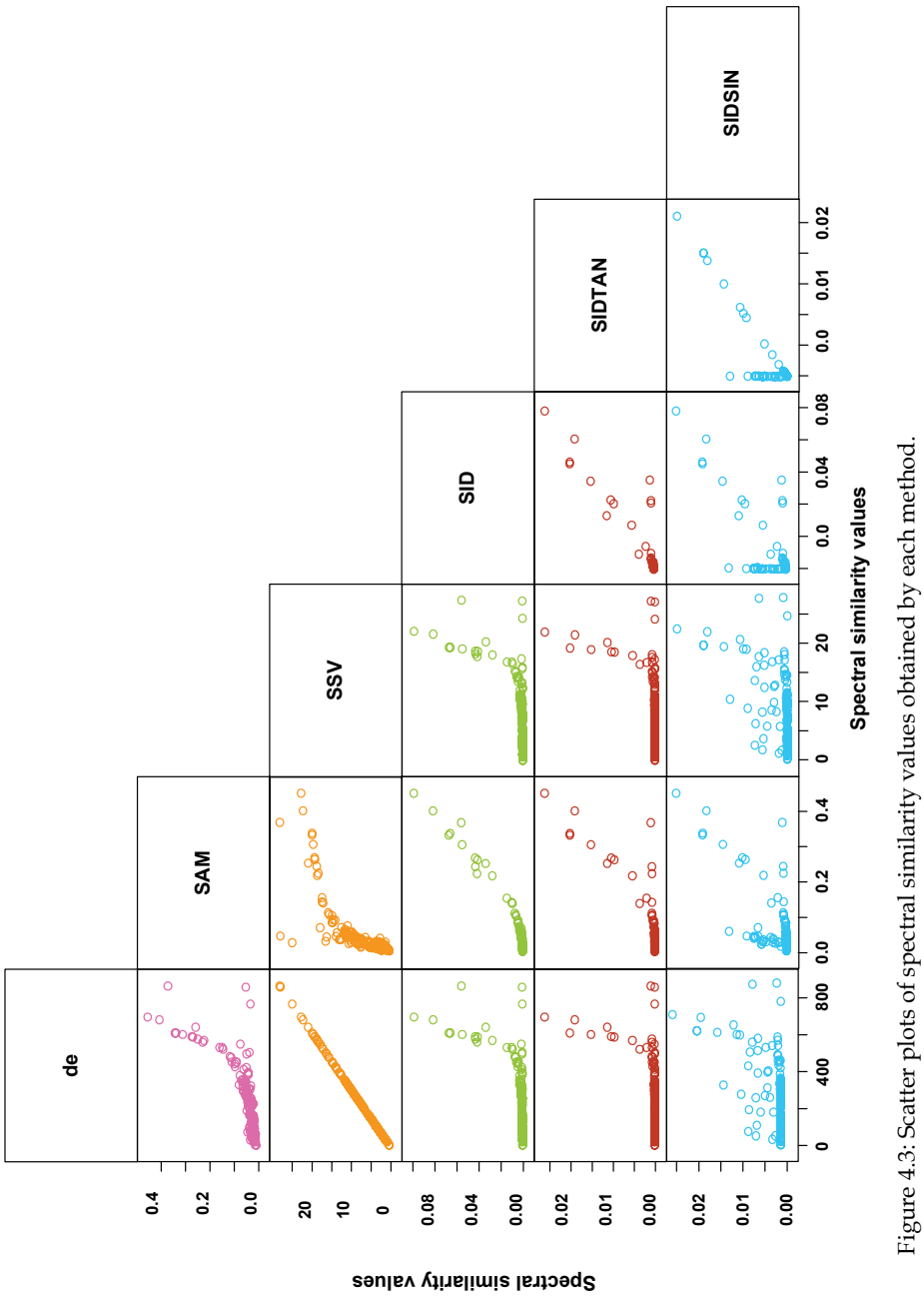

Figure 4.3: Scatter plots of spectral similarity values obtained by each method.

absolute reflectance, SAM is based on spectral angle, and SSV is combination of de and SAM, the lower correlation between SAM values and SSV values as compared to the correlation between de values and SSV values indicates that SSV values are influenced more by absolute reflectance than by spectral angle. The scatter plots also show that SAM values have high correlation with similarity values obtained by the three stochastic techniques, whereas de and SSV values have poor correlations with similarity values obtained by the three stochastic techniques. This signifies that similarity values obtained by the three stochastic techniques are strongly influenced by spectral angle rather than by magnitude of reflected energy.

4.3.4.4 Numerical classification of spectral similarity values

The spectral similarity values were input to the Wards method of hierarchical numerical classification to determine classes of various levels of similarities and whether the obtained classes are meaningful in terms of levels of soil salinity. Figure 4.4 shows the dendrograms based on similarity values of reflectance spectra of all soil samples treated with $MgCl_2$ and with $MgSO_4$ solutions. The initial two classes at the highest levels of each dendrogram are further subdivided into multiple groups at the succeeding levels as the similarity values increases (i.e., the dissimilarity among spectra decreases). The generated five groups at the third level (the EC of each soil sample is shown at the bottom of the dendrograms) suggest the possibility of classifying the quantified spectral similarity values into soil salinity classes that correspond with the classes defined by US salinity laboratory (Richards, 1954). In other words, the induced spectral variations due to salt concentrations are sufficient enough to generate clusters that are in agreement with international standard salinity classes.

Figure 4.5 shows the dendrograms based on similarity values of reflectance spectra of soil samples with silty clay loam texture and sub-irrigated with NaCl and KCl solutions. The two classes at the highest level of the dendrograms are subdivided at the next level with multiple subdivisions within the subclasses. Based on the EC of each soil sample (shown at the bottom of the dendrograms), the three classes at the second level have poor agreement with soil salinity classes as defined by Richards (1954). For example, the EC of soil samples treated with NaCl in the class 1a ranges between 4.4 and 30.5 dS/m, whereas EC of soil samples treated with KCl ranges between 3.2 to 45.6 (dS/m). However, despite of the poor classifications, the spectral similarity values have relatively good correlation with the EC values of soil samples with silty clay loam textures (Table 4.3). This suggests that discrimination (or classification) of salt-affected soils based on their reflectance spectra can be potentially improved due to strong correlation between soil EC and other spectral characteristics such as reflected energy (albedo) and absorption features parameters.

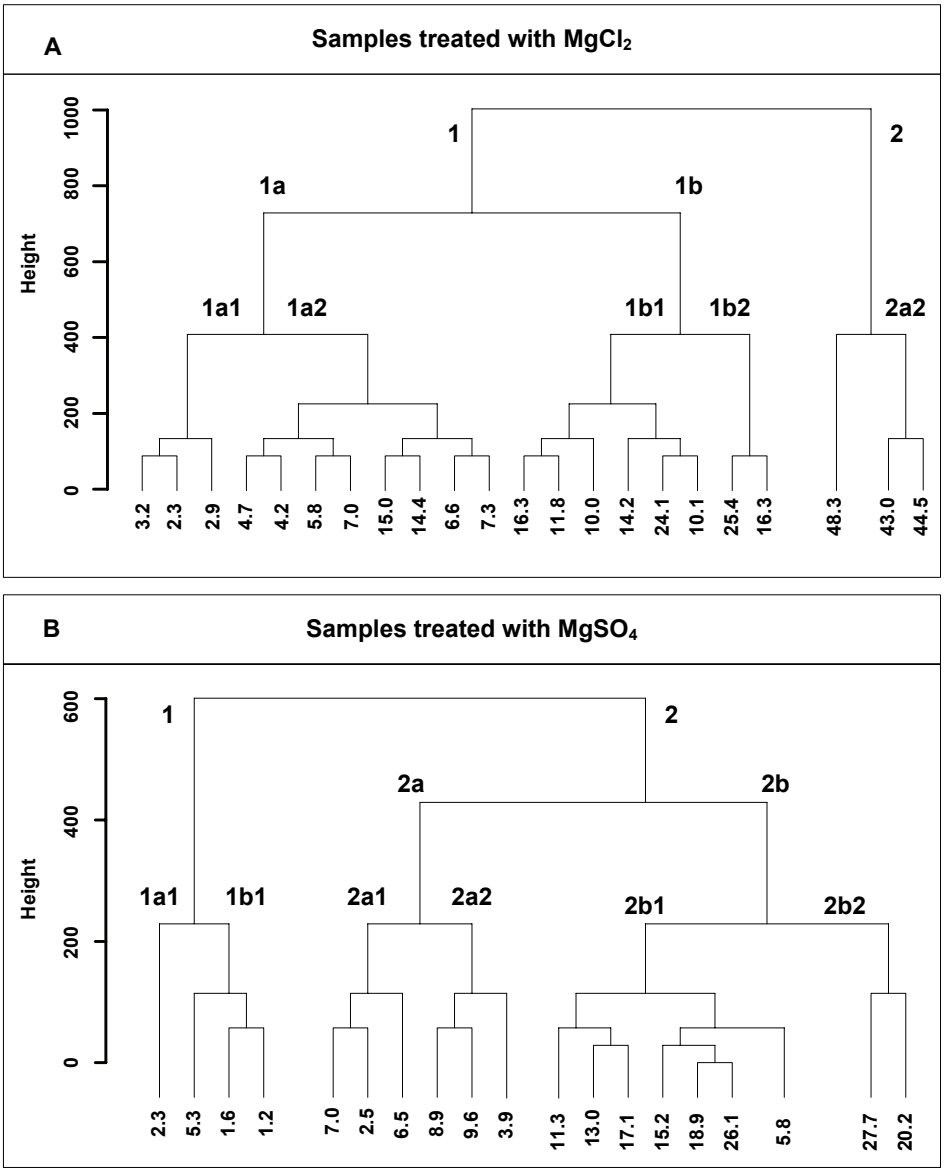

Figure 4.4: Dendrograms indicating salinity classes based on similarity values obtained by using the six spectral matching techniques on the reflectance spectra of soil samples (silty clay loam, sandy loam and sand texture) treated with $MgCl_2$ (5-A) and $MgSO_4$ (5-B) solutions. The values at the bottom of the dendrograms represent EC of soil samples at the time of spectral measurements.

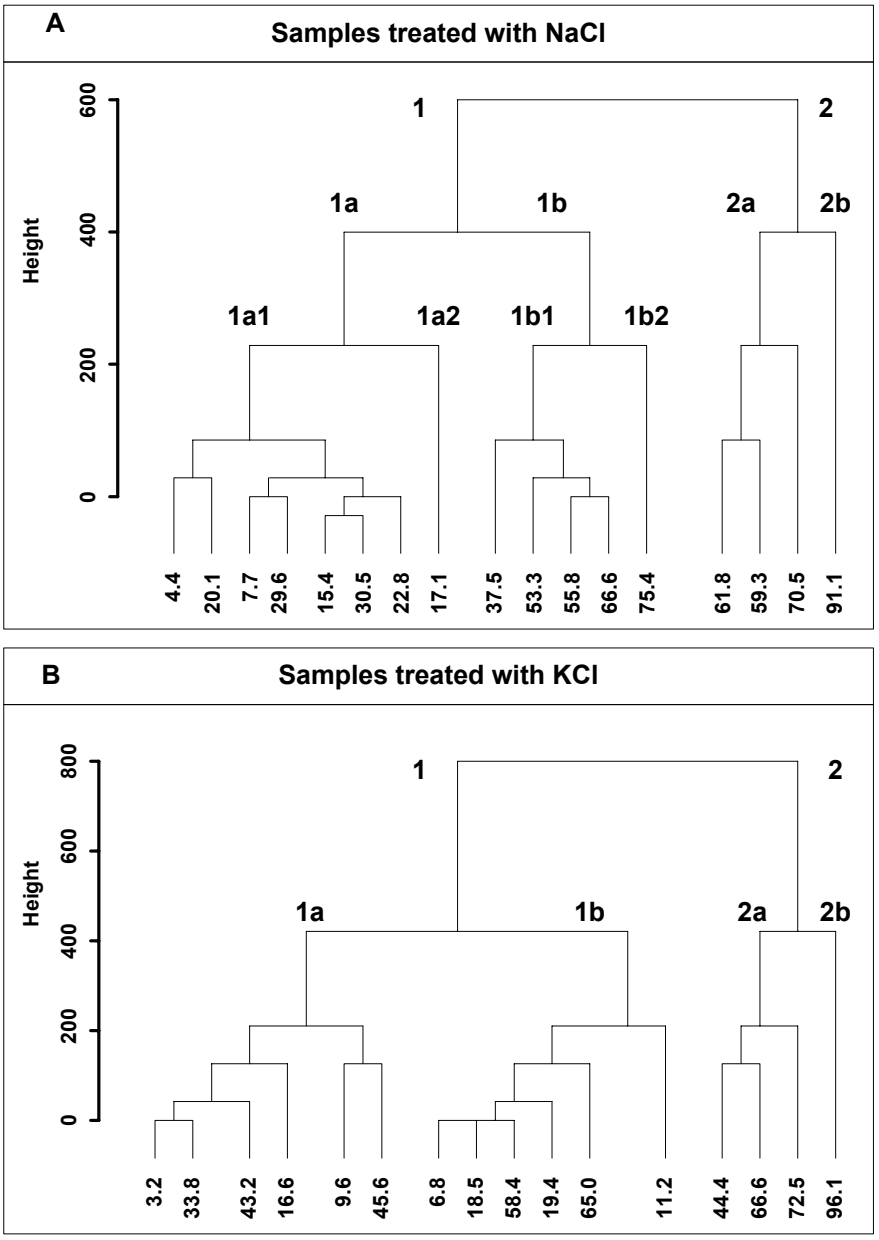

Figure 4.5: Dendrograms indicating salinity classes based on similarity values obtained by using the six spectral matching techniques on the reflectance spectra of soil samples with silty clay loam texture and sub-irrigated with NaCl (5-A) and KCl (5-B) solutions. The values at the bottom of the dendrograms represent EC of soil samples at the time of spectral measurements.

4.3.5 Statistical differences

Following the international standard salinity classes (Richards, 1954), the spectral reflectance data for the soil-affected soil samples were classified according to ranges of EC as > 4, 4 - 8, 8 – 16, 16 – 32 and > 32 dS/m. The classes of spectral reflectance data for the salt-affected soil samples are then used in the U-test. The spectral reflectance data for soil samples treated with $MgCl_2$ and $MgSO_4$ are selected to illustrate statistical comparison between spectral reflectance data divided according to the international standard salinity classes. The results of this test indicate whether the spectral reflectances of the salt-affected soil samples are significantly different or similar between the salinity classes.

There are five classes of $MgCl_2$-treated soil samples and four classes of $MgSO_4$-treated soil samples. Figures 4.6a and 4.6b show the median spectra for each salinity class of the soil samples treated with $MgCl_2$ and $MgSO_4$, respectively. The median spectra shows that spectral features at around 1400 and 1900 nm become broader while spectral features at around 2204 nm are degraded as soil salinity increases. The median spectra also show decrease in albedo, especially further than 1350 nm, as soil EC increases.

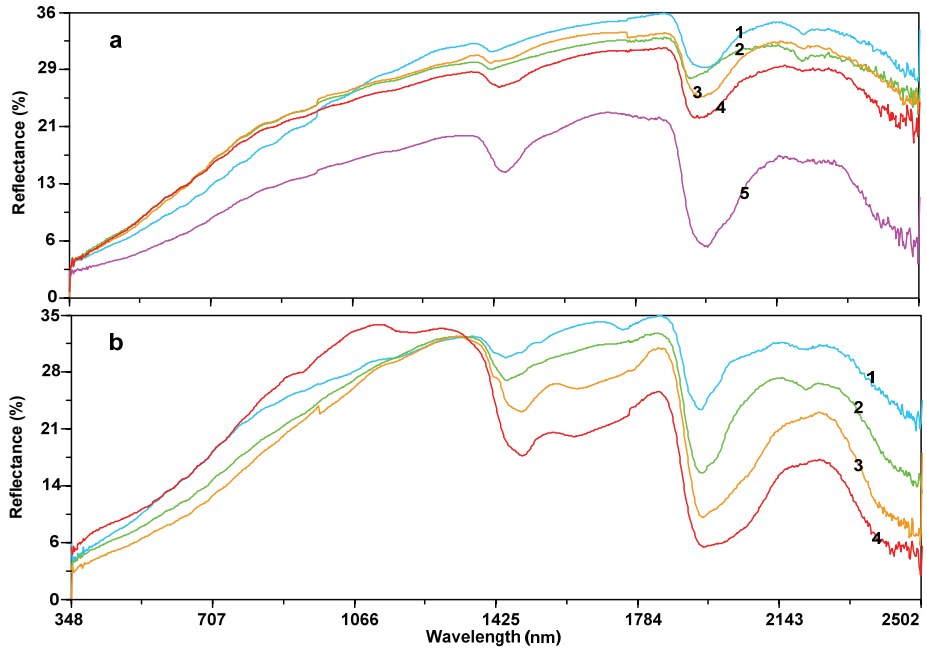

Figure 4.6: The median spectra of each salinity class of the soil samples treated with (a) $MgCl_2$ and (b) $MgSO_4$. The number on each curve represents a salinity class (1 = < 4 dS/m; 2 = 4 - 8 dS/m; 3 = 8 - 16 dS/m; 4 = 16 - 32 dS/m; 5 = > 32 dS/m).

To statistically test the null hypothesis (see section 4.2.3.2), 16 pairs of classes of spectral reflectance data (10 pairs for the $MgCl_2$-treated soil samples and six pairs for the $MgSO_4$-treated soil samples) were used in the U-test. The results indicate that the significance levels for the U-tests are mostly less than 0.02 and are less than the critical level of $\alpha = 0.05$. This means that the spectral reflectances of the salt-affected soil samples are significantly different between the salinity classes.

Figures 4.7a and 4.8a illustrate the results of the U-test for all possible pairs of classes of reflectance data of the salt-affected soil samples. Each figure shows grey areas representing frequency plots of salinity class pairs with significant difference in reflectance per band in the wavelength range of 350 - 2500 nm. In general, bands that maximise the discrimination between salinity classes are located in near (NIR) and shortwave infrared (SWIR) regions of the spectrum. The continuum removed of median reflectance spectra of severely salt-affected samples (i.e., high EC values) are shown on the frequency plot in order to visualize the position of the spectral features in relation to significant differences in reflectance occurring at every band.

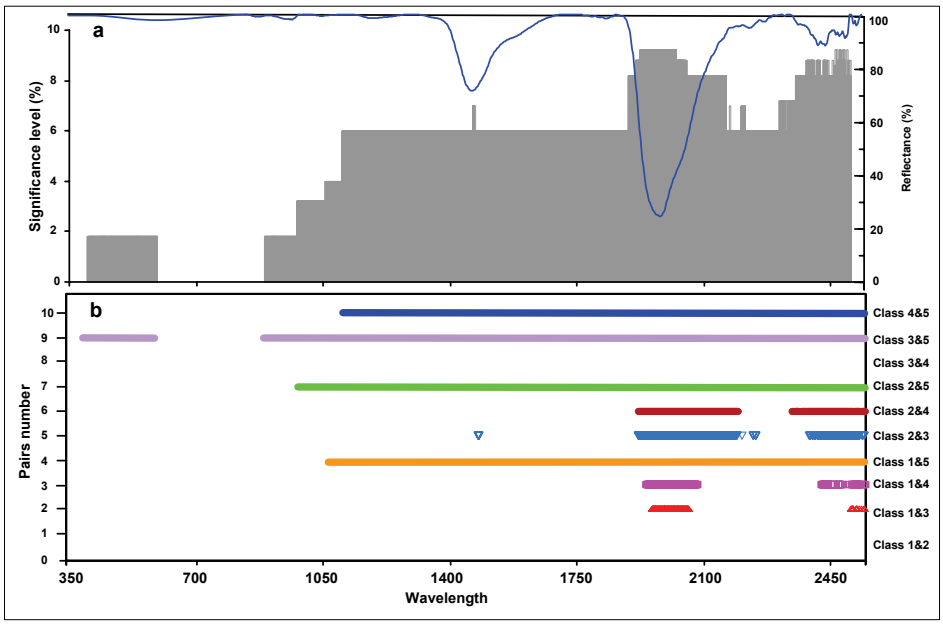

Figure 4.7: (a) Frequency plot of significant difference in reflectance per wavelength band for MgCl2-rich soil samples subjected to the U-test at critical significance level of $\alpha = 0.05$. The grey areas indicate the wavelength regions where two classes of reflectance data are significantly different $\alpha = 0.05$. (b) Waveband positions where classes of reflectance data are significantly different. (Classes = soil salinity class: 1 = < 4 dS/m; 2 = 4 - 8 dS/m; 3 = 8 - 16 dS/m; 4 = 16 - 32 dS/m; 5 = > 32 dS/m).

Figure 4.7b and 4.8b show the waveband positions where reflectance data for the different salinity classes are significantly different. For example, at around 1900 nm, eight pairs (out of a possible 10) of classes of reflectance data are significantly different. The significant differences in reflectance of the salt-affected soil samples in the salinity classes do not cover the same number of wavebands and occur at different wavelength positions. The variations in reflectance of soil samples with slight to moderate salinities are small and are mostly not significantly different per waveband in the VIS region. Therefore, in Figure 4.7a, the grey areas illustrated in the VIS regions are only due to the significant differences in reflectance of soil samples in class 3 and class 5.

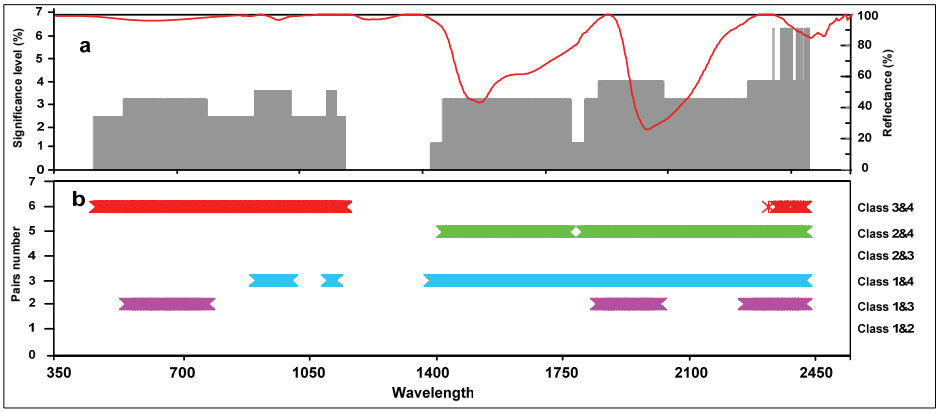

Figure 4.8: (a) Frequency plot of significant difference in reflectance per waveband for samples rich in $MgSO_4$. (b) The waveband positions where classes of reflectance are significantly different according to U-test at $\alpha = 0.05$. (Classes = soil salinity class: 1 = < 4 dS/m; 2 = 4 - 8 dS/m; 3 = 8 - 16 dS/m; 4 = 16 - 32 dS/m; 5 = > 32 dS/m).

4.4 Discussion

In the previous sections, variations in reflectance spectra responses of soils with different salt concentrations have been studied in detail by comparing spectral similarity values obtained from a series of the soil samples with various EC. Spectral matching techniques and a numerical classification technique were used to quantify spectral variations and determine statistical differences between the salinity classes. The Mann Whitney U-test was used to examine whether the spectral variations between the salinity classes were statistically significant.

Comprehensive analysis of the VIS, NIR and SWIR regions of reflectance spectra of the salt-affected soil samples, using spectral matching techniques, indicates significance differences in reflectance magnitude, absorption strength

and spectral angle. Although at the first sight it seems that the two types of spectral matching techniques (deterministic and stochastic) produced similar results, a number of differences can be highlighted by zooming in the data (Tables 4.2 and 4.3). For example, the results derived from stochastic techniques are influenced only by shape of the spectra and not by absolute reflectance. Therefore, there is a good match between results obtained from SAM (a deterministic technique) and the results derived from spectral information divergence (SID), SID (TAN) and SID (SIN). Furthermore, the values obtained from SID (TAN) and SID (SIN) are, in general, lower than the values obtained by SID and the values obtained by the deterministic techniques. However, the advantages are with the deterministic techniques, since any similarity or dissimilarity concerning absolute reflectance, spectral angle or combinations are taken into account.

The spectral matching data (Tables 4.2 and 4.3) show significant correlation between soil EC and spectral similarity measures, meaning that spectral similarity between the samples changes accordingly to the salt concentration in soil. The results also show that, salt type and soil texture influence the variations in correlation between values of EC and values of spectral similarity (Table 4.3). For example, for the same type of texture, the soil samples treated with $MgCl_2$ and $MgSO_4$ produced spectral responses that are highly dissimilar to the spectra of a non-saline soil sample, whereas the contrary is observed for the samples treated with KCl, NaCl, and Na_2SO_4. The effect of soil texture is pronounced in correlation coefficients presented in Table 4.3. The results show, for example, different spectral responses of the soil samples treated with KCl due to the soil textures. The susceptibility of soil to injury by exchangeable sodium is related to total surface area (external and internal) which is a function of soil texture and type of clay minerals (Richards, 1954). For example, the coarse-textured soils with dominate kaolinite clay mineral is less affected by excessive exchangeable sodium than fine-textured soil with dominate montmorillonite. The results, however, suggest that further analysis is required to determine how much of variation in soil reflectance spectra is due to soil texture.

The values obtained from the different spectral matching techniques were used to determine their potential in soil salinity classification and whether variations in derived classes are sufficient to provide bases for aggregation in classes that are in agreement with standard international salinity classes. The hierarchical classification of spectral similarity values show that, depending on type of salt that affect soils, derived soil salinity classes are in either good or poor correspondence with international soil salinity classes based on values of EC. This means that spectral similarity values can be potentially useful in saline soil classification but with relative degrees of success depending on type of salts.

The results of the Mann-Whitney U-test (Table 4.4) indicate that 90 percent of all possible pairs of soil salinity classes have statistically different spectra in the wavelength range between 350 – 2500 nm. The results of the U-test also indicates further that, wavelengths greater than 1900 nm provide crucial spectral information that can be used to discriminate between salinity classes. The contribution of spectral information derived from the VIS region of the saline samples spectra is minor.

The results of this study based on laboratory spectral data can not be fully employed yet considering up-scaling to image spectra. In general, the resolving capacity of many air-borne and space-borne remote sensing data is insufficient to resolve some of the spectral features found in laboratory spectral data. This is due to a combination of factors such as wider bandwidth, spatial resolution and atmospheric effect. For example, most of the spectral features at around 1400 and 1900 nm, which are crucial in discrimination of salt-affected soils, would not be available in image data due to the effect of atmospheric water absorption windows. Using air-borne hyperspectral imageries, perhaps the general spectrum shape is an effective alternative for classification of saline soils. The issues highlighted here call the attention for further investigations both on the technological advances to improve the resolving capacity of optical remote sensing sensors and on applications to develops methods that facilitate robust integration between laboratory and image spectra.

The studies presented here to determine relationships between reflected spectra and salinity of soils generally fall within the univariate approaches. However, the results have implication to move further on to multivariate approaches. For example, the results of the Mann-Whitney U-tests imply that a number of wavelength bands in NIR and SWIR regions of the measured reflectance spectra could be useful in estimation of degree of soil salinity. A possible multivariate approach to test this implication is through partial least squares regression, which is now gaining extensive applications to integrate chemometics and spectrometry (Rossel, et al., 2005; Hansen and Schjoerring, 2003; Galera, et al., 1996). Other multivariate approaches e.g., neural networks may also yield promising results.

4.5 Conclusions

The results of this study show that high spectral resolution laboratory data provides opportunities for spectral analysis and characterization of salts abundance in soil. The research provides insight and better understanding of soil spectral response due to salt variations to eventually improve capability of classification algorithms with regard to discrimination of the saline areas.

The results confirm that spectral similarity measures can be used as diagnostic indicators to differentiate among salt-affected soils spectra, since absolute reflectance, absorption strength and spectral angle proportionally vary with salt concentrations in soils. Comparison between results of deterministic and stochastic spectral matching techniques shows that the deterministic techniques are advantageous, because all the spectral aspects causing variations contribute in the calculated similarity values.

The results of hierarchical numerical classification method applied to spectral similarity values confirm that the spectral variations in salt-affected soils are sufficient to provide bases for aggregation in classes that are in agreement with standard international salinity classes as defined by US salinity laboratory.

The results of the Mann-Whitney U-test show that the differences between the reflectance spectra associated with the observed salinity classes are statistically significant. The results confirm that wavelengths in the NIR and SWIR regions contain the most crucial information and can be used to as a guideline to select diagnostic wavebands to discriminate between salinity classes based on spectral reflectance.

The established spectral parameters in laboratory data cannot be fully employed considering up-scaling to image spectra. This calls the attention for further investigations to improve sensor capabilities and to develop new approaches of data integration of various sources.

Chapter 5

Interference of salt and moisture on soil reflectance *

Abstract

This paper presents an approach to investigate the relation between soil salt and moisture contents through modelling of soil spectra using an inverted Gaussian function. The approach is tested on experimental and field data of soil physico-chemical properties and their spectral reflectance. The experimental data were obtained under laboratory controlled conditions, where soil samples with various degrees of salinity were prepared and then their properties such as spectral reflectance, electrical conductivity and moisture content were measured. The field data were measured in-situ at regularly-spaced grids in an area in northeast Thailand known to be affected by salinization and high groundwater level. The SWIR region of the experimental and field soil spectra were then fitted with an inverted Gaussian function. Parameters of the fitted curve such as functional depth, distance to the inflection point and area were

* This chapter is based on:

Farifteh, J., Tolpekin, V., Van der Meer, F., Sukchan, S. (2006d). Salinity modelling by inverted Gaussian parameters of soil reflectance spectra. Under review, *International Journal of Applied Earth Observation and Geoinformation*.

used as predictors in a regression analysis to predict soil moisture contents and salinity levels. Estimation of salinity levels was successful using experimental measurements for samples rich in $MgCl_2$ and $MgSO_4$ but not for NaCl. Amongst the calculated inverted Gaussian parameters, the area under the fitted curve provided the most accurate estimations. The results demonstrate the relative utility of high spectral resolution data for salinity studies of experimental data. The poor estimation of soil moisture and soil salinity using the field data confirmed that combination of salts and moisture in soil cause anomalies and therefore, variations neither in salt nor in moisture contents can be modelled accurately on the basis of quantification of soil reflectance alone.

Key word: soil salinity, soil moisture content, Gaussian function, remote sensing, hyperspectral, soil reflectance

5.1 Introduction

Quantification of salt variations in soil using hyperspectral data is challenging, since most of the spectral features that are diagnostic of salt minerals or salt-affected soils are masked due to atmospheric effect (Farifteh et al., 2005b) and because of significant variability of other soil chemical and physical properties (Irons et al., 1989; Ben-Dor, et al., 1999). Soil is a complex mixture of inorganic solids consisting primarily of crystalline minerals and noncrystalline substances, organic matter, air, and water or a solution containing a variety of dissolved compounds (Jackson et al., 1986; Irons et al., 1989). Therefore, soil reflectance is influenced by the inherent scattering and absorption properties of these components and their size and arrangement in relation to the soil, air and water (Liu, et al., 2002). However, salt and moisture as a soil component will thus influence the soil reflectance along with other characteristics such as physical structure and observation conditions (Epema, 1993; De Jong 1992; Irons et al., 1989; Musick and Pelletier, 1988; Baumgardner et al., 1985; Stoner and Baumgardner, 1981).

The effect of variations in soil chemical and physical properties on soil spectra can be minimized under controlled laboratory conditions and thus, the influence of salt contents on soil reflectance can be determined (Farifteh et al., 2006a, b). Laboratory study of salt-affected soil spectra showed that an increase in soil salinity induces changes in soil reflectance which, in many ways, are similar to the spectra of soils with various moisture contents. The results reported by Farifteh et al. (2006b) suggests substantial similarity with what has been reported by Whiting et al. (2004) for soil with various moisture contents. The similarities between the effects of salt and water on soil spectra show the need for further research.

One of the most frequently used functions in predicting soil moisture is the inverted Gaussian (IG), which has large potential application in discrimination of soil moisture contents and might have similar application in predicting soil salinity level. In a number of literatures, successful applications of Gaussian functions in modelling absorption bands have been addressed. Miller et al. (1990) found IG reflectance model to be an effective quantitative representation of the shape and position of the vegetation red edge reflectance. Most recently, Whiting et al. (2004) estimated soil moisture content (SMC) through fitting an IG function to a continuum removed soil spectra in the SWIR region. There are many more examples in which the IG method was used as a quantitative tool to analyze reflectance spectra (Schlerf et al., 2005; Liu et al., 2002; Sunshine et al., 1990; Roush and Singer, 1986; Clark 1981; McCord et al., 1981; Smith and Strens, 1976). In this study fitting an IG curve to salt-affected soils spectra was applied since it has the advantages of using the general shape of spectrum and is independent from diagnostic absorption bands and their parameters. In addition, since it has been successfully used for estimation of moisture, it has the potential to demonstrate the effect of SMC on estimation of salt and vice versa.

The objective of this chapter is to investigate the potential of IG function in quantification of salts variations in soil and to demonstrate whether estimations of SMC are influenced by presence of soil salt content (SSC) and vice versa. To achieve this aim, two sets of data were collected. The first data set was obtained under controlled laboratory measurements (see chapter 3) where salt amount in soil samples are varied while other soil constitutes including soil moisture were almost similar. This data set was used to show whether the IG algorithm can be used to quantify and predict salinity from soil reflectance spectra. The second data set is the result of in-situ field measurement where, in general, topsoil was roughly similar but salt and moisture were varied independently. This data set is used to demonstrate whether quantifications and estimations of soil salt contents under field conditions where salt and moisture coexists, using the same algorithm, is feasible.

5.1.1 Test areas

The data used in this study were collected from three different areas. The soil samples used in a laboratory experiment were collected from the island of Texel in the northwest of The Netherlands and Hajdunanas area in northeast Hungary. The site where in-situ soil and reflectance data were collected is located in northeast Thailand (see chapter 1, Figure 5.1). The details of the test areas are given in chapter 1.

From field observations, two representative grid areas (grids 1 and 6) were selected due to similarity in soil textures and variations in salts and moisture

contents. For example, data from grid 1 do not show any trend with neither salts nor SMC, meaning that the measurements obtained from points with various salts and moisture. Whereas, the data from grid 6 suggests strong positive correlation with both soil salt and SMC, indicating points with low salt contents have also less moisture. The detailed characteristics of the two data sets are discussed in the following sections of this chapter.

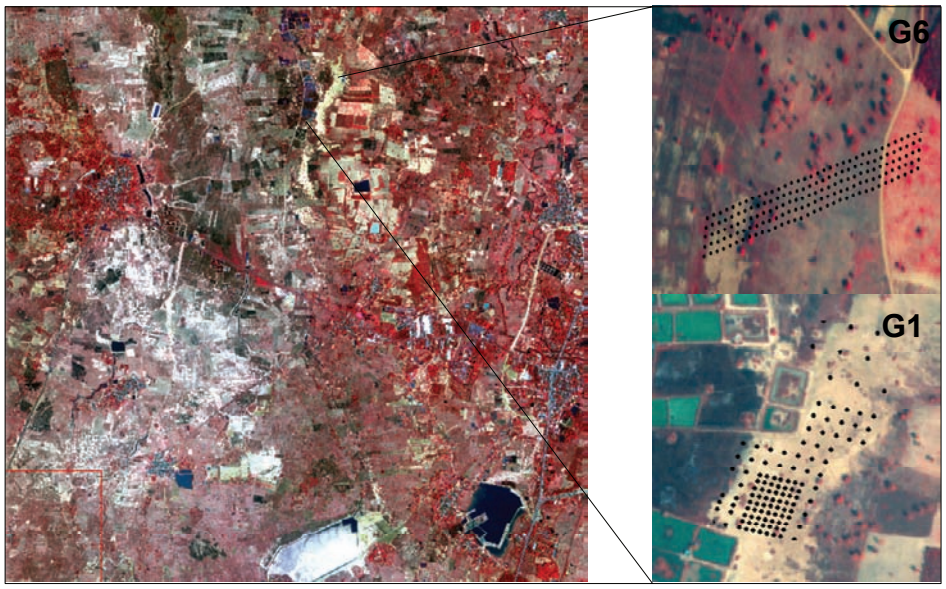

Figure 5.1: The Location of the grid areas in NE Thailand on a Quick-bird image. As it can be seen from grid 1 (G1), several large water bodies are at west side of the area which highly affect the soil moisture contents. The moisture variations in the area are influenced by texture of soil profile and surface morphology.

5.2 Methods and materials

5.2.1 Data acquisition

5.2.1.1 Experimental measurements

Experimental data were obtained in laboratory, where salt concentrations in a number of soil samples were changed by sub-irrigating them with prepared saline water of various densities using different technical salt grades (halite, bischofite and epsomite) and distilled water (see chapter 2). The samples were then dried at room temperature and then spectral reflectance and soil properties such as pH, electrical conductivity ($EC_{1:2}$), exchangeable cations and moisture

content were measured by known laboratory methods. A portable ASD FieldSpec FR spectrometer was employed for reflectance measurements. The detailed procedure of the setting and measurements is described in chapter 2.

5.2.1.2 Field measurements

In the field, soil physico-chemical properties were measured for 302 observation points. The measurements were carried out within two grid areas (size of approximately 340 x 100 m.), at intervals of 5, 10, 20 and 40 meters. At each observation point, soil moisture contents and soil apparent electrical conductivity (EC_a) at vertical (EC_{av}) and horizontal (EC_{vh}) dipole were measured simultaneously along with soil reflectance.

The soil moisture was measured using the Thetaprobe sensor. The instrument measures the soil moisture volume percentage by applying the Frequency Domain technique (FDR) means measuring changes in the dielectric constant (Eijkelkamp, 2005). It has an accuracy of 5% with standard calibration and the range of measurements varies between 5 - 55 volumetric moisture content.

Soil apparent conductivity was measured at 539 points (at intervals of 5 and 10 m) by EM-38, which is a geophysical exploration equipment that works on the basis of electromagnetic induction principle and designed to have several applications including mapping terrain conductivity. The instrument makes use of the response of ground to the propagation of electromagnetic fields, which are composed of an alternating electric intensity and magnetizing force (Kearey and Brooks, 1994). It offers rapid surveys made by placing the instrument on the ground and recording the meter reading in horizontal dipole and vertical dipole providing depths of exploration of 1.5 m and 0.75 m, respectively. The depths are based upon the orientation (vertical vs. horizontal), height, and spacing of the source electrical coils (Doerge et al., 2002). Disturbances/anomalies can be expected due to the presence of metals, power lines, etc. However, in order to obtain useful data, field-specific calibration is necessary (Hartsock et al., 2000), which may be possible at large scale, for instance at field parcel level.

The field spectra were obtained in the range between 350 – 2500 nm using ASD FieldSpec FR spectrometer and contact probe with 25^o field of view.

In order to validate and calibrate the in-situ field measurements, 121 soil samples were collected from a selected number of observation points in each grid. These samples were collected from depth 0-10 cm and from a reprehensive spot at each grids one soil sample was collected at four depths (0 - 20, 20 - 40, 60 - 80 and 120 -140 cm). Laboratory facilities in LDD in Thailand were used to

obtain validation and calibration data of physico-chemical properties of the 121 soil samples following the standard laboratory methods (Van Reeuwijk, 1993).

5.2.2 Modelling salt and moisture variations

5.2.2.1 Application of IG function

Absorption features observed in visible and near-infrared spectra are usually considered to be inherently Gaussian-like in shape and can be modelled with the Gaussian function (Clark and Roush, 1984). The IG function to represent spectral shape of an absorption band is defined as (Miller et al., 1990):

$$R(\lambda) = R_s + (R_0 - R_s)\exp\left(\frac{-(\lambda_0 - \lambda)^2}{2\sigma^2}\right) \quad [1]$$

where R_s is the maximum reflectance, R_0 is the minimum reflectance, λ_0 is the central minimum or peak position wavelength, λ is wavelength and σ is the Gaussian function deviation parameter describing the width of the Gaussian peak. The IG function can be fitted to different portion of spectra, where most spectral variations occur, by connecting the maximum reflectance wavelength to the function centres. Whitting et al. (2004) used the fundamental water absorption band at 2800 nm as the function centre based on the evidence given in Bishop et al. (1994) and Liu et al (2002). This peak position is beyond the range of the 'FieldSpec FR' spectrometer and therefore a fitting algorithm is needed to extrapolate the IG function to this point.

For this study, the fundamental water absorption band at 2800 nm was also used as the functional centre, since most salt minerals (e.g., hydroxyl group) exhibit a strong sharp band in the region 3650 - 3700 cm^{-1} (near 2750 nm) depending on what the OH is directly attached to, and where it is located in the mineral. The water of hydration usually exhibits a strong sharp band near 3600 cm^{-1} and one or more near 3400 cm^{-1} (see details in chapter 1). Water adsorbed by clay minerals and organic matter on soil surface areas (hygroscopic) and the free water influence the soil albedo due to the fact that the medium surrounding the particles changes from air to water (Ishida et al., 1991).

5.2.2.2 Model requirements

The parameters needed to estimate salt and moisture contents in saline soils, using IG function, are obtained in three steps: pre-processing, parameter calculation and accuracy assessment.

Pre-processing activities start with smoothing of reflectance spectra using convolution filters. It continues with conversion of relative reflectance to natural log and normalization of log reflectance by the maximum log reflectance. According to Whiting et al. (2004), the normalized natural log of reflectance can provide an optimum fit and normalization of the spectra to the maximum log of reflectance is essential since it enhances the effect of a shift in position of the maximum reflectance.

Parameter calculation involves determination of local maximum reflectance, its corresponding wavelength, and calculation of fitting parameters. Local maxima are used to define a general shape of the continuum, which provides the generalization of the spectrum (Bishop, 1988). There are number of techniques, such as first and second derivatives, wavelet transformation and convex hull, which can be used to determine local maxima in soil spectrum. Whiting et al. (2004) found that convex hull provides better results as compared to derivatives, since it is less susceptible to random variability in the spectra. A program in IDL language was developed to generate convex hull boundary points from the spectral plot values and to provide a sequential list of convex hull points along which the IG function is fitted to the shortwave region of spectrum from the point of maximum reflectance (λ_i) to the functional centre (λ_0) at 2800 nm (Figure 5.2). Other model parameters such as functional depth (Rd), distance (σ) to the inflection point and area of one side of the function were then calculated.

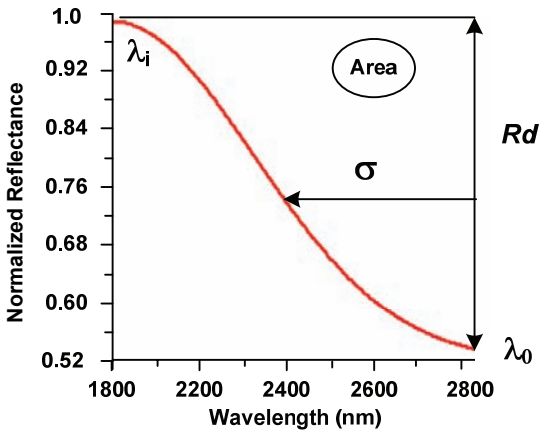

Figure 5.2: The IG model parameters required for estimating soil salinity. λ_i is the point of maximum reflectance in spectrum, λ_0 is the peak centre, Rd is the depth and σ is the distance to inflection point.

The third step involves application of the derived IG model parameters, as prediction variables x_{ij} ($j=1,\ldots,p$) in a linear regression function to estimate soil salt contents, y_i, for an unknown sample. The linear regression function for sample, i, has the form [2]:

$$y_i = \alpha_0 + \sum_{j=1}^{p} \beta_j x_{ij} + \varepsilon_i \qquad [2]$$

The S-Plus and Matlab packages were used in this study to perform statistical analysis for model regressions and validation replicates.

5.2.2.3 Model validation

Validation of IG modelling of salt variation was assessed by calculating the root mean squared error, RMSE [3] and RMSE%:

$$RMSE = \sqrt{\frac{\sum (Y' - Y)^2}{n}} \qquad RMSE\% = 100\frac{RMSE}{\overline{Y}} \qquad [3]$$

where Y and Y' are predicted and measured salt content ($EC_{1:2}$), respectively, $\overline{Y}$ is the mean of the measured $EC_{1:2}$ and n is the number of fitted spectra. The estimates of the error are in units of salt content. The validation was applied to each and every sample taken out from calibration sets that were used to create prediction models. The coefficient of determination (R^2) was calculated to show the strength of the predictive models, whereas the root mean square error (RMSE) and the relative root mean square error (RMSE%) were calculated to indicate the accuracy of the estimations for unknown samples.

5.3. Results

5.3.1 Soil physico-chemical properties

5.3.1.1 Experimental measurements

Descriptive statistics of properties of the salt-affected soil samples measured at the laboratory condition are summarised in Table 5.1. The moisture contents of soil samples are very low showing no relationship with $EC_{1:2}$ (see chapter 3, Figure 3.2), indicating that the effect of moisture on reflectance of each soil sample is minimal. This data set allows examining the potential of IG function in predicting soil salinity under laboratory conditions where all the soil constitutes, including moisture, are similar except for the soil salt contents.

Table 5.1: Summary statistics of measured properties of soil samples after sub-irrigating with saline water and dried at room temperature.

Rich in NaCl			Rich in $MgCl_2$			Rich in $MgSO_4$		
Sample	**SMC***	**$EC_{1:2}$**	**Sample**	**SMC***	**$EC_{1:2}$**	**Sample**	**SMC***	**$EC_{1:2}$**
Minimum	0.002	0.2	Minimum	0.001	2.3	Minimum	0.003	1.2
Mean	0.01	22.6	Mean	0.02	15	Mean	0.033	10.7
Median	0.01	18.6	Median	0.01	11	Median	0.028	8.9
Maximum	0.02	75.4	Maximum	0.1	48	Maximum	0.084	27.7
Std. Dev.	0.006	18.5	Std. Dev.	0.02	14	Std. Dev.	0.024	8.2
SE mean	0.001	3.2	SE mean	0.004	2.9	SE mean	0.006	1.9
Skewness	0.17	1.2	Skewness	2.96	1.4	Skewness	0.839	0.77
Kurtosis	- 1.3	1.3	Kurtosis	11	1.2	Kurtosis	- 0.15	- 0.4
CV%	0.6	0.8	CV%	1.3	0.9	CV%	0.7	0.8
Sample size	n =37			n = 22			n = 22	

* SMC = soil moisture contents in percentage, $EC_{1:2}$ values are in dS/m, Std. Dev. = standard deviation

5.3.1.2 Field measurements

The summary statistics of field measurements are presented in Table 5.2. The results of particle size analysis showed that the topsoil, in both grid areas are similar and has a sandy texture. The soil textures in the grid areas varied slightly with depths. The variations in sand (2.0 - 0.05 mm), silt (0.5 - 0.005 mm) and clay (< 0.005 mm) percentages with regard to depth classes are illustrated in (Figure 5.3). The amount of sand in both sample areas decreases with depth while the clay percentage slightly increases and silt contents do not shows any changes in relation to depth.

The EM-38 at vertical and horizontal dipole mode was used to measure soil apparent electrical conductivity (EC_a) at 539 points (354 in grid 1 and 185 in grid 6). The EC_a data generated from each site showed a good linear relationship between EC_{av} (apparent conductivity at vertical mode) and EC_{ah} (apparent conductivity at horizontal mode) in both grid areas (R^2 of 0.83 for grid 1 and 0.95 for grid 6). Figure 5.4 illustrates the measurements in both grids. Theoretically, the measured EC_{av} should be greater than the measured EC_{ah} (EM-38 manual, 2003). However, there were several measurements, particularly in severely saline areas, where EC_{ah} was greater than EC_{av}. In such cases, the distributions of soil salinity are inverted as suggested by Corwin and Rhoades (1984). Some of theses disturbances are probably related to high ground water levels in saline areas.

In order to validate and calibrate the field measurements, several samples (48 in grid 1 and 73 in grid 6) were collected from the topsoil. The relations between

the laboratory and the field measurements for soil EC_a and moisture content are presented in Figure 5.5. The figure shows variations in EC_{av} and SMC along two lines (2 and 5, east-west direction) in grid 6 (see Fig 5.1). The data suggest a relatively good fit between field and laboratory measurements.

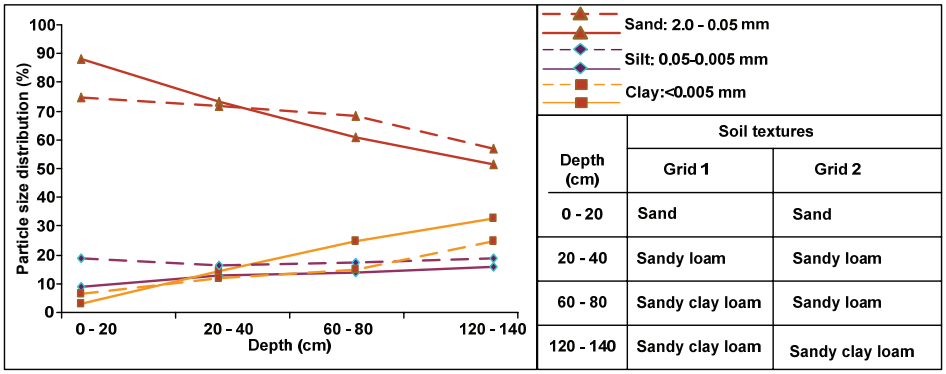

Depth (cm)	Soil textures	
	Grid 1	Grid 2
0 - 20	Sand	Sand
20 - 40	Sandy loam	Sandy loam
60 - 80	Sandy clay loam	Sandy loam
120 - 140	Sandy clay loam	Sandy clay loam

Fig. 5.3: Particle size distribution in soil profile. The solid and dashed lines represent particles variations in grids 1 and 6, respectively. Soil texture classes observed at four different depths in the two grid areas are shown at right side.

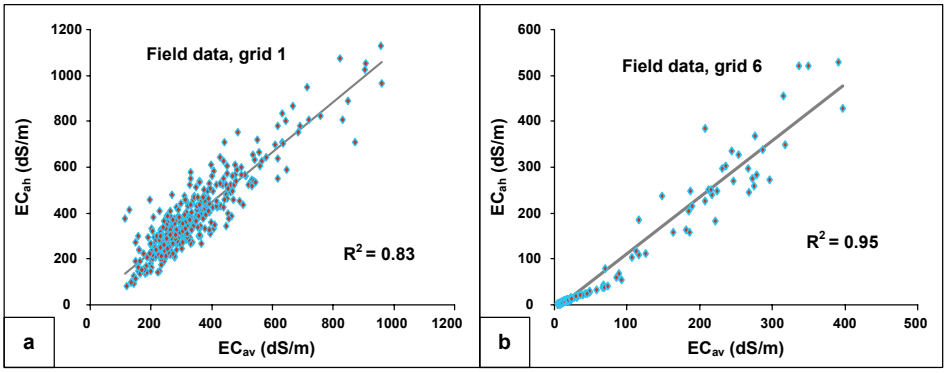

Fig. 5.4: Plot of EC_{av} (vertical dipole mode) versos EC_{ah} (horizontal dipole mode) measured in a) grid 1 (n = 354) and b) grid 6 (n = 185).

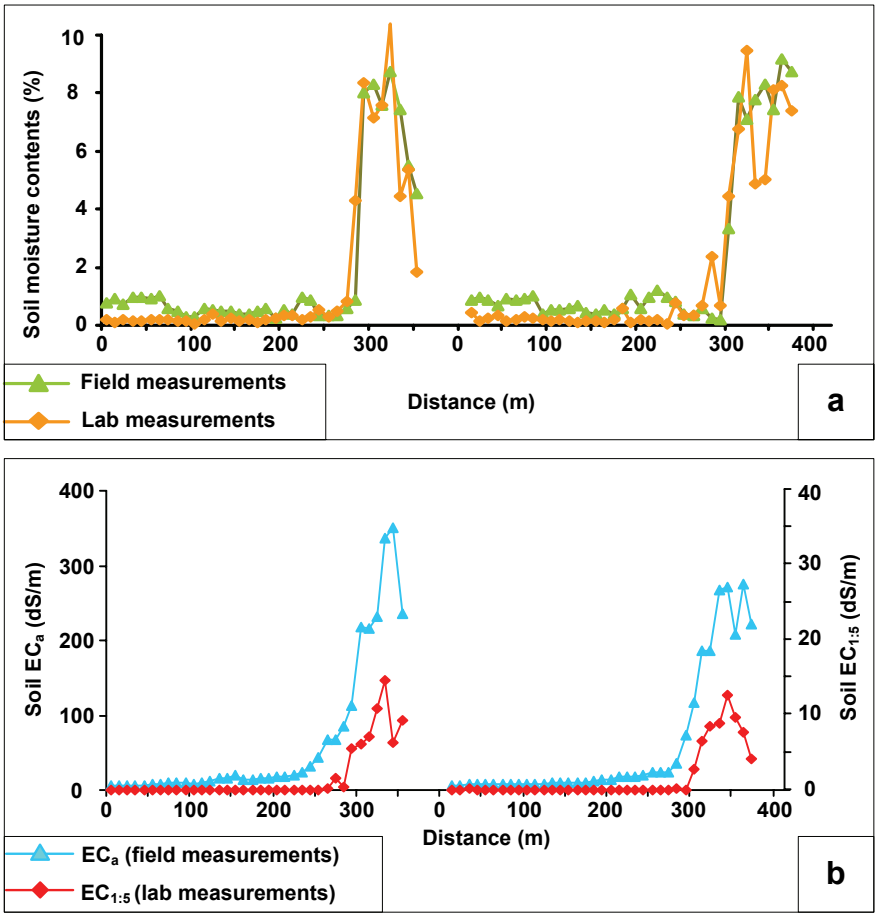

Figure 5.5: Relation between field (FDR) and laboratory (gravimetric) measurements along two lines (2 and 5, east-west direction) in grid 6. a) Soil moisture contents (%) measured in the field using the Thetaprobe sensor and in the laboratory. b) Soil EC_{av} measured in field and soil $EC_{1:5}$ measured in the laboratory.

Visual interpretation of Figure 5.4 also shows that in grid 6 the low EC measurements are belonging to the area where the SMC is low and vice versa (Table 5.2). This is due to the field condition, since most of the lowland areas, where the groundwater level is close to the surface, are affected by salts. It has to be emphasized that the soil EC and soil moisture contents are two independent variables and current correlation is related to the explained field conditions. However, the measurements in grid 1 ware obtained from lowland area where salinity is relatively high and availability of moisture in soil is

depend largely on variation of texture in soil profile and slightly due to surface micro morphology. Under these circumstances, the EC_a and SMC showed no agreement and therefore very poor correlation. However, soil reflectance in two grid areas is largely affected by both salt and moisture but in different way.
In order to quantify the magnitude of the explained relationship between the field measurements, the coefficient of determination (R^2) was calculated between soil EC and SMC. Figure 5.6 shows soil EC versus SMC. The R^2 value of 0.81 suggests a relatively strong correlation between in-situ measured soil EC_{av} and SMC in grid 6. Contrary to grid 6, the relationship between soil EC and moisture content in grid 1 is very poor (R^2 = 0.05).

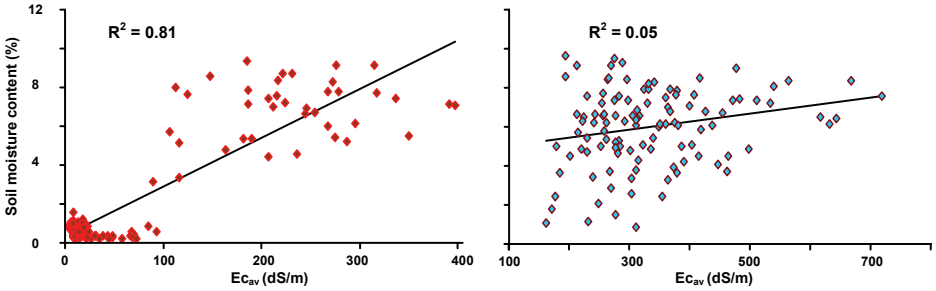

Figure 5.6: Scatter-plot of soil moisture content versus EC_{av} measured in grids 1 (left) and 6 (right).

Table 5.2: Descriptive statistics of soil properties measured in the field

Statistical properties	Grid 1			Grid 6		
	EC_{av} (dS/m)	EC_{ah} (dS/m)	SMC (%)	EC_{av} (dS/m)	EC_{ah} (dS/m)	SMC (%)
Minimum	163	138	0.8	5	2	0.2
Mean	336	379	6	62	65	1.9
Median	311	358	6.3	15	8	0.7
Maximum	956	1130	9.6	397	528	9.3
Standard dev.	125	161	2	95	119	2.6
SE M	11.5	15	0.2	7	8.7	0.2
Skewness	1.8	1.5	0.5	1.8	2.1	1.6
Kurtosis	5.2	4.1	-0.1	2.1	3.8	1.1
CV%	0.4	0.4	0.3	0.1	0.1	0.1
Sample size (n)	n = 117			n = 185		

SEM = standard error of the mean, CV = coefficient of variation (standard deviation/Mean)

5.3.2 Soil reflectance spectra

5.3.2.1. Experiment data

Positions and parameters (depth width, area and asymmetry) of absorption bands in salt-affected soil spectra vary as salt concentration in soil changed. The absorption features further than 1400 nm become broader and the positions of the maximum reflectance tend to shift toward shorter wavelengths as the overall reflectance descend or ascend, depending on the type of salt, with increase of salinity. The laboratory spectra from soil samples treated with epsomite are used to demonstrate this phenomenon (Figure 5.7). The moisture contents of the samples (see Table 5.1) at the time of the spectral measurements range between 0 to 0.05% limiting influence of soil moisture. Since soil moisture was controlled and other soil constituents, except for EC, were the same, the observed spectral variation can be related to the salt concentration. The soil samples presented in Figure 5.7 have $EC_{1:2}$ between 1.6, to a 27.7 dS/m. The spectral characteristics of soil samples suggest potential application of IG function to model soil salinity on the bases of the spectral variations.

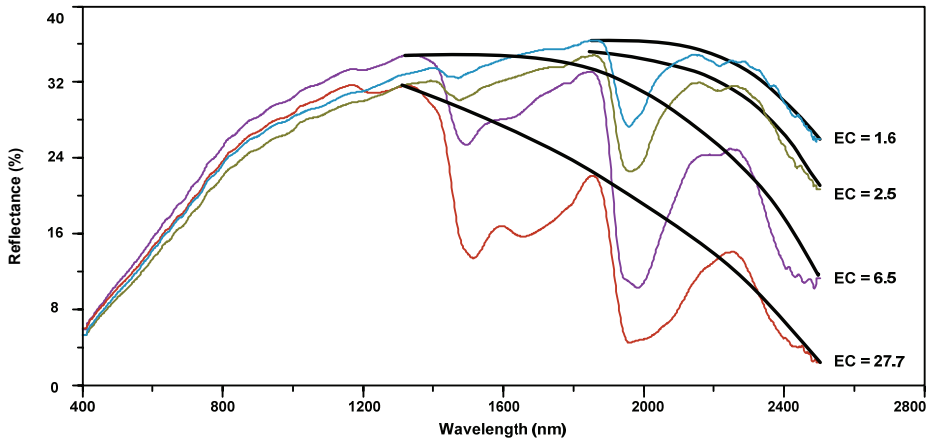

Figure 5.7: Laboratory spectra of salt-affected soil samples rich in epsomite ($MgSO_4$). The points of maximum reflectance (λ_i) shift towards shorter wavelengths as salinity level increase. The bold lines illustrate the general pattern in SWIR region. The EC are in dS/m.

5.3.2.2 Field data

The variability in field soil reflectance is depicted in Fig.5.8. The graph shows the spectral characteristics of the soil at the low and high salinity states (Figure 5.8a) and moisture contents (Fig. 5.8b) in each site. In general, wet soils have lower reflectance (albedo) than dry soils. Likewise, salt-affected soils generally

have a relationship with albedo depending on salt types, even though this correlation is poor in grid 1. Because soil salinity and soil moisture are independent variables, the data indicate that spectral variations due to increase of salt in soil can be obscured by strong affects of soil moisture. The correlation between soil overall reflectance (albedo) and soil EC in grid 1 is very poor. Generally speaking, albedo is not a good indicator for salt concentrations in soils.

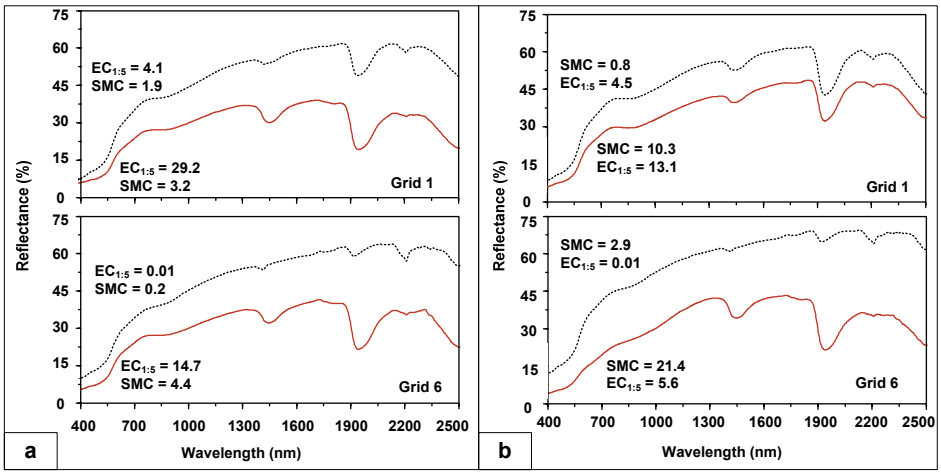

Figure 5.8: Spectra of soil in field area. Information for grid 1 is shown in the upper graphs and for grid 6 in the lower graphs. a) Soil reflectance variability mainly due to variations in soil EC. b) Soil reflectance variability mainly due to soil moisture variations.

5.3.3 Model of salts variations

5.3.3.1 Experimental data

At the laboratory condition, the model data include soil samples with three different textures and rich in a single salt such as halite, bischofite and epsomite. In total, 81 soil samples spectra were used to calculate the IG model parameters fitted to salt content. For the samples rich in $MgSO_4$, the amplitude (*Rd*), the area within the Gaussian curve (*A*) and the distance to the inflection point (σ) of the function are shown to be good indicators of salinity (Figure 5.9 and Table 5.4). The regression fit of the amplitude (*Rd*) and of the area within the Gaussian curve to the salt content of soil rich in $MgCl_2$ have high correlation of coefficients (R^2) of 0.81 and 0.82, respectively (Fig. 5.9 and Table 5.4). The fit parameters calculated for samples rich in NaCl show no relationship with salt content and provide unsatisfactory estimation of soil salinity. The results from the laboratory data suggests that application of the IG function in salinity study depends on the salt types.

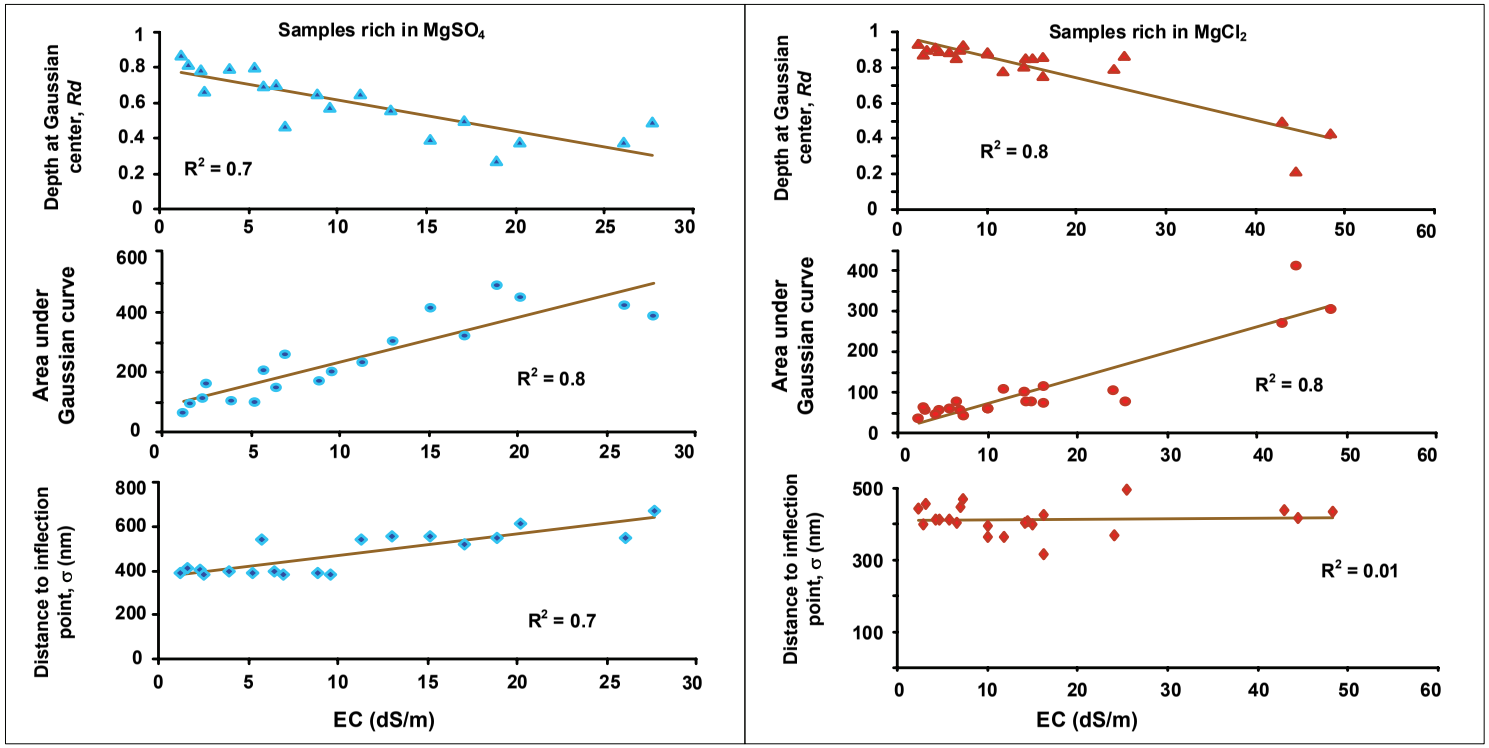

Figure 5.9: Linear relationship between soil salinity levels for $MgSO_4$ (left) and $MgCl_2$ (right) and IG model parameters calculated from soil spectra obtained from laboratory samples.

The number of hull points in the SWIR region ranged from 7 to 59 points for all the samples (n = 81). For samples rich in $MgCl_2$ and $MgSO_4$, the number of points, generally, increase with the level of salinity while for the rest of the samples (rich in NaCl) showed no relationship. The goodness of fit, in terms of RMSE between the actual and the estimated hull point reflectance, varies from 0.06 to 0.76. The RMSE exceeds 0.38 for only a few numbers (12) of spectra. In general, high RMSE is related to samples with an EC above 16 dS/m. For samples rich in $MgCl_2$ and $MgSO_4$, the RMSE increases with salinity levels, while for the other salt type no trend is observed.

5.3.3.2 Field measurements

The calculated IG model parameters showed that the number of the convex hull points in the SWIR region ranged from 15 to 72 and from 7 to 33 in grids 1 and 2, respectively. The convex hull points showed no relationship with soil EC_{av} in both grids. The RMSE between the actual convex hull points and the estimated reflectance ranges between 0.095 to 1.39 and between 0.0276 to 1.181 in grids 1 and 2, respectively.

The IG model parameters calculated from field spectra were plotted versus the soil EC_{av} (Figures 5.10 and 5.11). The results of multi regression fit of the Area, σ and Rd (dependent variables) to soil EC_{av} and SMC (independent variables) in grid 1 and 2 are given in Table 5.3. The results, shows how far the observed correlations are influenced by the two variables (SSC and SMC). The R^2 values calculated between the model parameters and EC_{av} and SMC indicates neither salts nor moisture can be modelled under field conditions. The strength and reliability of the relationships are quantified in term of R^2 and p-values, respectively. The R^2 values calculated from residuals show the percentage of variations that have not been explained by EC_{av}, SMC and interaction of them. Based on the data in Table 5.3, less than 3 % of observed variations in grid 1 are explained by EC_{av}, SMC and interaction of them. In grid 2, only sigma shows a relatively better correlation with EC_{av}.

The poor relationships between model parameters and soil EC_{av} discussed above is due to the combined affects of salt and moisture on soil reflectance spectra. Increase of salt and moisture in soil influence the soil spectra, generally, in same region of the wavelength and almost in the same way depending on salt type. This causes large anomalies in calculated model parameters. The affects of salt and moisture on IG model parameters illustrated in Figure 5.12, using weighted least squares algorithm. It showed that e.g., the area (A) is influenced more by moisture rather than salt especially in grid 6, while sigma (σ) is more effected by salt and Rd by both. However, the results suggest that modelling salt or moisture variation in soil would be very complex when the survey area is influenced by both salts and moistures.

It is emphasized that the observed poor correlation may also be related to the salt type, since results from laboratory data showed that the model parameters are influenced by salt types. The dominant salt type in the field area is halite (Kohyama et al., 1993) and as it can be seen from the laboratory results the IG model parameters showed no correlation with soil EC for the samples rich in NaCl. In addition, the poor correlation is also due to the field conditions where non to slightly saline soils have very low soil moisture while moderate to severely saline soils contained larger amount of moisture. Under this field conditions, it is not possible to illustrate quantitatively the affects of salts or moisture on the IG model parameters.

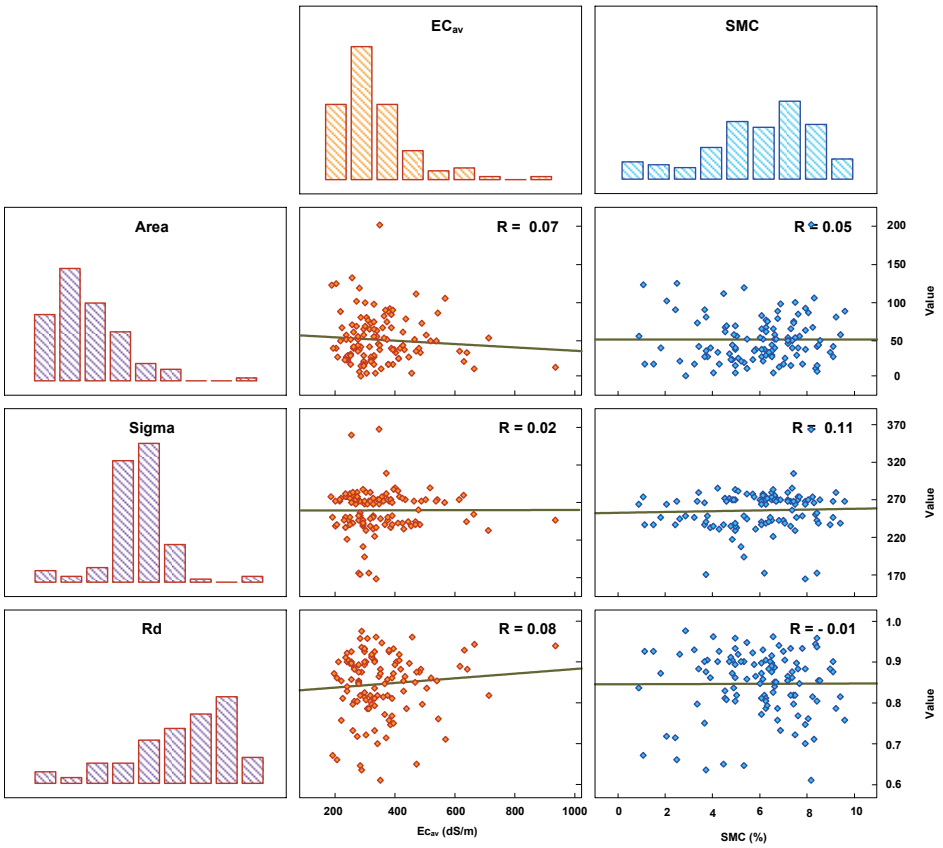

Figure 5.10: Scatter plots of calculated IG model parameters versus soil EC_{av} and soil moisture contents measured in the grid 1. Plots with diamond and triangles represent EC_{av} and SMC, respectively.

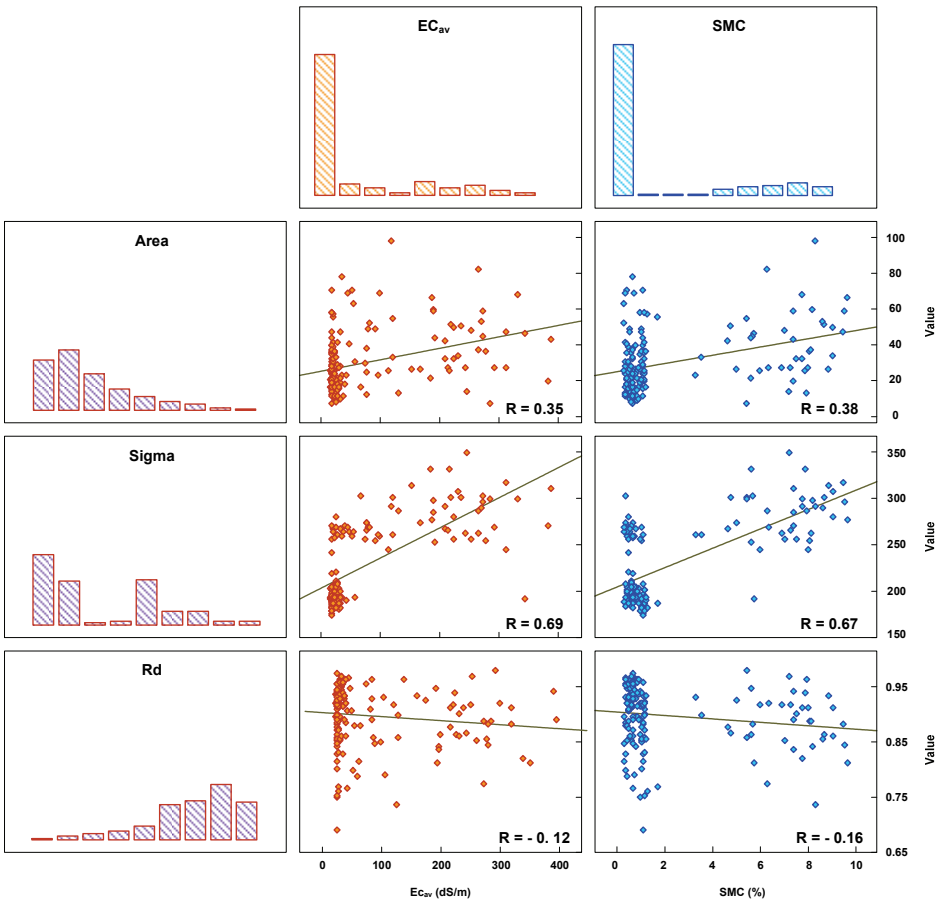

Figure 5.11: Scatter plots of calculated IG model parameters versus soil EC_{av} and soil moisture contents measured in the grid 6. Plots with diamond and triangles represent EC_{av} and SMC, respectively.

Table 5.3: Statistics representing the correlation between IG model parameters and SMC and EC_{av} in grid areas (1 and 6).

Grid areas	IG model parameters	Multiple				SMC			Ec_{av}			EC_{av} & SMC		
		R^2	P-value	R^2 Re.	Inter.	R^2	Pr (F)	Beta 1	R^2	Pr (F)	Beta 2	R^2	Pr (F)	Beta 3
Grid 1	Area	0.03	0.406	0.974	99.92	0.002	0.618	-5.38	0.007	0.372	-0.17	0.017	0.173	0.022
	Sigma	0.013	0.698	0.987	263.3	0.013	0.234	1.644	0.0	0.949	-0.01	0.0	0.966	0.001
	Rd	0.024	0.442	0.976	0.712	0.0	0.886	0.016	0.01	0.349	0.001	0.016	0.182	0.0
Grid 6	Area	0.16	0.0	0.84	20.6	0.14	0.0	3.74	0.0	0.766	0.086	0.018	0.068	-0.02
	Sigma	0.54	0.0	0.46	193.1	0.45	0.0	11	0.04	0.0	0.524	0.05	0.0	-0.07
	Rd	0.03	0.158	0.97	0.912	0.02	0.046	-0.01	0.0	0.6	0.0	0.01	0.334	0.0

Re.= residuals, Beta 1, 2, and 3 represent regression coefficients, Inter = intercept.

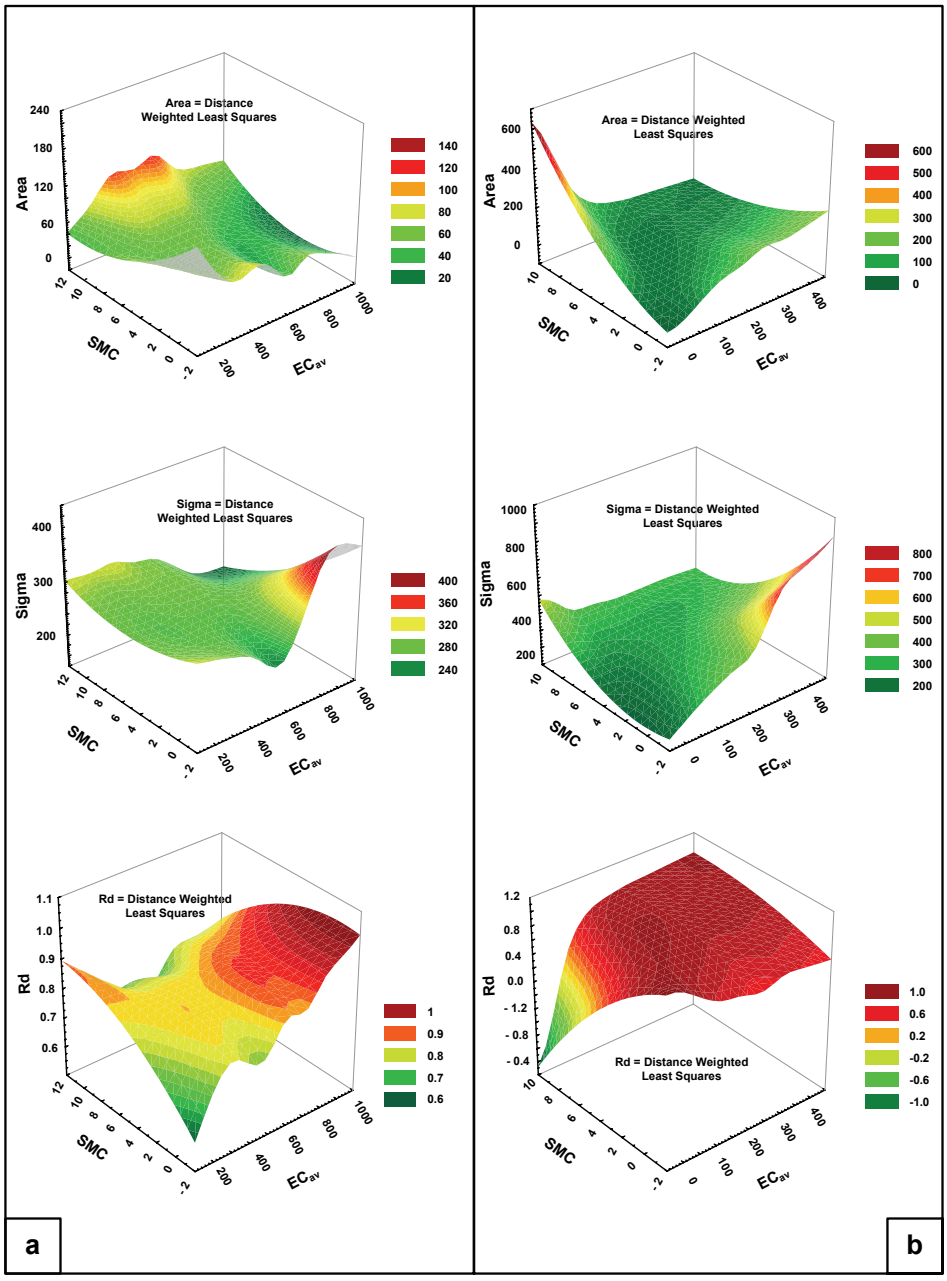

Figure 5.12: Relations between IG parameters (Rd, sigma and Area) and soil EC_{av} and moisture contents. a and b represents observation points in grids 1 and 6, respectively.

5.3.3.3 Validity of the models

Validations of predictive models of soil salt contents based on IG parameters are summarized in Table 5.4. Predictive models using experimental data show significant correlation between IG parameters and soil salt contents. The results from experimental data suggest that predictive regression models are robust for samples affected with salt types such as $MgCl_2$ and $MgSO_4$ but not with NaCl (Table 5.4). Linear spectral models to predict salinity level (EC) gave root mean square errors (RMSE) between 0.8 and 2.9 dS/m and R^2 values between 0.68 and 0.82. Amongst the three types of salts ($MgCl_2$, $MgSO_4$ and NaCl), only for $MgCl_2$ and $MgSO_4$ could the salinity levels be predicted with $RMSE_{CV}$ lower than 1.2 dS/m (roughly equivalent to RMSE% lower than 5.7). In most cases, predictive models using area under fitted curve gave better results than models using distance to inflation point (σ) or depth at Gaussian centre (*Rd*).

Table 5.4: Coefficient of determination (R^2), root mean square error (RMSE) and relative root mean square error (RMSEP) between measured and predicted soil salinity ($EC_{1:2}$) for different salt minerals. Numbers of sample used are 37, 22 and 19 for samples rich in NaCl, $MgCl_2$ and $MgSO_4$, respectively.

Soil samples rich in :	**Soil salinity Gaussian model accuracy**														
	R^2			**RMSE**			**RMSE%**			**Slope (β)**			**Intercept (ε)**		
IGMP	**Rd**	**σ**	**A**	**Rd**	**σ**	**A**	**Rd**	**σ**	**A**	**Rd**	**σ**	**A**	**Rd**	**σ**	**A**
NaCl	0.1	0.11	0.1	3.4	3.4	3.4	12.3	12.4	12.4	0.001	-0.7	0.8	0.9	464	44
$MgCl_2$	0.8	0.01	0.8	1.2	2.9	1.2	5.7	13	5.5	-0.01	1.4	6.3	1.0	411	8.3
$MgSO_4$	0.7	0.7	0.8	1.0	1.0	0.8	5.4	5.3	4.2	-0.01	9.6	15	0.8	371	82

IGMP = IG model Parameters, σ = distance to inflection point, *Rd* = depth and *A* = area.

5.4. Discussion and conclusions

The present study investigates the interference of salt and SMC on soil reflectance and their influence on modelling either soil salinity or soil moisture. The method described here might be suitable as an alternative method for quantifying salt variations in soil if the affects of soil moisture minimized. The advantage of this method is related to its ability to use the general shape of spectrum and its IG model parameters rather than diagnostics absorption bands parameters.

The IG model parameters of soil reflectance spectra, in general, are sensitive to position of maximum reflectance point on soil spectrum (Figure 5.2), which can

be a function of soil constituents. Salt minerals and water, as part of soil compositions, influence the magnitude of soil reflectance at various wavelengths in spectral range between 350 to 2500 nm. For example, salt minerals, such as epsomite or bischofte in soils causes shift in the positions of maximum reflectance. The shift occurs along X- (wavelength) and Y-axes (reflectance). Based on the results, quantification of salts or moisture contents of salt-affected soils could be relatively complicated. For example, parameters of an IG curve fitted to a spectrum of low moisture soil with large amount of salts can be the same as the ones measured from a curve fitted to spectra of non-saline soil with high moisture content. In other words, the amount of moisture in soil causes anomalies in estimation of salts contents and vice versa when estimating moisture content from salt-affected soils. In the case of soil samples rich in NaCl, the variations in salts changed only the soil albedo (shift on Y-axis) in NIR-SWIR regions while the positions of maximum reflectance point remain relatively unchanged. Under such circumstances, the salt contents of soil were poorly estimated using the derived IG model parameters.

Estimation of soil salinity levels using IG model parameters of soil spectra was successful, however, with laboratory measurements but not with field measurements. Statistically significant predictive regression models could be established for all the soil sample rich in $MgCl_2$ and $MgSO_4$, but not for samples rich in NaCl. Amongst the calculated IG model parameters, the area under fitted curve provided generally the most accurate models, whereas the distance to inflection point (σ) provided the least accurate models. The results demonstrate the relative utility of IG model parameters of high spectral resolution data for salinity studies at laboratory conditions.

The poor correlation between soil EC_{av} and IG model parameters for the field spectral data can be explained mainly by variations in salt types and influence of soil moisture on soil spectra. The dominant salt in the field area is halite, which has a weak effect on the general shape of soil spectra to provide bases for predictive regression modelling. Whereas, the soil moisture contents introduced large anomalies in calculated IG model parameters of field spectra. This result in a poor relationship between soil salinity level and IG model parameters and also strong relationship between salinity level and soil moisture which, indicating features exhibited by soil spectra are dominated by water rather than the salt.

The results suggest, therefore, that estimation of soil moisture using the same approach can be undermined by accumulation of salts in the soil. The results indicate that further studies are required to determine calibrating coefficients that can be used to eliminate the background spectra caused by soil moisture contents. Such information is critical for adjusting soil spectra obtained from the field or spectra derived from hyperspectral imagery in order to link spectral

variations to soil salinity levels. Up-scaling of results to airborne hyperspectral data, however, is even more complicated since other interfering factors such as variation in soil constituents (e.g., soil organic matter content) or soil surface roughness would influenced the soil reflectance as well.

Chapter 6

Quantitative analysis of salt-affected soil reflectance spectra: A comparison of two adaptive methods*

Abstract

In this chapter the possibility of estimating salt concentrations in soils from measured reflectance spectra is studied using partial least squares regression (PLSR) and artificial neural network (ANN). Performance of these two adaptive methods has been compared in order to examine linear and non-linear relationship between soil reflectance and salt concentration.

Experiment-, field- and image-scale data sets were prepared consisting of soil EC measurements (dependent variable) and their corresponding reflectance spectra (independent variables). For each data set, PLSR and ANN predictive models of soil salinity were developed based on soil reflectance data. The predictive accuracies of PLSR and ANN models were assessed against independent validation data sets not included in the calibration or training phase.

---

* This chapter is based on:

Farifteh, J., Van der Meer, F., Atzberger, C., Carranza, E.J.M., (2006). Quantitative analysis of salt-affected soil reflectance spectra: A comparison of two adaptive methods (PLSR and ANN). In Press, *Remote Sensing of Environment*.

The results of PLSR analyses suggest that an accurate to good estimation of EC can be made based on models developed from experiment-scale data ($R^2 > 0.81$ and RPD (ratio of prediction to deviation) > 2.1) for soil samples salinized by bischofite and epsomite minerals. For field-scale data sets, the PLSR predictive models provided approximate quantitative EC estimations ($R^2 = 0.8$ and RPD = 2.2) for grids 1 and 6 and poor estimations for grids 2, 3, 4 and 5. The salinity estimations from image-scale data sets by PLSR models were very reliable to good (R^2 between 0.86 and 0.94 and RPD values between 2.6 and 4.1) except for sub-image 2 ($R^2 = 0.61$ and RPD = 1.2).

The ANN models from experiment-scale data set revealed similar network performances for training, validation and test data sets indicating a good network generalization for samples salinized by bischofite and epsomite minerals. The RPD and the R^2 between reference measurements and ANN outputs of theses models suggest an accurate to good estimation of soil salinity ($R^2 > 0.92$ and RPD > 2.3). For the field-scale data set, prediction accuracy is relatively poor ($0.69>R^2>0.42$). The ANN predictive models estimating soil salinity from image-scale data sets indicate a good estimation ($R^2 > 0.86$ and RPD > 2.5) except for sub-image 2 ($R^2 =0.6$ and RPD=1.2).

The results in this chapter show that both methods have a great potential for estimating and mapping soil salinity. Performance indexes from both methods suggest large similarity between the two approaches with PLSR advantages. This indicates that the relation between soil salinity and soil reflectance can be approximated by a linear function.

Keywords: soil salinity, salt-affected soils, modelling, hyperspectral, remote sensing, geophysics, partial least square regression, artificial neural network

6.1 Introduction

The salinity problem

Elevated concentrations of soluble salts at surface or near-surface soil horizons are a major problem with severe worldwide economical and social consequences. Excessive salt concentrations in soils accelerate land degradation processes and decrease crop yields and agricultural production (FAO, 1988). Increased salt concentrations lead also to other major soil degradation phenomena such as soil dispersion, sealing and crust formation and structural changes, which result in unstable and compacted soil (Agassi et al., 1981; Tanji, 1990; De Jong, 1994). Consistent and early stage identification of soil salinisation processes as well as assessment of extent and degree of severity are vital in

terms of sustainable land management, especially in semi-arid areas where harsh climatic conditions together with rapidly increasing population densities require agricultural intensification and land use changes (Fauck, 1977; Frenkel and Meiri, 1985). The discussed issues together with the advances in the field of data acquisition are the motivation for developing robust modelling techniques for detecting salt-affected areas. Robust approaches should have predictive capabilities based on establishing empirical relationships between soil physico/chemical properties and soil reflectance and must be applicable to non-surveyed areas having geographical conditions similar to known salt-affected areas.

Remote sensing of soil salinity

The development of methods to map salt-affected soils using optical remote sensing data in combination with field measurements has been the objective of several studies during the last two decades (e.g., Dehaan and Taylor, 2003 and 2002; Ben-Dor et al., 2002; Evans and Caccetta 2000; Rao et al., 1998; Szilagyi and Baumgardner 1991; Everitt et al., 1988). A review of these investigations is given in Farifteh et al. (2006) and Metternicht and Zinck (2003). The methods that have already been developed range from simple visual interpretation of hardcopy satellite images (Verma et al., 1994) to sophisticated spectral unmixing techniques (Dehaan and Taylor, 2002; 2003). Field measurements range from soil sampling, laboratory analysis to in-situ electromagnetic (EM) measurements. Ground-based EM measurements of soil electrical conductivity are generally accepted as the most effective method to quantify soil salinity (Dehaan and Taylor, 2002). Field measurements are, however, costly, time consuming and only provide point information. Therefore new mapping tools such as optical imagery are studied for more efficient ways to detect and map salt-affected soils.

Optical remote sensing data seem to be well adopted for mapping soil salinity, as reflectance measurements have already been successfully used to model various soil properties (Ben-Dor, 2002; Irons et al., 1989). However, the application of remotely sensed data in salinity studies is difficult. Firstly, diagnostic features of salt-affected soils are generally weak because of poor salt crystallization (Hunt et al., 1972). Secondly, mapping of soil salinity is difficult because many other soil chemical and physical properties (e.g., moisture, surface roughness, organic matter) also influence soil reflectance (Irons et al., 1989; Ben-Dor, et al., 1999). Finally, from a remote platform the recorded reflectance is often the (mixed) result of several surface components (i.e., mixed pixel problem) (Dehaan and Taylor, 2003), and at the same time atmospheric scattering and absorption processes mask salts diagnostic features (Richards and Jia, 2005; Cloutis, 1996). With the development of hyperspectral sensors, spectral features related to characteristic absorption bands of salt minerals can be mapped with

more detail (Cloutis, 1996). This should enable better detection and mapping of soil salinity. However, a disadvantage of hyperspectral sensor is that the signal-to-noise ratio decreases, as smaller wavebands receive less energy. Detecting and mapping salinity by use of remote sensing is therefore challenging, since most of salt minerals are spectrally featureless and because the strength of signals representing salt-affected soils are relatively weak compared to the "noise" resulting from other interfering factors. Whether the recent efforts in modelling and predicting salinity are able to overcome these limitations and to provide a relatively accurate estimation is a question that yet has to be answered.

Linear and non-linear modelling techniques

Multivariate techniques such as partial least square regression (PLSR) and artificial neural networks (ANN) have been widely used as calibration tools in chemometrics. Both techniques have been applied to model the relationship between several chemical and physical soil properties and spectral data (Udelhoven et al., 2003; Yang et al., 2003).

The PLSR approach could model several response variables simultaneously while effectively dealing with strongly collinear and noisy independent variables (Wold et al., 2001). A large number of studies reported successful results and potential applications of PLSR in various disciplines (e.g., Hatonen et al., 1999; Lindberg et al., 1983). The PLSR algorithm has inferential capability, which can be used to model a possible linear relationship between salt concentrations in soils and measured reflectance spectra.

Artificial neural nets (ANN) have the ability to model any linear or non-linear relationships between a set of input and output variables (Yang et al., 2003; Huang and Foo, 2002; Maier and Dandy, 2001). Hence, as relationship between soil salinity and soil reflectance may not be linear, ANN methods can be advantageous in examining relationship between soil salinity and soil reflectance.

Objectives

The aim of this chapter is to investigate performance of PLSR and ANN for estimation of salt concentrations in soils based on spectral reflectance measurements. To make an in-depth investigation and comparison of performance of PLSR and ANN, the study was carried out at three different scales and using different data sets in four different study regions. The two already mentioned algorithms (PLSR and ANN) were first applied to data obtained from a laboratory experiment and then to field-measured data. Next, the two methods were tested using hyperspectral image data obtained by the air-borne HyMap sensor.

6.2 Characteristics of the test sites

The data sets used in this study were collected from four different areas (Table 6.1, see also section 1.5 in chapter 1). The experiment-scale data set were derived from the soil samples collected (i) from the island of Texel in the northwest of The Netherlands, and (ii) in the Tedej area in northeast Hungary (Table 6.1). The field data set was obtained in 2004 (Oct. to Jan.) from a test site (Muangpia) with an area of approximately 55 square km situated near Khon Kaen city in northeastern Thailand (see also section 1.5 in chapter 1)). The image data set belongs to the test area in Western Australia (Toolibin lake), which is situated at approximately 200 km south-east of Perth close to the town of Narrogin. Figure 6.1 shows the location of the grids area in Northeast of Thailand and the hyperspectral sub-images of Toolibin Lake from Western Australia where the developed PLSR and ANN were tested. The detailed information of the study areas is given in chapter 1 section 1.5.

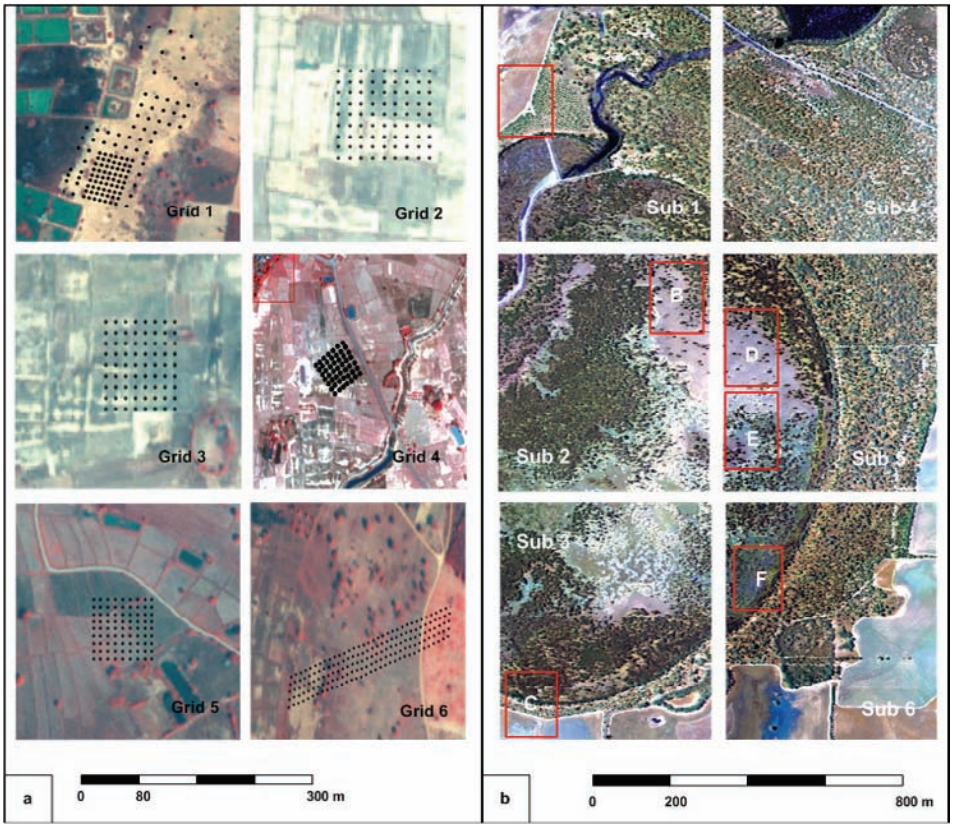

Figure 6.1: a) Grid areas in the Northeast Thailand where in-situ field measurements were carried out. b) Hyperspectral image (HyMap) from Toolibin Lake in Western Australia where salinity was predicted and mapped.

Table 6.1: Description of the data sets used in this study (see Table 1.4).

Location	Type of data sets	Soil texture	Subset number	Name of subsets	Number of samples
Texel Island	Laboratory experiment	Sand Sandy loam	1 2	KCl NaCl	43 48
Tedej		Silty clay loam	3 4	$MgCl_2$ $MgSO_4$	22 30
Muangpia	Field measurements	Sand Sandy loam Loam Sandy clay loam	1 2 3	Grids 1&6 Grids 2-5 All grids	302 316 628
Toolibin Lake	Hyperspectral imagery and field measurements	See chapter 1	1 2 3 4 5	Sub-image 1 Sub-image 2 Sub-image 3 Sub-image 5 Sub-image 6	1060 3412 3469 1999 1237

6.3 Materials and Methods

6.3.1 Data descriptions

The experimental data sets were obtained, in laboratory, from soil samples that were air-dried, crushed and passed through a 0.2 mm sieve and then sub-irrigated with saline water of various densities using different technical salt grades (e.g., halite, sylvite, bishofite, and epsomite). The experimental set-up ensured that soil moisture contents remained low, thus minimizing the effect of soil moisture on the measured spectra. Soil moisture content of soil samples never exceeded 0.05 %, with more than ¾ of samples having moisture contents of less than 0.02 percent. The detailed description of data and laboratory procedures can be found in chapter 3. Detailed soil information of the areas where soil sample were collected (Texel and Tedej) can be found in Kloosterhuis et al. (1986), and Kardev´an et al. (2003), respectively.

The field data sets from Thailand includes soil reflectance, soil apparent electrical conductivity (EC_a) and soil moisture content, which were measured in six grids at intervals of 5, 10, 20 and 40 meters. These data were combined in two sets due to similarity between the top soil (0-20 cm) textures. One data set consists of data from grids 1 and 6 (soil texture sand) and the other data set includes data from grids 2, 3, 4 and 5 (sandy loam to loam). The variations in sand (2.0 – 0.05 mm), silt (0.05-0.005 mm) and clay (< 0.005 mm) percentages of the data are illustrated in Figure 6.2. Details of procedures of the field measurements and the technical specifications of the instruments that were used are reported in chapter 5. Detailed soil information for Thailand test site can be found in Mitsuchi et al. (1989).

Data sets in the Toolibin area consist of image data acquired by the air-borne hyperspectral sensor HyMap of the HyVista Corporation (pixel size 3.5 m) and electrical conductivity measurements. The HyMap hyperspectral scanner provides 128 bands across the wavelength region of 0.45 – 2.5 µ with contiguous spectral coverage (except in the atmospheric water vapour bands) and bandwidths between 15 – 20 nm (HyVista, 2004). The hyperspectral image was taken on November 20th 1998 and was georeferenced and corrected for atmospheric effects by CSIRO Office in Perth. The hyperspectral imagery covers an area where corresponding soil EC_a measurements are at hand. In the same period as the hyperspectral data were obtained, soil salinity was measured at intervals of approximately 3 meter using the EM-38 (geophysics instrument).

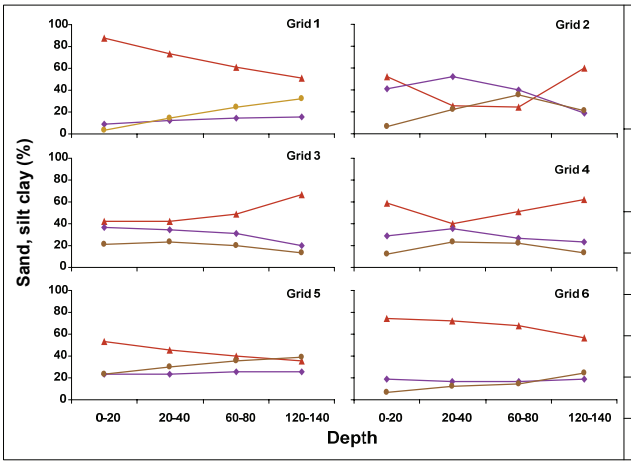

Grid	Soil texture at different depth			
	0-20	20-40	60-80	120-140
1	Sand	Sandy loam	Sand clay loam	Sand clay loam
2	Sandy loam	Silty loam	Clay loam	Sand clay loam
3	Loam	Loam	Loam	Sandy loam
4	Sandy loam	Loam	Sand clay loam	Sandy loam
5	Sand clay loam	Sand clay loam	Clay loam	Clay loam
6	Sandy	Sandy loam	Sandy loam	Sand clay loam

Figure 6.2: Particle size distribution and soil texture classes observed at four different depths in the grid areas in Northeast Thailand. The data presented here are from one representative sample in each grid. Each grid covers an area of about 100 by 100 meters (see Figure 6.1a).

6.3.2 Partial least square regression model (PLSR)

PLSR is a method that specifies a linear relationship between a set of dependent (response) variables, *Y*, and a set of predictor variables, *X*. The general idea of PLSR is to extract the orthogonal or latent predictor variables, accounting for as much of the variation of the dependent variable(s). Detailed description of the PLSR technique can be found in Geladi and Kowalski (1986) and Wold et al. (2001).

In this study, PLSR was used to model correlation between soil reflectance spectra (predictor variables) and salinity (response variable). A schematic representation of the method is given in Figure 6.3, based on a review of Wold

et al. (2001) and the tutorial of Geladi and Kowalski (1986). The PLSR modelling was performed using software developed by Viscarra Rossel (2005). Application of PLSR method takes into account the matrices *T, U, W* and *C* (Figure 6.3), which contain useful information that describes the linear relationship between the response and predictor variables. The score matrices *T* and *U* describe the similarities or dissimilarities (e. g., relationships) between response and predictor variables. The weight matrices *W* and *C* define how the variables are combined to form the quantitative relationship between *X* and *Y*.

Reflectance data in wavelength range between 400-2450 nm were used for the PLSR analysis. For every scale of the study (experiment, field, image), the data used to build the PLSR models were randomly divided into calibration and prediction sets. For the experiment-scale, two-thirds of the data were used for calibration and one-third for prediction. For the field-scale and image-scale studies, with large amount of data, 50% were used for calibration and 50% for prediction. Among the measured field spectra, a few differed considerably (checked by visual inspection) from the rest and thus were left out. With regard to the HyMap image, from total number of 128 bands, 117 bands were used for the analysis. From total number of 128 bands, 11 bands (1, 2, 3, 64, 65, 66, 95, 96, 97,127 and 128) contained large amount of noise, and therefore, were not used for the analysis. To reduce processing load (PLSR software limitation), the HyMap data set was split into six sub-images (Figure 6.1b). Each sub-image (except sub-image 4) contains a large number of EC_a observations, varying between 1000 measurements in sub-image 1 to 3500 in sub-image 3 (see Table 6.1). Prediction models were developed independently for each sub-image. The prediction models were then used to map soil salinity within the six small representative windows (Figure. 6.1b, A, B, C, D, E & F) due to software limitation. Notice that electrical conductivity measurements (i.e., using the EM-38 instrument) assess the entire soil rofile, whereas the soil reflectance (field or air-borne measurements) is influenced by only the first few millimetres. Hence, a close relation can be expected only if the salt minerals are well distributed within the soil profile.

All spectral data used for building the PLSR models were transformed to log (1/R), corrected for light scattering using multiplicative signal correction (MSC) techniques and smoothed with a running median filter (size 3 or 5 data points) (Viscarra Rossel, 2005). Before analysis, the transformed spectral data sets were further centred or standardized (mean of zero and standard deviation of one) in order to make their distribution fairly symmetrical (transformation), to focus the model on important variables (scaling), to ease interpretation and increase numerical stability (centre), and to remove the size of the observation (normalize) if it is irrelevant (Jackson, 1991).

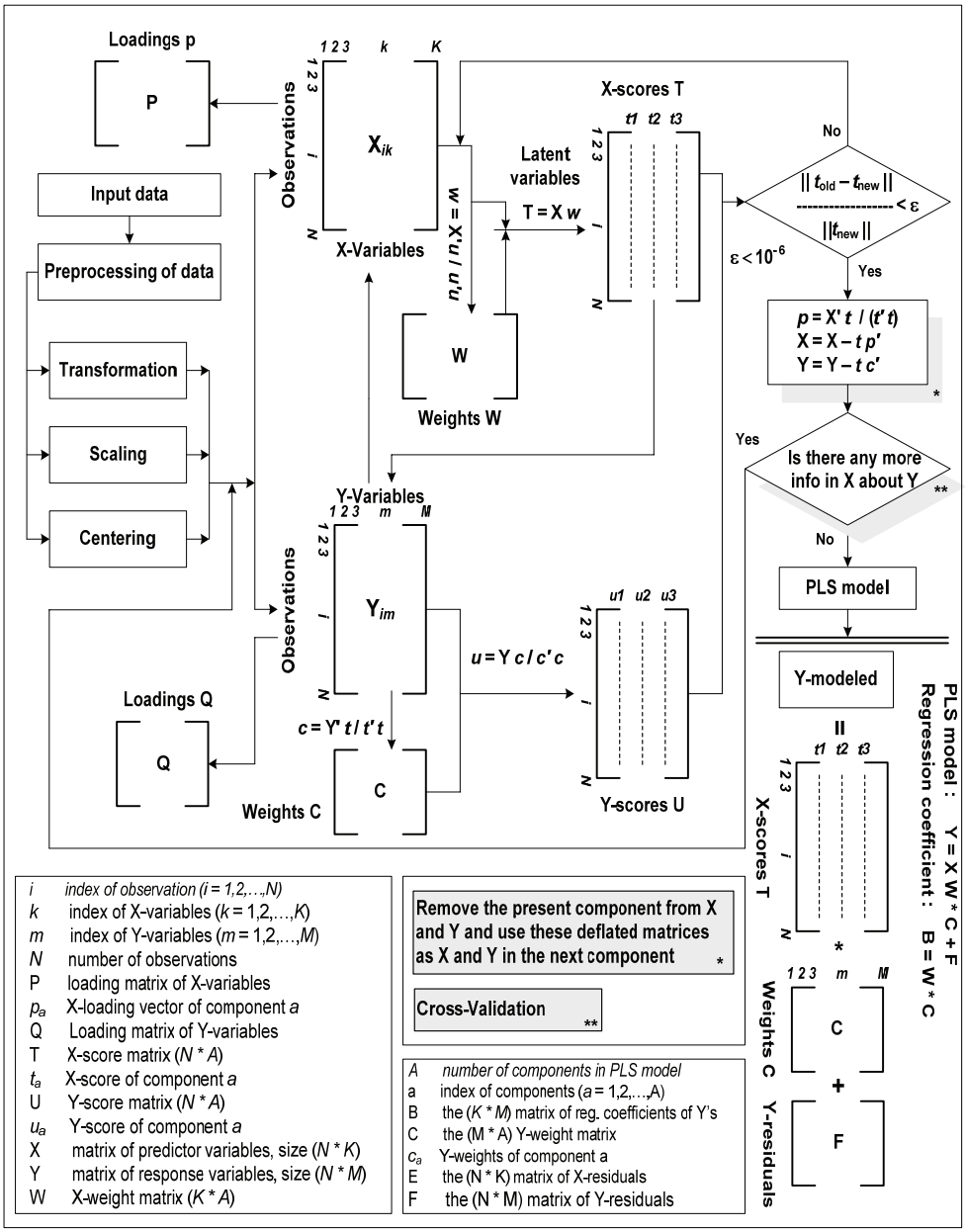

i	*index of observation (i = 1,2,…,N)*
k	index of X-variables (*k* = 1,2,…,*K*)
m	index of Y-variables (*m* = 1,2,…,*M*)
N	number of observations
P	loading matrix of X-variables
p_a	X-loading vector of component *a*
Q	Loading matrix of Y-variables
T	X-score matrix (*N* * *A*)
t_a	X-score of component *a*
U	Y-score matrix (*N* * *A*)
u_a	Y-score of component *a*
X	matrix of predictor variables, size (*N* * *K*)
Y	matrix of response variables, size (*N* * *M*)
W	X-weight matrix (*K* * *A*)

A	*number of components in PLS model*
a	index of components (*a* = 1,2,…,A)
B	the (*K* * *M*) matrix of reg. coefficients of Y's
C	the (M * A) Y-weight matrix
c_a	Y-weights of component a
E	the (N * K) matrix of X-residuals
F	the (N * M) matrix of Y-residuals

Figure 6.3: PLSR algorithm and data arrangement based on procedure described in Wold et al. (2001).

6.3.3 Artificial neural network model (ANN)

An artificial neural network (ANN) consists of a large number of highly interconnected processing elements (nodes or units), which simulate basic functions of biological neurons. Figure 6.4 illustrates a simple one-neuron model within an artificial network, where an input vector is passed through the neuron for providing an output value. A neural network is composed of several (sometime thousands) of such processing units where unidirectional connections between them are provided by a corresponding weighting vector. Such networks are called multiple-layer networks and have the ability "to learn" the relationship between input and output data. A multiple-layer system consists of input, hidden and output layers. The theory and mathematical basis of ANNs have been extensively described in Haykin (1999) and Bishop (1995).

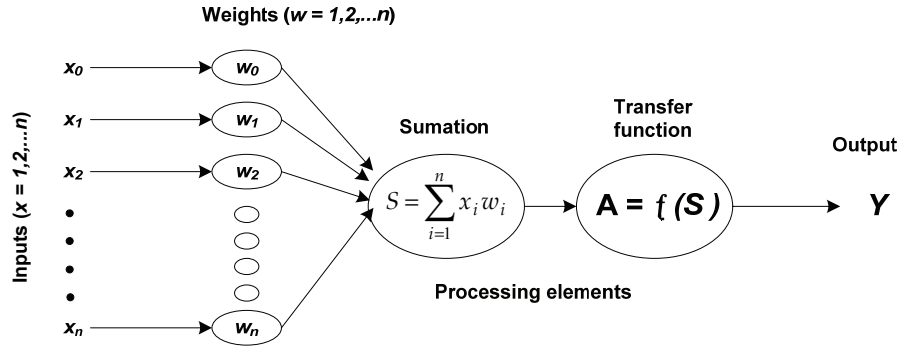

Figure 6.4: A basic artificial neuron; an example of one-neuron model structure.

In this study, a multiple-layer feed-forward backpropagation network with three layers was used: input, hidden and output layer. This type of network generally provides better performances in comparison to other types (Hornik et al., 1989). Tan-sigmoid transfer functions (non-linear) and linear transfer functions were selected for the hidden and output layers, respectively. Using a tan-sigmoid function in the hidden layer allows to approximate only non-linear relations present between input and output layers (Haykin, 1999). The number of neurons in the hidden layer can be defined using a formula recommended by Fletcher and Goss (1993) or using a trial-and-error approach as suggested by Chang et al. (2004). The number of neurons in the hidden layer is of great importance, as too many neurons may cause over-fitting problems (Huang and Foo, 2002). For improving network generalization, Demuth and Beale (2004) recommended to use a network that is just large enough to provide an adequate fit between predictor and response variables. To avoid over-fitting problems and to provide an effective means to stop the time demanding training phase,

the so called "early stopping" approach has been used (Demuth and Beale, 2004).

The network input layer used in this study relates to reflectance, while the network output layer relates to soil salinity. Data preprocessing techniques (centering or standardizing to a mean of zero and standard deviation of one) and principal component analysis (PCA) were applied to the inputs to normalize the reflectance data and to reduce the data dimension. The numbers of neurons used for training the networks were varied systematically between five and 13 to allow subsequent selection of the most appropriate network size based on the performance on the test dataset (Adeloye and De Munari, 2005). For ANN modelling, the computer software MatLab and the Neural Network Toolbox were used (Demuth and Beale, 2004).

In each scale of the study, each data set was divided into three subsets, one for training (half of input data), one for validation (a quarter) and one for testing (a quarter of input data). The Levenberg-Marquardt algorithm (Demuth and Beale, 2004), which provides a fast optimization, was used for network training. The performance of a trained network was assessed by comparing the mean squared error (MSE) and root mean squared error (RMSE) calculated from training, validation and testing data subsets. Only a training data subset is used for updating the network weights and biases. During training, error with respect to validation data subset is monitored. When the validation error increases for a specified number of iterations, the training is stopped. Error with respect to testing data subset is not monitored during training, but is quantified to assess the final performance of a trained ANN model.

6.3.4 Quantification of prediction errors

To quantify performance of salinity-reflectance models based on PLSR and ANN methods, various parameters between estimated values (Y') and independent reference measurements (Y) were calculated (Table 6.2): root mean square error (RMSE), relative RMSE (RMSE%), mean and relative mean absolute errors (MAE and MAE%). Both MAE and RMSE indicate absolute estimation errors, but RMSE is more sensitive to outliers and thus, RMSE% and MAE% are also calculated. To analyse the goodness of estimated values versus the observed values, three other model performance parameters were calculated (Miehle et al., 2006; Williams, 2001; Nash and Sutcliffe, 1970): coefficient of determination (R^2), model efficiency (ME) and ratio of prediction to deviation (RPD). Detailed descriptions and definitions of these model performance parameters are given in Taylor (1997) and Cacuci (2003). The equations for quantification of the model performance parameters are given in Table 6.2.

Table 6.2: Equations* for quantification of errors of prediction.

$RMSE = \sqrt{\frac{\sum (Y' - Y)^2}{n}}$	$RMSE\% = 100 \frac{RMSE}{\overline{Y}}$
$MAE = \frac{\sum_{i=1}^{n} \lvert Y_i' - Y_i \rvert}{n}$	$MAE\% = 100 \frac{MAE}{\overline{Y}}$
$RPD = \frac{SDP}{\left(\sum (Y' - Y)^2 - \left\{\left[\sum (Y' - Y)\right]^2 / N\right\} / N - 1\right)^{1/2}}$	
$SDP = \left\{\sum y'^2 - \left[\left(\sum y'\right)^2 / N\right] / (N - 1)\right\}^{1/2}$	
$ME = 1 - \frac{\sum_{i=1}^{n} (Y' - Y)^2}{\sum_{i=1}^{n} (Y_i - \overline{Y})^2}$	

* Y and Y' are measured and predicted values, respectively, SDP is the standard deviation of prediction, $\overline{Y}$ and $\overline{Y'}$ are averages of the observed and predicted values, respectively, n is the number of observations.

The R^2 and RPD indicate strength of statistical correlation between measured values and predicted values both for PLSR and ANN predictive models. A predictive model is accurate if R^2 and RPD values are higher than 0.91 and 2.5, respectively (Williams, 2001). R^2 between 0.82-0.9 and RPD higher than 2 indicate a good prediction, whereas the R^2 of an approximate prediction is considered to lie between 0.66-0.81 with a RPD of higher than 1.5. R^2 between 0.5-0.65 indicates a poor relationship. MAE and ME indices were also used to examine the performance of the PLSR and ANN predictive models. MAE and ME values indicate degree of agreement between measured and predicted values; hence, they provide a measure of prediction model efficiency (Nash and Sutcliffe, 1970). Larger values MAE% and RMSE%, thus mean high prediction errors while ME values close to 1 indicate small errors in prediction values. To examine the performance of PLSR-calibration models RMSE and RPD values is analysed. Generalization of the ANN-training, validation and test models was analysed using the R^2 and RMSE values calculated from each data sets (training, validation and test).

6.4. Results and discussion

6.4.1 Soil reflectance and band combinations for salinity indices

For a preliminary analysis, 2-D correlograms of coefficient of determination (R^2) were constructed by sequential regression of reflectance ratios against soil EC (Figure 6.5). The reflectance ratios include all possible pair combinations of narrow bands in the range 400 - 2450 nm.

For the experiment-scale data sets, the 2-D correlograms show several "hot spots" indicating relatively broad regions of high correlation between reflectance ratios and soil EC. The "hot spots" indicate wavelength combinations with R^2 values higher than 0.7. Apparently, the best performing band combinations are those in NIR and SWIR regions of the soil spectra. The reflectance spectra of salt-affected soil samples rich in $MgSO_4$ and $MgCl_2$ provide high R^2 over larger portions of NIR and SWIR regions, indicating potential for estimation of salinity levels (Figure 6.5a). For soil samples rich in NaCl and KCl, the number of well performing band combinations is limited and with low R^2 values.

For the field-scale data sets, 2-D correlograms (Figure 6.5b) show that the reflectance spectra of salt-affected soils with sandy texture (grids 1 and 6) have better correlations with EC_a and that the potential spectral bands for salinity estimation are in the NIR and SWIR regions of the soil spectra. On the contrary, reflectance spectra of salt-affected soils with sandy loam to loam texture in grids 2, 3, 4 and 5 have weak correlations with EC_a. The saline soil in grids 2, 3, 4 and 5, because of their texture and location in the lowlands where the groundwater level is close to the surface (1.5 to 2 m), also have higher moisture content than saline soils in grids 1 and 6. Consequently, the relationships between EC_a and reflectance of saline soils in grids 2, 3, 4 and 5 are poorer as compared to those in grids 1 and 6.

For the image-scale data sets, the magnitude R^2 values between EC_a and reflectance ratios (Figure 6.5c) are similar to those with the experiment-scale data sets and are mostly higher than those with the field-scale data sets. "The hot spot" in Figure 6.5c indicates that potentially useful spectral bands for salinity estimation are those in the NIR and SWIR regions.

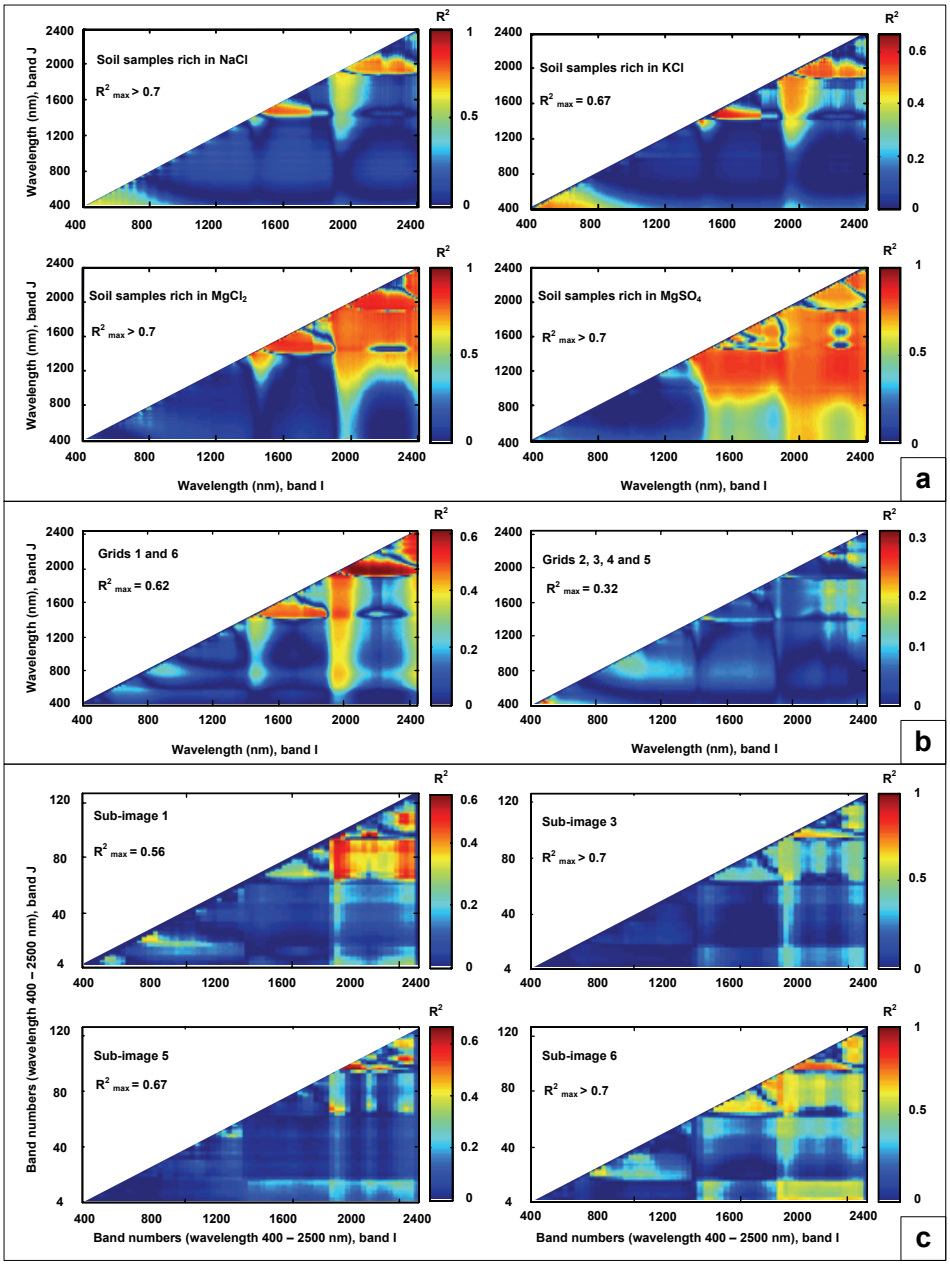

Figure 6.5: The 2-D correlogram represents the R^2 values between the ratio index (wavelength I / wavelength J) and EC for the laboratory and 4 different salt solutions (a), field measurements (b) and airborne hyperspectral image (c).

6.4.2 PLSR model for salinity estimations

Application of the PLSR algorithm to the various data sets resulted in calibration models and examples of PLSR calibration model parameters are illustrated in Figure 6.6. The optimal number of latent variables (or orthogonal factors) that can be used for salinity estimation can be defined through analysis of RMSECV and RPD values of the calibration models. The predictive ability of individual *X*- and *Y*-variables as a function of the number of PLSR factors can be identified by the amount of variation in both *X* and *Y* data explained by the latent variables.

For all the data sets, more than 95% of variations are explained by the first five latent variables (Table 6.3). The contribution of each wavelength (band) can be visualized by analysis of the computed loading weights (LWs). Computed LWs stress further the results of 2-D correlograms analysis that spectral bands useful for salinity estimation are those in NIR and SWIR regions. Strong co-variation between soil EC_a and soil reflectance in the NIR and SWIR regions can also be visualized in the form of positive and negative peaks of the regression coefficients *B* (Figure 6.7). The statistics of estimated *Y*-variable given in Table 6.3 show how well soil salinity can be estimated from reflectance data by application of the PLSR methods.

For experiment-scale data, the RMSE and RPD values together with the total variation in *Y* explained by model variables indicate that the calibration models for soil samples treated with NaCl, $MgCl_2$ and $MgSO_4$ are performed better than calibration model soil samples treated with KCl (Table 6.3). For field-scale data sets the performance of calibration models are poor. For image-scale data sets, the RPD and RMSE values and the explained variation in *Y* derived from all the calibration models, except for sub-image 2, suggest reliable prediction ability (Table 6.3). The PLSR-calibration models developed for each data set at each scale were then used to estimate soil salinity. The accuracy of the estimated salinity values and the performance of predictive models were deduced for the experiment-, field- and image-scale data sets based on the performance statistics derived from measured and predicted salinity values and on the calculated model performance indices (Table 6.4).

For the experiment-scale data, the results show that accurate predictions of EC can be made based on PLSR models developed from samples rich in $MgSO_4$ and $MgCl_2$ (Figure 6.8a and Table 6.4). For samples rich in KCl and NaCl, the predictions of EC can be considered good, because the R^2 values are higher than 0.81 and the RPD of prediction varies between 2.1 to 6.3. This is also indicated by the low RMSE and MAE values and high ME values (Table 6.4) obtained from PLSR-predictive models for the same data sets. The higher salinity prediction accuracy for soil samples rich in $MgSO_4$ and $MgCl_2$ can be attributed

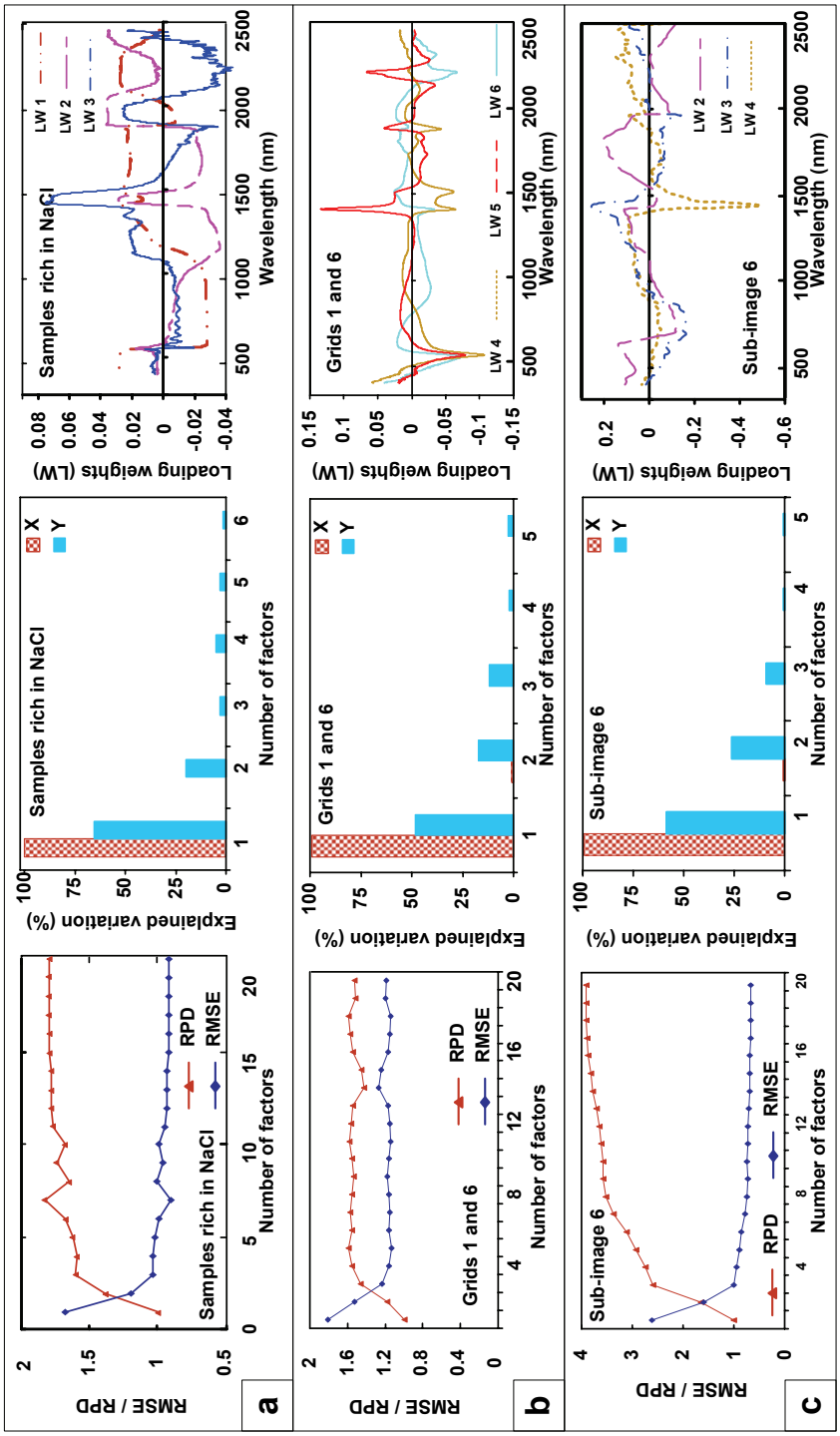

Figure 6.6: Parameters of PLSR calibration model. a, b and c, represents three representative examples selected from laboratory, field and hyperspectral data, respectively.

Table 6.3: Performance statistics of PLSR calibration models

Data-scale	Data sets	Nr.	RMSE	R^2	RPD	Explained variations by model variables (%)				
						X1	X2	Y1	Y2	Total Y
Experiment-scale	KCl	7	33	0.78	1.0	99.7	0.15	59.5	20.7	95.9
	NaCl	6	15	0.81	2.0	99.8	0.14	65.2	19.8	97.6
	$MgCl_2$	12	18	0.92	1.0	99.4	0.64	58	31.7	100
	$MgSO_4$	6	41	0.98	2.0	97.7	2.25	72.1	18.5	99.8
Field-scale	Grids 1& 6	11	14	0.80	1.6	99.2	0.7	48.1	17.4	86.4
	Grids 2 to 5	19	59	0.60	1.5	99.8	0.1	85.1	3.8	97.8
	All grids	12	87	0.60	1.6	99.4	0.4	64.7	7.9	90.4
Image-scale	Sub-image 1	20	97	0.86	2.4	99.9	0.02	61	11	96.0
	Sub-image 2	22	72	0.61	1.6	99.9	0.02	96	1.2	98.5
	Sub-image 3	30	101	0.87	2.7	99.9	0.05	64	14	95.6
	Sub-image 5	23	73	0.91	3.0	99.9	0.03	71	7.7	97.6
	Sub-image 6	19	67	0.94	3.9	99.9	0.06	58	26	98.0

Nr. = Number of latent variable used by calibration model. X_1, X_2 = Explained variations X (%) by latent variables 1 and 2 respectively. Y_1, Y_2 = Explained Y-variations (%) by latent variables 1 and 2 respectively. Total Y = Total explained Y-variation by number of latent variables used for prediction. RPD is a ratio showing accuracy of the PLSR calibration model (Not reliable 1.5 < RPD > 2.5 reliable).

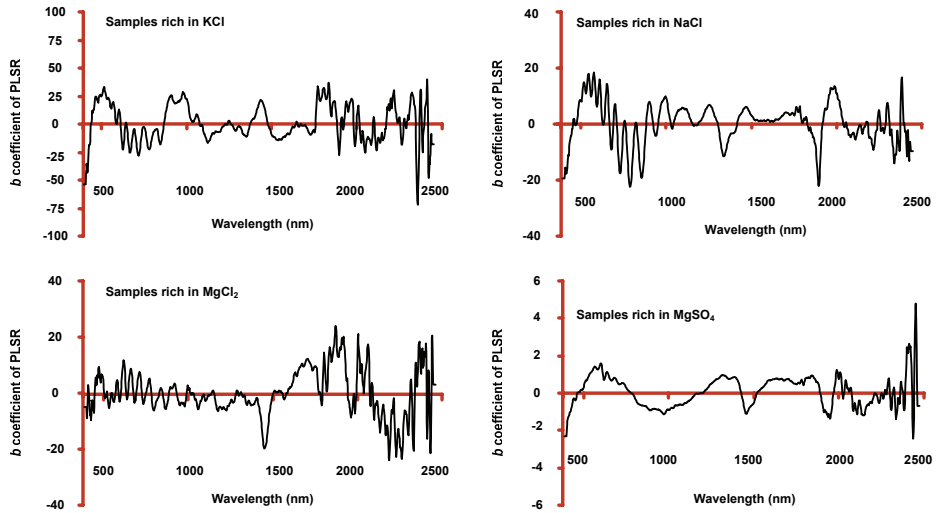

Figure 6.7: Regression coefficients of *B* derived from PLS calibration model for 4 salt types of laboratory data.

to: 1) salt-induced absorption bands at around 1488, 1630, 1946, and 1556, 1451 and 1952 nm (chapters 2 and 3), 2) enlargement of width and area of absorption bands at around 1400 and 1900 nm due to increase in salt concentration in soil, 3) a strong decrease in soil albedo with increasing soil salinity, and 4) shift of the maximum reflectance shoulder towards shorter wavelengths as the salt concentration increases (chapter 4). For soil samples salinized by KCl and NaCl, the predicted EC_a values are on average higher than the measured EC_a (Table 6.5). The high RMSE, MAE values and the low ME values (Table 6.4) confirm the large differences between measured EC_a and EC_a values predicted by PLSR models for these samples (KCl and NaCl).

The field-scale data sets resulted in generally poor relationships between EC_a values and soil reflectance (Table 6.4). The high RMSE% and MAE% and low ME values indicate large variations between measured and estimated EC_a values for the field-scale data. The field data from grids 1 and 6 provide slightly better prediction results (R^2 = 0.8 and RPD = 2.2), while the R^2 and RPD values in grids 2-5 are low (R^2 = 0.6 and RPD=1.3). Note that (a) the experimental-scale data sets were obtained from laboratory-dried soil samples, (b) the field-scale data sets were obtained in-situ in an area with tropical climate, and (c) the image-scale data sets pertain to an area with semi-arid climate. Therefore, the poor soil salinity estimations from reflectance spectra resulting from the field-scale data sets are mostly likely due to high soil moisture.

Table 6.4: Performance statistics of PLSR predictive models

Data-scales	Data sets	R^2	RMSE	RMSE%	MAE	MAE%	ME	RPD	Nr.	PLSR coefficients	
										Slope	Intercept
Experiment-scale	KCl	0.78	13.1	37.1	11.1	31.2	0.74	1.5	8	0.687	13.4
	NaCl	0.81	12.8	33.3	10.4	27.1	0.75	1.7	6	0.712	16.5
	$MgCl_2$	0.92	4.4	28.0	3.3	21.1	0.90	3.5	12	1.01	-1.21
	$MgSO_4$	0.98	1.3	11.6	1.0	9.0	0.97	6.2	6	1.01	0.142
Field-scale	Grids 1& 6	0.80	70.0	44.0	50.0	32.0	0.78	2.1	10	0.883	25.1
	Grids 2 to 5	0.60	60.0	28.0	47.0	22.0	0.50	1.4	23	0.784	32.7
	All grids	0.60	88.0	48.0	68.0	37.0	0.56	1.5	17	0.830	36.1
Image-scale	Sub-image 1	0.86	87.4	29.8	66.6	22.7	0.86	2.6	22	0.897	22.8
	Sub-image 2	0.61	73.5	13.0	56.0	9.9	0.60	1.2	16	0.628	217.0
	Sub-image 3	0.87	101.0	27.8	76.6	21.1	0.86	2.5	22	0.875	31.2
	Sub-image 5	0.91	67.1	19.6	48.5	14.1	0.91	3.1	19	0.916	14.2
	Sub-image 6	0.94	63.2	20.5	40.0	13.0	0.94	4.2	16	0.927	36.9

Nr. = Optimal number of latent variable used by predictive model.

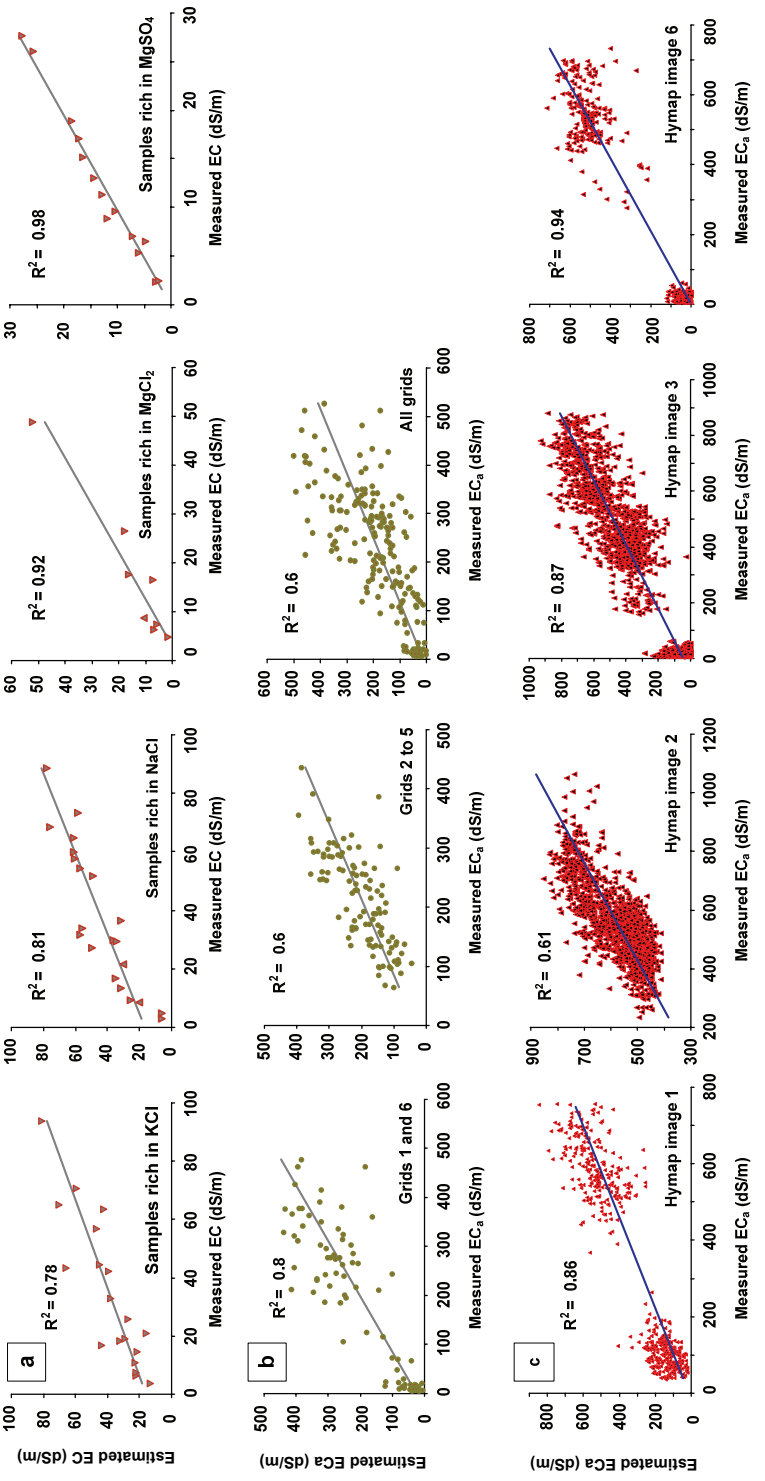

Figure 6.8: Scatter plots of measured vs. predicted EC_a derived from PLSR analysis of soil reflectance.

Table 6.5: Descriptive statistics of measured and predicted EC by PLSR and ANN models. The statistics are from the data used for testing and validation of the models.

Data scale	Data sets	Minimum			Mean			Median			Maximum			Std. Dev.			SE Mean			Skewness			Kurtosis			N
		MY	PY	AY	MY	PY	AY	MY	PY	AY	MY	PY	AY	MY	PY	AY	MY	PY	AY	MY	PY	AY	MY	PY	AY	
Experiment-scale	KCl	3.9	13.3	1	35	39	27	27	38	27	96	81	71	26	19	23	6	4.4	5.2	0.8	0.7	0.5	-0.2	-0.2	-0.9	19
	NaCl	3.0	6.0	9.1	38	44	39	33	49	29	91	78	94	26	20	24	5.6	4.4	5.2	0.4	0.3	0.9	-0.9	-0.6	-0.2	21
	$MgCl_2$	3.2	1.7	6.6	16	15	14	11	9.0	10	48	52	43	15	16	12	5.4	5.7	4.3	1.7	2.2	2.5	2.8	5.5	6.7	8
	$MgSO_4$	1.6	-0.7	3.8	12	12	11	10	12	10	28	28	26	8	8	7	2.1	2.2	1.9	0.7	0.4	0.7	-0.2	-0.5	-0.5	15
Field-scale	Grids 1& 6	5.0	-74	13	160	166	158	121	136	126	477	437	462	151	150	137	15	15	14	0.38	0.23	0.6	-1.4	-1.4	-1.0	100
	Grids 2 - 5	65	-26	90	211	198	212	212	185	215	436	394	352	80	84	65	7.7	8.1	6.3	0.25	0.24	-0.1	-0.6	-0.4	-1.0	108
	All grids	5.0	-131	10	186	166	192	194	160	203	477	498	451	122	132	100	8.5	9.1	7.0	0.02	0.53	-0.1	-0.9	-0.3	-0.7	208
Image-scale	Sub-image 1	32	-107	-23	293	282	295	128	200	209	713	823	695	235	222	219	10.2	9.6	9.5	0.4	0.4	0.29	-1.6	-1.2	-1.6	530
	Sub-mage 2	278	411	358	566	562	568	551	532	538	1069	850	833	117	92	91	2.8	2.2	2.2	0.9	0.9	0.99	1.1	-0.2	0.1	1736
	Sub-image 3	5.8	-198	-94	363	359	362	409	381	373	880	929	938	270	253	250	6.5	6.1	6.0	0.03	0.02	0.03	-1.3	-1.1	-1.2	1747
	Sub-image 5	3.7	-161	-79	343	340	342	459	444	461	647	758	686	220	211	207	6.9	6.7	6.5	0.8	0.8	0.78	-1.2	-1.0	-1.1	999
	Sub-image 6	4.8	-128	-80	308	294	308	470	453	484	734	713	672	262	257	256	10.5	10.4	10	0.1	0.2	0.17	-1.8	-1.8	-1.9	618

SE Mean = mean standard error of the mean, MY = measured EC, PY = predicted EC by PLSR models, AY=Predicted EC by ANN models, N= sample size.

For the image-scale data sets, the R^2, RPD, and ME values of predictive models of sub-image 1, 3, 5 and 6 are satisfactory (Table 6.4). Even though the results of the PLSR analysis of the image-scale data sets suggest high correlation between soil spectra and EC_a values, it has to be remembered that spectral variations at the image level can also be due to variations in vegetation density and type (land cover), soil moisture, soil type and reflectance of other scene components within a pixel area. It is noted also that the measured EC_a values represent salinity of the soil profile (1.5 m depth), whereas the image reflectance data pertain only to land surface. Despite this important difference, the good to high co-variation between the measurements is remarkable. For sub-image 2 the low R^2, RPD and ME values indicate poor linear relationship between the measured EC_a and soil reflectance. Whereas, the low RMSE% and MEA% values suggest considerable similarity between measured and estimated EC_a. This discrepancy (poor relationship but low estimation errors) probably suggests non-linear relationship between soil salinity and soil reflectance, but then the PLSR made a good linear fit.

6.4.2.1 Salinity mapping using PLSR models

Using the HyMap hyperspectral imagery, the PLSR calibration models developed for the image-scale data sets were employed to map variations in soil salinity in each of the six small representative windows (70 x 100 pixels) of sub-images 1, 2, 3, 5 and 6 in the Lake Toolibin area in Western Australia (see Figure 6.1b). The restriction to small windows was necessary as the PLSR software package used can not handle larger data sets. For each window, a salinity map was created from predicted EC_a values recoded into seven salinity classes (Figure 6.9). As part of a post-classification processing, prior to map presentation, each map is smoothed with a median filter (size 7x7) to suppress high frequency variations (e.g., noise) and to portray only the general soil salinity pattern.

Descriptive statistics derived from the salinity maps (Table 6.6) show that the maximum of estimated EC_a values in some of the selected areas (Figures 6.9d and e) are higher than the maximum of measured EC_a vaues, whereas in other areas (Figures. 6.9a, c and f) the estimated EC_a values have a similar range as the measured EC_a values (see Table 6.5).

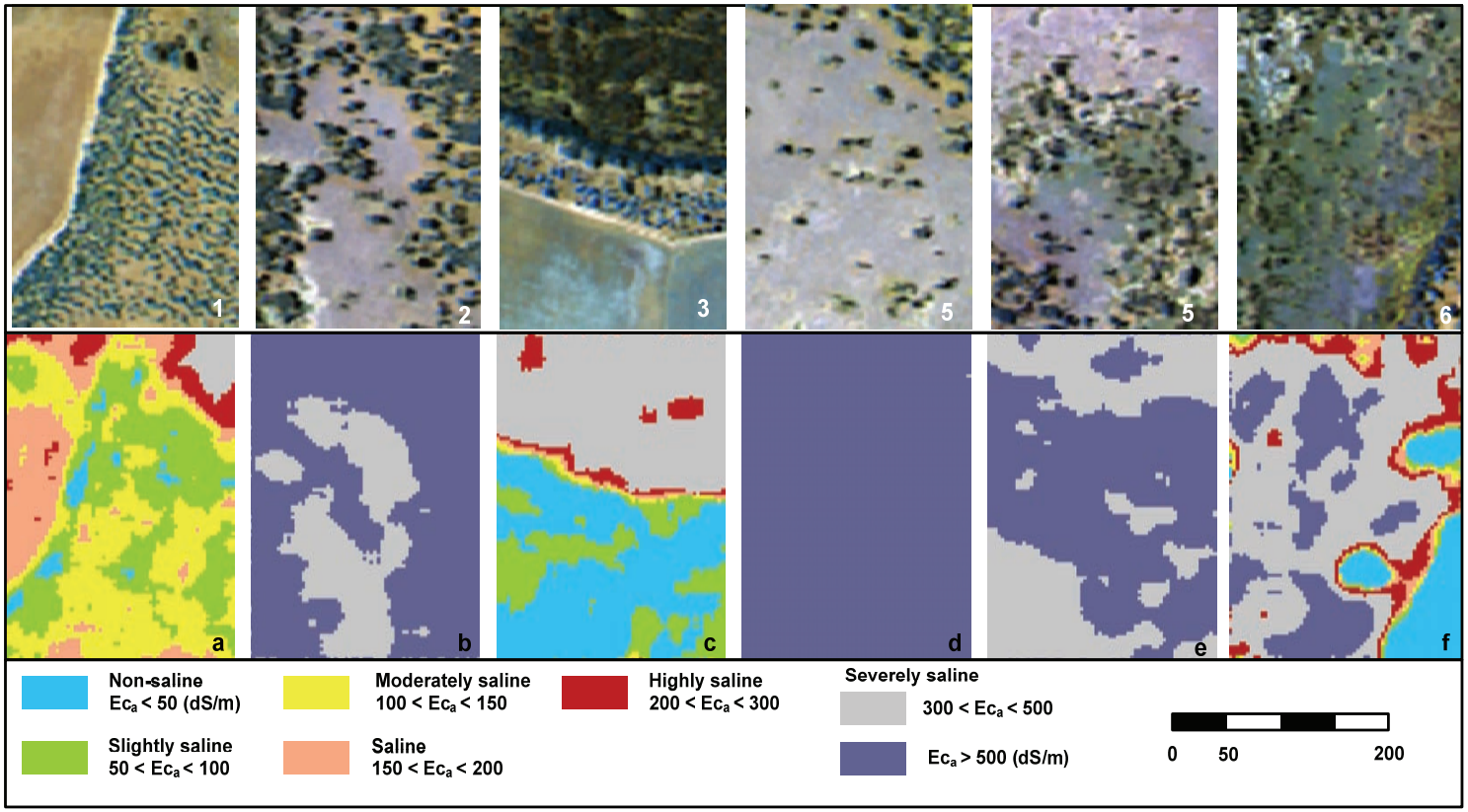

Figure 6.9: Salinity maps (a, b, c, d, e and f) resulted from PLSR analysis applied to windows (70 x 100 pixel) of hyperspectral images (A, B, C, D, E and F). Location of map a to f is indicated in Figure 6.1.

Table 6.6: Summary statistics derived from salinity maps.

Statistics	Sub-image a		Sub-image b		Sub-image c		Sub-image d		Sub-image e		Sub-image f	
	PLSR	ANN	PLSR	ANN	PLSR	ANN	PLSR	ANN	PLSR	ANN	PLSR	ANN
Minimum	0	0	456	418	0	0	785	0	514	334	0	0
Maximum	449	434	564	625	448	615	1088	519	1354	609	703	673
Mean	128	123	515	503	176	296	992	438	839	508	372	487
Std. dev.	63	60	21	26	154	164	34	68	125	30	176	150

6.4.3 Neural network model for salinity estimations

For the experiment-scale data sets, four ANN models were developed (one for each salt mineral). The R^2 and RMSE are generally highest and lowest, respectively, for the training models (Table 6.7). This is probably because the weights and biases are optimized during training. RMSE at various phases of learning for training, validation and test data sets is illustrated in Figure 6.10. Overall, ANN models for soil samples salinized with $MgCl_2$ and $MgSO_4$ have higher R^2 and lower RMSE and MAE values than ANN models for soil samples salinized with KCl and NaCl. The R^2 and RMSE values for the training model and the poorer R^2 and RMSE values for the validation and test models indicate that the ANNs models learned quite well but have poor generalization ability, probably because of small size of data sets.

For the field-scale data sets, the R^2 values of validation and test data sets (e.g., grid 1 & 6) are mostly lower than for the training data set (Table 6.7). This suggests that the ANN models for the field-scale data did not learn quite well and thus have poor generalization ability (Figure 6.10). In general, soil salinity prediction accuracy using the field-scale data sets is relatively poor. As already mentioned before (§ 4.2), the poor accuracy of estimated EC_a based on the field-scale data sets is presumably related to the field and climate conditions and/or accuracy of the field equipments.

For image-scale data sets, the ANNs models are satisfactory. The high R^2 values obtained from most of the sub-image data sets indicate that the ANN models mostly learned quite well and mostly have good generalization ability (Figure 6.10). The estimates of EC_a values in sub-images 1, 3, 5 and 6 ($0.86 < R^2 < 0.96$ and $2.5<RPD<4.9$) are very good. This is also supported by RMSE, MAE and ME values. In sub-image 2, estimates of EC_a values are poor (Table 6.7). The correlations between measured and estimated soil EC_a at the various phases of ANN modelling (training, validation and testing) are illustrated in Figure 6.11. The results in Figure 6.11 and Table 6.7 indicate generally that hyperspectral imagery provides suitable data for soil salinity mapping over large areas, if an accurate salinity model from ground data in a representative training site is available.

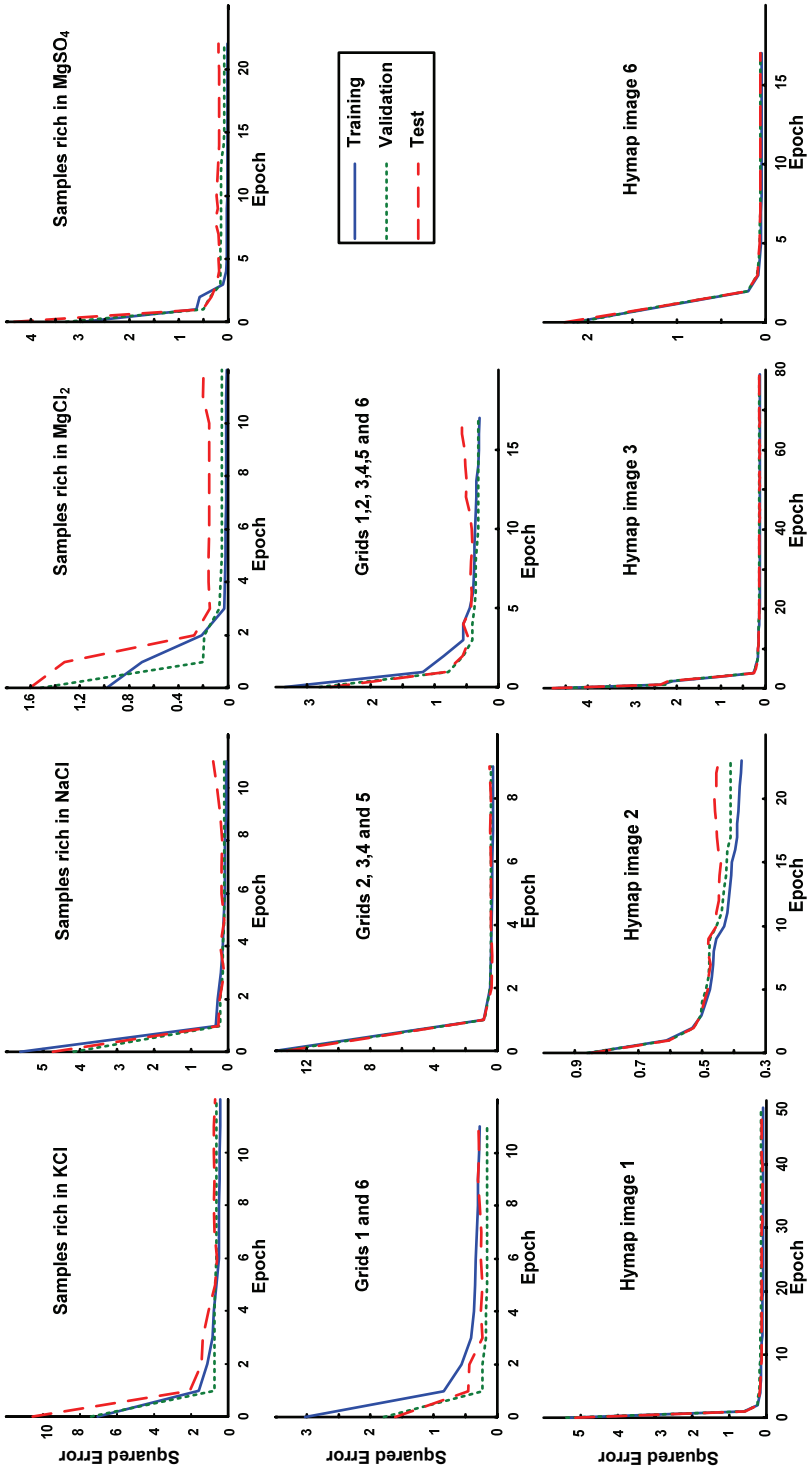

Figure 6.10: MSE at various phase of learning for training, validation and test data sets for laboratory, field and airborne imageries.

Table 6.7: ANN model parameters for soil salinity (EC_a) estimation.

Data-scale	Data sets	RMSE			R^2			Predictive model parameters							Nr. Of ite.	Nr. of neu.
		Tra.	Val.	Test	Tra.	Val.	Test	R^2	ME	RMSE	RMSE%	MAE	MAE%	RPD		
Experiment-scale	KCl	16.1	17	13.6	0.65	0.5	0.9	0.73	0.56	15.7	44.3	13.6	38.3	1.7	10	9
	NaCl	3.45	8.5	9.4	0.98	0.86	0.86	0.87	0.84	9.4	24.5	7.7	20.1	2.5	14	9
	$MgCl_2$	1.8	3	5.4	0.98	0.98	0.88	0.89	0.79	5.3	33.8	4.3	27.3	2.3	13	5
	$MgSO_4$	0.55	2.3	2.8	0.99	0.87	0.91	0.97	0.96	1.4	12.5	0.9	7.7	5.0	20	5
Field-scale	Grids 1 & 6	105	82	89	0.69	0.72	O.60	0.65	0.56	91.0	57.0	65	41.0	1.5	11	9
	Grids 2 - 5	66	61	62	0.42	0.41	0.42	0.46	0.17	59.0	28.0	46	22.0	1.1	16	9
	All grids	89	78	78	0.67	0.54	0.50	0.59	0.39	79.0	42.0	61	32.0	1.3	12	9
Image-scale	Sub-image 1	86	87	90	0.87	0.86	0.85	0.86	0.84	90.3	30.8	59.7	20.4	2.5	25	7
	Sub-image 2	73	75	77	0.6	0.58	0.56	0.60	0.15	67.1	11.9	47.2	8.3	1.2	75	11
	Sub-image 3	100	101	102	0.86	0.86	0.86	0.86	0.89	89.3	24.6	63.4	17.5	2.5	89	13
	Sub-image 5	68	71	72	0.9	0.9	0.89	0.89	0.80	68.2	19.9	42.4	12.4	2.9	30	11
	Sub-image 6	45	52	51	0.97	0.96	0.96	0.96	0.96	61.4	20.0	35.7	11.6	4.9	58	11

Tra. = Training, Val. = Validation, Nr. of ite. = Number of iterations, Nr. of neu. = Number of neurons

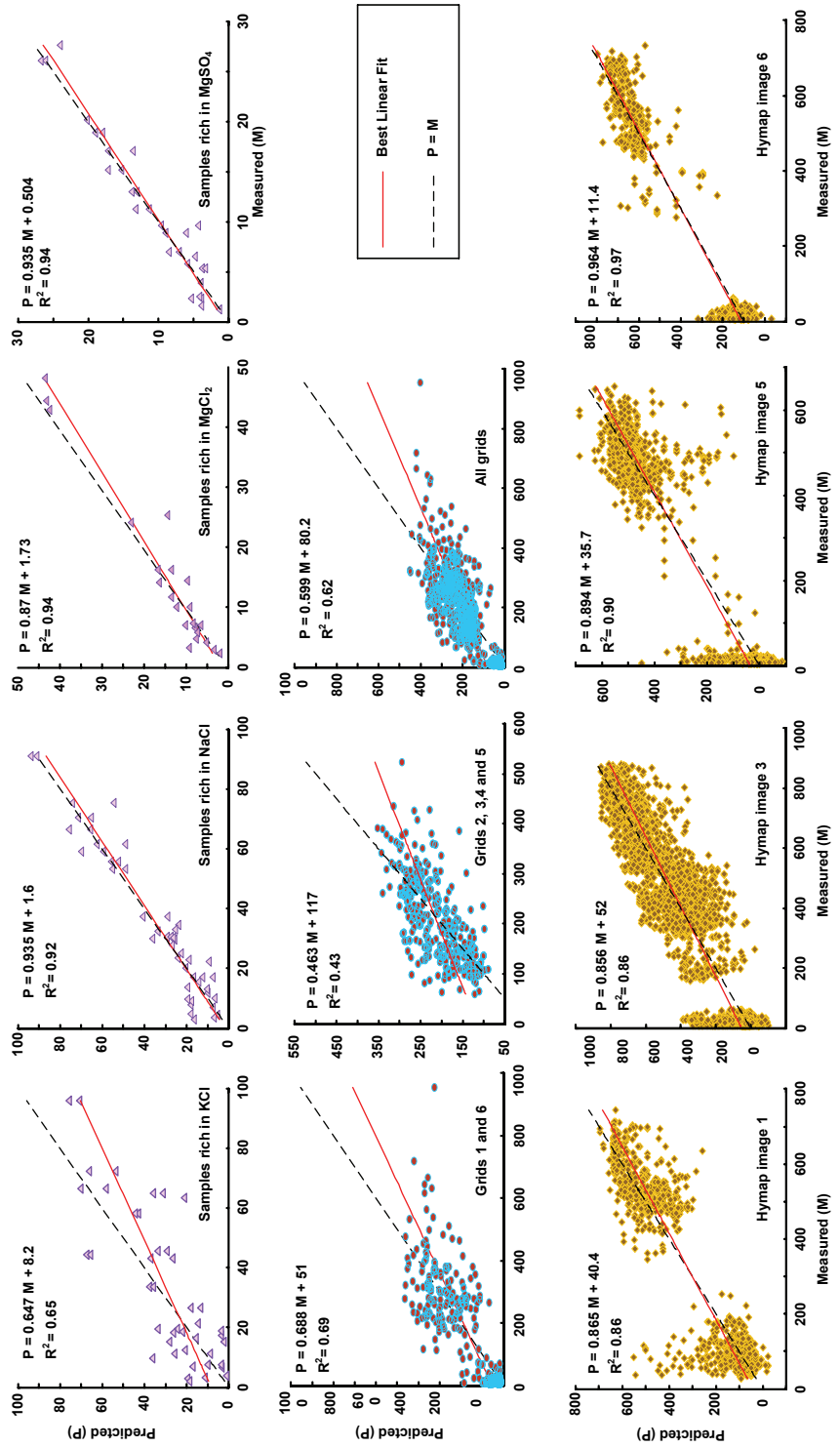

Figure 6.11: Scatter plots of measured EC_a vs. predicted EC_a derived from ANN analysis of soil reflectance.

6.4.3.1 Salinity mapping using ANN models

The image reflectance data in the six small representative windows (70 x100 pixels) selected from the hyperspectral image (see Figure 6.1) were used in the ANN models previously trained with the image-scale data sets to map the spatial distribution of soil salinity. For each window, a salinity map was created with a maximum of 7 salinity classes (Figure 6.12). A median filter (window size 7x7) was applied to the maps of estimated EC_a values as a post-classification technique to reduce high frequency variations and to smooth the boundaries between soil salinity classes.

The descriptive statistics derived from the salinity maps show that the predicted EC_a values in the selected areas are quite lower than the observed EC_a values. For example, the maximum observed EC_a values in sub-images 2, 3 and 5 are 1069, 880 and 647 (dS/m), respectively (see Table 6.5), while the maximum predicted EC_a values in the salinity maps within the same sub-images are 625, 615 and 609 (dS/m), respectively (see Table 6.6). The tendency of ANNs to underestimate EC_a, is not clear but probably, can be associated to data distribution, spectral characteristics of the imagery (mixed pixel; e.g., influence of land cover specially vegetation) or ANN generalization.

6.4.4 PLSR vs. ANN

To properly compare robustness of PLSR-predicted EC_a values vis-à-vis ANN-predicted EC_a values with respect to corresponding measured EC_a values, the statistical parameters used earlier (§ 4.2 and 4.3) to assess the performances of individual models cannot be used appropriately to compare between PLSR and ANN models because of the differences in data treatment in each of the two modelling techniques. In order to have uniform basis upon which to judge whether soil salinity predictions based on reflectance data are robust if PLSR is used or if ANN is used, these three sets of EC_a values were assumed to be replicate measurements by different methods and one-way analysis of variance (ANOVA) was performed. One-way ANOVA was performed in two sets, one set by using measured and PLSR-predicted EC_a values and another set by using measured and ANN-predicted EC_a values. The null hypothesis in either set of one-way ANOVA is that a set of measured EC_a values and a corresponding set of predicted EC_a values have, with respect to variance, identical means. This null hypothesis is tested by calculating an F-value and comparing this with a critical F-value at a certain significance level. The calculated F-values not only allows further assessment of individual PLSR or ANN salinity-reflectance models but also provide bases, in terms of magnitude of calculated F-values and their corresponding p-values, to judge if a PLSR model is better than its corresponding ANN model or vice versa.

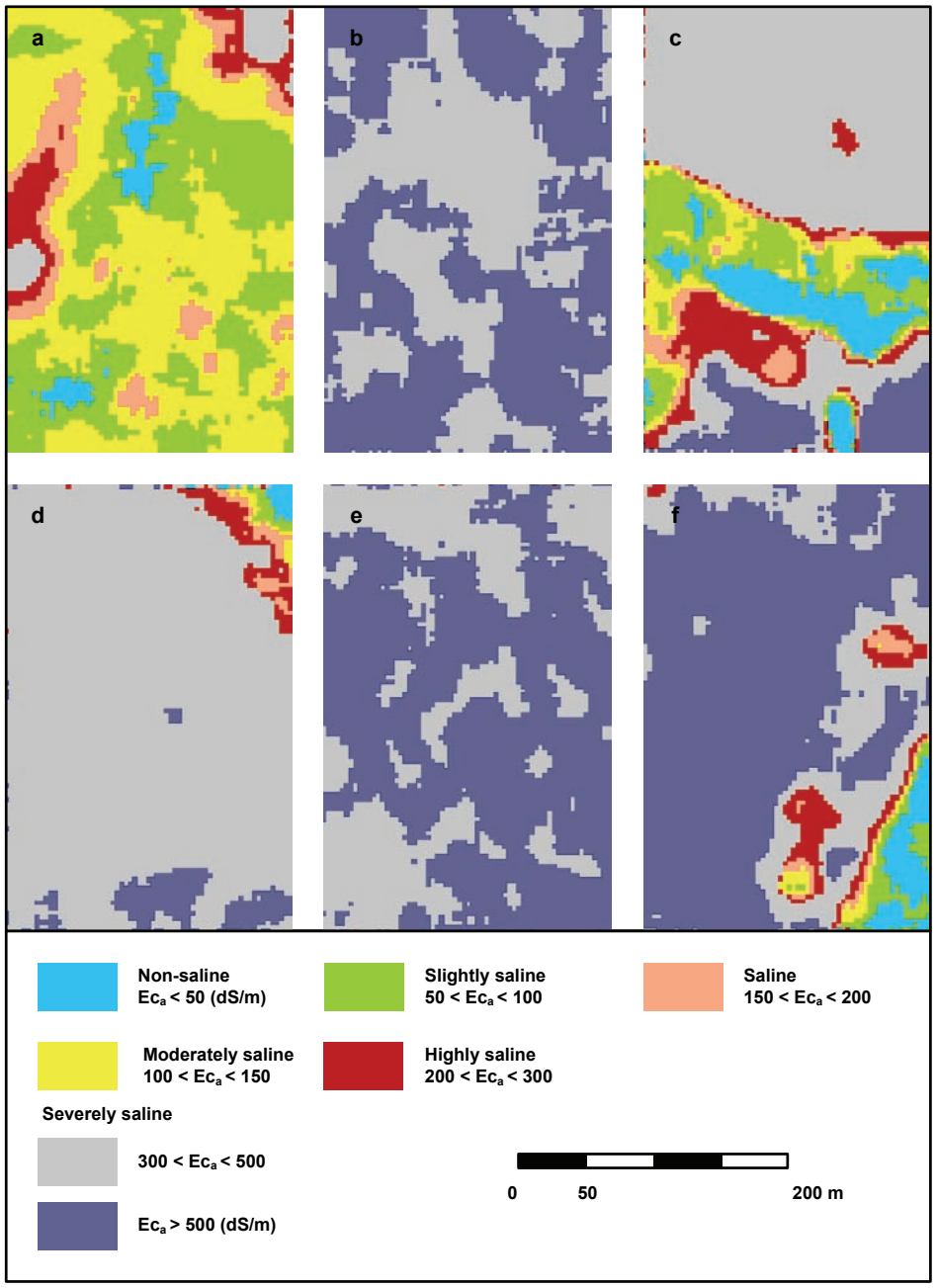

Figure 6.12: Salinity maps (a, b, c, d, e and f) resulted from estimated values by ANN models applied to six windows (70 x 100 pixels) selected from hyperspectral images (see Figure 6.10: A, B, C, D, E and F).

For the experimental-scale data sets, the calculated F-values between measured and PLSR-predicted EC_a values and between measured and ANN-predicted EC_a values are all statistically smaller than the corresponding critical F-values (Table 6.8). These results suggest that the sets of predicted EC_a values, either by PLSR or ANN, are statistically identical to their corresponding sets of measured EC_a values. It can also be gleaned from Table 6.8, that the F-values and corresponding p-values are consistently better for soil samples treated with $MgCl_2$ or $MgSO_4$ than for soil samples treated with KCl. This result sustains the results described and discussed in the previous sections (§ 4.2 and 4.3) that soil salinity prediction based on reflectance data would be dependent on salt types. The sizes of the experimental-scale data sets are small, however, so that the suggestion of these results as to performance of the individual models might not be conclusive really. In addition, the p-values of calculated F-values do not show a clear pattern to suggest that PLSR-predicted EC_a values are better than ANN-predicted EC_a values or vice versa.

Table 6.8: Results of one-way ANOVA between measured and PLSR-predicted EC_a values and between measured and ANN-predicted EC_a values. p-value significant at $p<0.05$

Data-scale	Data sets	PLSR		ANN		F critical	df
		F	p-value	F	p-value		
Experiment-scale	KCl	0.2130	0.6472	1.0518	0.3119	4.11	1 , 36
	NaCl	0.5755	0.4525	0.0019	0.9658	4.08	1 , 41
	$MgCl_2$	0.0173	0.8972	0.0612	0.8082	4.60	1 , 14
	$MgSO_4$	0.0099	0.9216	0.0015	0.9699	4.20	1 , 29
Field-scale	Grids 1&6	0.0909	0.7633	0.0083	0.9274	3.89	1 , 198
	Grids 2-5	1.3460	0.2473	0.0093	0.9234	3.89	1 , 214
	All grids	2.6568	0.1039	0.2830	0.5950	3.86	1 , 414
Image-scale	Sub-image 1	0.6543	0.4188	0.0166	0.8976	3.85	1 , 1058
	Sub-image 2	1.4275	0.2323	0.3378	0.5611	3.84	1 , 3470
	Sub-image 3	0.1498	0.6988	0.0043	0.9478	3.84	1 , 3492
	Sub-image 5	0.0841	0.7719	0.0104	0.9188	3.85	1 , 1996
	Sub-image 6	0.7960	0.3725	0.0027	0.9582	3.85	1 , 1234

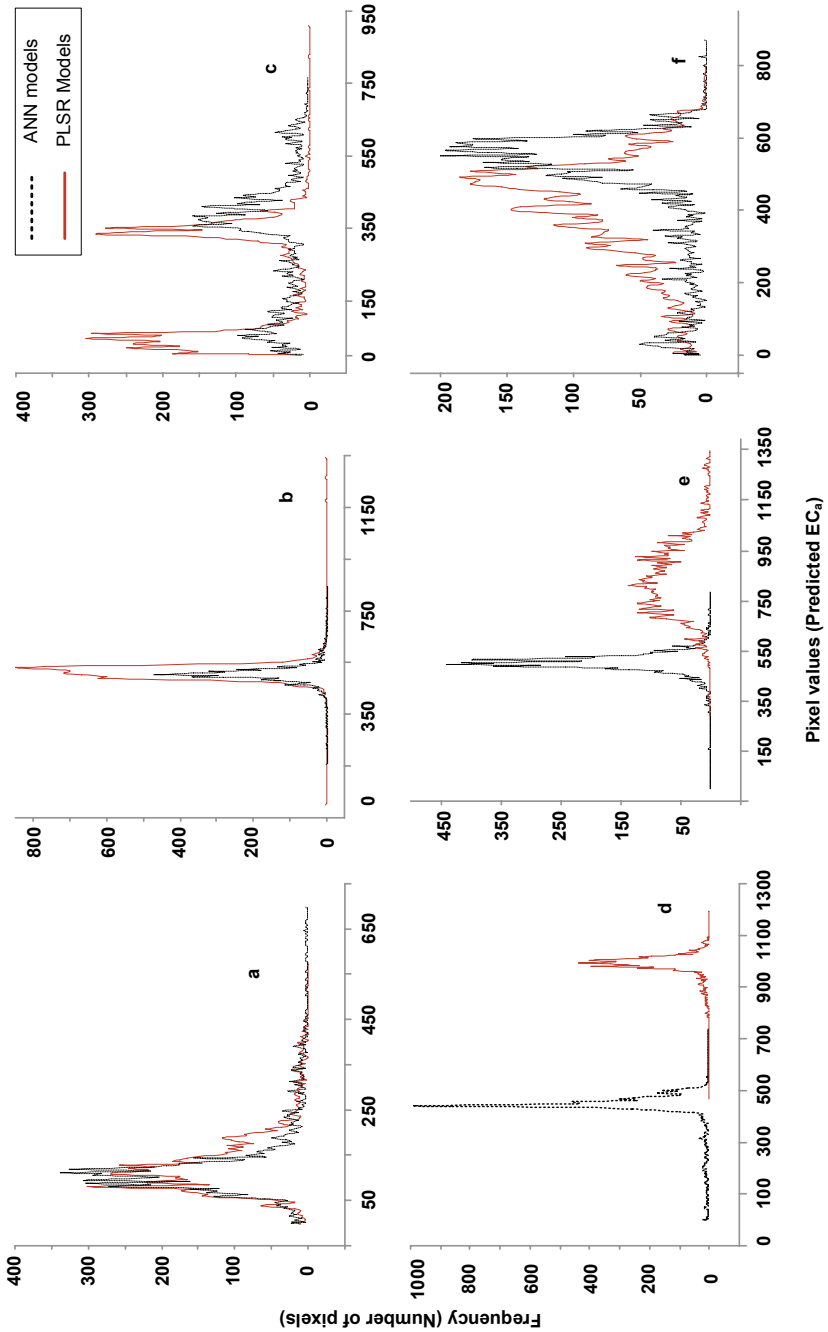

Figure 6.13: Histogram calculated from salinity maps (see Figures 6.9 and 6.12) produced from PLSR and ANN predicted values. Plot a to f refers to map a to f in Figure 6.9 and the location of a to f is indicated in figure 6.1.

For the field-scale data sets, the calculated F-values between measured and PLSR-predicted EC_a values and between measured and ANN-predicted EC_a values (Table 6.8) suggest that the sets of predicted EC_a values, either by PLSR or ANN, are statistically identical to their corresponding sets of measured EC_a values. The F-values and corresponding p-values are lower and higher, respectively, for either PLSR or ANN models in grids 1 and 6 (lower soil moisture due to soil sandy texture) than in grids 2-5 (high variation in soil moisture due to soil sandy loam to loam texture). This result suggests further that high soil moisture content will render ineffective soil salinity estimation from reflectance data. The p-values of calculated F-values between measured and PLSR-predicted EC_a values are consistently much smaller than the p-values of calculated F-values between measured and ANN-predicted EC_a values. These results indicate that based on the field-scale data sets, modelling of relationship between soil salinity and soil reflectance via ANN modelling would result in slightly better soil salinity predictions than via PLSR modelling. The results thus further suggest that, in areas with tropical climate, soil salinity prediction based on reflectance data would be better via ANN modelling than via PLSR modelling.

For the image-scale data sets, the results of the one-way ANOVA (Table 6.8) indicate that the sets of predicted EC_a values, either by PLSR or ANN, are statistically identical to their corresponding sets of measured EC_a values. The results of the one-way ANOVA also suggest that modelling of salinity-reflectance relationship in soils and thus soil salinity mapping based on reflectance would be more robust through ANN modelling than through PLSR modelling. The salinity maps predicted from the image-scale data sets (Figure 6.9 and 6.12), suggest considerable agreement between PLSR and ANN predicted values for salinity maps a, b, c and f; whereas, for salinity maps d and e, the predictions of the PLSR models exceed those of the ANN models (Table 6.8). The histograms of these sub-images show that the predicted values of the ANN models have smaller range and distributions closer to the average (see Table 6.6 and Figure 6.13). The summary statistics (see Table 6.6) also shows that the minimum and maximum values predicted by PLSR models are often higher than the ones predicted by the ANN models. The differences between the salinity maps produced by PLSR and ANN are illustrated in Figure 6.14. The maps have been prepared by subtracting PLSR predictions (Figure 6.9) from ANN predictions (Figure 6.12). The resulting difference maps were than normalized to obtain an index between -1 to 1. Positive values show areas where PLSR predictions are higher and negative values represent areas where ANN prediction values are higher. Values close to zero represent areas of similar predictions and pixels with values close to 1 or -1 represent maximum differences between the two methods.

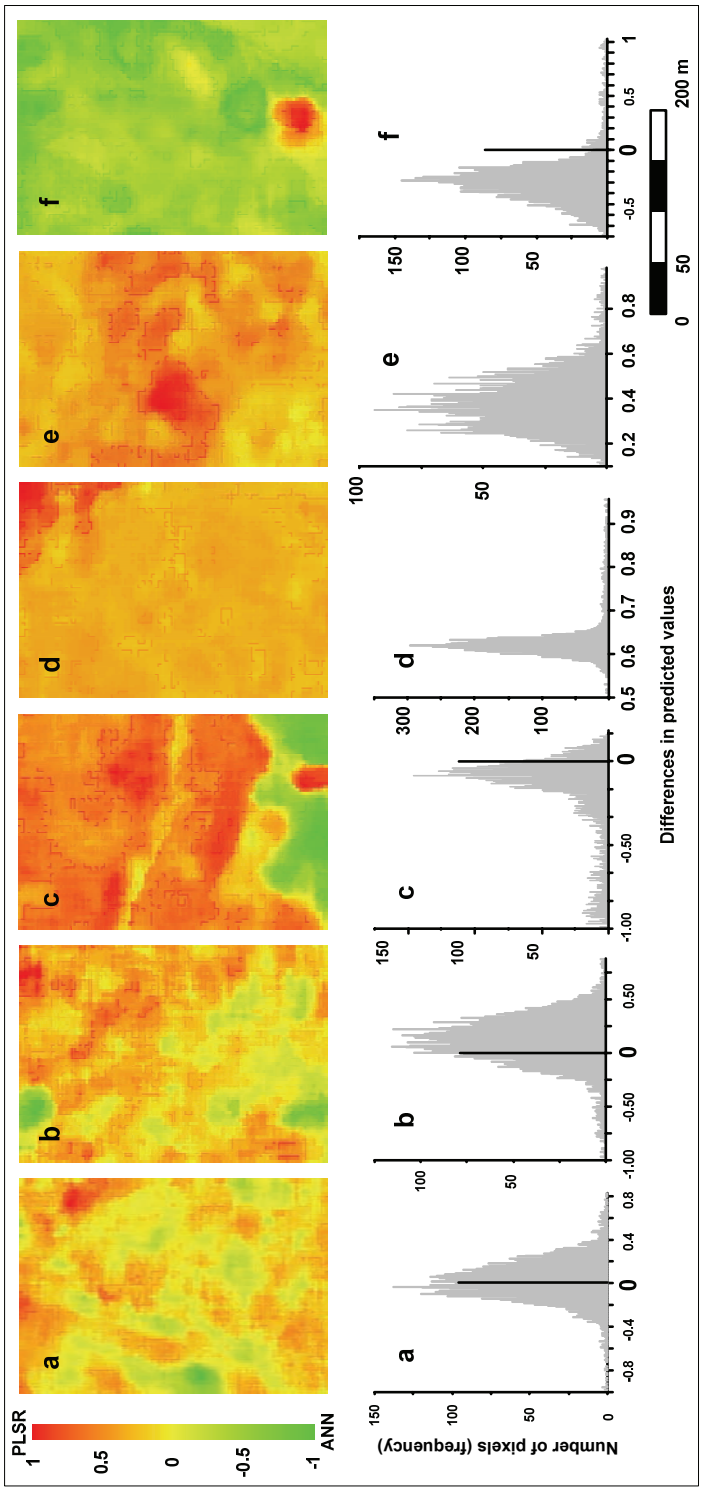

Figure 6.14: Maps a, b, c, d, e and f illustrate the differences between PLSR and ANN prediction values. The calculated histograms from these maps show the distribution of the data in each map.

In summary for calibration of salinity-reflectance relationships and for prediction of soil salinity using reflectance data, the statistics performance calculated between measured and PLSR-predicted EC values and between measured and ANN-predicted EC values show that for the experiment- and field-scale data sets both methods perform similarly, whereas for the image-scale data sets the ANN modelling slightly outperforms the PLSR modelling. The performance differences between these two methods, however, are not large and therefore, soil salinity based on soil reflectance can be predicted and mapped by either PLSR or ANN.

6.5 Conclusions

This research in this chapter examines PLSR and ANN modelling for estimation of soil salinity from spectral data obtained at experiment-, field- and image-scale data sets. Results show that either of two methods is satisfactory for establishing relationships between soils EC. The results allow drawing the following conclusions:

- Both PLSR and ANN modelling permit reliable estimations of soil EC and mapping of soil salinity levels at experiment- and image-scale). The fact that the PLSR approach gave results as reliable as the ANN approach shows that relation between soil salinity and soil reflectance can be described by linear models.

- The major differences between PLSR and ANN algorithm relate to the computation time for establishing the models and the reproducibility of the final models. Network training may take a long time and even with the same data set models developed at the end of every training session are different, since the learning process is started from randomly initialised weights and biases. On the contrary, the PLSR algorithm always results in identical calibration models for the same data set.

- The poor performances of the PLSR and ANN models based on the field-scaled data sets and the better performances of the both method based on the experimental- and image-scale data, in general, suggest the following. Application of PLSR or ANN to estimate soil salinity from reflectance data would be ineffective in areas with tropical climate, unless reflectance data are "demoisturized" or unless the simultaneous yet individual influence of soil moisture and soil salinity on reflected energy are understood and separated a-priori.

- With regard to the field-scale data sets it is unclear what exactly caused the lower accuracy compared to the experiment- and image-scale data sets. Part of the problem has been attributed to the high soil moisture content, soil

texture and tropical climate conditions of the study area as well as the accuracy of the field equipments. Further research works are needed to investigate these factors.

- PLSR and ANN modelling techniques have a high capacity for detecting salt-affected areas at an early stage of salinisation, which is a major development for improving agricultural practices at scales ranging from farms to states.

Chapter 7

Synthesis:
Information on soil salinity modelling; integration of surface and near-surface remotely sensed measurements

Is there any knowledge in the world which is so certain that no reasonable man could doubt it? (Russell, 1912).

Abstract

This chapter provides a summary on quantification of salt variations in soils, including the main research achievements and the results, as presented in chapter 2 to 6. Issues related to salts formation and their excessive accumulations in soil as well as their detrimental affects on soil physical/chemical properties and soil productivities are reviewed (see chapter 2). The proposed conceptual framework includes detecting the early stage of salinization by use of integrating surface and near-surface remotely sensed measurements. Study of spectral characteristics of salt-affected soils under controlled laboratory conditions during an experiment revealed insight knowledge, which provided guidelines for the next phases of the research. The experimental results provide the basis for quantification of similarities or dissimilarities that exhibited in soil reflectance spectra due to various amount of salt in soil. These observed degrees of similarities were used to generate clusters following the standard salinity classes as suggested by US salinity laboratory. The experimental study also showed that effects of salt and moisture on soil

reflectance spectra are significantly similar. This led to examination of the interference of both substances (salt and moisture contents) on soil reflectance, using inverted Gaussian function parameters to predict soil salt and moisture contents. In an up-scaling phase, the previous findings were used to develop modelling tools and predict the degree of soil salinity using hyperspectral image and in-situ geophysics measurements. For four different study areas in The Netherlands, Hungary, Thailand and Australia, statistical and mathematical algorithms such as spectral matching, Gaussian function, partial least squares regression and artificial neural networks showed considerable potentials for quantification and estimating degree of salinity. The research has provided sets of data and scientific methods that have considerable application in soil salinity monitoring and assessments, modelling and predicting early stage of salinization. The research has also provided new research orientations that are useful at local and global scale for developing strategies. Such strategies can efficiently be used for a better management and a sustainable use of land which would be beneficial to both farmers and governments.

7.1 Overview of the research

Excessive salts precipitation in soil profiles develops to the formation of salt-affected soils affecting the physical, chemical and biological properties of the soil, and eventually leads to partial or complete loss of soil productivity. Soil salinity has a large impact in arid and semi-arid regions where lands are extremely needed to supply food and fibre for their rapidly increasing population, while human-induced factors and natural conditions are highly contributing to expansion of saline areas. This conflictive situation is a major concern at local and global scales where enormous efforts had focused on slowing down the salinization and preventing its progression. As a part of these efforts, scientific studies have been carried out to combat salinization. These studies focus on providing comprehensive understanding of the process, developing methods and algorithms, and providing various application tools. In general, optical remote sensing, electromagnetic geophysics and solute modelling are the three most used disciplines for detection, estimation and mapping of salt-affected soils. Each of these methods has advantages, but also constraints which make their use limited in terms of prediction of possible salinization problems and the early stage detection of salinization. Chapter two shows that more accurate estimation and mapping of soil salinity is feasible if predictive modelling tools with integration capability can be developed that combine surface and near-surface measurements. Beside technological advances in data acquisition methods, this is what motivated the research reported in this dissertation.

The research objective was to develop modelling procedures for quantifying soil salt contents (SSC) on basis of variations observed in soil reflectance spectra. The main focus of the research is to develop predictive models for quantitative salt contents in soils on the bases of the integrated use of soil reflectance spectra and geophysical surveys. Briefly, the research covers (*i*) development of the conceptual model for salinization risk assessment; (*ii*) development of the spectrometric techniques for recognizing the presence and abundance of salts in soils; (*iii*) quantifying similarities between salt-affected soils spectra with different electrical conductivity; (*iv*) establishing a relationship between soil properties and soil spectra in laboratory; (*v*) field application of laboratory experiment achievements, using in-situ surface and near-surface measurements; (*vi*) up-scaling using air-borne imageries combined with field data; and (*vii*) predicting and mapping saline areas using modelling tools (integrated approach) and evaluating the results.

The aim of the is chapter (7) is to synthesize main findings and practical outputs of this study and discuss their usability as related to monitoring soil salinization in terms of further applications. Furthermore, it provides some recommendations for the development of applications and for future research.

7.2 Salinity study in a broad perspective

Formation, movement and accumulation of salts have a substantial influence on several aspects of soils, mainly on their physical, chemical and biological properties. Excessive soil degradation and decrease of soil's suitability to grow craps and provide other services are among immediate detrimental effects caused by increase of salt in soil. The damages caused by salts in urban areas are mostly on roads, buildings underground services and drinking water.

Extensive scientific studies, most of them discussed in this dissertation attempt to provide practical methods for monitoring soil salinity in order to provide accurate information for development of sustainable land management strategies. Remote sensing data, geophysical survey, and solute transport modelling are the most commonly used tools and techniques in the identification, large scale mapping and monitoring of the salt-affected areas.
Remote sensing has been widely used to detect and map salt-affected areas with focus on variations in topsoil reflectance due to salt accumulations in soils. Solute transport modelling is used to predict the salt distribution in the soil with focus on dynamics of the salt movement regimes especially in sub-surface. Near-surface geophysics sensors are widely used to map and monitor salt-affected areas with focus on soil profile.

In practice, each of these methods has its advantages and disadvantages which are described in chapter 2. Briefly, the main constraints of remote sensing are related to sensors capabilities that do not allow extracting information from the third dimension of soil the profile: the sub-surface part. Concerning solute modelling, the main restriction is related to the fact that the information derived from a solute model represents the points where the field data were collected and the results have to be interpolated. The main constrain of geophysical survey is related to the fact that the measurements are representing an average apparent conductivity of the materials (as bulk) at a certain depth and influenced also by changes in mineralogy, intensity of alteration and water content. Remote sensing has the advantages of providing high temporal resolution, since thousands of medium to high-resolution imageries from the earth surface are available. Solute transport modelling has the advantage of providing subsoil information on dynamics of the salt movement regimes which can be used as complementary data in combination with remote sensing. Near-surface geophysics has the advantage of efficiently being used to highlight conductive areas where no surface expression of salt is evident.

Considering the complexity of salinization as summarized above, an integrated approach was conceptualized for this research which is presented in chapter 2. This novel method overcomes a number of the early mentioned limitations and constraints and benefited from the advantages of each method. The integrated method involved an up-scaling, where combination of hyperspectral remote sensing and in-situ geophysics measurements with statistical and mathematical modelling tools provided possibilities for estimation and mapping salt-affected area.

However, the application of the suggested research framework has been evaluated partly in this research and will be completed in the near future. It demands further investigation to demonstrate its full potential in predicting, mapping and monitoring salt-affected areas. The focus of such an investigation should be on exploring the possibilities of integrating remote sensing and solute modelling data which has not been evaluated in the study.

7.3 Spectroscopy of salt-affected soils

Salt-affected soils contain various proportions of cations (Na^+, Mg^{++}, K^+, and Ca^{++}) and anions (Cl^-, SO_4^{--}, CO_3^{--} and HCO_3^-) that eventually appear in soil in the form of a (1) salt crust as the result of evaporation, (2) deposit as the result of precipitation, or (3) solution as the result of dissolving in water. Theoretically, they can directly be detected by optical remote sensing since salt minerals have diagnostic spectral signatures occurring in the VNIR-SWIR region. However, this is true only when the salt accumulation in soil is large

enough to crystallize and form salt minerals at the surface, which is mostly not the case. In the experimental study presented in chapter 3, soil samples with large variations in salts was created and used to examine the affect of salt on soil reflectance spectra. While, under the controlled experimental set up, the other soil constituents, including soil moisture contents, were kept almost constant in the period of experiment.

Spectral analyses revealed that salt-affected soil samples do not exhibit all of the diagnostic absorption features that can be found in the spectra of the dominant salt minerals. It showed that the number and clearness of diagnostic bands reduces as the salt concentration in the samples decreases. The results showed that an increase in soil salinity induces changes in soil reflectance for wavebands higher than 1300 nm, particularly in the water absorption bands (around 1400 and 1900 nm). It also revealed that the relation between salinity level and albedo and/or spectral reflectance may be positive or negative, depending on salt mineral and soil type. It was found that spectral responses of soils with different salt contents, in many ways, are similar to the spectra of soils with various moisture contents. The observed absorption features at further than 1400 nm were broaden, the position of maximum reflectance were shifted toward shorter wavelengths and overall reflectance were changed proportionally as salts concentration were increased in soil. The continuum-removed (CR) spectra indicate a strong negative correlation between increase of soil EC and changes in absorption bands parameters (depth, width and area).

A guideline for further studies was provided based on the laboratory experiment results presented in chapter 3 which are:

- Study of salt-affected soil, using hyperspectral data, should largely focus on spectral variations in NIR and SWIR region of soil spectra rather than individual diagnostic absorption signature.

- Quantification of salt-abundances in soil, at up-scaling phase, should mainly focus on using general shape of spectrum rather than absorption bands parameters (depth, area, etc.), since most of the spectral features that diagnose salt minerals or salt-affected soils are masked in an image due to atmospheric effect.

- Further studies are required to unravel the influence of soil moisture contents on the relation between salinity level and spectral reflectance.

7.4 Development of quantification algorithms

The techniques used to quantify variations in soil reflectance spectra are described in chapters 4 and 5. In chapter 4, stochastic and deterministic spectral

matching techniques (similarity measures) were used to determine differences between reflectance spectra of saline and non-saline soil samples. Comprehensive analysis of the visible, near and shortwave infrared regions of reflectance spectra of the salt-affected soil samples by use of spectral matching techniques indicates considerable differences in reflectance magnitude, absorption strength and spectral angle. The results show significant correlations between soil EC and spectral similarity measures, indicating that similarity between the samples' spectrum decreases as the salt concentration in soil increases. The results confirm that spectral similarity measures can be used as diagnostic indicators to differentiate among salt-affected soils spectra obtained from laboratory experiment.

The values obtained from the different spectral matching techniques were also used to determine their potential in soil salinity classification. The results of hierarchical numerical classification method applied to spectral similarity values confirm that the spectral variations in salt-affected soils are sufficient to provide bases for aggregation in classes that are in agreement with standard international salinity classes as defined by US salinity laboratory.

The significance of the observed spectral differences between salt-affected soil samples spectra was statistically examined. The Mann-Whitney U-test employed to examine null hypothesis, indicates no significant difference between the median of individual waveband reflectance measurements for soil samples within each salinity class while difference between two classes is statistically significant. The results show that the differences between the reflectance spectra associated with the observed salinity classes are statistically significant.

According to the guidelines presented in section 7.3, further research is required to define the influence of moisture on salt-affected soil reflectance spectra and to search for an alternative method that use the general shape of the spectra rather than diagnostic absorption signature or absorption bands parameters (depth, with, etc.) in order to estimate soil salinity. Both of these issues were addressed in chapter 5. The interferences of salts and moisture contents on soil reflectance were examined through modelling using an inverted Gaussian function. The algorithm was employed because:

- It is one of the most frequently used functions in predicting soil moisture effectively. Therefore, under conditions where there are no affects of salt on soil spectra the algorithm should be able to predict the soil moisture content accurately. On the contrary, if there are interferences due to soil salt contents, the model would not be capable of estimating soil moisture contents and probably soil salinity.

- It was found suitable since the previous studies (chapters 3 and 4) suggested that the spectral responses of soils with different salt contents, in many ways, are similar to the spectra of soils with various moisture contents.

- The IG function can be fitted to different portions of spectra by connecting the maximum reflectance wavelength, meaning it uses the general shape of the spectrum independently from diagnostic absorption bands and their parameters.

This modelling approach was first tested on experimental data sets where the affects of the soil constituents, including soil moisture contents, were kept almost constant while large variations in soil salt contents was created. This was an attempt to confirm whether the applied algorithm has any potential application in salinity modelling. The results of fitting an IG function to SWIR region of the soil spectra showed that parameters of the fitted curve such as functional depth, distance to the inflection point and area can be used as predictors in regression analysis to predict soil salinity depending on the dominant salt types in soil. This means application of IG modelling approach is limited in salinity studies.

The approach was further used to test field data sets where the in-situ measured soil reflectance spectra were largely influenced by both salts and moistures. The poor correlation between soil EC_{av} and IG model parameters for the field spectral data can be explained mainly due to salt type and influence of soil moisture. The dominant salt in the field area is halite, which has a weak effect on the general shape of soil spectra to provide bases for predictive regression modelling, as it is also observed from experimental data sets. However, large anomalies observed in calculated IG model parameters of field spectra caused by soil moisture contents.

The poor estimation of soil moisture contents using the field data confirmed the influence of salts on soil reflectance spectra and its contribution to causing incongruity in model calculations. Therefore, the results suggest that estimation of soil moisture using the same approach can be undermined by accumulation of salts in soil. This means further studies are required to determine calibrating coefficients that can be used to eliminate the background spectra caused by either salts or moisture.

7.5 Modelling algorithm and integrated approach

In the study presented in chapter 4, the results suggested multivariate approaches such as partial least squares regression (PLSR) or artificial neural

networks (ANN) may have potentials in estimation of soil salinity. It is also proposed in chapter 2 that soil salinity modelling should be based on integration of soil reflectance measurements obtained from remotely sensed sensors with (*i*) data obtained from geophysical survey, (*ii*) data derived from solute and modelling, or (*ii*) data obtained from both methods.

Following the guidelines, an investigation was conducted to examine the possibility of predicting salt concentrations in soils by use of PLSR and ANN analysis on the bases of soil reflectance measured by field and airborne spectrometers and soil property measured by geophysical sensor (EM-38). The results presented in chapter 6 showed that both methods are very effective for establishing relationships between soil reflectance and soil EC. The performance indexes calculated from predicted values from both methods, generally, suggest large similarity between the two approaches even though comparing the individual predicted values by each model showed much less agreement between predicted values especially for image dataset. While for field data sets, the complex field situations influence the PLSR and ANN predictive models resulting in poorer estimations of salinity compare to the experiment data.

The significant correlation established between soil EC and soil reflectance at laboratory level by both methods provided the basis for up-scaling toward the air-borne hyperspectral data. In the up-scaling process, the accurate laboratory experiment data were replaced with the pixel reflectance derived from hyperspectral imageries and in situ EC_a measured by geophysical instruments. The accurate estimation of soil salinity by both methods (PLSR and ANN), at up-scaled level, provides possibility of integrating sub-surface geophysical electromagnetic measurements and surface reflectance derived from air-borne hyperspectral imageries. This means, progressing from two non-unique salt identification methods towards a unique and new approach with prediction capabilities, which could lead to early detection of salinization. This integrated method can be consider as a major development in terms of management of agricultural practices and would be a great benefit to both farmers and states.

7.6 Conventional methods and new developments

Study of salinity by use of remote sensing has been limited since most often reflectance values measured by sensors can not be related to physical properties of soil that influenced by salts. In general, indirect indictors (e.g., vegetation cover density and type) that are more easily detectable by remote sensing sensors are often employed for mapping salt-affected areas. Furthermore, remote sensing sensors are incapable of extracting information from the third dimension of soil profile, while salinization occurs both at the surface and the near-surface. That has been the case in last decades where detection and

classification of saline area by use of remote sensing has not been adequate and mostly resulted in differentiation between non and severely saline areas. With regard to soil salinity and remote sensing, generally, those approaches that are based on convention methods have not provided new information rather than verification of existing knowledge.
The developed methods presented in this dissertation aim to overcome the aforementioned issues. The main differences between the developed methods and convention methods are on use knowledge-based approach and integration of surface and sub-surface measurements obtained for two different remotely sensed sensors. Knowledge-based systems offer large potential for extracting information from remotely sensed data on bases of explicit knowledge about the objects and processes, use of ancillary data, and an iterative procedure to adjust the calculated results (optimization). Both PLSR and ANN modelling methods presented in chapter six uses training data sets to learn about the object and develop calibration algorithms that eventually can be used for identification and prediction of the object under study. In the developed methods, geophysical measurements were used as ancillary data for calibration and training purposes. The geophysics technology has the advantage of effectiveness for cropped land and can efficiently be used to highlight conductive areas where no surface expression of salt is evident. Therefore, the calibration and training models are not biased by land cover. However, they might be influenced by land cover where the cover is strongly influenced by soil salt contents.

Beside the new methods discussed above, there are several other new developments in the presented study, which are:

- The proposed conceptual framework in chapter 2 is a new concept in salinity study. It provides the possibility to progress from three non-unique salt identification methods towards a unique approach with potential application to detect early stages of salinization.

- The laboratory experiment and the detailed study to the spectral response of salt solutions presented in chapter 3 and 4 provided insights that have not been described in previous studies as it has been extensively discussed here. In addition, the designed experiment is original.

- The quantification of soil spectral response in relation to variations in salt concentration presented in chapter 4 provided physical evidences on salt affects on soil reflectance. The employed algorithms were able to quantify the magnitude and the strength of the relationship between soil salt contents and the observed quantified spectral variations in soil reflectance.

7.7 Future work

Research such as salinity study by use of remote sensing, solute modelling and geophysical survey that cover a wide field are always involved with problem of selection, especially if it has to be completed in a short period of time. A compromise that includes achieving the research aims and meets the time limit is needed to be made and therefore, this study focused only on the most important related issues and not covering all the aspects that have been mentioned in proposed conceptual framework in chapter 2.

The research presented here, illustrates some of possibilities that can be achieved in detecting, predicting and monitoring soil salinity, especially at the early stage. However, the application of the developed methods can be extended to focus mainly on research areas that were not covered in this study. A practical extension of the present works can be on the use of information or data obtained from solute modelling on the dynamic regime of salts in soil profile. The possibilities to integrate remote sensing and solute modelling, or remote sensing, geophysical survey and solute modelling need to be further explored. A more accurate estimation of salinity and wider applications can be expected from such integrated approach.

Another area that needs additional attention concerns the soil moisture contents and its influence on reflectance spectra of salt-affected soils. Further studies are required in order to determine the calibrating coefficients that can be used to eliminate the background spectra caused by soil moisture contents. In this regard, there are various techniques and data that need to be explored, especially the potential of ground-penetrating radar (GPR) and high-resolution thermal infrared (TIR) data.

A third area that still needs research is related to selecting an optimal integration technique, since in this study the focus was on knowledge-based approach. There are several other techniques such as overlying, conditional probability and evidential reasoning that also can be used for data integration. Therefore, further research it is recommended to explore the possibilities that can be offered by other integration methods.

At last, the extension of the current research lies on evolution of the new development compare to conventional methods in term of the final results. A realistic assessment of what has been presented in this study can be made by characterization of uncertainties associated with the output salinity maps as they are compared with a salinity map obtained from field measurements. The new developed method and various other conventional methods can be used to create several salinity maps that can be used as an input for uncertainty analysis.

References

Abdulghani, S.A. (1963). Relations between photo - interpretation and soil survey in Texel island. MSc thesis, *ITC*, Enschede, The Netherlands.

Adeloye A.J., De Munari, A. (2005). Artificial neural network based generalized storage–yield–reliability models using the Levenberg–Marquardt algorithm. *Journal of Hydrology*, Vol. 326, 1-4, 215-230.

Agassi, M., Shainberg, I. Morin, J. (1981). Effect of electrolyte concentration and soil sodicity on infiltration rate and crust formation. *Soil Sci. Soc. Am. J.* 45:848-851.

Anderson, C.A., Bro, R., (2000). The N-way toolbox for Matlab. *Chemometrics and intelligent Laboratory Systems*, 52, 1-4.

Australian Heritage Commission (1995). Five Australian wetlands recognised for their heritage value. *Media Release*, 12 December 1995.

Bailiff, I.K., Barnett, S. M. (1994). Characteristics of infrared-stimulated luminescence from a feldspar at low temperatures. *Radiation Measurements,* Volume 23, Issues 2-3, pp. 541-545.

Bastiaanssen, W.G.M., Molden, D.J., Makin, I.W. (2000). Remote sensing for irrigated agriculture: examples from research and possible applications. *Agricultural water management*, 46: 137-155.

Baumgardner, M.F., Silva, L.F., Biehl, L.L., Stoner, E.R. (1985). Reflectance properties of soils. Adv. Agron., 38: l-44.

Bedidi, A., Cervelle, B., Madeira, J., Pouget, M. (1990). Moisture effects on spectral characteristics (visible) of lateritic soils. Soil Sci. 153, 129-141.Ben-Dor, E. (2002) Quantitative remote sensing of soil properties. *Advanced in Agronomy*, pp. 75.

Ben-Dor, E. (2002). Quantitative remote sensing of soil properties. Advanced in Agronomy, 75: 173-243.

Ben-Dor, E., Irons, J. R., Epema, G. F. (1999). Soil reflectance. In A. N. Rencz (Ed.), Remote sensing for the earth sciences: *Manual of remote sensing* (pp. 111 –188). New York: Wiley.

Ben-Dor, E., Patkin K., Banin A., Karnieli A. (2002). Mapping of several soil propeties using DAIS-7915 hyperspectral scanner data – a case study over clayey soils in Israel. *Int. Journal of Remote sensing*, vol. 23, no. 6, 1043 – 1062.

Bhagavantan, S., Venkatarayuda, T. (1939). Raman effect in relation to crystal structure. In: Proceedings of the Indian Academy of Science. Section A, *Mathematical and physical science*.

Bishop, C. (1995). Neural Networks for Pattern Recognition. *Oxford University Press*, New York.

Bishop, J.L. (1988). The effects of water, octahedral cation substitution and exchangeable cation composition on the shortwave infrared reflectance spectrum of montmorillonite. MS Thesis, *Stanford University*, Stanford, California, 37 p.

Bishop, J.L., Pieters, C.M., Edwards, J.O. (1994). Infrared spectroscopic analyses on the nature of water in montmorillonite. *Clays & Clay Min*., Vol. 42, 6, pp. 702-716.

Bowers, S.A., Hanks, R.J. (1965). Reflection of radiant energy from soils. *Soil Sci.,* 190: 130-138.

Buringh, P. (1978). Food production potential of the world. In: Radhe Sinha (ed.). The World Food Problem; Consensus and Conflict. *Pergamon Press*. 477-485.

Burrough, P.A. (1996). Opportunities and limitations of GIS-based modelling of solute transport at the regional scale. In: Corwin, D.L., Loague, K., (Eds), Applications of GIS to the modelling on non-pointed source pollutants in the vadose zone. *SSSA Spec. Pub*. 48: SSSA: Madison, WI.

Burt, R. (2004). Soil survey laboratory methods manual SSIR42. Edition4. Soil survey investigations report; 42. *USDA*, Natural Resources Conservation Service (NRCS).

Butters, G.L., Jury W.A. (1989). Field scale transport of bromide in an unsaturated soil, 2. Dispersion modelling. *Water resource research*, 25: 1583-1589.

Cacuci, D.G., 2003. Sensitivity & Uncertainty Analysis, Volume 1: Theory. Chapman & Hall/CRC. 304 p.

Chang, C-I. (2003). Hyperspectral Imaging: Techniques for Spectral Detection and Classification, *Kluwer Academic/Plenum Publishers*, New York.

Chang, Y.M., Chang, L.C., Chang, F.J. (2004). Comparison of static feedforward and dynamic-feedback neural networks for rainfall runoff modeling. *Journal of Hydrology,* 290, 297–311.

Clark, R.N. (1981). Water frost and ice: The near-infrared spectral reflectance 0.65-2.5 μm. *J. of Geophysical Res*., Vol. 86, B4, pp. 3087-3096.

Clark, R. N. (1999). Spectroscopy of rocks and minerals, and principles of spectroscopy, in Rencz, A.N., (Ed.), *Manual of Remote Sensing*, Vol. 3, John Wiley, New York, p 3- 58, 1999.

Clark, R. N., Roush, T. L. (1984). Reflectance spectroscopy: Quantitative analysis techniques for remote sensing applications. *J. of Geophysical Res*., Vol. 89, B7, 6329–6340.

Clark, R.N., Swayze, G.A., Livo, K.E., Kokaly, R.F., King, T.V., Dalton, J. B., Vance, J. S., Rockwell, B. W., Hoefen, T., McDougal, R.R. (2002). Surface reflectance calibration of terrestrial imaging spectroscopy data: *a tutorial using AVIRIS in proc. of the 10th Airborne Earth Science Workshop, JPL* pub. 2-1.

Clark, R. N., Swayze, G.A., Livo, K.E., Kokaly, R.F., Sutley, S.J., Dalton, J.B., McDougal, R.R., Gent, C.A., (2003). Imaging spectroscopy: Earth and planetary remote sensing with the USGS Tetracorder and expert systems, *J. Geophys. Res*., 108(E12), 5131.
Available at: *http://speclab.cr.usgs.gov/PAPERS/tetracorder*

Cloutis, E.A. (1996). Hyperspectral geological remote sensing: evaluation of analytical techniques. *Int. J. Remote Sensing*, 17: 2215-2242.

Congalton R.G., and Green, K. (1999). Assessing the accuracy of remotely sensed data : principles and practices. Mapping Sciences Series; *2. Boca *Raton etc. Lewis*. 137 p. 0-87371-986-7.

Corwin, D.L. (1996). GIS Application of deterministic solute transport models for regional-scale assessment of non-point source pollutants in the vadose zone. Soil Sci. Soc. Am., 677 S. Application of GIS to the modelling of non-point source pollutants in the vadose zone, Ch. 5, *SSSA special publication* 48: 69-100.

Corwin, D.L., Rhoades, J.D. (1984). Measurements of converted electrical conductivity profiles using electromagnetic induction. *Soil Sci. Soc. Am. J.* 48, pp. 288-291.

Corwin, D.L., Sorensen, M., Rhoades, J.D. (1989). Field-testing of models which identify soils susceptible to salinity development. *Geoderma*, 45:1, 31- 64.

Crowley, J.K. (1991a). Visible and Near-Infrared (0.4-2.5□□m) reflectance spectra of playa evaporite minerals. *Journal of geochemical research*, 96: no. B10, 16231-16240.

Crowley, J.K., 1991b. Spectral reflectance analysis of playa evaporate minerals - potential for use in playa geochemical studies and mineral resource exploration. In: Raines, G.L., Lisle, R.E., Schafer, R.W., Wilkinson, W.H., (Eds.), Geology and Ore Deposits of the Great Basin. Symposium Proceedings: 255-262. *Geological Society of Nevada*, Reno, Nevada.

Csillag F., L. Pasztor Biehl, L.L. (1993). Spectral band selection for the characterization of salinity status of soils. *Remote sensingof Enviorn.* 43, pp. 231-242.

Dehaan R., Taylor G.R. (2003). Image-derived spectral endmembers as indicators of salinization**,** *Int. Journal of Remote Sensing*, Vol. 24, no. 4, 20, 775-794

Dehaan, R.L., Taylor, G.R. (2002). Field-derived spectra of salinized soils and vegetation as indicators of irrigation-induced soil salinization. *Remote Sensing of Environ*., 80, 406-417.

De Jong S.M. (1992). The Analysis of spectroscopical data to map soil types and soil crusts of Mediterranean eroded soils. *Soil Technology*, vol. 5, 199–211.

De Jong, S.M. (1994). Applications of reflective remote sensing for land degradation studies in a Mediterranean environment. Nederlandse Geografische Studies, 177, *Utrecht University, Utrecht, The Netherlands*. 237 p.

Demattê, J.A.M., Campos, R.C., Alves, M.C., Fiorio P.R., Nanni, M.R., (2004). Visible–NIR reflectance: a new approach on soil evaluation. *Geoderma*, Vol. 121, Issues 1-2, 95-112

Demuth, H., Beale, M. (2004). Neural Network Toolbox for use with MatLab. User's guide version 4. *The Math Works, Inc. 3 Apple Hill Drive*, Natick, MA 01760-2098.

Derver, J.I. (1982). The Geochemistry on natural waters, 2ed ed., Prentice Hall, New Jersey, 437 p.

Diaz L., Herrero, J., (1992). Salinity estimates in irrigated soils using electrical induction. *Soil Science*, 154: 151-157.

Doerge, T., Kitchen, N.R, Lund, E.D. (2002). Soil electrical conductivity mapping. Potash and Phosphate institute (PPI). *Site-Specific management guidelines*. SSMG-30.

Drake, N.A. (1995). Reflectance spectra of evaporate minerals (400-2500 nm): Application for remote sensing. *Int. J. Remote Sensing*, vol. 16, no. 14, 2555-2571.

Driessen, P.M., Schoorl, R., (1973). Mineralogy and morphology of salt efflorescences on saline soils in the Great Konya Basin, Turkey. *J. Soil Science,* 24, 436–442.

Du Y., Chang, C-I., Ren, H., Chein-Chi, C., Jensen, J.O., D'Amico, F.M. (2004). New hyperspectral discrimination measure for spectral characterization. *Optical Engineering*, Vol. 43 No. 8, 1777-1786.

Duckworth, J. (1998). Spectroscopic quantitative analysis. In J. Workman, & A. W. Springsteen (Eds.), Applied spectroscopy. A compact reference for practitioners, San Diego,7 *Academic Press*, 93–164.

Duda, R.O., and Hart, P.E. (1973). Pattern recognition and scene analysis. *John Willey & Sons Inc*.

Dwivedi, R.S., Sreenivas, K. (1998). Delineation of salt-affected soils and waterlogged areas in the Indo-Gangetic plains using IRS-1C LISS-III data. *Int. J. Remote Sensing*, Vol. 19, no. 14, 2739-2751.

Dwivedi, R.S., Sreenivas, K., Ramana, K.V., (1999). Inventory of salt-affected soils and waterlogged areas: A remote sensing approach. *Int. J. Remote Sensing,* Vol. 20, no. 8, 1589-1599

Eijkelkamp (2005). Available at: *http://www.eijkelkamp.nl/*

Eklund, P.W., Kirkby, S.D., Samlim, A. (1998). Data mining and soil salinity analysis. *Int. j. Geographical information science*, vol. 12, no. 3, 247 – 268.

El-Kadi, A.I., Oloufa, A.A., Eltahan, A.A., Malik, H.U. (1994). Use of a Geographic information system in site-specific ground-water modelling. *Ground water*, 32: 617-625.

Epema, G. (1993). Mapping surface characteristics and their dynamics in a desert area in southern Tunisia with Landsat TM. Ph.D. thesis, *Agricultural University of Wageningen*.

Escadafal, R. (1994). Soil spectral properties and their relationships with environmental examples from arid regions. In: Hill J., Megier, J., (Eds), Image spectrometry - a tool for environmental observation. *ECSC, EEC, EAEC, Brussels and Luxembourg*. 71-87.

Evans, F.H., Caccetta P.L. (2000). Broad-scale spatial prediction of areas at risk from dryland salinity. *Cartography*, vol. 29, no.2.

Everitt, J., Escobar, D., Gerbermann, A., Alaniz, M. (1988). Detecting saline soils with video imagery. *PE&RS*, 54: 1283-1287.

FAO (2006). FAO field guide, 20 things to know about the impact of salt water on agricultural land in ACEH province. At: *http://www.fao.org/ag/tsunami/docs/saltwater-guide.pdf*

FAO (1988). Salt-affected soils and their management. FAO, *Soils Bulletin* 39, Rome.

Farahani, H.J. (2004). Soil Electrical conductivity mapping of agricultural fields. USDA-ARS Water Management Unit, AERC-Colorado State University. At: *http://www.colostate.edu/Depts/SoilCrop/extension/Newsletters/2002/Sensors/SoilEC.htm*

Farifteh, J., Bouma A., van der Meijde, M. (2004). A new approach in the detection of salt affected soils; Integrating surface and subsurface measurements. *In 10th European meeting of environmental and engineering geophysics*. Utrecht, The Netherlands, 6–9 Sept. P059.

Farifteh, J., Farshad, A. (2002). Remote sensing and modelling of topsoil properties, a clue for assessing land degradation. In: *17th world congress of soil science*. 14-21 August 2002, Bangkok, Thailand. Symposium 52, 865-1 – 865-11.

Farifteh, J., Farshad, A., George R.J. (2006a). Assessing salt-affected soils using remote sensing, solute modelling, and geophysics. *Geoderma*, Vol. 130, 3-4, 191-206.

Farifteh, J., van der Meer, F., Carranza, E.J.M. (2006b). Similarity measures for spectral discrimination of saline soils. (*In press, Int. J. of Remote Sensing*).

Farifteh, J., van der Meer, F., van der Meijde, M., Atzberger, C. (2006c). Spectral characteristics of salt-affected soils: A laboratory experiment. *Under review, Geoderma*.

Farifteh, J., Tolpekin, V., Van der Meer, F., Sukchan, S. (2006d). Salinity modeling by inverted Gaussian parameters of soil reflectance spectra. *Under review, Int. J. of JAG*.

Farifteh, J., van der Meer, F., Atzberger, C., Carranza, E.J.M. (2006e). Quantitative analysis of salt-affected soil reflectance spectra: A comparison of two adaptive methods (PLSR and ANN). *Under review, Remote Sensing of Environment*.

Farmer, V.C. (1974). The InfraRed Spectra of Minerals, (ed.) *Mineralogical Society*, London, 539 p.

Farr, T. G., Bates, B., Ralph, R. L., Adams, J. B. (1980). Effects of Overlapping Optical Absorption Bands of Pyroxene and Glass on the Reflectance Spectra of Lunar Soils. LUNAR AND PLANETARY SCIENCE XI, P. 276-278. Available at: *http://adsabs.harvard.edu/cgi-bin/nph-bib_query?bibcode=1980LPI....11..276F&db_key*

Fauck, R. (1977). Influences of agricultural practices on soil degradation. In : *FAO Soil Bulletin No. 34* : Assessing soil degradation.

Ferraro, J.R. (1971). Low frequency vibrations in inorganic and coordination compounds, *Plenum*, New York.

Fletcher, D., Goss, E. (1993). Forecasting with neural networks: an application using bankruptcy data. *Information and Management*, 24, 159-167.

Frenkel, H., Meiri, A. (1985). Soil salinity: two decades of research in irrigated agriculture. *Van Nostrand Reinhold*. ISBN: 0-442-22583-0, 441 p.

Gaffey, S.J. (1986). Spectral reflectance of carbonate minerals in the visible and near infrared (0.35-2.55 microns): calcite, aragonite, and dolomite. *American Mineralogist*, Vol. 71, Issue 1-2, pp. 151-162.

Gaffey, S.J. (1987). Spectral reflectance of carbonate minerals in the visible and near infrared (0.35-2.55 □m): Anhydrous carbonate minerals. *Journal of Geophysical Research*, vol. 92, no. B2, 1429-1440.

Geladi, P Kowalski, B.R. (1986). Partial least-squares regression: A tutorial. *Analytica Chimica Acta*, Vol. 185, 1-17.

Galera, M.M., Vidal, J.L.M., Frenich, A.G., Gil García, M.D. (1996). Determination of cypermethrin, fenvalerate and *cis*- and *trans*-permethrin in soil and groundwater by high-performance liquid chromatography using partial least-squares regression. *Journal of Chromatography A*, Volume 727, 1, 39-46.

George, R.J., Bennett, D.L. (2000). Airborne geophysics provides improved spatial information for the management of dryland salinity. In: Conacher A.J., (Ed), *Land Degradation*. 305-319.

George, R.J., Woodgate, P. (2002). Critical factors affecting the adoption of airborne geophysics for management of dryland salinity. *Exploration Geophysics,* 33, 84-89.

George, R.J., Beasley, R., Gordon, I., Heislers, D., Speed, R., Brodie, R., McComnell, C., Woodgate, P. (1998). The national airborne geophysics project - national report. Evaluation of airborne geophysics for catchment management. At: *www.ndsp.gov.au*

Gilliland, M.W., Baxter-Potter, W. (1987). A geographic information system to predict non-point source pollutant potential. Water Resource Bulletin, 23: 281-291.

Goetz, A.F., Vane, G., Soloman, J.E., Rock, B.N. (1985). Imaging spectrometry for earth remote sensing. *Science*, 228, 1147.

Goetz, A.F.H., Herring, M. (1989). The high resolution imaging spectrometer (HIRIS) for EOS. IEEE Trans. *Geo. Rem. Sens*., 27, 136-144.

Griffiths, D.H., King, R.F. (1981). Applied geophysics for geologists and engineers: the elements of geophysical prospecting. *Pergamon Press*. Second edition. 230.

Haaland, D.M., Thomas E.V. (1988a). Partial least squares methods for spectral analyses. 1. Relation to other quantitative calibration methods and the extraction of qualitative information. *Analytical Chemistry*, 60, 1193-1202

Haaland, D.M., Thomas, E.V. (1988b). Partial least squares methods for spectral analyses. 2. Application to simulated and glass spectral data. *Analytical Chemistry*, 60, 1202-1208

Hansen, P.M., Schjoerring, J.K. (2003). Reflectance measurement of canopy biomass and nitrogen status in wheat crops using normalized difference vegetation indices and partial least squares regression. *Remote Sensing of Environment,* Vol. 86, 4, 542-553.

Hapke, B. (1993). Theory of reflectance and emittance spectroscopy, Series: Topics in Remote Sensing (No. 3), pp. 304–305. New York: *Cambridge University Press*.

Hartsock, N.J., Mueller, T.G., Thomas, G.W., Barnhisel, R.I., Wells, K.L., Shearer S.A. (2000). Soil electrical conductivity variability. *Proceedings of 5th international conference on precision Agriculture. Madison*, WI.p.ASA Misc. Publ., ASA, CSSA, and SSSA.

Hatchell, D.C. (1999). Analytical Spectral Devices (ASD) Technical Guide. 4th Edition. Available online at: *www.asdi.com*

Hatonen, J., Hyotyniemi, H., Miettunen, J., Carlsson, L.E. (1999). Using image information and partial least squares method to estimate mineral concentrations in mineral flotation. IPMM 99: *Proceedings of the Second International Conference on Intelligent Processing and Manufacturing of Materials*, Vol. 1, pp. 459-464. Honolulu, HI; USA; 10-15 July.

Haykin, S. (1999). Neural Networks: A Comprehensive Foundation. 2ed edition, *Prentice-Hall Inc.*, New Jersey.

Hearn, SJ. (1988). Soil Conservation and Management Strategies for the Toolibin Catchment. Western Australian Department of Agriculture. Technical Report No. 75. Division of Resource Management.

Herzberg, G. (1945). Infrared and Raman spectra of Polyatomic molecules. *D. Van Nostrand Company*, Inc. New york.

Hick, P.T., Davis, J.R., Steckis, R.A. (1984). Mapping salinity in Western Australia using remotely sensed data. Satellite remote sensing. *Proc. 10th anniversary conference, Reading 1984 (Remote Sensing Society, University of Reading), published by Arkansas University,* Fayetteville, Department of Electrical Engineering, 343-350.

Hick, P.T., Russell, W.G.R. (1990). Some spectral considerations for remote sensing of soil salinity. *Aus. J. Soil Res.,* 28: 417-431.

Hill J., Sommer, S., Mehl W., and Megier, J. (1996). A conceptual framework for mapping and monitoring the degradation of Mediterranean ecosystems with remote sensing. In: Hill J. and Peter D., (Eds), The use of remote sensing for land degradation and desertification monitoring in the Mediterranean basin. *State of the art and future research. Experts workshop 13 to 15 June, Valencia (Spain)*.

Homayouni, S., Roux, M. (2004). Hyperspectral image analysis for material mapping using spectral matching. Available at:

http://www.isprs.org/istanbul2004/comm7/papers/10.pdf

Hornik, K., Stinchcombe, M., White, H. (1989). Multylayer feedforward networks are universal approximators. *Neural Networks*, 2, 5, 359–366.

Howari, F.M., Goodell, P.C., Miyamoto, S. (2002). Spectral properties of salt crusts formed on saline soils. *Journal of Environmental Quality*, Vol. 31, no. 5, 1453-1461

Howlett, A., Roach, M.J., Reid, J.E., 2001. Geophysical characteristics of salinization at cape Portland, NE Tasmania. *Exploration Geophysics*, 32: 214-218.

Huang, Z., Turner, B.J., Dury, S.J., Wallis, I.R. Foley, W.J. (2004). Estimating foliage nitrogen concentration from HyMap data using continuum removal analysis. *Remote Sensing of Environment*. 93, 18-29.

Huang, W., Foo, S. (2002). Neural network modelling of salinity variation in Apalachicola River. *Water Res.*, 36, 1, 356-362.

Hunt, G.R. (1980). Electromagnetic radiation: The communications link in remote sensing. In: B.S. Siegal and A.R.Gillespie (Editors), *Remote Sensing in Geology*. Wiley: New York. 545.

Hunt G.R., Salisbury, J.W. (1970). Visible and near-infrared spectra of minerals and rocks. I. Silicate minerals. *Modern Geology*. 1, 283-300.

Hunt G.R., Salisbury, J.W. (1971). Visible and near-infrared spectra of minerals and rocks. II. Carbonates. *Modern Geology*. 2, 23-30.

Hunt, G., Salisbury J.W. (1976). Visible and near infrared spectra of minerals and rocks: XII. Metamorphic rocks. *Modern Geology*, 5: 219-228.

Hunt G.R., Salisbury, J.W., Lenhoff, C.J. (1971). Visible and Near-infrared spectra of minerals and rocks. IV. Sulphides and Sulphates. *Modern Geology*. 3, 1-14.

Hunt G.R., Salisbury, J.W., Lenhoff, C.J. (1972). Visible and Near-infrared spectra of minerals and rocks. V. Halides, Phosphates, Arsenates, Vanadates and Borates. *Mod. Geology*. 3, 121-132.

HyVista, 2004; HYVista corporations, Airborne Hyperspectral Surveys and Information Products. Available at: *http://www.hyvista.com/main.html*

Irons, J.R., Weismiller, R.A., Petersen, G.W. (1989). Soil reflectance. In: Asrar, G., (Ed), Theory and Applications of Optical Remote Sensing. Wiley Series of Remote Sens., *J. Wiley & Sons*, New York, NY. 66-106.

Ishida, T., Ando, H., Fukuhara, M. (1991). Estimation of complex refractive index of soil particles and its dependence on soil chemical properties. *Remote Sensing of Environ*. 38, 173-182.

Jackson, J.E. (1991). A User's Guide to Principal Components, *J. Wiley & Sons*, New York, 1991.

Jackson, M.L., Lim, C.H., Zelazny, L.W. (1986). Oxides, hydroxides, and aluminosilicates. In: Klute, A., (Ed), Methods of soil analysis, part 1. Agronomy 9. *American Society of Agronomy*: Madison, Wisconsin. 101-1 50.

Jain, S., Sharma, K., Manchanda, M., and Singh, C. (1988). Physiographic soil classification from multi remote sensing data. *Proceedings of the 9th Asian Conference on Remote Sensing.* No. 23-29, Bangkok, Thailand, vol. 17, 1-8.

Johnson, C.K., Doran, J.W., Duke, H.R., Wienhold, B.J., Eskridge, K.M., and Shanahan J.F. (2001). Field-Scale electrical conductivity mapping for delineating soil condition. *Soil Sci. Soc. Am. J.,* 65: 1829-1837.

Jolly, I.D. (1998). The impact of flooding on modelling salt transport processes to streems. *Environmental Modelling & Software*, 13: 87-104.

Jury, W.A. (1982). Simulation of solute transport using a transfer function model. *Water Resour.Res.,* 18: 363-368.

Kardev´an, P., Vekerdy, Z., R´oth, L., Sommer, S., Kemper, T., Jordan, G., Tam´as, J., Pechmann, I., Kov´acs, E., Hargitai, H., L´aszl´o, F. (2003). Outline of scientific aims and data processing status of the first Hungarian hyperspectral data acquisition flight campaign, HYSENS 2002 Hungary. In M. Habermeyer, A. M¨ulle, & S. Holzwarth (Eds.), *Proceedings of the 3rd EARSeL workshop on imaging spectroscopy, Herrsching, Germany* (pp. 324–332).

Kearey, P., Brooks, M. (1994). An introduction to geophysical exploration. *Blackwell scientific publication*. Second edition.

Keränen, P., Kaarna, A., Toivanen, P. (2003) Spectral Similarity Measures for Classification in Lossy Compression of Hyperspectral Images. *In A.B., Serpico (Ed.), Image and signal processing for remote sensing VIII. Proceedings of the 9'th International Symposium on Remote Sensing,* SPIE Vol. 4885, March 2003, 285-296, Crete, Greece, Sept. 23-27.

Klein, C., Hurlbut, C.S. (1999). Manual of mineralogy. 21st edition. *John Wiley & Sons*, INC. New York.

Kloosterhuis, J.L., Steur, G.G.L., Heijink, W., 1986. Bodemkaart van Nederland schaal 1 : 50.000 : toelichting bij het kaartblad Texel. *Wageningen : Stiboka*. 133 p. + 2 krt. ISBN: 90-327-0218-1

Kohyama, K., Wichaidit, P., Pramojance, P., Sukchan, S., and Wada, H. (1993). Salinization in the watershed of Northeast Thailand. In: ADRC (ed.) *Research activities of ADRC contributed to agricultural development in Northeast Thailand*. Khon Kaen. Thailand.

Kruse, F.A. (1995). Mapping spectral variability of geologic targets using Airborne Visible/Infrared Imaging Spectrometer (AVIRIS) data and a combined spectral feature/unmixing approach. In M.R., Descour et al. (Eds): *Image Spectrometry, Proceedings SPIE-The International society for optical Engineering*, 17018 April 1995, Orlando, Florida.

Kruse, F. A., Lefkoff, A. B., Boardman, J. B., Heidebrecht, K. B., Shapiro, A. T., Barloon, P. J., Goetz, A. F. H. (1993) The Spectral Image Processing System (SIPS) - Interactive Visualization and Analysis of Imaging spectrometer Data. *Remote Sensing of Environm.*, Vol. 44, pp. 145-163.

Kumar. L., Schmidt, K.S., Dury, S., Skidmore, A.K. (2001). Review of hyperspectral remote sensing and vegetation science. In: van der Meer, F., (Ed) Hyperspectral remote sensing. *Kluwer Academic press*: Dordrecht.

Lane, R., Green, A., Golding, C., Owers, M., Pik, P., Plunkett, C., Sattel, D., Thorn, B., (2000). An example of 3D conductivity mapping using the TEMPEST airborne electromagnetic system. *Exploration Geophysics*, 31: 162-172.

LDD (1991). Map of salt-affected area (scale 1:100,000). Ministry of agricultural and cooperation, *Land Development Department (LDD), Soil Survey and Classification Division. Khon Kaen, Thailand*.

Lehmann, E.L. (1998). Nonparametrics : statistical methods based on ranks. Revised first edition. *Prentice Hall Inc.* Upper Saddle River, NJ 07458. 463 p. ISBN: 0-13-997735-X.

Lesch, S.M., Strauss, D.J., Rhoades, J.D. (1995). Spatial prediction of soil salinity using electromagnetic induction techniques 1. Statistical prediction models: A comparison of multiple linear regression and cokriging. *Water Resources Res.*, 31: 373-386.

Lide, D.R. (1993). Handbook of chemistry and physics, 74th edition. *CRC Press*.

Lindberg, W., Persson, J.A., Wold S. (1983). Partial Least-Squares Method for Spectrofluorimetric analysis of mixture of humic acid and ligninsulfonate. *Ana. Chem*. Vol. 55, pp. 643 – 648.

Liu, W., Bareta F., Gu, X., Tong, Q., Zheng, L., Zhang B. (2002). Relating soil surface moisture to reflectance. *Remote Sensing of Enviror.*, 81, 238– 246.

Lobell, D.B., Asner, G.P. (2002). Moisture effects on soil reflectance. *Soil Science Society of America Journal*, 66, 722– 727.

Lund, E.D., Wolcott, M.C., Hanson, G.P., (2001). Applying nitrogen site-specifically using soil electrical conductivity maps and precision agricultural technology. In: 2nd Int. nitrogen conference on Science and policy. *Potomac Md*, 14-18 Oct.

Mabbut, J.A. (1977). Desert Landforms. *The MIT Press. Cambridge*, 340P.

Mabbut, J.A. (1984). Landform of Australian desert. In F., El-Baz, (Ed), Desert and arid lands. *Martinus Nijhoff Publishers*, The Hague, the Netherlands.

Maier, H.R., Dandy, G.C. (2001). Neural network based modelling of environmental variables: A systematic approach. *Mathematical and Computer Modelling*, Vol. 33, 6-7, 669-682.

Mainguet, M. (1991). Desertification. Natural Background and Human mismanagement. *Springer-Verlag*. Berlin. ISBN: 3-540-52519-X, 306 p.

Manchanda, M., Iyer, H. (1983). Use of Landsat imagery and aerial photographs for delineation and categorization of salt-affected soils of part of north-west India. *Journal Indian Society Soil Science*, 31, 263-271.

Max, J.J., Chapados, C. (2001). IR Spectroscopy of aqueous alkali halides solutions: Pure salt-solvated water spectra and hydration numbers. *Journal of chemical physics*, Vol. 115, 6, 2664 – 2675.

Max, J.J., de Blois, S., Veilleux, A., Chapados C. (2001). IR Spectroscopy of aqueous alkali halides. Factor analysis. *Can. J. Chem.* 79(1), 13-21.

McCord, T.B., Clark, R.N., Hawke B.R., McFadden, L.A., Owensby, P.D., Pieters C.M., Adams, J.B. (1981). Moon: near-infrared spectral reflectance, a first good look. *J. of Geophysical Research,* Vol. 86, B11, 10883-10892.

McGowen, I., Mellyon, S. (1996). Detection of dryland salinity using single and multi-temporal Landsat imagery. *Proceedings of the 8th Australian remote sensing conference, Canberra*. 26-34.

McFadden, L. A., Goldman, N. (2004). Mineralogical Interpretation of 433 Eros with Modified Gaussian Method. *American Astronomical Society*, 36 #4. Available at: *//adsabs.harvard.edu/cgi-bin/*

McNeill, J.D. (1980a). Electrical conductivity of soils and rocks. *Geonics Ltd*., Tech. Note TN-5, Mississauga, Ontario.

McNeill, J.D. (1980b). Electromagnetic terrain conductivity measurement at low induction numbers. *Geonics Limited*, Technical note TN-6, Mississauga, Ontario.

Metternicht, G.I., Zinck, J. A. (2003). Remote sensing of soil salinity: potentials and constraints. *Remote Sensing of Environ.* Vol. 85, Issue 1, 25, 1-20.

Metternicht, G.I., Zinck, J.A. (1996). Modelling salinity-alkalinity classes for mapping salt-affected topsoils in the semiarid valleys of Cochabamba (Bolivia). *ITC Journal*, 125-135.

Miehle, P., Livesley, S.J., Liw, C., Feikemaz, P.M., Adams M.A., Arndt, S.K. (2006). Quantifying uncertainty from large-scale model predictions of forest carbon dynamics. *Global Change Biology*, 12, 1421–1434.

Miller, J. R., Hare, E. W., Wu, J. (1990). Quantitative characterization of the vegetation red edge reflectance: 1. An inverted-Gaussian reflectance model. *Int. J. of Remote Sensing,* 11, 1755–1773.

Mitsuchi, M., Wichaidit, P., Jeungnijnirund, S. (1989). Soils of the Northeast Plateau, Thailand, Technical Bull. *Trop. Agr. Res. Center*, 25-55.

Moenke, H., 1962, Mineralspektren, I. *Akademie-Verlag*, Berlin.

Moon, A.M., Bonham-Carter, G.F. (1992). On knowledge-based approach of integrating remote sensing, *geophysical and geological information; IGARSS*, 92.

Moore, D.S., McCabe, G.P. (2003). Introduction to the practice of statistics. Forth ed. W.H. *Freeman and Co.*, New York. 828 p.

Mougenot, B., Pouget, M., Epema, G.F. (1993). Remote sensing of salt-affected soils. *Remote Sensing Reviews,* 7: pp. 241-259.

Mulder, N.J. (1994). A theory of knowledge based image analysis with application to SAR data of agriculture; *Proceeding of European Optical Society and International Society of Optical Engineering Symposium*; 26-30 Sept, 1994, Rome, Italy.

Musick, H.B., Pelletier, R.E. (1988). Response to soil moisture of spectral indexes derived from bidirectional reflectance in thematic mapper wavebands. *Remote Sensing of Environment*, Vol. 25, 2, 167-184.

Nakamoto, K. (1963). Infrared spectra of inorganic and coordination compounds. *John Wiley &Sons*, INC., New York.

NASA (2001). Introduction to the Hyperion Instrument & Data Processing. Available at: *http://eo1.gsfc.nasa.gov/miscPages/Workshop/Sec-03.pdf*

Nash, J.E., Sutcliffe, J.V. (1970). River flow forecasting through conceptual models, 1: a discussion of principles. *Journal of Hydrology*, 10, 282–290.

Nyquist R.P., Kagel, R.O. (1971). Infrared spectra of inorganic compounds (3800-45 cm-1). *Academic Press*, New York.

Paul, J.L., Tanji, K.K., Anderson, W.D. (1966). Estimating soil and saturation extract composition by a computer mrthod. Soil. Sci. Society of America Proc. 30: 15 – 17.

Peng, W. (1998). Synthetic analysis for extracting information on soil salinity using remote sensing and GIS: A case study of Yanggao basin in China. *Environ.l Manage.,* 22, 1, 153–159.

PimaView User Manual (1999). User manual. *Integrated Spectronics Pty Ltd*. Document Ref. No. ISPL-PV-3.1-01.

Pinty, B., Verstraete, M.M., Iaquinta, J., Gobron, N. (1996). Advanced modelling and inversion techniques for the quantitative characterization of desertification. In: Hill, J., Peter, D., (Eds), The use of remote sensing for land degradation and desertification monitoring in the Mediterranean basin. *State of the art and future research. Experts workshop* 13 to 15 June Valencia (Spain).

Pishkar, A.R. (2003). Analysis of the relationship between soil salinity dynamics and geopedologic properties, a case study of the Goorband area, Iran . MSc thesis, *ITC*, Enschede, The Netherlands.

Pracilio, G., Street, G.J., Chakravartula, P.N., Angeloni, J.R., Sattel, D., Owers, M., Lane, R. (1998). Lake Toolibin SALTMAP survey, interpretation report. National Dryland Salinity Program, Airborne Geophysical Surveys to assist planning for salinity control. *World Geoscience Corporation Limited, 65 Brockway Road, Floreat. W.A. 6014, Australia*

Rao, B.R.M, Sankar, T., Dwivedi, R.S., Thammappa, S.S., Venkataratnam, L., Sharma, R., Das, S. (1995). Spectral behaviour of salt-affected soils. *Int. J. Remote Sensing*, Vol. 16, no. 12, 2125-2136.

Rao, B.R.M., Dwivedi, R.S., Sreenivas, K., Khan, Q.I., Ramana, K.V., Thammappa, S.S., Fyzee, M.A. (1998). An inventory of salt-affected soils and waterlogged areas in the Nagarjunsagar Canal Command Area of Southern India, using space-borne multispectral data. *Land Degradation and Development*, 9: 357-367.

Reynolds, J.M. (1997). An introduction to applied and environmental geophysics. *Wiley & Sons*. 796.

Richards, L. A. (1954). Diagnosis and improvement of saline and saline and alkali soils, (Agricultural Handbook No. 60), US Department of Agricultural, Washington, DC.

Rhoades, J.D., Corwin, D.L. (1981). Determining soil electrical conductivity-depth relations using an inductive electromagnetic soil conductivity meter. *Soil Sci. Soc. Am. J.*, 45: 255-260.

Rhoades, J.D., Lesch, P.J., Shouse, P.J., Alves, W.J. (1989). New calibrations for determining soil electrical conductivity-Depth relations from electromagnetic measurements. *Soil Sci. Soc. Am. J.,* 53:74-79.

Ross, S.D. (1974). Sulphatee and other oxy-anions of Group VI. In: V. C. Farmer (Ed.), The InfraRed Spectra of Minerals, *Mineralogical Society*, London, 423-444.

Rossel, R.A.V., Walvoort, D.J.J., McBratney, A.B., Janik L.J., Skjemstad, J.O. (2005). Visible, near infrared, mid infrared or combined diffuse reflectance spectroscopy for simultaneous assessment of various soil properties. *Geoderma,* Vol. 131, 1-2, 59-75.

Rossel, R.A.V. (2005). ParLeS version 2.1a. Pre-processing of data, Principal Component Analysis and Partial Least Squares Regression with Leave-one-out Cross Validation. Available at: *//www.usyd.edu.au/su/agric/acpa/people/rvrossel/soft01.htm*

Rozanov, B.G. (1990). Human impacts on evolution of soils under various ecological conditions of the world. P. 53-62. In: *Proc. of the 14th Int. Cong. of Soil Sci.,* 12–18 August, Kyoto, Japan. Plenary papers.

Roush, T.L., Singer, R.B. (1986). Gaussian analysis of temperature effects on the reflectance spectra of mafic minerals in the 1-mm region. *J. Geophys. Res*., 91, 10301-10308.

Sah, A.k., Eiumnoh, A., Murai, S., Parkpian, P. (1995). Mapping of salt-affected soils using remote sensing and geographic information systems: A case study of Nakhon Ratchaslma, Thailandl . *Proceedings of the 16th Asian Conference Remote sensing.* 20-24 Nov. G-3-1 – G-3-6.

Savitzky A., Golay, M.J.E. (1964). Smoothing and Differentiation of Data by Simplified Least Squares Procedures. *Anal. Chem*. 36(8), 1627–1639.

Schoups, G., Hopmans, J.W. (2002). Model of vadose zone solute transport with root water and solute uptake. In: *17th world congress of soil science*. 14-21 August 2002, Bangkok, Thailand. Symposium 54.

Schwarz J. Staenz K. (2001). Adaptive Threshold for Spectral Matching of Hyperspectral Data. *Canadian Journal of Remote Sensing*, vol. 27, No 3, pp. 216-224.

Schmidt, K.S., Skidmore, A. K. (2003). Spectral discrimination of vegetation types in a coastal wetland. *Remote Sensing of Environment,* Vol. 85, Issue 1, 25, 92-108.

Schmidt, K.S., Skidmore, A.K., Kloosterman, E.H., van Oosten, H., Kumar, L., Janssen, J.A.M. (2004). Mapping coastal vegetation using an expert system and hyperspectral imagery. *Photogrammetric Engineering and Remote Sensing*, Vol. 70, no. 6, 703-715.

Schwarzott M., Baurecht D., Fringeli, U.P. (2001). Solvation effects in aqueous solutions investigated by FTIR-ATR spectroscopy. *The first International Conference on Advanced Vibrational Spectroscopy,* ICAVS-1. August 19-24, Turku, Finland. At: http://www.bpc.univie.ac.at/biophysik/pub.html

Schlerf, M., Atzberger, C., Hill, J., (2005). Remote sensing of forest biophysical variables using HyMap imaging spectrometer data. *Remote Sensing of Environment*, Vo. 95, 2, 177-194.

Shao, X., Ma, C. (2003). A general approach to derivative calculation using wavelet transform. *Chemometrics and Intelligent Laboratory Systems*, vol. 69, Issues 1-2, 28, 157-165.

Sharma, B.R., and Bhargava, G.P. (1988). Landsat imagery for mapping saline soils and wetlands in northwest India. *Int. J. Remote sensing*, 9: 39-44.

Shepherd, K.D., Walsh, M.G. (2002). Development of reflectace spectral libraries for characterization of soil properties. *Soil Sci. Soc. Am.*, Vol. 66, no. 3.

Sinanuwong, S., Takaya, Y. (1974). Saline soils in Northeast Thailand. *South East Asian Studies,* Vol. 12, pp. 105-120.

Skidmore, A.K. (1989). An expert system classifies eucalypt forest types using Thematic Mapper data and a digital terrain model. *Photogrammetric Engineering & Remote Sensing*, Vol. 55, no.10, 449-1464.

Smith G., Strens, R.G.J. (1976). Intervalence transfer absorption in some silicate, oxide and phosphate minerals. In: R.G.J. Strens (ed), The Physics of Minerals and Rocks. *John Wiley & Sons*, Inc., New York. 583-612.

Sparks, D. L. (1995). Environmental soil chemistry. *Academic press*, *Inc.* San Diego, 267 p.

Spenneman, G.H.R. (1997). Urban salinity as a threat to cultural heritage places. A primer on the mechanics and effects of chloridation, Johnstone Centre of Parks, Recreation and Heritage, *Charles Sturt University*, Albury, NSW.

Spitz, K., Moreno, J. (1996). A practical guide to groundwater and solute transport modelling. *John Wiley & Sons*, Inc.

Steven, M.D., Malthuis, T.J., Jaggard, F.M., Andieu, B. (1992). Monitoring responses of vegetation to stress. In: Cracknell, A.P., Vaughan, R.A., (Eds), *Remote sensing from research to operation: Proceedings of the 18th Annual Conference of the remote sensing society*'. University of Dundeep.

Stoner, E.R. (1979). Physicochemical, site, and bidirectional reflectance factor characteristics of uniformly moist soils. *PhD. thesis, Purdue Univ*ersity.

Stoner, E.R., Baumgardner M.F. (1981). Characteristic variations in reflectance of surface soils. *Soil Sci. Soc. Am. J.*, 45: 1161-1165.

Street, G.J., Pracillio, G., Anderson-Mayes, A. (2002). Interpretation of geophysical data for salt hazard identification and catchment management in southwest Western Australia. *Exploration Geophysics*, 33: 65-72.

Sunshine, J. M., Pieters, C. M., Pratt, S. F. (1990). Deconvolution of mineral absorption bands—An improved approach. *Journal of Geophysical Res.- Solid Earth and Planets*, 95, 6955– 6966.

Szabolcs, I. (1974). Salt affected soils in Europe. *Martinus Nijhoff*, The Hague. 63.

Szilagyi, A., Baumgardner, M.F. (1991). Salinity and spectral reflectance of soils. In: *Proc. Am. Soc. Photogramm. R. Sens. Sympo. Baltimore* U.S.A. 25-29 March 1991, ASPRS 430- 437.

Tanji, K. K. (1990). Agricultural Salinity Assessment and Management. American Society of Civil Engineers Manuals and Reports on Engineering Practice No. 71, *American Society of Civil Engineers*, New York, NY. 619 P.

Taylor, G., Dehaan, R. (2000). Salinity mapping with hyperspectral imagery.

At: *//www.bees.unsw.edu.au/research/remote_sensing/salinity1.html*

Thomas, D.S.G. (1997). Arid zone geomorphology : process, form and change in drylands. Second edition. *John Willey & Sons Ltd*. 713 P.

Triantafilis, J., Odeh, I.O.A., McBratney, A.B. (2001). Five geostatistical models to predict soil salinity from electromagnetic induction data across irrigated cotton. *Soil Sci. Soc. Am. J.*, Vol. 65, no. 3, 869-878

Trudgill, T., (Ed.), (1995). Solute modelling in catchment systems. *John Wiley & Sons Ltd*. Chichester,486 P.

TSG user manual (2005). At:

//members.ozemail.com.au/~pima/TSG%20Pro%20MainFrame.htm

Udelhoven, T., Emmerling, C., Jarmer, T. (2003). Quantitative analysis of soil chemical properties with diffuse reflectance spectrometry and partial least-square regression: A feasibility study. *Plant and Soil,* 251: 319–329.

Upadhyaya, S., Teixeira, A. (2002). Sensors for Information Gathering. Available at: *http://www.precisionag.org/PDF/ch10.pdf*

USGS (2007). At:*//crustal.usgs.gov/projects/remote_sensing/products.html*

Van Dam, J.C., Huygen, J., Wesseling, J.G., Feddes, R.A., Kabat, P., van Walsum, P.E.V., Groenendijk, P., Van Diepen, C.A. (1997). Theory of SWAP version 2.0. Simulation of water flow, solute transport and plant growth in the Soil-Water-Atmosphere-Plant environment. *DLO Winand Staring Centre*, Technical Document 45, Wageningen, The Netherlands.

Van der Meer, F. (2000a). Imaging Spectrometry for Geological Application. In: R.A. Meyers (Ed.) Encyclopedia of analytical chemistry, 8601-8638. *John Wiley & Sons LTD*, Chichester.

Van der Meer, F. (2000b). Spectral curve shape matching with a continuum removed CCSM Algorithm. *int. j. of remote sensing*, vol. 21, 16, 3179–3185.

Van der Meer, F., Bakker, W.W., Scholte, K., Skidmore, A., De Jong, S., Clevers, J., Epema, G. (1999). Simulation of MERIS data: potentials and limitations for mapping (soil) mineralogy. *JAG., Vol. 1, 3*. 196-204.

Vane G., Goetz, A. F. H. (1993). Terrestrial imaging spectrometry: current status, future trends, *Remote Sensing Environ.*, 44, p. 117 - 126.

Van Reeuwijk, L.P. (1993). Procedures for soil analysis. Technical paper No. 9. *International soil reference and information centre (ISRIC).* Wageningen. The Netherlands.

Van Wesenbeeck, I.J., Kachanoski, R.G. (1994). Special scale dependence of in situ solute transport. *Soil Sci. Soc. Am.*, 55: 3-7.

Vaughan, P.J., Simunek, J., Suarez, D.L., Corwin, D.L., Rhoades, J.D. (1996). Unsatchemgeo: Modelling water flow and multicomponent solute transport in a GIS context. "Applications of GIS to the modelling of non-point source pollutants in the vadose zone". *SSSA special publication no*. 48, Madison, WI., 235-246.

Verkerk, G., Broens, J.B., Kranendonk, W., van der Puijl, F.J., Sikkema, J.L., Stam, C.W. (1992). Binas, Informatieboek vwo/havo voor het onderwijs in de natuurwetenschappen. *Wolters-Nordhoff bv*. Groningen, The Netherlands. ISBN 90-01-89372-4.

Verma, K.S., Saxena, R.K., Barthwal, A.K., Deshmukh, S.N. (1994). Remote sensing technique for mapping salt affected soils. *Int. J. Remote Sensing*, 15: 1901-1914.

Verstraete, M.M., Pinty, B., Myneni, R. (1994). Understanding the biosphere from space: Strategies to exploit remote sensing data. In: *Proceeding of the 6th ISPRS international symposium on physical measurements and signatures in remote sensing*. Val d'Isere, France, 17-21 January 1994, CNES. 993-1004.

Vink, A.P.A. (1949). Bydrage tot de kennis van loess en dekzanden in het byzonder van de zuidoostelijke Veluwe. Thesis Wageningen University, The Netherlands.

Vlotman, W.F., (Ed), (2000). EM-38 workshop proceedings. New Delhi, Feb 4. Special Reports no:10. *ILRI*, The Netherlands.

Wagenet, R.J., Hutson, J.L. (1996). Scale-dependency of solute transport modelling/GIS applications. *J. Environ. Qual.* 25: 499 – 510.

Webster, R., Oliver, M.A. (1990). Statistical methods in soil and land resource survey. *Oxford University Press.*

White, W.B. (1974). The carbonate minerals. In. V. C. Farmer (Ed.), The InfraRed Spectra of Minerals, Mineralogical Society Monograph 4, 227-284., *Mineralogical Society*, London, 539 p.

Whiting M.L., Li, L., Ustin, S.L. (2004). Predicting water content using Gaussian model on soil spectra. *Remote Sensing of Environment*, vol. 89, 4, 535-552.

Wilkinson, G.G. (1996). A review of current issues in the integration of GIS and remote sensing data. *Int. J. Geographical Information Systems*, Vol. 10, Issue 1, 1996, 85-101.

Williams, P. C. (2001). Implementation of near infrared technology. *In Near infrared technology in the agricultural and food industries* (ed. P. C. Williams and K. H. Norris), 145-171. *American Association of Cereal Chemists*, St Paul, Minnesota.

Williams, B.G., Fiddler, FT. (1983). The use of electromagnetic induction for locating subsurface saline material. P.189-196. In: Relation of groundwater quantity and quality. *Proceedings of the Hamburg symposium*. IAHS publ.146.

Wishart, D. (1969). Mode Analysis: A Generalization of Nearest Neighbor which Reduces Chaining Effects. In A.J. Cole (Ed.), Numerical Taxonomy, *Academic Press*, 282-311.

Wold, S., Sjöström, M., Eriksson, L. (2001). PLS-regression: a basic tool for chemometrics. *Chemometrics and intelligent Lab. Systems*, 58(2), 109-130.

Yamamoto, Y., Sukchan, S. (2003). The Conformity of agricultural land use and physical suitability using by multi-temporal satellite imagery in Khon Kaen District, Northeast Thailand. *Asian Journal of Geoinformatics*, Vol.4, No. 1, pp.31-38.

Yang, H., Griffiths, P.R., Tate, J.B. (2003). Comparison of partial least squares regression and multi-layer neural networks for quantification of nonlinear systems and application to gas phase Fourier transform infrared spectra. *Analytica Chimica Acta*, 489, 125–136.

Yemefack, M., Rossiter, D.G., Njomgang, R. (2005). Multi-scale characterization of soil variability within an agricultural landscape mosaic system in southern Cameroon. *Geoderma,* 125, 117-143.

Summary

In the literature, a compound process (a series of processes, together) termed as salinization/alkalinization, is referred to as the most frequently occurring land degradation type in semi and arid regions. These processes are the product of a complex interaction of various factors, which cause changes within a time period of about a decade, generally irreversible, resulting in increase of salt in soils. Excessive salts precipitation in soil profile develops to the formation of salt-affected soils affecting the physical, chemical and biological properties of the soil, and eventually leads to partial or complete loss of soil productivity. It has a large impact in semi-arid regions where the lands are extremely needed for agricultural practices to supply required food and fibre for their rapidly increasing population, while human-induced factors and natural conditions are highly contributing to expansion of saline areas. This conflictive situation is a major concern at local and global scales where enormous efforts had focused on slowing down the salinization and preventing its progression. As a part of these efforts, enormous scientific studies had been carried out to combat salinization. These studies had focused on providing comprehensive understanding of the process, developing methods and algorithms, and providing various application tools. Optical remote sensing, electromagnetic geophysics and solute modelling are the three most used disciplines for detection, prediction and mapping of salt-affected soils.

A review of techniques and methods that used to detect salt-affected areas allows establishing a discussion leading to development of a new conceptual framework for the research. This study focuses on defining the underlying problems that prevent accurate estimation of soil salinity levels from remote sensing and is based on the philosophy of solving one problem at a time and providing answers that contribute to solve another problem in hand. Following such an ideology, the presented research was started with an experimental study under controlled laboratory conditions to provide the basics but very essential information of spectral characteristics of salt-affected soils and the underlying factors. This information was used to build the foundation of the current investigation in order to develop modelling tools that use both spectral reflectance and electromagnetic measurements (geophysics). Therefore, developing modelling procedures for quantifying salt contents in soils on the basis of variations in soil reflectance spectra is the main focus of this research. Can a salinity warning system that employs modelling techniques be developed to detect areas in early stage of salinity where the soils are potentially at risk become the main question to be answered. To do so, a new conceptual model and new approach needed to be developed. The developed conceptual framework suggests the use of knowledge-based approach and integration of surface and sub-surface measurements. Knowledge-based systems offer large

potential for extracting information from remotely sensed data on bases of explicit knowledge about the objects and processes, use of ancillary data, and an iterative procedure to adjust the calculated results (optimization). Beside the mentioned issues, the research also focused on the development of spectrometric techniques for recognizing the presence and abundance of salts in soils, quantifying similarities between salt-affected soils spectra with different electrical conductivity, establishing a relationship between soil properties and soil spectra in laboratory, field application of laboratory achievements using in-situ surface and near-surface measurements, predicting and mapping saline areas using modelling tools, and evaluating the results.

Briefly, the main findings and conclusions of the research are:

Conceptualization of an approach where detection of an early stage of soil salinity via integrating surface and near-surface information into modelling process in a GIS environment were promised.

The results from experimental study provided detailed information on salt-induced spectral features and their potential involvement in predicting soil salinity. The analysis of the relationship between salt concentrations in soil samples and their spectral responses revealed the complexity of salts identification and quantification of salinity levels. The findings provided a perspective for developing spectrometric techniques to recognize the presence and abundance of salts in soils.

The used spectral matching techniques provided an insight and a better understanding of soil spectral response due to salt variations. The results illustrates that spectral similarity measures are suitable diagnostic indicators to differentiate among salt-affected soils spectra. It shows that differences observed in absorption strength, absolute reflectance and spectral angle in the near and shortwave infrared regions of salt-affected soils are proportionally varied with the amount of salts in soils. The results of numerical classification method show that the spectral variations are sufficient to provide a basis for aggregation in classes that are in agreement with the standard international salinity classes. The statistical test showed that the differences between the reflectance spectra associated with the observed salinity classes are statistically significant.

The study of interaction between salt and moisture in soil and their effects on soil spectra showed that accurate quantification of soil salt contents largely depends on availability of free water (moisture) in the soil. The results confirm the influence of salts on soil reflectance spectra and its contribution to causing incongruity. They also suggest that prediction of soil moisture using spectral reflectance can be hampered by the accumulation of salts in soil.

The developed methods, both PLSR and ANN, were very effective for establishing relationships between soil reflectance and soil EC. The significant correlation established between soil EC and soil reflectance at laboratory level by both methods provided the basis for up-scaling toward the air-borne hyperspectral data. In the up-scaling process, the accurate laboratory data were replaced with the pixel reflectance derived from hyperspectral imageries and in situ EC_a measured by geophysical instruments. The accurate prediction of soil salinity by both methods (PLSR and ANN), at up-scaled level, provides possibility of integrating sub-surface geophysical electromagnetic measurements and surface reflectance derived from air-borne hyperspectral imageries. This means, progressing from two non-unique salt identification methods towards a unique and new approach with prediction capabilities, which could lead to early detection of salinization. The new integrated method can be considered as a major development towards a sustainable agricultural management.

Samenvatting

Verzouting en alkalinizatie wordt algemeen gezien als de meest voorkomende vormen van land degradatie in semi-aride en aride gebieden. Beide processen zijn het resultaat van de complexe interactie van een aantal factoren, die in het algemeen binnen een periode van zo'n tien jaren een onomkeerbare verandering veroorzaakt, resulterend in een toename van de hoeveelheid zout in de bodem. Een hoge mate van neerslag van zouten in het bodemprofiel resulteert in een aantasting van de fysische, chemisch en biologische eigenschappen van de verzoute bodem. Uiteindelijk leidt dit tot een gedeeltelijk of zelfs permanent verlies van productiviteit van de bodem. Dit heeft grote gevolgen in semi-aride gebieden, waar een grote behoefte is aan landbouwgrond om in de voedselbehoefte van de snel toenemende bevolking te voorzien, terwijl tegelijkertijd door menselijke invloed de hoeveelheid verzoute bodems zich uitbreidt. Deze problematische situatie is tot grote zorg. Zowel op lokaal niveau als op wereldschaal worden enorme inspanningen gedaan om processen van bodemverzouting af te remmen en tegen te gaan. Ook wordt er veel geïnvesteerd in wetenschappelijke studies ten behoeve van de bestrijding van verzouting. In dergelijke studies wordt veelal de nadruk gelegd op kennisopbouw over de verzoutingsprocessen, op de ontwikkeling van methoden en technieken, en op de levering van toepasbare gereedschappen. Aardobservatie in het optische domein, elektromagnetische geofysica en de modellering van (in water) opgeloste stoffen zijn de drie vakgebieden, die het meest worden toegepast voor de detectie, voorspelling en kartering van verzoutte bodems.

Op basis van een overzicht van bestaande methoden en technieken die worden gebruikt voor de detectie van door zout aangetaste bodems is een nieuw conceptueel raamwerk ontwikkeld voor dit onderzoek. In deze studie wordt de nadruk gelegd op de analyse van de problemen die nauwkeurige bepaling van de mate van bodemverzouting met behulp van aardobservatie in de weg staan. Uitgangspunt hierbij is het één voor één oplossen van problemen, waarbij het antwoord op het ene probleem wordt gebruikt om het volgende probleem op te lossen. Dit idee volgend startte het onderzoek met een experimentele studie onder gecontroleerde laboratorium omstandigheden om de spectrale kenmerken van door zout aangetaste bodems te bepalen. De informatie die dit opleverde is gebruikt als basis voor de ontwikkeling van een serie modellen die zowel gebruik maken van spectrale reflectie, als van elektromagnetische (geofysische) metingen. De nadruk in dit onderzoek ligt aldus op de ontwikkeling van modelleerprocedures voor het kwantificeren van het zoutgehalte in bodems op basis van variatie in bodemreflectie spectra. De hoofdvraag hierbij is: kan een waarschuwingssysteem worden ontwikkeld dat in staat is gebieden te detecteren, die in een vroeg stadium van

bodemverzouting verkeren? Om deze vraag te beantwoorden zijn een nieuw conceptueel model alsmede een nieuwe methode van aanpak benodigd. Het te ontwikkelen conceptuele raamwerk veronderstelt de inzet van een kennisgedreven aanpak en de integratie van zowel oppervlakte- als ondergrondse metingen. Kennisgedreven systemen bieden goede mogelijkheden voor het genereren van informatie uit aardobservatiegegevens op basis van expliciete kennis van de betrokken objecten en processen, het gebruik van aanvullende gegevens en een iteratieve procedure om berekende gegevens te optimaliseren. Naast de hierboven beschreven nadruk, richt dit onderzoek zich ook op de ontwikkeling van spectroscopische technieken voor de detectie van het zoutvoorkomen in bodems, op de kwantitatieve, vergelijkende analyse van spectra van door zout aangetaste bodems met verschillende elektrische geleidbaarheid, op het vaststellen van relaties tussen bodemkenmerken en bodemspectra onder laboratoriumcondities, op de toepassing in het veld van de resultaten van laboratoriumanalyses bij in-situ metingen, en op de modelmatige voorspelling en kartering van door verzouting aangetaste gebieden.

De belangrijkste bevindingen and conclusies van het onderzoek zijn als volgt:

De ontwikkeling van een modelleringmethodiek is beoogd die door integratie van informatie van het bodemoppervlak en van de ondergrond de detectie van bodemverzouting in een vroeg stadium mogelijk maakt.

De resultaten van de experimentele studie hebben gedetailleerde informatie opgeleverd over invloed van zouten op de spectrale kenmerken van bodems en het mogelijke gebruik hiervan in de voorspelling van bodemverzouting. De analyse van de relatie tussen zoutconcentratie in bodemmonsters en hun spectrale karakteristiek geeft aan dat het herkennen van zoutvoorkomen in bodems en het kwantificeren van verschillende niveaus van bodemverzouting een complexe aangelegenheid is. Er zijn geen eenduidige verschillende spectra of verschillende absorptiebanden voor diverse zouten noch voor diverse zoutconcentraties. De versschillen zijn zeer subtiel en veranderen van situatie tot situatie. Deze bevindingen hebben als uitgangspunt gediend voor de ontwikkeling van spectrometrische technieken voor de detectie en van de aanwezigheid van zouten in bodems en van de mate van bodemverzouting.

De gebruikte technieken voor spectrale vergelijking ('spectral matching') hebben geleid tot een beter inzicht in de spectrale kenmerken van bodems onder invloed van variaties in zoutvoorkomen. De onderzoeksresultaten illustreren dat spectrale gelijkenis functies kunnen dienen als diagnostische indicatoren voor het differentiëren van de verschillende spectrale karakteristieken van door verzouting aangetaste bodems. Het geeft ook aan dat onderscheidden verschillen in mate van absorptie, in absolute reflectie en in spectrale hoek, in zowel het nabije en kortegolf golflengte bereik, proportioneel

veranderen met de hoeveelheid zoutvoorkomen in bodems. De resultaten van de toegepaste numerieke classificatie methode geven aan dat de gevonden spectrale verschillen voldoende basis vormen voor een groepering in spectrale klassen die in overeenstemming is met internationale standaarden voor classificatie van bodemverzouting. De resultaten van de statistische U-test laten statistisch significante verschillen tussen reflectie spectra enerzijds en bodemverzoutings klassen anderzijds zien.

Uit analyse van de interactie tussen zout in de bodem en bodemvocht en het resulterende effect op bodemreflectie spectra blijkt dat de nauwkeurigheid in kwantificering van de concentratie in bodemzout voor een groot deel afhangt van de hoeveelheid vrij water in de bodem. De resultaten van dit onderzoek bevestigen de invloed van zoutvoorkomen op bodemreflectie spectra en de bijbehorende variatie die dat veroorzaakt. De resultaten geven ook aan dat voorspelling van de hoeveelheid bodemvocht met gebruik van spectrale reflectie technieken kan worden belemmerd door de accumulatie van zouten in de bodem.

De in dit onderzoek ontwikkelde partial least squares regression (PSLR) en artificial neural network (ANN) methodieken zijn erg effectief gebleken voor het vaststellen van de relatie tussen bodemreflectie en elektrische geleidbaarheid van de bodem. De significante correlatie tussen de elektrische geleidbaarheid van de bodem en bodemreflectie, zoals vastgesteld onder laboratorium condities, heeft de basis gevormd voor opschaling naar hyperspectrale gegevens verkregen met vliegtuigen. In deze opschaling zijn de laboratoriumgegevens vervangen door zowel reflectiegegevens op pixel basis van hyperspectrale beelden, en in-situ meting van elektrische geleidbaarheid van de bodem met geofysische instrumenten. Voornoemde PLSR en ANN methodieken zijn succesvol toegepast in de voorspelling van bodemverzouting op de schaal van hyperspectrale beelden. Dit biedt mogelijkheden voor de integratie van ondergrondse geofysische, elektromagnetische metingen met oppervlaktegegevens over bodemreflectie verkregen uit hyperspectrale beelden uit vliegtuigen. Hiermee worden twee afzonderlijke methodes voor het detecteren van het zoutvoorkomen in de bodem samengevoegd tot een nieuwe, geïntegreerde methode van aanpak die de mogelijkheid tot voorspelling van bodemverzouting biedt. Dit kan daadwerkelijk leiden tot de detectie van bodemverzouting in een eerder stadium. Deze nieuwe methodiek kan daarmee een belangrijke bijdrage leveren aan het verbeterd beheer van landbouwgebieden.

Acknowledgments

The research presented in this dissertation was supported by several individuals and institutes over the last few years and would not have been accomplished without their contributions. I start with a word of apology and sincere thanks to many individuals who have assisted me with their knowledge or friendship during this research but are not mentioned here.

I am grateful to Prof. F. van der Meer, Prof. S. de Jong, Dr. M. van der Meijde and Dr. E.J.M. Carranza for their support, supervision and constructive discussions, which considerably improved the context of this dissertation.

Special gratitude is due to Prof. K. Harmsen for his crucial support during the early phase of the research and to Prof. A. Zinck for his contributions to my initial research proposal. I extend my gratitude to Dr. G. Metternicht and Dr. R. George for scientific support and providing access to the Toolibin catchment database. I am very grateful for support during the fieldwork from the staff of the soil survey and land use planning of LDD in Thailand, especially Mr. S. Sukchan, Mrs. P. Kuneepong and Mr. A. Suchinai. Special gratitude to ITC colleagues: Ir. B. Krol, Dr. H. van der Werff, Drs. B. de Smeth, Drs. J. Kooistra, Ir. G. Reinink and many others who had contributed to this research in different ways. I wish to express my gratitude to all fellow PhD candidates for their friendship, support, tea breaks, lunches, dinners, etc.

Lastly, my sincere thanks go to my parents, sisters, brothers and my friends for their support and care.

Author's publications

Farifteh, **J.**, F. van der Meer, M., C. Atzberger, Carranza, E.J.M., 2007. Quantitative analysis of salt-affected soil reflectance spectra: A comparison of two adaptive methods (PLSR and ANN). In press; *Remote Sensing of Environment*.

Farifteh, J., van der Meer, F., and E.J.M., Carranza, 2007. Similarity measures for spectral discrimination of salt-affected soils. In press; *International Journal of Remote Sensing*.

Farifteh, **J.**, van der Meer, F., van der Meijde, M., Atzberger, C. 2007. Spectral characteristics of salt-affected soils: A laboratory experiment. Under review; *Geoderma*.

Farifteh, J., Tolpekin, V., van der Meer, F., Sukchan, S. 2007. Salinity modeling of soil reflectance spectra. Under review; *International journal of Applied Earth Observation and Geoinformation*.

Farifteh, J., Farshad, A., and George, R.J., 2006. Assessing salt-affected soils using remote sensing, solute modelling and geophysics. *Geoderma,* 130, 191-206.

Farifteh, J., Soeters, R., 2006. Origin of the biancane and calanchi, East Aliano, southern Italy. *Geomorphology*, 77, 142-152.

Farifteh, J., van der Meer, F., van der Meijde M., Farshad, A., 2005. Spectral characteristics of salt-affected soils; Impact on imaging spectroscopy. *4th Workshop on Imaging Spectroscopy "Imaging Spectroscopy, New quality in environmental studies*". Warsaw, Poland, 27-29 April 2005.

Farifteh J., Bouma, A., van der Meijde, M. 2004. Detecting salt affected soils; Integrating surface and sub-surface measurements. Conference *Near Surface, 10th European Meeting of Environmental and Engineering Geophysics*, Utrecht, The Netherlands, 6-9 September 2004.

Farifteh, J., Farshad, A., 2002. Remote sensing and modelling of topsoil properties, a clue for assessing land degradation. *17 World congress of Soil Science*. 14-21 August 2002, Thailand.

Farifteh, J., Soeters, R., 1999. Factors underlying piping in the Basilicata region, southern Italy, *Geomorphology*, volume 26 (1999) 239-251.

Van Zuidam, R.A., **Farifteh, J**., Eleveld. M. Tao, C., 1998. Developments in remote sensing, dynamic modelling and GIS applications for integrated coastal zone management. Journal of Coastal Conservation 4: 191 – 202, 1998, © EUCC; *Opulus Press Uppsala*.

Van Westen, C., **Farifteh, J.,** 1997. ILWIS 2.1 for Windows; Users' Guide. *International Institute for Geo-information Science and Earth Observation (ITC)*, Enschede, The Netherlands, 511 p.

Mohammed, S.O., Farshad, A., **Farifteh, J.,** 1996. Evaluating land degradation for Assessment of land vulnerability to desert conditions in the Sokota area, Nigeria, Land Degradation and development, Vol. 7. *John Wiley & Sons, Ltd.*, 1996.

Farifteh, J., 1994. A Model for the Geomorphological Development of an area in the east of Alianello (Basilicata, Southern Italy), MSc. Thesis, *ITC*. The Netherlands.

Mahmoudi, F., and **Farifteh, J.,** 1990. Geomorphological Characteristics of Deserts of Iran, oral presentation in International workshop on remote sensing in Tehran, Iran.

Farifteh, J., 1990. Quantitative Analysis in Geomorphology, *Tehran University*, Tehran, Iran, 368 p., (in Farsi).

Farifteh, J., 1988. Geomorphological evolution of Dashtyari Plain, "Baluchistan". Iran Desert Research Centre, *Tehran University*, Tehran, Iran, 112 p., (in Farsi).

Farifteh, J., 1987: Systems of Climate Classification. A case study of semi-arid and arid regions of Iran. *Iran Desert Research Centre, Tehran University,* Tehran, Iran, 223 p., (in Farsi).

ITC Dissertations

1. **Akinyede** (1990), Highway cost modelling and route selection using a geotechnical information system
2. **Pan He Ping** (1990), 90-9003-757-8, Spatial structure theory in machine vision and applications to structural and textural analysis of remotely sensed images
3. **Bocco Verdinelli, G.** (1990), Gully erosion analysis using remote sensing and geographic information systems: a case study in Central Mexico
4. **Sharif, M**. (1991), Composite sampling optimization for DTM in the context of GIS
5. **Drummond, J.** (1991), Determining and processing quality parameters in geographic information systems
6. **Groten, S.** (1991), Satellite monitoring of agro-ecosystems in the Sahel
7. **Sharifi, A.** (1991), 90-6164-074-1, Development of an appropriate resource information system to support agricultural management at farm enterprise level
8. **Zee, D. van der** (1991), 90-6164-075-X, Recreation studied from above: Air photo interpretation as input into land evaluation for recreation
9. **Mannaerts, C.** (1991), 90-6164-085-7, Assessment of the transferability of laboratory rainfall-runoff and rainfall - soil loss relationships to field and catchment scales: a study in the Cape Verde Islands
10. **Ze Shen Wang** (1991), 90-393-0333-9, An expert system for cartographic symbol design
11. **Zhou Yunxian** (1991), 90-6164-081-4, Application of Radon transforms to the processing of airborne geophysical data
12. **Zuviria, M. de** (1992), 90-6164-077-6, Mapping agro-topoclimates by integrating topographic, meteorological and land ecological data in a geographic information system: a case study of the Lom Sak area, North Central Thailand
13. **Westen, C. van** (1993), 90-6164-078-4, Application of Geographic Information Systems to landslide hazard zonation
14. **Shi Wenzhong** (1994), 90-6164-099-7, Modelling positional and thematic uncertainties in integration of remote sensing and geographic information systems
15. **Javelosa, R.** (1994), 90-6164-086-5, Active Quaternary environments in the Philippine mobile belt

16. **Lo King-Chang** (1994), 90-9006526-1, High Quality Automatic DEM, Digital Elevation Model Generation from Multiple Imagery
17. **Wokabi, S.** (1994), 90-6164-102-0, Quantified land evaluation for maize yield gap analysis at three sites on the eastern slope of Mt. Kenya
18. **Rodriguez, O.** (1995), Land Use conflicts and planning strategies in urban fringes: a case study of Western Caracas, Venezuela
19. **Meer, F. van der** (1995), 90-5485-385-9, Imaging spectrometry & the Ronda peridotites
20. **Kufoniyi, O.** (1995), 90-6164-105-5, Spatial coincidence: automated database updating and data consistency in vector GIS
21. **Zambezi, P.** (1995), Geochemistry of the Nkombwa Hill carbonatite complex of Isoka District, north-east Zambia, with special emphasis on economic minerals
22. **Woldai, T.** (1995), The application of remote sensing to the study of the geology and structure of the Carboniferous in the Calañas area, pyrite belt, SW Spain
23. **Verweij, P.** (1995), 90-6164-109-8, Spatial and temporal modelling of vegetation patterns: burning and grazing in the Paramo of Los Nevados National Park, Colombia
24. **Pohl, C.** (1996), 90-6164-121-7, Geometric Aspects of Multisensor Image Fusion for Topographic Map Updating in the Humid Tropics
25. **Jiang Bin** (1996), 90-6266-128-9, Fuzzy overlay analysis and visualization in GIS
26. **Metternicht, G.** (1996), 90-6164-118-7, Detecting and monitoring land degradation features and processes in the Cochabamba Valleys, Bolivia. A synergistic approach
27. **Hoanh Chu Thai** (1996), 90-6164-120-9, Development of a Computerized Aid to Integrated Land Use Planning (CAILUP) at regional level in irrigated areas: a case study for the Quan Lo Phung Hiep region in the Mekong Delta, Vietnam
28. **Roshannejad, A.** (1996), 90-9009-284-6, The management of spatio-temporal data in a national geographic information system
29. **Terlien, M.** (1996), 90-6164-115-2, Modelling Spatial and Temporal Variations in Rainfall-Triggered Landslides: the integration of hydrologic models, slope stability models and GIS for the hazard zonation of rainfall-triggered landslides with examples from Manizales, Colombia
30. **Mahavir, J.** (1996), 90-6164-117-9, Modelling settlement patterns for metropolitan regions: inputs from remote sensing

31. **Al-Amir, S.** (1996), 90-6164-116-0, Modern spatial planning practice as supported by the multi-applicable tools of remote sensing and GIS: the Syrian case

32. **Pilouk, M.** (1996), 90-6164-122-5, Integrated modelling for 3D GIS

33. **Duan Zengshan** (1996), 90-6164-123-3, Optimization modelling of a river-aquifer system with technical interventions: a case study for the Huangshui river and the coastal aquifer, Shandong, China

34. **Man, W.H. de** (1996), 90-9009-775-9, Surveys: informatie als norm: een verkenning van de institutionalisering van dorp - surveys in Thailand en op de Filippijnen

35. **Vekerdy, Z.** (1996), 90-6164-119-5, GIS-based hydrological modelling of alluvial regions: using the example of the Kisaföld, Hungary

36. **Pereira, Luisa** (1996), 90-407-1385-5, A Robust and Adaptive Matching Procedure for Automatic Modelling of Terrain Relief

37. **Fandino Lozano, M.** (1996), 90-6164-129-2, A Framework of Ecological Evaluation oriented at the Establishment and Management of Protected Areas: a case study of the Santuario de Iguaque, Colombia

38. **Toxopeus, B.** (1996), 90-6164-126-8, ISM: an Interactive Spatial and temporal Modelling system as a tool in ecosystem management: with two case studies: Cibodas biosphere reserve, West Java Indonesia: Amboseli biosphere reserve, Kajiado district, Central Southern Kenya

39. **Wang Yiman** (1997), 90-6164-131-4, Satellite SAR imagery for topographic mapping of tidal flat areas in the Dutch Wadden Sea

40. **Saldana-Lopez, Asunción** (1997), 90-6164-133-0, Complexity of soils and Soilscape patterns on the southern slopes of the Ayllon Range, central Spain: a GIS assisted modelling approach

41. **Ceccarelli, T.** (1997), 90-6164-135-7, Towards a planning support system for communal areas in the Zambezi valley, Zimbabwe; a multi-criteria evaluation linking farm household analysis, land evaluation and geographic information systems

42. **Peng Wanning** (1997), 90-6164-134-9, Automated generalization in GIS

43. **Lawas, C.** (1997), 90-6164-137-3, The Resource Users' Knowledge, the neglected input in Land resource management: the case of the Kankanaey farmers in Benguet, Philippines

44. **Bijker, W.** (1997), 90-6164-139-X, Radar for rain forest: A monitoring system for land cover Change in the Colombian Amazon

45. **Farshad, A.** (1997), 90-6164-142-X, Analysis of integrated land and water management practices within different agricultural systems under semi-arid conditions of Iran and evaluation of their sustainability

46. **Orlic, B.** (1997), 90-6164-140-3, Predicting subsurface conditions for geotechnical modelling
47. **Bishr, Y.** (1997), 90-6164-141-1, Semantic Aspects of Interoperable GIS
48. **Zhang Xiangmin** (1998), 90-6164-144-6, Coal fires in Northwest China: detection, monitoring and prediction using remote sensing data
49. **Gens, R.** (1998), 90-6164-155-1, Quality assessment of SAR interferometric data
50. **Turkstra, J.** (1998), 90-6164-147-0, Urban development and geographical information: spatial and temporal patterns of urban development and land values using integrated geo-data, Villaviciencia, Colombia
51. **Cassells, C.** (1998), 90-6164-234-5, Thermal modelling of underground coal fires in northern China
52. **Naseri, M.** (1998), 90-6164-195-0, Characterization of Salt-affected Soils for Modelling Sustainable Land Management in Semi-arid Environment: a case study in the Gorgan Region, Northeast, Iran
53. **Gorte B.G.H.** (1998), 90-6164-157-8, Probabilistic Segmentation of Remotely Sensed Images
54. **Tegaye, Tenalem Ayenew** (1998), 90-6164-158-6, The hydrological system of the lake district basin, central main Ethiopian rift
55. **Wang Donggen** (1998), 90-6864-551-7, Conjoint approaches to developing activity-based models
56. **Bastidas de Calderon, M.** (1998), 90-6164-193-4, Environmental fragility and vulnerability of Amazonian landscapes and ecosystems in the middle Orinoco river basin, Venezuela
57. **Moameni, A.** (1999), Soil quality changes under long-term wheat cultivation in the Marvdasht plain, South-Central Iran
58. **Groenigen, J.W. van** (1999), 90-6164-156-X, Constrained optimisation of spatial sampling: a geostatistical approach
59. **Cheng Tao** (1999), 90-6164-164-0, A process-oriented data model for fuzzy spatial objects
60. **Wolski, Piotr** (1999), 90-6164-165-9, Application of reservoir modelling to hydrotopes identified by remote sensing
61. **Acharya, B.** (1999), 90-6164-168-3, Forest biodiversity assessment: A spatial analysis of tree species diversity in Nepal
62. **Akbar Abkar, Ali** (1999), 90-6164-169-1, Likelihood-based segmentation and classification of remotely sensed images

63. **Yanuariadi, T.** (1999), 90-5808-082-X, Sustainable Land Allocation: GIS-based decision support for industrial forest plantation development in Indonesia

64. **Abu Bakr**, **Mohamed** (1999), 90-6164-170-5, An Integrated Agro-Economic and Agro-Ecological Framework for Land Use Planning and Policy Analysis

65. **Eleveld, M.** (1999), 90-6461-166-7, Exploring coastal morphodynamics of Ameland (The Netherlands) with remote sensing monitoring techniques and dynamic modelling in GIS

66. **Yang Hong** (1999), 90-6164-172-1, Imaging Spectrometry for Hydrocarbon Microseepage

67. **Mainam, Félix** (1999), 90-6164-179-9, Modelling soil erodibility in the semiarid zone of Cameroon

68. **Bakr, Mahmoud** (2000), 90-6164-176-4, A Stochastic Inverse-Management Approach to Groundwater Quality

69. **Zlatanova, Z.** (2000), 90-6164-178-0, 3D GIS for Urban Development

70. **Ottichilo, Wilber K.** (2000), 90-5808-197-4, Wildlife Dynamics: An Analysis of Change in the Masai Mara Ecosystem

71. **Kaymakci, Nuri** (2000), 90-6164-181-0, Tectono-stratigraphical Evolution of the Cankori Basin (Central Anatolia, Turkey)

72. **Gonzalez, Rhodora** (2000), 90-5808-246-6, Platforms and Terraces: Bridging participation and GIS in joint-learning for watershed management with the Ifugaos of the Philippines

73. **Schetselaar, Ernst** (2000), 90-6164-180-2, Integrated analyses of granite-gneiss terrain from field and multisource remotely sensed data. A case study from the Canadian Shield

74. **Mesgari, Saadi** (2000), 90-3651-511-4, Topological Cell-Tuple Structure for Three-Dimensional Spatial Data

75. **Bie, Cees A.J.M. de** (2000), 90-5808-253-9, Comparative Performance Analysis of Agro-Ecosystems

76. **Khaemba, Wilson M**. (2000), 90-5808-280-6, Spatial Statistics for Natural Resource Management

77. **Shrestha, Dhruba** (2000), 90-6164-189-6, Aspects of erosion and sedimentation in the Nepalese Himalaya: highland-lowland relations

78. **Asadi Haroni, Hooshang** (2000), 90-6164-185-3, The Zarshuran Gold Deposit Model Applied in a Mineral Exploration GIS in Iran

79. **Raza, Ale** (2001), 90-3651-540-8, Object-oriented Temporal GIS for Urban Applications

80. **Farah, Hussein** (2001), 90-5808-331-4, Estimation of regional evaporation under different weather conditions from satellite and meteorological data. A case study in the Naivasha Basin, Kenya

81. **Zheng, Ding** (2001), 90-6164-190-X, A Neural - Fuzzy Approach to Linguistic Knowledge Acquisition and Assessment in Spatial Decision Making

82. **Sahu, B.K.** (2001), Aeromagnetics of continental areas flanking the Indian Ocean; with implications for geological correlation and reassembly of Central Gondwana

83. **Alfestawi, Y.** (2001), 90-6164-198-5, The structural, paleogeographical and hydrocarbon systems analysis of the Ghadamis and Murzuq Basins, West Libya, with emphasis on their relation to the intervening Al Qarqaf Arch

84. **Liu, Xuehua** (2001), 90-5808-496-5, Mapping and Modelling the Habitat of Giant Pandas in Foping Nature Reserve, China

85. **Oindo, Boniface Oluoch** (2001), 90-5808-495-7, Spatial Patterns of Species Diversity in Kenya

86. **Carranza, Emmanuel John** (2002), 90-6164-203-5, Geologically-constrained Mineral Potential Mapping

87. **Rugege, Denis** (2002), 90-5808-584-8, Regional Analysis of Maize-Based Land Use Systems for Early Warning Applications

88. **Liu, Yaolin** (2002), 90-5808-648-8, Categorical Database Generalization in GIS

89. **Ogao, Patrick** (2002), 90-6164-206-X, Exploratory Visualization of Temporal Geospatial Data using Animation

90. **Abadi, Abdulbaset M.** (2002), 90-6164-205-1, Tectonics of the Sirt Basin – Inferences from tectonic subsidence analysis, stress inversion and gravity modelling

91. **Geneletti, Davide** (2002), 90-5383-831-7, Ecological Evaluation for Environmental Impact Assessment

92. **Sedogo, Laurent G.** (2002), 90-5808-751-4, Integration of Participatory Local and Regional Planning for Resources Management using Remote Sensing and GIS

93. **Montoya, Lorena** (2002), 90-6164-208-6, Urban Disaster Management: a case study of earthquake risk assessment in Carthago, Costa Rica

94. **Ahmad, Mobin-ud-Din** (2002), 90-5808-761-1, Estimation of Net Groundwater Use in Irrigated River Basins using Geo-information Techniques: A case study in Rechna Doab, Pakistan

95. **Said, Mohammed Yahya** (2003), 90-5808-794-8, Multiscale perspectives of species richness in East Africa
96. **Schmidt, Karin** (2003), 90-5808-830-8, Hyperspectral Remote Sensing of Vegetation Species Distribution in a Saltmarsh
97. **Lopez Binnquist, Citlalli** (2003), 90-3651-900-4, The Endurance of Mexican Amate Paper: Exploring Additional Dimensions to the Sustainable Development Concept
98. **Huang, Zhengdong** (2003), 90-6164-211-6, Data Integration for Urban Transport Planning
99. **Cheng, Jianquan** (2003), 90-6164-212-4, Modelling Spatial and Temporal Urban Growth
100. **Campos dos Santos, Jose Laurindo** (2003), 90-6164-214-0, A Biodiversity Information System in an Open Data/Metadatabase Architecture
101. **Hengl, Tomislav** (2003), 90-5808-896-0, PEDOMETRIC MAPPING, Bridging the gaps between conventional and pedometric approaches
102. **Barrera Bassols, Narciso (**2003), 90-6164-217-5, Symbolism, Knowledge and management of Soil and Land Resources in Indigenous Communities: Ethnopedology at Global, Regional and Local Scales
103. **Zhan, Qingming** (2003), 90-5808-917-7, A Hierarchical Object-Based Approach for Urban Land-Use Classification from Remote Sensing Data
104. **Daag, Arturo S.** (2003), 90-6164-218-3, Modelling the Erosion of Pyroclastic Flow Deposits and the Occurrences of Lahars at Mt. Pinatubo, Philippines
105. **Bacic, Ivan** (2003), 90-5808-902-9, Demand-driven Land Evaluation with case studies in Santa Catarina, Brazil
106. **Murwira, Amon** (2003), 90-5808-951-7, Scale matters! A new approach to quantify spatial heterogeneity for predicting the distribution of wildlife
107. **Mazvimavi, Dominic** (2003), 90-5808-950-9, Estimation of Flow Characteristics of Ungauged Catchments. A case study in Zimbabwe
108. **Tang, Xinming** (2004), 90-6164-220-5, Spatial Object Modelling in Fuzzy Topological Spaces with Applications to Land Cover Change
109. **Kariuki, Patrick** (2004), 90-6164-221-3, Spectroscopy and Swelling Soils; an integrated approach
110. **Morales, Javier** (2004), 90-6164-222-1, Model Driven Methodology for the Design of Geo-information Services
111. **Mutanga, Onisimo** (2004), 90-5808-981-9, Hyperspectral Remote Sensing of Tropical Grass Quality and Quantity

112. **Šliužas, Ričardas V.** (2004), 90-6164-223-X, Managing Informal Settlements: a study using geo-information in Dar es Salaam, Tanzania
113. **Lucieer, Arko** (2004), 90-6164-225-6, Uncertainties in Segmentation and their Visualisation
114. **Corsi, Fabio** (2004), 90-8504-090-6, Applications of existing biodiversity information: Capacity to support decision-making
115. **Tuladhar, Arbind** (2004), 90-6164-224-8, Parcel-based Geo-information System: Concepts and Guidelines
116. **Elzakker, Corné van** (2004), 90-6809-365-7, The use of maps in the exploration of geographic data
117. **Nidumolu, Uday Bhaskar** (2004), 90-8504-138-4, Integrating Geo-information models with participatory approaches: applications in land use analysis
118. **Koua, Etien L.** (2005), 90-6164-229-9, Computational and Visual Support for Exploratory Geovisualization and Knowledge Construction
119. **Blok, Connie A.** (2005), Dynamic visualization variables in animation to support monitoring of spatial phenomena
120. **Meratnia, Nirvana** (2005), 90-365-2152-1, Towards Database Support for Moving Object Data
121. **Yemefack, Martin** (2005), 90-6164-233-7, Modelling and monitoring Soil and Land Use Dynamics within Shifting Agricultural Landscape Mosaic Systems
122. **Kheirkhah, Masoud** (2005), 90-8504-256-9, Decision support system for floodwater spreading site selection in Iran
123. **Nangendo, Grace** (2005), 90-8504-200-3, Changing forest-woodland-savanna mosaics in Uganda: with implications for conservation
124. **Mohamed, Yasir Abbas** (2005), 04-15-38483-4, The Nile Hydroclimatology: impact of the Sudd wetland (Distinction)
125. **Duker, Alfred, A.** (2005), 90-8504-243-7, Spatial analysis of factors implicated in *mycobacterium ulcerans* infection in Ghana
126. **Ferwerda, Jelle, G.,** (2005), 90-8504-209-7, Charting the Quality of Forage: Measuring and mapping the variation of chemical components in foliage with hyperspectral remote sensing
127. **Martinez, Javier** (2005), 90-6164-235-3, Monitoring intra-urban inequalities with GIS-based indicators. With a case study in Rosario, Argentina

128. **Saavedra, Carlos** (2005), 90-8504-289-5, Estimating spatial patterns of soil erosion and deposition in the Andean region using Geo-information techniques. A case study in Cochabamba, Bolivia
129. **Vaiphasa, Chaichoke** (2006), 90-8504-353-0, Remote Sensing Techniques for Mangrove Mapping
130. **Porwal, Alok** (2006), 90-6164-240-X, Mineral Potential Mapping with Mathematical Geological Models
131. **Werff, Harald van der** (2006), 90-6164-238-8, Knowledge-based remote sensing of complex objects: recognition of spectral and spatial patterns resulting from natural hydrocarbon seepages
132. **Vlag, Daniël van de** (2006), 90-8504-384-0, Modeling and visualizing dynamic landscape objects and their qualities
133. **Joshi, Chudamani** (2006), 90-8504-470-7, Mapping cryptic invaders and invisibility of tropical forest ecosystems: *Chromolaena odorata* in Nepal
134. **Bandara, K.M.P.S.** (2006), 90-8504-406-5, Assessing irrigation performance by using remote sensing
135. **Dilo, Areti** (2006), 90-8504-461-8, Representation of and Reasoning with Vagueness in Spatial Information. A system for handling vague objects
136. **Debba, Pravesh** (2006), 90-8504-462-6, Sampling scheme optimization from hyperspectral data
137. **Huisman, Marco** (2006), 90-6164-246-9, Assessment of rock mass decay in artificial slopes
138. **Lemmens, Rob** (2006), 90-6164-250-7, Semantic interoperability of distributed geo-services
139. **Chacón Moreno, Eulogio** (2007), 90-8504-559-2, Ecological and spatial modeling: Mapping ecosystems, landscape changes, and plant species distribution in Llanos del Orinoco, Venezuela
140. **Amer, Sherif** (2007), 90-6164-253-1, Towards Spatial Justice in Urban Health Services Planning
141. **Obakeng, Obolokile Thothi** (2007), 90-6164-254-X, Soil moisture dynamics and evapotranspiration at the fringe of the Botswana Kalahari, with emphasis on deep rooting vegetation
142. **Cho, Moses Azong** (2007), 978-90-8504-622-6, Hyperspectral remote sensing of biochemical and biophysical parameters